

# Laboratory experimental procedures for the compression and shear characterisation of historical brick masonry

Thesis by compendium of publications

Doctoral Thesis by:  
Jorge Segura Domingo

Supervised by:  
Pere Roca Fabregat  
Luca Pelà

Barcelona, [November 2020](#)

Departament d'Enginyeria Civil i Ambiental

Programa de Doctorat en Enginyeria de la Construcció



UNIVERSITAT POLITÈCNICA  
DE CATALUNYA  
BARCELONATECH

# DOCTORAL THESIS

*This page is intentionally left blank.*

# **Laboratory experimental procedures for the compression and shear characterisation of historical brick masonry**

Doctoral Thesis submitted in fulfilment of the requirements for the  
*Degree of Doctor of Philosophy in Construction Engineering*

By

JORGE SEGURA DOMINGO

Barcelona, November 2020

*Thesis by compendium of publications*



**Universitat Politècnica de Catalunya**  
Departament d'Enginyeria Civil i Ambiental  
Programa de Doctorat en Enginyeria de la Construcció

*Thesis Supervisors:*

Prof. Pere Roca Fabregat

Assoc. Prof. Luca Pelà

*Board of Examiners:*

Prof. Humberto Varum – Universidade do Porto

Prof. Climent Molins Borrell – Universitat Politècnica de Catalunya

Assoc. Prof. Guido Camata – Università degli Studi “G. d’Annunzio” Chieti – Pescara

*To Yasmina*

*This page is intentionally left blank.*

*Manifiesto es que los antiguos de buena gana usaron de ladrillos en lugar de piedras. Yo creo cierto que los hombres al principio guiados por falta y necesidad de las cosas, pusieron en uso el hacer edificios de ladrillos, y que después que se consideró este género de edificio cuan fácil de hacer y cómodo para el uso, y apto para la gracia, y firme y constante para durar, llevaron adelante el edificar, y así las otras cosas como las cosas reales de ladrillo. Finalmente después que o por caso, o por industria percibieron que el fuego valía para firmar y espesar los ladrillos perseveraron en levantar con ladrillos todas las cosas a cada paso.*

*De Re Aedificatoria*, Leon Battista Alberti (15<sup>th</sup> c.)  
Spanish translation from latin by Francisco de Lozano in 1582

*Insensibly one begins to twist facts to suit theories, instead of theories to suit facts.*

Sherlock Holmes in *A scandal in Bohemia*  
Arthur Conan Doyle (1891)

*This page is intentionally left blank.*

# Acknowledgements

A PhD thesis should be, by definition, original and innovative, and the result of an individual effort. The doctorate is in fact a degree awarded individually. However, this thesis is devoted to one of the oldest building materials, and, as it is the case of historical constructions, which were characterized by the collective effort of a community, it is the result of my work during the last 5 years together with the collaboration of many other people. I want to express my sincere gratitude to all of them.

If we establish a metaphor of this thesis with a masonry wall, a first group of people would symbolize the units or blocks, which made the thesis possible, providing soundness and strength.

- My deepest appreciation goes to my two supervisors. Professor Pere Roca gave me the opportunity to start this process and the first economical support. I thank him for receiving me in his office a certain day of 2014 when I was not even a master's student. I thank him for his kindness, for teaching with passion, for his perennial availability, and, particularly, for his scientific and professional rigour. I thank also him for having a solution for whatever problem I could face. I thank Luca Pelà for his confidence, his sense of humour, his friendliness, for his enthusiasm. The meetings at his office and his uncountable e-mails have been the seeds of this thesis. I thank him for his detailed reviews and his accuracy. Thanks for believing in me and encouraging me.
- Financial support from different Spanish ministries is acknowledged. Research projects MICROPAR (BIA2012-32234), MULTIMAS (BIA2015-63882-P) and SEVERUS (RTI2018-099589-B-I00) partially funded this work. I also thank the Department of Civil and Environmental Engineering of UPC for awarding me a scholarship during the first months, and AGAUR – Generalitat de Catalunya for an FI scholarship over three years.
- Given the prevailing experimental character of this thesis, the staff of the Laboratory of Structures of Camins deserve a special gratitude. Tomás García, Carlos Hurtado and Camilo Bernad helped me with great ideas and solved any need

I encountered. Special thanks go for their help to prepare the diagonal testing setup. My particular appreciation goes, undoubtedly, to Jordi Cabrerizo and Robert McAloon, to whom I owe very much and whose affection and willingness to help me I will always remember. They are both like units of the best stone of Montjuic.

- I want also to thank Xavi Montornés, Manolo and José for the construction of the masonry specimens, as well as the Kerakoll company for providing the building mortar. Paolo Casadei and Patricio Contreras are acknowledged because of that.
- Fruitful collaborations along these years allowed me to reach this goal. Fabricio Avilés guided me during my first weeks in the laboratory. Diego Aponte illustrated me with his knowledge on mortars and has shown always an appreciated interest in my work. Ernest Bernat carried out the laboratory campaign in Terrassa and has granted me with his patience and scientific value. I also had the pleasure to co-supervise the master's thesis of Mateo Ugolini, Pietro Salvatoni and Myronas Drygiannakis. I learnt a lot during the process. Thanks to all of them.

A good mortar is necessary to bind the units. A second group of people shared the trip with me and acted as mortar, specially to distribute the stresses uniformly.

- I wish to thank the colleagues and staff of DECA: Mylene, Janill, Tai, Rubén, Celia, Razmik, Carlos, Andrés, Noemí, Rosa Olea, Clara, Loreto, Rolando, Amir, Nuria, Nikola, Pablo, and Andressa, for their happiness and for creating a nice place to work in. Many thanks go to my office partners, Edu and Cristina, for their support and long conversations.
- Special thanks go to the Team Roca & Friends. Thanks to Naveen, Irene, Daniela, Chiara and Corrado. My appreciation goes to Sara, for her pink elegance; to Camilla, for her irony; to Belén, for being the first one; to Albert, for his endless speeches; to Fernando and Laura, for bringing Alicante to Barcelona; to Maria José and Elena, for being our friends; to Francesco, for his social commitment; to Ulric, for his strength; to Bora, for his support beyond the sea. I thank Savvas for his help and guidance; I thank Nirvan for his peaceful presence and his eternal kindness; I thank Philip for his friendship. I thank Lara for being my research partner.

A single wall means nothing without proper boundary conditions. The last group of people is the ground and the place where this thesis was built on.

- I thank my whole family for their continuous love. I thank Silvia, Manolo and Irene for their visits and affection.
- I thank Sara for sharing her sister with me. Rosario and Rachid took me in their home. All this long time, they have helped us, advised us, and taken care of us. Thank you.
- Her father was a stonemason; her husband was a bricklayer able to build Catalan vaults. My grandmother Ascensión does not know anything else about masonry, but I know she is happy for me. I owe her very much.
- My parents and my sister have always supported me unconditionally. They have paid the highest price: the time I was abroad. I will compensate them soon.

All the thanks go to Yasmina. She is the force of gravity that makes everything stable.

*This page is intentionally left blank.*

# Abstract

Masonry has been used for millennia to build all sort of constructions. As a result, a significant part of the building stock around the world is made of masonry. In the need of structural assessment, structural analysis tools, as well as strength criteria proposed in building codes, require the knowledge of the mechanical properties of the materials.

However, the mechanical characterisation of masonry is still difficult and challenging, due to its composite nature and its complex mechanical behaviour. In fact, it is possible to find contradictions among standards, lack of definition for certain procedures, or even lack of standards for certain tests.

This thesis aims to contribute with the critical analysis of some of these testing procedures and provide possible improvements for a specific type of masonry. Four lines of research have been identified, which cover tests in laboratory and in situ to characterise the behaviour in compression and in shear. The specific type of masonry on which the experimental campaigns are carried out is the traditional type of brickwork that was extensively used in Barcelona during the 19th and 20th c. In spite of its relevance, this type of masonry is in need of further characterisation.

A preliminary research was necessary to find a historical-like mortar with a relatively fast hardening and low mechanical properties. The modification of hydraulic lime based commercial mortars with the addition of limestone filler is investigated. Small amounts of filler enhance the mechanical properties of the mortar. High amounts of filler reduce the mortars' strengths and make it suitable to replicate historical-like masonry in laboratory.

The first line of research on testing procedures covered the compressive characterisation of masonry on prismatic standard specimens. European and American standards differ in the type of specimen to consider, running bond walls and stack bond prisms, respectively. This work compares experimental results obtained from both types of specimen and also obtained from two types of loading, monotonic and cyclic.

The second line of research involves an experimental campaign that investigates the possibility of using 90 mm cylinders extracted from existing walls to characterise the compressive behaviour of masonry. Four examples of masonry have been investigated,

including cylinders extracted from three existing buildings of Barcelona. The results obtained with 90 mm cylinders compare well to those obtained with the well-known 150 mm cylinders.

The third line of research deals with the characterisation of the shear response of masonry in laboratory. The standard triplet specimen consisting of three units and two mortar joints present some interpretation problems related to the non-simultaneous failure of the two joints. This experimental campaign studies the possibility of using couplet specimens of only one mortar joint to determine the shear parameters. For the two types of brickwork investigated, couplets provide higher estimations of the shear parameters with respect to triplets.

The last line of research investigates the diagonal compression test, a testing procedure applicable both in situ and in laboratory for shear characterisation. First, an experimental campaign is presented. The experimental results are used to calibrate a numerical model, which is applied to investigate the actual states of stresses and to find correlating coefficients between the test results and the mechanical properties of masonry.

The combination of all the former researches provides a set of reference values for the mechanical properties of the traditional brickwork of Barcelona. Nevertheless, the scientific findings, methods, and criteria presented in this thesis, even if derived for a specific type of brickwork, may be of application for the characterisation of other types of masonry around the world.

**Keywords:** Masonry · Brickwork · Mechanical characterisation · Laboratory testing · Compression · Shear · Existing buildings · Historical constructions · Handmade bricks · Lime mortar · Barcelona

# Resum

L'obra de fàbrica ha estat utilitzada durant mil·lennis per construir tota mena d'estructures. Davant la necessitat de verificacions estructurals, les eines d'anàlisi, així com els criteris de resistència dels codis de construcció, requereixen el coneixement de les propietats mecàniques dels materials.

Malauradament, la caracterització mecànica de l'obra de fàbrica no es tasca fàcil i continua suposant un desafiament, per la seva natura composta i el seu complex comportament. De fet, és possible trobar contradiccions entre normes, manca de definició per alguns procediments i, inclús, inexistència de normes per alguns tipus de test.

Aquesta tesi aspira a contribuir a l'anàlisi crítica d'algunes d'aquestes tècniques d'assaig i proveir-ne possibles millores per a un tipus d'obra de fàbrica específic. Quatre línies de recerca s'han identificat, que abasten tests en laboratori i in situ per caracteritzar el comportament a compressió i a tallant. El tipus específic de material sobre el qual es duran a terme les campanyes experimentals és la fàbrica de maó tradicional que va ser extensament utilitzada a Barcelona durant els segles XIX i XX. Tot i la seva rellevància, aquest tipus de material continua necessitant una caracterització més detallada.

Una recerca preliminar fou necessària per trobar un morter pseudo-històric amb febles propietats mecàniques. La modificació de morters comercials de calç hidràulica amb l'addició de filler calís és investigada. Petites quantitats de filler milloren les propietats mecàniques del morter. Majors quantitats de filler redueixen les resistències del morter i el fan apropiat per replicar fàbriques de tipus històric al laboratori.

La primera línia de recerca sobre tècniques d'assaig va estudiar la caracterització a compressió amb espècimens prismàtics estàndards. Les normes americanes i europees difereixen en el tipus d'espècimen considerat, prismes apilats i petits murets, respectivament. Aquest treball compara resultats experimentals obtinguts amb els dos tipus d'espècimen i també obtinguts amb dos tipus d'aplicació de càrrega, monòtona i cíclica.

La segona línia de recerca desenvolupa una campanya experimental que investiga la possibilitat d'utilitzar cilindres de 90 mm de diàmetre extrets de murs existents per caracteritzar la resposta a compressió. Quatre exemples d'obra de fàbrica s'han investigat, incloent cilindres

extrets de tres edificis de Barcelona. Els resultats obtinguts amb els cilindres de 90 mm es comparen satisfactòriament amb els obtinguts amb els ja coneguts cilindres de 150 mm.

La tercera línia de recerca tracta la caracterització en laboratori de la resposta a tallant de l'obra de fàbrica. La tripleta estàndard formada per tres maons i dos junts de morter presenta alguns problemes d'interpretació relacionats amb la fallada no simultània dels dos junts. La campanya estudia la possibilitat d'utilitzar bipletes compostes de tan sols un junt de morter per determinar els paràmetres a tallant. Pels dos tipus de material estudiats, les bipletes proporcionen majors estimacions de les propietats a tallant que les tripletes.

L'última línia de recerca estudia el test de compressió diagonal, una tècnica aplicable in situ i al laboratori per caracteritzar el comportament a tallant. Es presenta una campanya experimental, els resultats de la qual s'utilitzen per calibrar un model numèric. Aquest s'aplica per investigar els estats de tensions reals i trobar coeficients de correlació entre els resultats del test i les propietats mecàniques de l'obra de fàbrica.

La combinació de les investigacions prèvies proporciona un conjunt de valors de referència per a les propietats mecàniques de la fàbrica de maó tradicional de Barcelona. Les conclusions científiques, mètodes i criteris presentats en aquesta tesi, tot i haver estat derivats per un tipus específic de fàbrica, poden ser d'aplicació per a la caracterització d'altres tipus de fàbrica arreu del món.

**Paraules clau:** Obra de fàbrica · Caracterització mecànica · Assaigs en laboratori ·  
Compressió · Tallant · Edificis existents · Construccions històriques · Maons de fabricació  
manual · Morter de calç · Barcelona

# Resumen

La obra de fábrica ha sido utilizada durante milenios para construir toda clase de estructuras. Ante la necesidad de verificaciones estructurales, las herramientas de análisis, así como los criterios de resistencia de los códigos de construcción, requieren el conocimiento de las propiedades mecánicas de los materiales.

Desafortunadamente, la caracterización mecánica de la obra de fábrica no es una tarea fácil y continúa suponiendo un desafío, por su naturaleza compuesta y su complejo comportamiento. De hecho, es posible encontrar contradicciones entre normas, falta de definición en algunos procedimientos o, incluso, inexistencia de normas para algunos tipos de test.

Esta tesis aspira a contribuir en el análisis crítico de algunas de estas técnicas de ensayo y proveer posibles mejoras en ellas para un tipo de obra de fábrica específico. Se han definido cuatro líneas de investigación que abarcan ensayos en laboratorio e in situ para caracterizar el comportamiento a compresión y a cortante. El tipo específico de material sobre el que se llevan a cabo las campañas experimentales es la fábrica de ladrillo tradicional que se usó extensamente en Barcelona durante los siglos XIX y XX. A pesar de su relevancia, este tipo de material continúa necesitando una caracterización más detallada.

Una investigación preliminar fue necesaria para encontrar un mortero pseudo-histórico con débiles propiedades mecánicas. La modificación de morteros comerciales de cal hidráulica con la adición de filler calizo es investigada. Cantidades pequeñas de filler mejoran las propiedades mecánicas del mortero. Mayores cantidades de filler reducen sus resistencias y lo hacen apropiado para replicar obras de fábrica de tipo histórico en el laboratorio.

La primera línea de investigación sobre técnicas de ensayo estudió la caracterización a compresión con especímenes prismáticos estandarizados. Las normas americanas y europeas difieren en el tipo de espécimen considerado, prismas apilados y pequeños muretes, respectivamente. Este trabajo compara resultados experimentales obtenidos con los dos tipos de espécimen y también obtenidos con dos tipos de aplicación de carga, monótona y cíclica.

La segunda línea de investigación gira sobre una campaña experimental que investiga la posibilidad de utilizar cilindros de 90 mm de diámetro extraídos de muros existentes para caracterizar la respuesta a compresión. Se han investigado 4 ejemplos de fábrica, incluyendo

cilindros extraídos de 3 edificios de Barcelona. Los resultados obtenidos con los cilindros de 90 mm se comparan satisfactoriamente con los obtenidos en los ya aceptados cilindros de 150 mm.

La tercera línea de investigación trata la caracterización en laboratorio de la respuesta a cortante de la obra de fábrica. La tripleta estándar formada por tres ladrillos y dos juntas de mortero presenta algunos problemas de interpretación relacionados con el fallo no simultáneo de las juntas. La campaña estudia la posibilidad de utilizar bipectas con una sola junta de mortero para determinar los parámetros a cortante. Para los dos tipos de material estudiados, las bipectas proporcionan mayores estimaciones de las propiedades a cortante que las tripletas.

La última línea de investigación estudia el ensayo de compresión diagonal, una aplicable in situ y en laboratorio para caracterizar el comportamiento a cortante. Se presenta una campaña experimental cuyos resultados se utilizan para calibrar un modelo numérico. Este se aplica para investigar los estados reales de tensiones y encontrar coeficientes de correlación entre los resultados del ensayo y las propiedades mecánicas de la obra de fábrica.

La combinación de las investigaciones previas proporciona un conjunto de valores de referencia para las propiedades mecánicas de la fábrica de ladrillo tradicional de Barcelona. Las conclusiones científicas, métodos y criterios presentados en esta tesis, aun habiendo sido derivados para un tipo específico de fábrica, pueden ser aplicados para la caracterización de otros tipos de fábrica en otras áreas geográficas.

**Palabras clave:** Obra de fábrica · Caracterización mecánica · Ensayos en laboratorio · Compresión · Cortante · Edificios existentes · Construcciones históricas · Ladrillos de fabricación manual · Mortero de cal · Barcelona

# Contents

Abstract .....	xiii
Resum .....	xv
Resumen .....	xvii
List of Figures .....	xxi
List of Tables .....	xxvii
1.Introduction .....	1
1.1. Motivation .....	3
1.2. Scope .....	5
1.3. Outline of the thesis - Compendium of publications .....	6
2.Literature review .....	11
2.1. Introduction .....	13
2.1.1. Overview .....	13
2.1.2. Mechanical behaviour of masonry .....	14
2.2. Mechanical characterisation needs for the structural assessment of masonry structures .....	20
2.2.1. Modelling strategies for structural analysis .....	21
2.2.2. Structural assessment in building codes .....	30
2.2.3. Summary of characterisation needs .....	35
2.3. Mechanical characterisation procedures .....	37
2.3.1. General aspects .....	37
2.3.2. Characterisation of masonry in compression .....	41
2.3.3. Characterisation of masonry in shear .....	50
2.3.4. Summary of characterisation procedures .....	59
2.4. Replication of historical-like masonry in laboratory .....	60
2.4.1. General aspects .....	60
2.4.2. Structural masonry in the city of Barcelona .....	62
2.5. Summary .....	68
3.Objectives and methodology .....	71
3.1. Objectives .....	73
3.2. Methodology .....	74
4.Materials .....	77
4.1. Introduction .....	79
4.2. Units .....	79
4.2.1. Units used to replicate historical-like brickwork .....	79

4.2.2.	Other units .....	81
4.3.	Mortars.....	82
4.3.1.	Mortar used to replicate historical-like brickwork.....	82
4.3.2.	Other mortars.....	83
4.4.	Additional materials .....	84
4.5.	Paper I – Influence of recycled limestone filler additions on the mechanical behaviour of commercial premixed hydraulic lime mortars.....	87
5.	Characterisation of masonry in compression.....	113
5.1.	Introduction.....	115
5.2.	Paper II – Monotonic and cyclic testing of clay brick and lime mortar masonry in compression.....	117
5.3.	Paper III – Experimental analysis of the size effect on the compressive behaviour of cylindrical samples core-drilled from existing brick masonry .....	149
5.4.	Discussion.....	187
6.	Characterisation of masonry in shear.....	193
6.1.	Introduction.....	195
6.2.	Paper IV – Experimental comparison of two testing setups for characterising the shear mechanical properties of masonry .....	197
6.3.	Paper V – Experimental and numerical insights on the diagonal compression test for the shear characterisation of masonry.....	227
6.4.	Discussion.....	271
7.	Conclusions .....	275
7.1.	Summary.....	277
7.2.	Conclusions.....	278
7.3.	Main contributions .....	287
7.4.	Suggestions for future work.....	289
	References .....	293

# List of Figures

Figure 1 Outline of the thesis. ....	8
Figure 2 Examples of different masonry typologies. a) Rubble stone masonry, b) ashlar stone masonry with dry joints, c) clay brick masonry, d) concrete block masonry. ....	14
Figure 3 Examples of stress vs. strain curves for mortar, brick and masonry prisms under uniaxial compression (from Binda et al. [5]). ....	16
Figure 4 Modes of failure for biaxial tests (examples on brick masonry by Dhanasekar et al. [8]). ....	17
Figure 5 Failure surface for biaxial tests in terms of normal stresses and angle of orientation of the bed joints planes (results for brick masonry obtained by Dhanasekar et al. [8]). ....	17
Figure 6 a) Limit domain and b) failure modes of a masonry pier under combined vertical and horizontal loading (from Calderini et al. [9]). ....	19
Figure 7 Examples of geometry-based models. a) Andreu et al. [17], b) Block et al. [18], c) Block and Lachauer [19], d) Chiozzi et al. [20]. ....	23
Figure 8 Examples of continuum models. a) Valente and Milani [21], b) Betti et al. [22], c) Elyamani et al. [23], d) Pelà et al. [24]. ....	24
Figure 9 Examples of block-based models. a) Interface-element-based approach by Lourenço and Rots [29], b) Contact-based approach by Pulatsu et al. [32] c) Textured continuum-based approach by Petracca et al. [31]. ....	26
Figure 10 Examples of macroelement models. a) Lagomarsino et al. [35], b) Calì et al. [36], c) Siano et al. [37], d) Rinaldin et al. [38] ....	28
Figure 11 a) and b) Examples of compressive tests on stack bond prisms, from Drougkas et al. [75] and Pelà et al. [83], respectively. c) and d) Examples of compressive tests on wallettes, from Parisi et al. [84] and Gumaste et al. [79], respectively. ....	43
Figure 12 a), b) and c) Examples of tests on 150 mm cylinders, from Brencich and Sterpi [102] , Matysek [104], and Pelà et al. [110] respectively. D) Example of test on 100 mm cylinders, from Sassoni et al. [107]. ....	45
Figure 13 a) Scheme of double flat jack test, from Jurina [98]. b) Application example on existing building by Binda and Tiraboschi [121]. ....	49
Figure 14 a) Example of test on standard triplet specimen, from Pelà et al. [145], b) Example of complex setup for testing couplet specimens, from Van der Pluijm [144]. ....	52
Figure 15 a) Example of in situ shove test from Ferretti et al. [155]. b) Scheme and example of Brazilian test on cylinders from Marastoni et al. [151]. c) Example of test on cylinder from Jafari et al. [154]. ....	54

Figure 16 Examples of diagonal compression tests. a) Test in vertical position by Parisi et al. [169] b) and c) In situ tests, from Borri et al. [164] and Ferretti et al. [155], respectively. d) Test on a strengthened wall by Mahmood and Ingham [165]. .....56

Figure 17 a) Axonometry by Paricio [197] of a typical rectangular building of the Eixample district in Barcelona. b), c) and d) Singular examples of industrial facilities of Barcelona made of brickwork: Fabra i Coats factory, Casaramona factory, and Can Batlló complex, respectively. ....65

Figure I.1 XRD diffractograms in the 5 – 60° 2θ angular region of the anhydrous premix. a) Fraction passing the 0.063 mm sieve, b) fraction retained in the 0.063 mm. ....94

Figure I.2 Determination of the particle size distribution chart of the premix aggregates. ....95

Figure I.3 Polarized light microscope images of limestone filler particles dispersed in oil. Magnification 100X. Scale 50 μm. ....96

Figure I.4 XRD diffractogram in the 5 – 60° 2θ angular region of limestone filler.....96

Figure I.5 Graphical representation of mortars proportioning, a) by percentage of total powder volume and b) by percentage of total powder weight. ....97

Figure I.6 Mortar testing setup. A) Three-point bending and b) compression tests. .... 100

Figure I.7 Flexural strength of mortars ( $f_{flex}$ ). Bars represent the average values at 14, 28 and 56 days for each mortar. Whiskers indicate the average values ± 1 standard deviation. .... 102

Figure I.8 Compressive strength of mortars ( $f_{comp}$ ). Bars represent the average values at 14, 28 and 56 days for each mortar. Whiskers indicate the average values ± 1 standard deviation. .... 102

Figure I.9 Ratio between compressive ( $f_{comp}$ ) and flexural strength ( $f_{flex}$ ) of mortars for each filler content at 14, 28 and 56 days. .... 105

Figure I.10 Correlation between compressive ( $f_{comp}$ ) and flexural strength ( $f_{flex}$ ) by combining the available data from all types of mortar and ages. .... 105

Figure I.11 Strength evolution of mortar MD with age. The dashed lines indicate the average value of the strengths considering all the individual results after 28 days. a) Flexural strength, b) compressive strength..... 107

Figure I.12 Stereo microscope images of hardened mortar MD joint sections after 56 days. Magnification 10X. .... 108

Figure I.13 a) XRD diffractogram in the 5 – 60° 2θ angular region of hardened mortar MD at 56 days after crushing and mechanical sieving; b) comparison of XRD diffractograms in the 15 – 55° 2θ angular region of anhydrous premix (see Figure I.1a) and hardened mortar MD at 56 days. .... 109

Figure II.1 Masonry specimens for compression strength tests according to a) EN 1052-1 [68], b) ASTM C1314 [66]. .... 120

Figure II. 2 Masonry samples, average dimensions. a) Running bond walls, b) Stack bond prisms. Common average thickness $t_s = 148$ mm. ....	125
Figure II.3 Experimental setups: a) Stack bond prisms, b) Running bond walls. ....	126
Figure II.4 Generic load (kN) vs. time (min) curve describing the adopted loading history. Load levels: A - 5% of an estimated maximum load ( $P_o$ ). B - 30% of an estimated maximum load ( $P_o$ ). C - Actual maximum load registered during the test ( $P_{max}$ ). D and F - Loads corresponding to 5% and 30% of the actual maximum load ( $P_{max}$ ), used as limits to compute the elastic modulus on the stress-strain curves. ....	128
Figure II.5 Stress vs. strain experimental curves for running bond walls. a) Detail of the three loading/unloading cycles, b) Full curves until failure. ....	130
Figure II.6 Failure of running bond walls. a) Crack pattern at peak load, b) State at the end of the test, c) Dismantled specimen. ....	131
Figure II.7 Stress vs. strain experimental curves of the stack bond prisms with monotonic loading. a) Detail of the three loading/unloading cycles and beginning of the second stage, b) Full curves until failure. ....	132
Figure II.8 Stack bond prisms after failure. a) Front view, b) Lateral view, c) Dismantled specimen. ....	132
Figure II.9 Stress vs. strain experimental curves of the stack bond prisms with cyclic loading until failure. a) SBP5, b) SBP6, c) SBP7. ....	133
Figure II.10 Normalized elastic modulus ( $E_{c,i}/E_{c,max}$ ) of the reloading branches vs. normalized compressive strain ( $\varepsilon_{r,i}/\varepsilon_p$ ), for the stack bond prisms tested under cyclic loading. ....	134
Figure II.11 Experimental (dashed) and analytical (solid) stress-strain curves for specimen SBP5. a) Analytical model by Facconi et al. [86], b) Analytical model by Sima et al. [291], with new calibration. ....	140
Figure II.12 Experimental (dashed) and analytical (solid) stress-strain curves for specimen SBP6. a) Analytical model by Facconi et al. [86], b) Analytical model by Sima et al. [291], with new calibration. ....	141
Figure II.13 New relationships for the model proposed by Sima et al. [291], obtained by curve fitting of the present work's experimental data. Notation according to [291]. a) Relationship between unloading strain – plastic strain ratio ( $r$ ) and the unloading damage ( $\delta_{un}$ ), b) Relationship between the final unloading stiffness – initial stiffness ratio ( $R$ ) and the unloading damage ( $\delta_{un}$ ), c) Relationship between the reloading damage ( $\delta_{re}$ ) and the unloading damage ( $\delta_{un}$ ). In the above, $r_c^2$ is the coefficient of determination R squared. ....	141
Figure III.1 a) Masonry wall built in the laboratory for the campaign “MA”, and b) core drilling of 150 mm and 90 mm cylindrical samples. ....	157

Figure III.2 Front and lateral views of regularized core samples of campaign “MA”: a) 150 mm cylinder and b) 90 mm cylinder. ....	157
Figure III.3 Experimental setups of campaign “MA” for a) 150 mm cylinder and b) 90 mm cylinder. ....	159
Figure III.4 Compressive stress-strain curves of core samples of campaign “MA”: a) 150 mm cylinders and b) 90 mm cylinders.....	160
Figure III.5 Typical failure of 150 mm cylinders in compression tests of campaign “MA”: a) appearance of the first crack at one side, b) further opening of the first crack and development of a second crack at the other side, and c) final sandglass failure.....	161
Figure III.6 Typical failure of 90 mm cylinders in compression tests of campaign “MA”: a) vertical cracks crossing the core from the top to the bottom mortar caps, and b) final sandglass failure. ....	162
Figure III.7 a) View of the building of the “Fabra i Coats” industrial complex in Barcelona studied in campaign “MB”, b) main façade of the residential building at Rambla de Catalunya Street in Barcelona studied in campaign “MC”, c) façade of the housing complex in the district of Ciutat Vella in Barcelona studied in campaign “MD”.....	165
Figure III.8 a) Façade wall investigated in “Fabra i Coats” factory and b) in-situ core drilling for campaign “MB”, c) inner wall of the analysed building in Rambla Catalunya street and d) in-situ core drilling for campaign “MC”, e) inner wall of the building in Ciutat Vella and f) in-situ core drilling for campaign “MD”.....	168
Figure III.9 Compressive stress-strain curves of campaign “MB”: a) 150 mm samples and b) 90 mm samples.....	169
Figure III.10 Compressive stress-strain curves of campaign “MC”: a) 150 mm samples and b) 90 mm samples.....	170
Figure III.11 Compressive stress-strain curves of campaign “MD”: a) 150 mm samples and b) 90 mm samples.....	171
Figure III.12 Modes of failure in the 150 mm (left) and 90 mm (right) core samples extracted from existing masonry buildings: a) and b) campaign “MB”, c) and d) campaign “MC”, e) and f) campaign “MD”. ....	172
Figure III.13 Comparison of compressive strengths ( $f_c$ ) results obtained for 150 mm and 90 mm cylinders for the four types of masonry investigated. ....	177
Figure III.14 Comparison of Young’s moduli ( $E$ ) results obtained for 150 mm and 90 mm cylinders for the four types of masonry investigated. ....	177
Figure III.15 Size effect on a) compressive strength and b) Young’s modulus obtained from 150 mm and 90 mm cylinders for the four types of masonry investigated in this research. ....	180
Figure IV.1 Geometric definition of the masonry specimens.....	204

Figure IV.2 Testing arrangements for a) triplets and b) couplets. ....	205
Figure IV.3 LVDTs position for each specimen type. Red squared dots indicate support of the LVDT, blue triangular dots indicate support of the contrasting element. See Figure IV.2 for an actual picture of the vertical LVDTs. ....	206
Figure IV.4 Shear strength $\tau_u$ vs. normal stress $\sigma$ plots for a) TL, b) CL, c) TC, and d) CC specimens. Red lines represent the regression corresponding to the Mohr-Coulomb failure criterion, with indication of the cohesion $c$ , the angle of friction $\phi$ and the coefficient of determination $R^2$ . ....	209
Figure IV.5 Curves for masonry made of hydraulic lime mortar and handmade bricks. a) Shear stress vs. shear displacement plot for triplets. b) Normal displacement vs. shear displacement plot for triplets. c) Shear stress vs. shear displacement plot for couplets. d) Normal displacement vs. shear displacement plot for couplets. ....	210
Figure IV.6 Curves for masonry made of Portland cement mortar and extruded bricks. a) Shear stress vs. shear displacement plot for triplets. b) Normal displacement vs. shear displacement plot for triplets. c) Shear stress vs. shear displacement plot for couplets. d) Normal displacement vs. shear displacement plot for couplets. ....	211
Figure IV.7 Schematic shear stress $\tau$ vs. displacement $\delta_s$ curves that show the corresponding areas for the two approaches to calculate second mode fracture energy: a) Cohesive fracture energy $G_f^{II}$ , b) Cohesive-frictional fracture energy taking into account the frictional dissipation up to a displacement corresponding to a 2.5% shear strain $G_f^{II}_{2.5\%}$ . ....	213
Figure IV.8 Shear secant modulus $G$ vs. shear strain $\gamma$ plots for a) TL, b) CL, c) TC, and d) CC specimens. ....	214
Figure IV.9 Comparative plots for different tested specimens of a) residual shear strength $\tau_{res}$ , b) strength degradation ratio SDR, c) cohesive fracture energy $G_f^{II}$ , and d) cohesive-frictional fracture energy $G_f^{II}_{2.5\%}$ . ....	222
Figure V.1 a) Coordinate system in the diagonal compressed wall. b) Mohr's circle representations of the stresses at the centre of the panel according to ASTM's and c) Frocht's approaches. ....	233
Figure V.2 Setup of the diagonal compression test. ....	239
Figure V.3 a) to e) Crack patterns at the end of the test for the five specimens. f) Pattern detail of wall URM_2 with cracks involving both bricks and mortar joints. ....	242
Figure V.4 a) Boundary conditions on the numerical simulation and position of the virtual LVDT for comparison. b) Discretized domain used for the macromodelling approach. ....	248
Figure V.5 Comparison between the load-strain curves of the experimental tests and the numerical analyses. No experimental curve is given for specimen URM_2 due to invalid readings of the LVDTs during the test. ....	252
Figure V.6 Contour of the maximum principal strains, $\epsilon_I$ , after the peak load. ....	252

Figure V.7 Contour of stresses in the linear range, expressed in terms of normalized stress  $\alpha$ . a) Normal stresses  $\sigma_x$  along X-axis [ $\sigma_y$  are not shown due to the problem's symmetry], b) shear stresses  $\tau_{xy}$ , and c) maximum principal stresses  $\sigma_I$ .....255

Figure V.8 Distribution of the maximum principal stresses along the axes of symmetry of the panel. Stresses are normalized and expressed in terms of the coefficient  $\alpha_I$ . The X-axis represents normalized lengths. The centre of the panel corresponds to the coordinate 0.5. ....256

Figure V.9 a) Evolution of stresses and b) relevant normalized values  $\square$  in the centre of the panel with increasing load. The load is normalized with respect to the maximum load attained during the analysis. ....259

Figure V.10 Evolution of tensile damage contour for different levels of imposed displacement  $\delta$ . The tensile damage index  $d^+$  ranges from 0 (intact material) to 1 (completely damaged material). a)  $\delta = 0.198$  mm,  $P = 0.82P_{max}$ , b)  $\delta = 0.216$  mm,  $P = 0.89P_{max}$ , c)  $\delta = 0.230$  mm,  $P = 0.95P_{max}$ , d)  $\delta = 0.244$  mm,  $P = P_{max}$ , e)  $\delta = 0.247$  mm,  $P = 0.92P_{max}$ .....260

Figure V.11 Sensitivity of the model to variations of different parameters, in terms of load – strain curves and coefficient  $\alpha_{I,calc}$ . a) Variation of input Young's modulus,  $E$ . b) Variation of input tensile strength,  $f_t$ . c) Variation of input tensile fracture energy,  $G_{ft}$ . d) Variation of parameter  $\kappa 1$ . ....263

Figure V.12 Effect of the panel side length on the coefficient  $\alpha_{I,calc}$ . Triangle dot indicates the value corresponding to the side length recommended in ASTM E519 [355] (1200 mm).....265

Figure V.13 Effect of the loading cap depth on the coefficient  $\alpha_{I,calc}$ . The X-axis indicates the loading cap depth normalized with respect to the panel side length. The triangle dot indicates the value corresponding to the ratio recommended in ASTM E519 [355] ( $1/8^{th}$ ).....266

# List of Tables

Table 1 Inventory of mechanical material properties used in different modelling strategies. Grey background indicates properties that are typically used in the corresponding strategy. Stripped background stands for properties that could be used within that strategy. <sub>HOM</sub> indicates that the property is used through a homogenization technique. ....	29
Table 2 Mechanical properties involved in building codes strength criteria. ....	35
Table 3 Main encountered needs for the different types of test investigated, classified by mechanical property and by test feature. Last column indicates the corresponding standard if applicable. ....	59
Table 4 Results obtained by Bergós in the laboratory of the Universitat Industrial de Barcelona before 1950 [189]. ....	67
Table 5 Summary of mechanical properties used by different authors in the seismic assessment of Barcelona buildings. ....	68
Table I.1 Mortars definition in terms of total powder volume by replaced by limestone filler. ....	97
Table I.2 Mortars proportioning by volume and by weight, and flow measured according to EN 1015-3 [250]. ....	98
Table I.3 Flexural strength of mortars ( $f_{flex}$ ). Average values at 14, 28 and 56 days for each mortar. Coefficients of variation shown in brackets. ....	101
Table I.4 Compressive strength of mortars ( $f_{comp}$ ). Average values at 14, 28 and 56 days for each mortar. Coefficients of variation shown in brackets. ....	102
Table II.1 Mechanical parameters of bricks ....	123
Table II.2 Mechanical parameters of mortar ....	124
Table II.3 Compressive strength, stiffness and strain at peak stress of running bond walls. ....	130
Table II.4 Compressive results of stack bond prisms. ....	132
Table II.5 Experimental and analytical compressive strength values (MPa). The coefficient of variation is indicated in brackets. ....	137
Table II.6 Experimental and analytical elastic modulus values (MPa). ....	138
Table II.7 Model input data for comparison with the experimental results of specimens SBP5 and SBP6. ....	140
Table III. 1 Experimental compressive strength of bricks ( $f_b$ ) and mortar joints ( $f_{m, DPT}$ ) in campaign “MA” executed on masonry built in the laboratory. ....	156
Table III.2 Compressive strength ( $f_c$ ) and Young’s modulus ( $E$ ) of 150 mm and 90 mm masonry cylinders in campaign “MA”. ....	162

Table III.3 Experimental compressive strengths of bricks ( $f_b$ ) and mortar ( $f_{m\_DPT}$ ) of campaigns “MB”, “MC” and “MD”.....	166
Table III.4 Compressive strengths ( $f_c$ ) and Young’s moduli ( $E$ ) of 150 mm and 90 mm masonry cylinders of campaign “MB”.....	173
Table III.5 Compressive strengths ( $f_c$ ) and Young’s moduli ( $E$ ) of 150 mm and 90 mm masonry cylinders of campaign “MC”.....	173
Table III.6 Compressive strengths ( $f_c$ ) and Young’s moduli ( $E$ ) of 150 mm and 90 mm masonry cylinders of campaign “MD”.....	173
Table III.7 Experimental estimation of masonry compressive strength ( $f_c^*$ ) vs. predictions from expressions of ACI [106] ( $f_{c,ACI}$ ) and EC6 [56] ( $f_{c,EC6}$ ). $\Delta$ % expresses the difference in percentage of the predictions with respect to the experimental estimation. ....	182
Table IV.1 Mechanical strengths of masonry components. Number of specimens and coefficients of variation are shown in brackets. ....	203
Table IV.2 List of tested specimens and applied normal stresses.....	208
Table IV.3 Ultimate shear strength $\tau_u$ , residual shear strength $\tau_{res}$ , strength degradation ratio $SDR$ , cohesive fracture energy $G_f^H$ and cohesive-frictional fracture energy $G_{f^H_{-2.5\%}}$ for all specimens and precompression levels. The average values for each precompression level of $SDR$ and $G_{f^H_{-2.5\%}}$ are indicated in square brackets. ....	213
Table IV.4 Cohesion ( $c$ ) and friction ( $\phi$ ) for different types of masonry available in the literature, with compressive strengths of mortar $f_m$ and of units $f_b$ .....	223
Table IV.5 Comparison of experimental results with design standard values.....	225
Table V.1 Mechanical properties of constituent materials (brick and mortar) and of masonry composite. ....	236
Table V.2 Experimental results. Maximum load, tensile strength and shear modulus of each specimen. ....	242
Table V.3 Experimental data-sets for numerical calibration. ....	243
Table V.4 Calibration of the numerical model with experimental results: Input data for the numerical analyses of the three data-sets, and comparison between experimental and numerical maximum loads. ....	251
Table V.5 Values of the parameters investigated in the sensitivity analyses. ....	262
Table V.6 Validation analyses of additional experimental campaigns from literature. Comparison between experimental and numerically predicted maximum load.....	268

**1**

# **Introduction**

*This page is intentionally left blank.*

## 1.1. Motivation

Masonry is a form of construction consisting of the arrangement of units that are laid dry or bound together by mortar. Among others, bricks, cut stones or concrete blocks may act as units, while mud, lime, gypsum or cement may act as binder. This great variety of possible components, some of which are easily available in nature, together with the simplicity of the technique, have motivated the extensive use of masonry from antiquity until today for building structural elements such as walls, columns, arches or vaults. Nowadays, a significant part of the existing building stock worldwide is made of load-bearing masonry members. In many instances, these buildings have a high cultural or architectural value.

The structural analysis of masonry constructions may be required in different situations. In the case of existing buildings, a structural evaluation may be necessary to design remedial measures after a seismic event or to address progressive damage or material decay experienced over the years or centuries. Sometimes, buildings need to be assessed for adaptive reuse projects or to ensure conformity with relevant new regulations. Preventive analyses of the actual vulnerability of constructions might be recommended as well, especially on earthquake prone areas. In addition, masonry is still the primary construction technique in many countries around the world and new buildings need to be properly designed.

At present, engineers and architects have at their disposal a wide and diverse collection of methods to carry out the assessment of masonry structures. This abundance of resources contrasts with the very limited means available at the times when most of these structures were built. For millennia, tradition and imitation were the only tools for designing masonry buildings. The classical architectural treatises from Renaissance to 19th century only included suggestions on good building practices and rules of thumb based mainly on proportionality. Some of these

rules were mere generalizations of empirical observations. Specifications based on a scientific approach did not appear until the first half of the 20th century for modern materials such as steel or concrete, while reports and standards devoted to masonry started to be published after the 1950s and were incorporated to modern building codes from 1970 onwards. In the case of existing masonry structures, recommendations were not specifically considered until very recently. From the 1980s onwards, an important and sustained research effort, supported by the increasing capabilities of computers, has provided powerful tools for the structural analysis of masonry, based on different approaches and considering different levels of detail.

Nevertheless, most of the available analysis methods rely on previous knowledge of the mechanical properties of masonry. Given its composite nature, as a material constituted by units and mortar, masonry presents a very complex mechanical behaviour that depends on the individual properties of the components, the interaction between them, their relative dimensions and arrangement, and the loading conditions. In consequence, its characterisation faces two major issues in the selection of a representative specimen and in the application of proper boundary conditions. When dealing with historical constructions, these difficulties increase as damage and impact on the structure should be reduced to a minimum in order to preserve its intrinsic value.

International and national organizations such as the American Society for Testing and Materials – ASTM-, the European Committee for Standardization – CEN- or the International Union of Laboratories and Experts in Construction Materials, Systems and Structures – RILEM-, among others, have issued and adopted standards and recommendations that deal with testing procedures of masonry. Nevertheless, and not surprisingly given the complexity of the subject, the current standards are not exempt of criticism. As a matter of fact, examples can be found of contradictions between standards, absence of specifications for certain properties, or

procedures that would need to be better detailed or clarified. The determination of the compressive strength, which is the single most important property of masonry, stands as a paradigmatic example: the choice of the testing specimen – small running bond wall or stack bond prism- would depend on the standard being applied.

These inconsistencies may entail difficulties for the common practitioner. Additionally, the lack of unified or precise criteria for certain aspects may hinder the necessary comparison between results from different researchers. The ultimate goal of this thesis is to help in the improvement of the characterisation procedures of masonry. Any contribution from research and academia could be incorporated into new or updated versions of the standards and codes. Eventually, the collective research effort will result in better designs and in more respectful interventions while guaranteeing the structural safety of new and existing buildings.

## **1.2. Scope**

The scope of this thesis is the critical analysis of the current procedures for the characterisation of masonry, and the contribution with possible improvements applicable to a specific type of masonry.

The following four criteria narrowed the scope of the thesis to adapt it to the limited availability of time and material resources:

- Delimit the selection of the testing procedures to be analysed to those related with the most important mechanical properties involved in the assessment and design of masonry structures. Set the focus of the thesis on the properties of masonry as a composite material. The detailed investigation of procedures required for the characterisation of components (units or mortar) is beyond the scope of this work.
- Systematically keep in mind applications to historical and existing constructions.

- Delimit experimental investigations to tests on a single type of masonry. Take advantage of the experimental campaigns to entirely characterise a type of material representative of traditional masonry assemblages. The traditional brickwork extensively used in the city of Barcelona during the 19<sup>th</sup> c. and the first half of the 20<sup>th</sup> c. has been selected.
- Prioritise the preparation of publications to increase the dissemination of the findings. The next section explains how this criterion has influenced the outline of this work.

The specific scientific objectives and the methodology of the thesis are presented in Chapter 3, based on the conclusions provided by the literature review presented in Chapter 2.

### **1.3. Outline of the thesis - Compendium of publications**

In agreement with the possibilities offered by the Universitat Politècnica de Catalunya, this doctoral thesis is presented as a compendium of publications. All of them are related to masonry characterisation and are published in a journal that belongs to the category Construction & Building Technology in Journal Citation Reports (JCR), classified within the first quartile (Q1) as required by the specific regulations of the Doctoral School.

The compendium comprises the following three papers:

- **Paper I:** J. Segura, D. Aponte, L. Pelà, P. Roca, Influence of recycled limestone filler additions on the mechanical behaviour of commercial premixed hydraulic lime based mortars, *Constr. Build. Mater.* 238 (2020), <https://doi.org/10.1016/j.conbuildmat.2019.117722>.

- **Paper II:** J. Segura, L. Pelà, P. Roca, Monotonic and cyclic testing of clay brick and lime mortar masonry in compression, *Constr. Build. Mater.* 193 (2018) 453-466, <https://doi.org/10.1016/j.conbuildmat.2018.10.198>.
- **Paper III:** J. Segura, L. Pelà, P. Roca, A. Cabané, Experimental analysis of the size effect on the compressive behaviour of cylindrical samples core-drilled from existing brick masonry, *Constr. Build. Mater.* 228 (2019), <https://doi.org/10.1016/j.conbuildmat.2019.116759>.

Additionally, two more papers have been prepared and are incorporated into this document.

On the date of submission of the thesis, these two last manuscripts are still under review:

- **Paper IV:** J. Segura, E. Bernat, V. Mendizábal, L. Pelà, P. Roca, L. Gil, Experimental comparison of two testing setups for characterising the shear mechanical properties of masonry. *Under review*.
- **Paper V:** J. Segura, L. Pelà, S. Saloustros, P. Roca, Experimental and numerical insights on the diagonal compression test for the shear characterisation of masonry. *Under review*.

All together, the five papers conform a corpus of research consistent with the thesis' scope.

The present document has been elaborated to create a coherent and continuous framework for the five papers to better expose the contributions of this work. Figure 1 shows the outline of the thesis. From now on, papers will be referred to with the numbering given above.

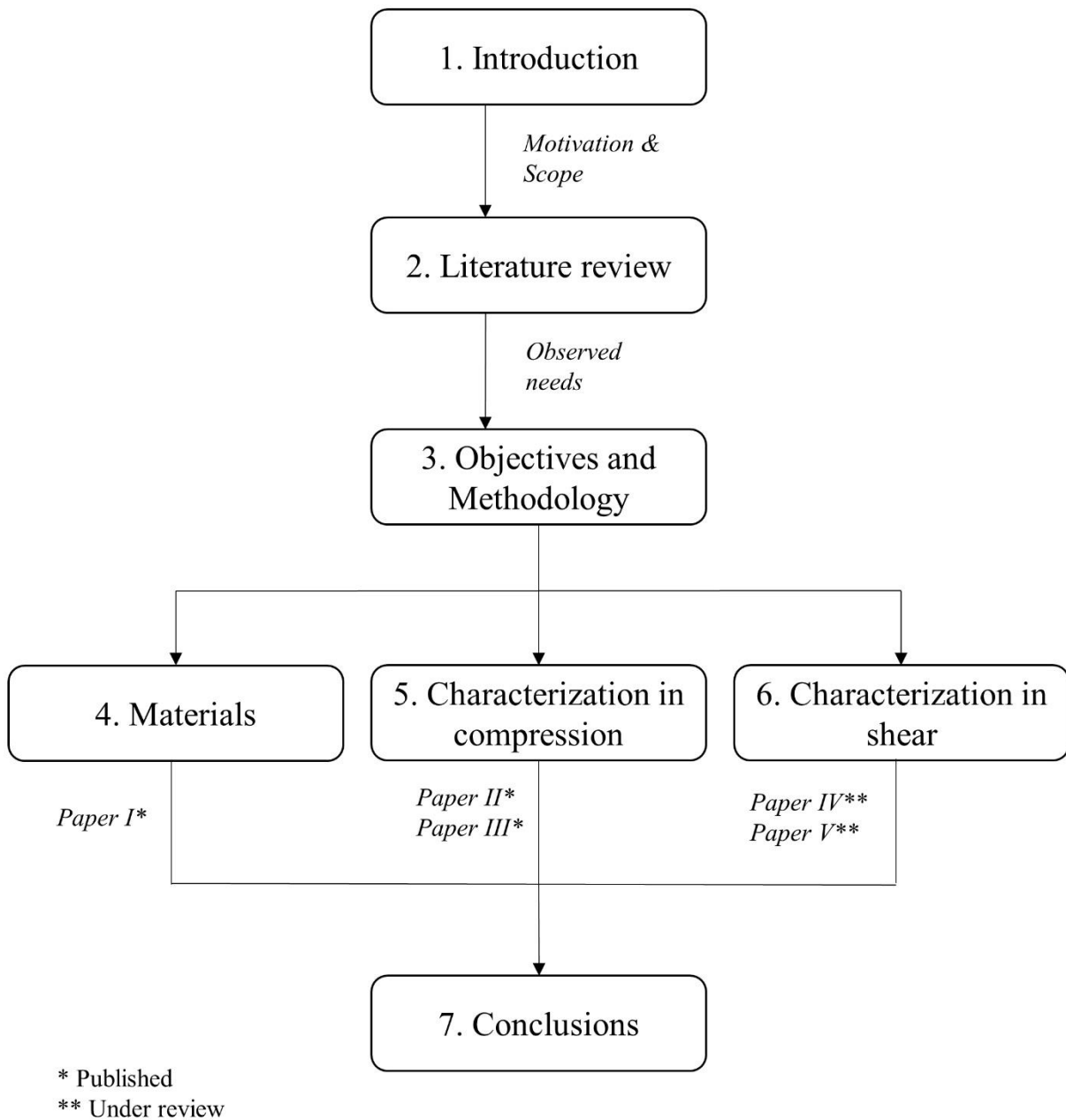


**Figure 1** Outline of the thesis.

The document is composed by seven chapters. Papers are reproduced in its integrity as subchapters within Chapters 4, 5 and 6.

Chapter 2 explores the current state of the art in relation with the characterisation of masonry. This chapter intends to narrow the scope of the thesis' aim and identify the needs for research. The chapter is divided in three main parts. The first part deals with the review of different available analysis methods and building codes, with the goal of identifying which are

the most relevant mechanical properties for structural analysis and assessment of masonry constructions. The second section offers an overview of the available characterisation procedures for the aforementioned mechanical properties. The needs presented in this section defined the main lines of this research. This second part delves into different aspects: the general difficulties and challenges associated with masonry characterisation, the existing procedures to determine the mechanical properties in compression, and the existing procedures to determine the mechanical properties in shear. Both laboratory and in situ approaches were considered in all cases. The third and final section of Chapter 2 aims to establish the type of masonry to be used for the experimental investigations. It was found that clay brick masonry made of lime mortar is one of the prevailing masonry typologies around the world. Particularly, this type of construction is the base for many buildings in the city of Barcelona, and is currently in need of better characterisation. The section also includes a short discussion on replicating historical-like materials in the laboratory. Overall, Chapter 2 presents a brief literature review that sets the context for the research, given that each of the papers includes a distinct introduction and state of the art.

Chapter 3 develops the scope of the thesis in accordance with the needs observed in Chapter 2. It describes the broad subjects addressed within the thesis and details the specific objectives pursued in each paper. The general methodology is also described.

Chapter 4 presents the materials used during the whole research to replicate a traditional form of brickwork. These materials are handmade clay bricks specially selected from a local manufacturer and a hydraulic lime based mortar whose design motivated the first paper of the compendium. Paper I is included as a section in the chapter and investigates the influence of limestone filler additions on the mechanical behaviour of hydraulic lime mortars. The chapter also mentions all the other materials that appear along the thesis.

Chapters 5 and 6 conform to the core of the thesis as they present the investigation on the characterisation procedures. Chapter 5 is devoted to the determination of mechanical properties in compression. After an introduction, the chapter includes Paper II and Paper III of the compendium. Paper II deals with the characterisation of masonry in laboratory with standard specimens. It investigates the influence of the specimen types and provides data for both monotonic and cyclic loading. Paper III delves in a characterisation technique specific for in situ inspections, which consists of extracting cylindrical cores from existing walls and testing them in a laboratory. This research explores the use of a new proposed specimen which is smaller than the standard one. The chapter includes a short discussion that compares the results from both papers.

Chapter 6 follows a parallel outline to that of Chapter 5 but devoted to the estimation of mechanical properties in shear. Besides an introduction and a discussion, this chapter includes Paper IV and Paper V. Paper IV covers the determination of shear properties of bed joints in a laboratory setting. It compares the standard triplet test with a proposed specimen consisting of only one joint. Paper V tackles the estimation of the shear strength from a different approach, by means of the diagonal compression test which can be applied in laboratory or in situ. The paper deals with the controversy that exists around the interpretation of this test.

Finally, Chapter 7 serves to summarize and unify the conclusions drawn in the preceding chapters, to highlight the main contributions, and to give suggestions for future work.

**2**

## **Literature review**

*This page is intentionally left blank.*

## 2.1. Introduction

### 2.1.1. Overview

The mechanical characterisation of a material refers to the different procedures that provide information on properties such as strengths or elastic parameters, which are required to carry out structural analyses and evaluate the structural performance and safety of a building. In the case of masonry<sup>1</sup>, the mechanical characterisation is a complex, non-univocal and still challenging subject that covers a great variety of issues. The literature review presented in this chapter aims to narrow the scope and define the lines of research and objectives of the thesis. In the last years, many authors have devoted their efforts to compose complete state-of-the-art summaries on these issues. Given that each of the papers included in the subsequent chapters incorporate a particular state of the art, the perspectives presented herein are short reviews on specific topics that aim to delineate the research context.

The following subsection 2.1.2. briefly introduces the mechanical behaviour of masonry, because its particular features have influence on the rest of the subjects addressed within the chapter, which contains three main sections. Section 2.2 answers what is a mechanical characterisation needed for and which are the main mechanical properties that require to be characterised. It is a purpose-oriented section that links this research with the real practice of engineers and architects. Section 2.3 delves into how the former mechanical properties are characterised. The section offers an overview on the different laboratory and in situ procedures available for masonry, and highlights possible areas of improvement that will be explored

---

<sup>1</sup> Masonry has been defined in Section 1.1 as a building technique. Nevertheless, for the sake of concision, it is common practice in the engineering field to use the term *masonry* also as a metonymy of the composite material made of units and mortar. This common practice is also applied in this work and masonry may refer to both the building technique and the composite material.

within the thesis. Section 2.4 aims to define which materials combination will be used to carry out the experimental investigations. As stated in the global aim of Section 1.2, this work intends to take advantage of the planned research to fully characterise one type of masonry. A last section, 2.5., summarizes the former findings.

### 2.1.2. Mechanical behaviour of masonry

Masonry is a composite material that results from the arrangement of units that are bound together with mortar or laid dry. Figure 2 displays some examples of different combinations of constituents that conform different masonry typologies. Despite this heterogeneity and the wide variety of possible combinations, masonry has some common features as a material.

As a consequence of its composite nature, masonry presents a very complex mechanical behaviour [1,2], which is influenced by the individual properties of the units and the mortar, their interaction, their relative dimensions, the arrangement of the pieces, and the direction and magnitude of loading.

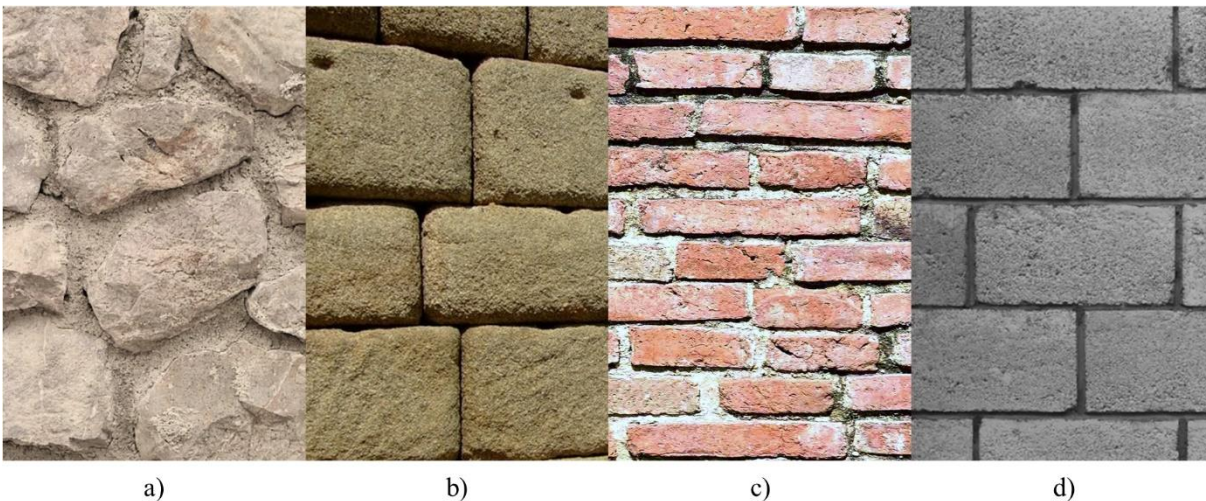


**Figure 2** Examples of different masonry typologies. a) Rubble stone masonry, b) ashlar stone masonry with dry joints, c) clay brick masonry, d) concrete block masonry.

Masonry behaviour is highly nonlinear as the result of the nonlinearities of the components and the source of weakness constituted by the interface or bond between components. The

response of the components is generally quasi-brittle, while the bond is characterised by a normal-stress dependent cohesive-frictional behaviour in shear and a cohesive response in tension [3].

The most relevant feature of masonry is its ability to withstand compression, compared to a very limited, even null in some cases, capacity in tension. Historically, this characteristic has been reflected in structural design, where masonry was used for building structural members subjected mainly to compression. The durability and resistance of this material are obvious in the light of the amount of existing constructions that were built centuries ago [4].

The behaviour of masonry in compression reflects its composite nature and the interaction between components. For instance, the case of brickwork is clearly illustrated in Figure 3, which shows three experimental stress-strain curves from a well-known research carried out by Binda et al [5]. In the figure, the curves show how the composite behaviour is the result of the contribution of both constituents, and how the composite strength lays within the strengths of brick and mortar. In the common case where units are stronger and stiffer than mortar, the resulting masonry strength is higher than the mortar's but lower than the units' strength. This fact has been traditionally explained by the difference in the stiffness of the materials and the particular states of stresses that are generated within the components [1,2]. While both bricks and mortar would tend to expand laterally under vertical compression, the difference in stiffness –in both Young's modulus and Poisson's ratio- would motivate bricks to prevent the free expansion of the mortar in the joint. This confinement creates a favourable triaxial compression state within the mortar, which is able to withstand higher stresses. Conversely, bricks are compressed vertically but are stretched laterally and eventually fail by tensile splitting.

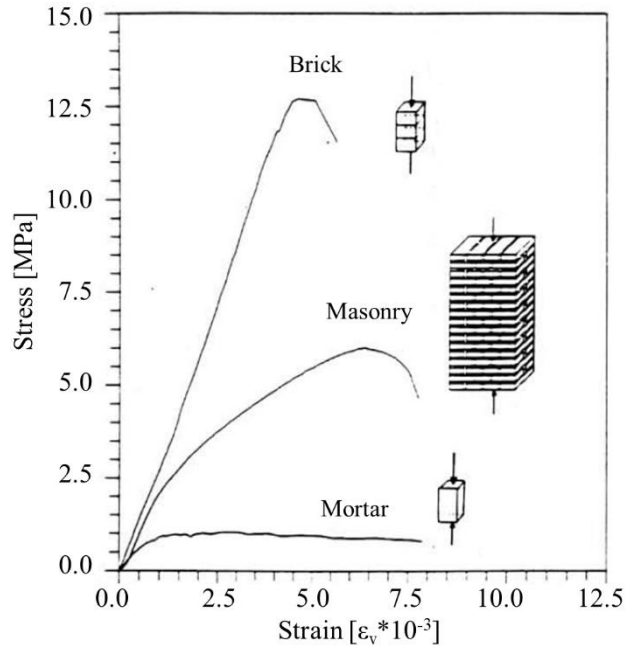


**Figure 3** Examples of stress vs. strain curves for mortar, brick and masonry prisms under uniaxial compression (from Binda et al. [5]).

Because of being composed by a superposition of layers of units and mortar, another feature of masonry is its anisotropy. The more regular the arrangement, the higher the influence of anisotropy; the more random the arrangement, the more valid would be the hypothesis of isotropy. Extreme cases could be a perfectly built brickwork and a very random rubble masonry. Page and co-workers carried out extensive experimental campaigns to investigate the anisotropy of brickwork under biaxial stresses [6–8]. Figure 4 illustrates the variation of the failure modes with the orientation of the loads with respect to the bed joints. The sketches exemplify the role played by mortars joints as discontinuity planes and lines of weakness. Figure 5 displays the failure surface that assembles all the experimental results. Two remarks are obvious: a) the much higher strength observed in compression than in tension, and b) the higher strength observed in compression when the load is applied perpendicularly to the bed joints than when it is applied obliquely or parallel to the bed joints

Angle $\theta$	Uniaxial tension	Other ratios $\sigma_1 / \sigma_2$	Uniaxial compression	Biaxial compression
0°				
22.5°				
45°				
67.5°				
90°				

**Figure 4** Modes of failure for biaxial tests (examples on brick masonry by Dhanasekar et al. [8]).

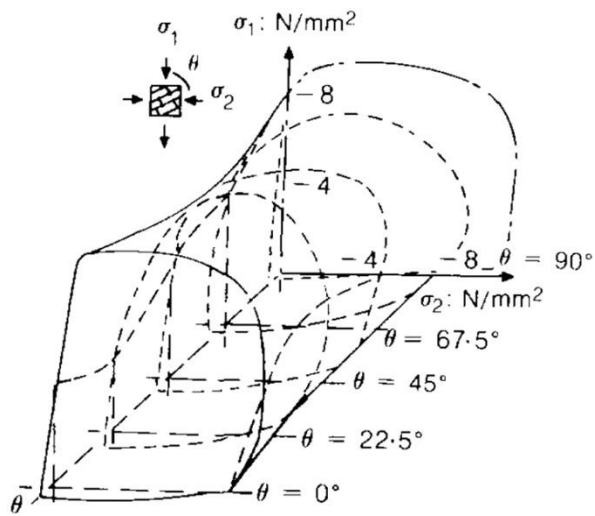


**Figure 5** Failure surface for biaxial tests in terms of normal stresses and angle of orientation of the bed joints planes (results for brick masonry obtained by Dhanasekar et al. [8]).

Combined with compression, masonry members may also need to withstand shear in instances such as soil settlements, wind loads, or seismic events. The resistance to in-plane loading is of paramount importance especially in the latter case, given the severe consequences that may be occasioned by an earthquake in terms of damage and casualties. The shear strength of masonry is another feature that depends on several parameters: the geometry and boundary conditions of the structural member, the masonry arrangement, the acting axial load, and the mechanical properties of the constituents [9]. Figure 6 exemplifies the influence of the acting axial load on the strength and failure modes of a masonry pier. For a pier of given slenderness and given masonry type, the shear response is characterised by the limit domain shown in Figure 6a associated to the failure modes depicted in Figure 6b. Failure modes A and C occur if the pier has a predominant flexural behaviour. For low levels of vertical load, the rotation of the pier about the toes produces horizontal cracks at the corners (A – rocking). For high levels of vertical load, the more compressed corner eventually presents a widespread damage pattern of sub-vertical cracks (C- crushing) [9]. In the case of predominant shear behaviour, two additional modes of failure may happen. Shear frictional sliding failure involves the sliding through a horizontal bed joint plane or a stepped diagonal line with no damage in the units (B1 in Figure 6). This failure is usually preceded by the opening of the flexural crack, which eventually reduces the resisting section. The other possible failure is diagonal cracking, that refers to the failure produced with the formation of a diagonal crack that passes through the mortar joints and the units (B2 in Figure 6).

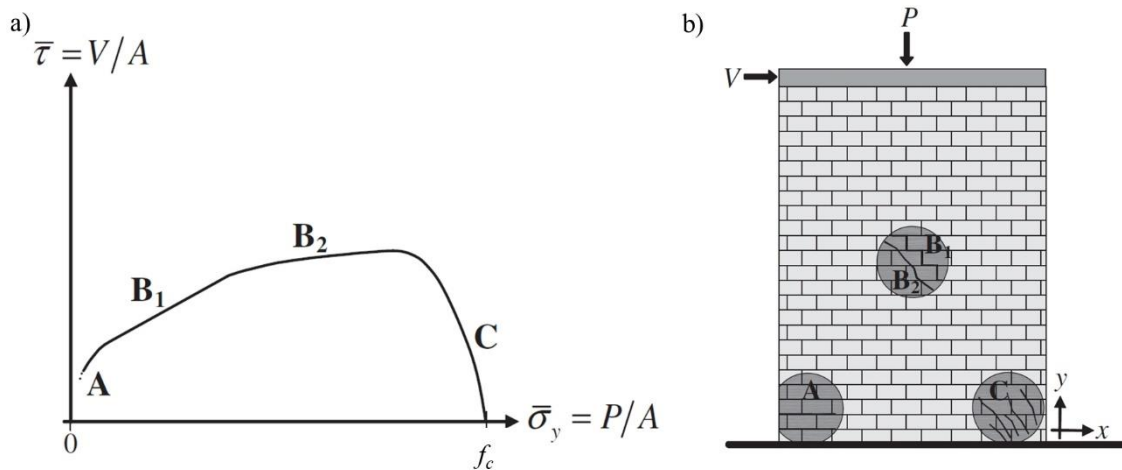


**Figure 6** a) Limit domain and b) failure modes of a masonry pier under combined vertical and horizontal loading (from Calderini et al. [9]).

A last feature of masonry that should be highlighted is its inherent variability. Beyond the differences of typology found between geographical areas or between buildings, masonry presents a high scattering in its properties within the single building. This fact is especially relevant in the case of historical constructions, due to the less industrialized processes of the time. The causes of variability are diverse and of different origins: a) variability within the raw materials, which could present chemical, physical or geometrical differences, b) variability during the construction and related to workmanship, e.g. the amount of water used for wetting the units or preparing the mortar, or bad practices resulting in non-constant mortar thicknesses and misalignments, and c) variability after the construction, related to the curing process, the loading history or the damage and decay experienced over the years. Overall, the material variability affects the structural performance by creating weaker areas and should be taken into account while designing characterisation campaigns.

## **2.2. Mechanical characterisation needs for the structural assessment of masonry structures**

Structural assessment is a procedure for checking whether a building satisfies the required limits of safety and serviceability appropriate to the actions under consideration. The complete assessment procedure involves the definition of the design context, the determination of actions, the performance of structural analysis, and, finally, the verification of the required limits.

To perform the structural analysis of a building, different input data are necessary. Other than the loads acting on the structure, input data include geometrical definition, soil conditions, construction details, damage and state of conservation, and mechanical properties of the materials, which are the subject of this thesis.

Material properties feed the structural models, which are used to determine the effects of the actions either on the structure -such as rotations- or on structural members -such as forces, moments, stresses or strains. It is then obvious that a better characterisation would increase the reliability of the structural analysis results. From a practical point of view, this observation is especially important. Most modern building codes are based on a limit state philosophy, also known as load and resistance factor design approach. In the case of existing buildings assessment, codes such as Eurocode 8-3 [10] or the Italian NTC [11] define different levels of knowledge that account for the uncertainties of the building. Improving the characterisation of the materials helps in reducing the uncertainties and allows a reduction of the safety factors applied during the analysis. Eventually, this better characterisation results in a safer and more respectful design.

This section explores the specific material properties that require to be known for the structural assessment of masonry buildings, with the aim of narrowing the scope of the work.

First, Section 2.2.1. reviews the different modelling strategies for structural analysis and identifies the most relevant properties in use. Second, Section 2.2.2. reviews current building codes to identify the properties used in safety verifications. The last Section 2.2.3. presents a summary.

### **2.2.1. Modelling strategies for structural analysis**

During the last decades, a great research effort has led to the development of a plethora of modelling strategies devoted to the analysis of masonry structures [12]. The complexity of the mechanical behaviour of the material, as described in Section 2.1.2., motivated the appearance of diverse approaches, which faced the subject of masonry analysis within different conceptual frameworks. D’Altri et al. [3] made an updated review of the different strategies, and proposed a classification consisting on four different categories: a) Geometry-based models, where the structure is modelled as a combination of rigid bodies and the equilibrium is usually investigated by means of limit analysis-based solutions; b) Continuum models, where masonry is modelled as a continuum deformable body, with no distinction between constituents; c) Block-based models, where the actual texture of masonry is taken into account, considering the blocks either rigid or deformable; and d) Macroelement models, where the structure is idealized into panel-scale structural members (typically piers and spandrels).

Although other classifications are possible, like the more traditional distinction between limit analysis, finite element methods (macromodelling and micromodelling) and discrete element methods with different subcategories, the proposal by D’Altri et al. [3] suits the objectives of this section because it is simple and makes order on the great variety of available modelling strategies. Therefore, the following exposition of the material properties required for each strategy is presented according to the aforementioned categorization. Table 1 (see Section

2.2.1.5) presents an inventory of the different material properties. For further details on the basics and features of each strategy, the reader is referred to [3,12].

### **2.2.1.1. Geometry-based models**

This exposition starts with geometry-based models because they constitute the category that requires the less amount of mechanical properties to be characterised. In fact, geometry-based models rely basically on the definition of the geometry as the only input. This modelling strategy is based on the application of limit analysis, i.e. the application of the limit theorems of plasticity. The static (lower bound) theorem is applied to assess the equilibrium of a structure, its static safety, and is especially suitable for the analysis of arches and vaults (see Figure 7a,b,c). Complementarily, the kinematic (upper bound) theorem is useful to study the possible collapse mechanisms, and is widely used for the assessment of the seismic vulnerability of buildings (see Figure 7d). In the prime formulation by Heyman [13], these theorems are of application under the following assumptions: i) compressive strength of masonry is infinite, ii) sliding between parts is prevented, iii) tensile strength of masonry is negligible. Therefore, procedures applying limit analysis approaches would not need theoretically the characterisation of any material property.

Nevertheless, given that masonry compressive strength is certainly not infinite, sliding may occur, and tensile strength is limited but not null, some authors have proposed innovative formulations that extend the possibilities of limit analysis and apply to the actual features of masonry. For instance, the concept of thrust zone adds geometric constraints that account for the limited compressive strength of the material [14,15]. More recently, Chiozzi et al. [16] proposed a new approach based on the kinematic theorem that requires three material properties as input: the compressive, tensile and shear strengths of masonry.

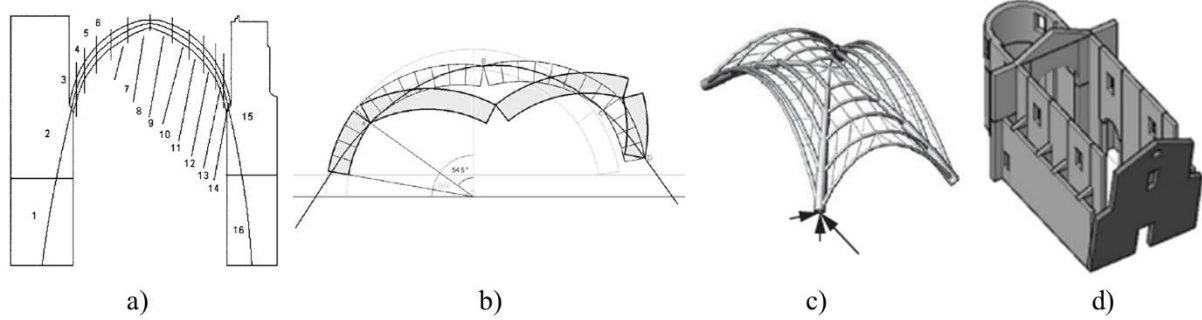


**Figure 7** Examples of geometry-based models. a) Andreu et al. [17], b) Block et al. [18], c) Block and Lachauer [19], d) Chiozzi et al. [20].

### 2.2.1.2. Continuum models

Continuum models consider masonry as a continuum deformable body. As a continuum, the actual texture of the material is not described and the required computational effort is, generally, lower than in more detailed approaches. The deformability condition needs the definition of homogeneous constitutive laws that approximate the overall mechanical response of the material. The use of homogenization techniques to derive constitutive laws is mentioned in the next section on block-based models.

Although non-fully coherent with the masonry mechanics described in Section 2.1.2., these homogeneous isotropic models have been extensively used because of their computational efficiency, their availability in finite element (FE) codes, and the reduced number of parameters that need to be characterised [3]. Consequently, they are especially suitable for large-scale structures given their ability to represent complex geometries and to integrate the randomness and irregularities found in many historical masonry buildings [21–24], as shown in the examples of Figure 8. In the case of more regular types of masonry, such as brickwork, orthotropy plays an important role. Different approaches have been developed to incorporate the effect of anisotropy, although they increase the computational needs and the number of mechanical properties to be determined [25–27].

Different approaches have been adopted to define the constitutive laws, which are based namely on fracture mechanics, on damage mechanics or on plasticity theory. The required input mechanical parameters vary depending on the selected theoretical framework [28]. A fracture or damage-based approach may need to be feed with tensile and compressive strengths of masonry, tensile and compressive fracture energies of masonry, and ultimate or crack strains. The plasticity-based models such as Mohr-Coulomb or Drucker-Prager involve also cohesion, friction angle and dilatancy angle. In all cases, the elastic properties of masonry (Young's modulus, Poisson's ratio) are necessary.

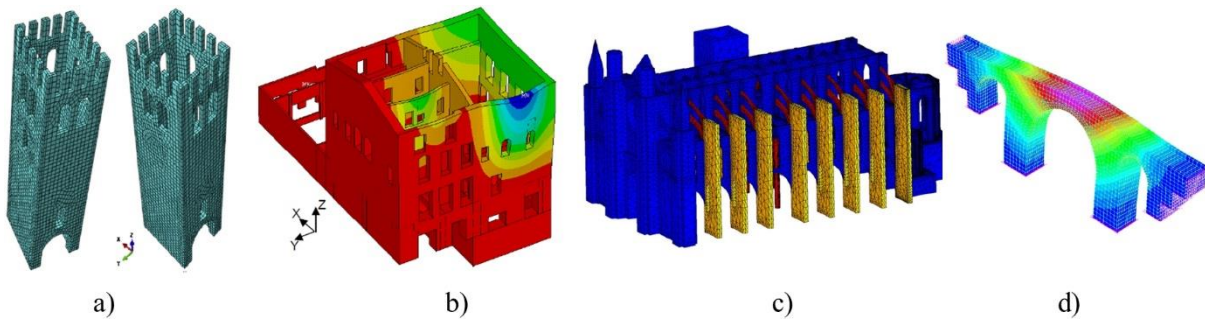


**Figure 8** Examples of continuum models. a) Valente and Milani [21], b) Betti et al. [22], c) Elyamani et al. [23], d) Pelà et al. [24].

### 2.2.1.3. Block-based models

In block-based models, masonry is considered as a heterogeneous material composed by different constituents: blocks (units) and joints (filled with mortar or empty). Consequently, these models describe the actual texture of masonry and are able to account intrinsically for the anisotropy of the material and the representation of the failure modes. Nevertheless, this modelling strategy is characterised by a huge computational demand, by a time-consuming preparation process, which also faces the possible lack of complete information about the actual masonry texture, and by the need of a large amount of different mechanical parameters to be characterised. Overall, its applicability is mostly reduced to academic purposes or high-level construction projects [3].

D’Altri et al. [3] classified the different existing block-based models into several subcategories, namely interface element-based approaches, contact-based approaches, and textured continuum-based approaches (see Figure 9). The differences among them lie in the formulation of the interaction between blocks and the level of detail. With regard to the subject of this thesis, the mechanical properties that need to be characterised also vary depending on the selected approach. As a matter of fact, one example of each subcategory is described below with the definition of all the required mechanical parameters. This list cannot be exhaustive, given the specificity and variety of the different approaches that are currently under development.

A classic example of interface-element-based model with a FE approach is the multisurface interface model proposed by Lourenço and Rots [29]. In this model, units are expanded in both directions by a mortar thickness and modelled with continuum elements. Mortar joints are then modelled with zero-thickness interface elements that concentrate all the possible nonlinearities. In addition, potential cracks within the units are introduced also with zero-thickness interface elements. The required mechanical properties to feed this model are as follows. Deformability is modelled through the Young’s modulus and Poisson’s ratio of the units, and the normal and shear stiffness of the joints. The latter two are determined from the elastic properties (Young’s modulus and shear modulus) of both units and mortar. The inelastic properties of the joints account for the different failure modes. Tensile strength of the joints or of unit – mortar interface, together with mode I fracture energy, stands for the tension mode. This mode also applies for the potential cracks. Initial cohesion of the joints, initial friction angle, residual friction angle, mode II fracture energy and dilatancy angle are required to represent the shear mode. The cap mode is defined with the compressive strength and three internal parameters.

An example of contact-based approach is provided in [30], which presents a modelling strategy based on the discrete element method (DEM). In DEM, discrete blocks interact mechanically with each other along their boundaries. In this example, blocks are considered rigid and all the system deformation is lumped at the joints, which are characterised by the joint normal and shear stiffness. The nonlinear contact behaviour is governed by a Mohr-Coulomb model characterised by tensile, cohesion and friction parameters (tensile strength, cohesion, and angle of friction for both horizontal and vertical joints).

The last subcategory is the textured continuum-based approach, where the actual texture of masonry is modelled in a FEM framework with distinction between blocks and joints, but without any interface between them. An example of this approach is given in [31], where a tension/compression damage model applies for both units and mortar joints. Coherently with the material model, this example requires the following mechanical properties for both units and mortar joints: Young's modulus, Poisson's ratio, tensile strength, tensile fracture energy, elastic limit in compression, compressive strength, residual compressive strength, and compressive strain at peak stress.

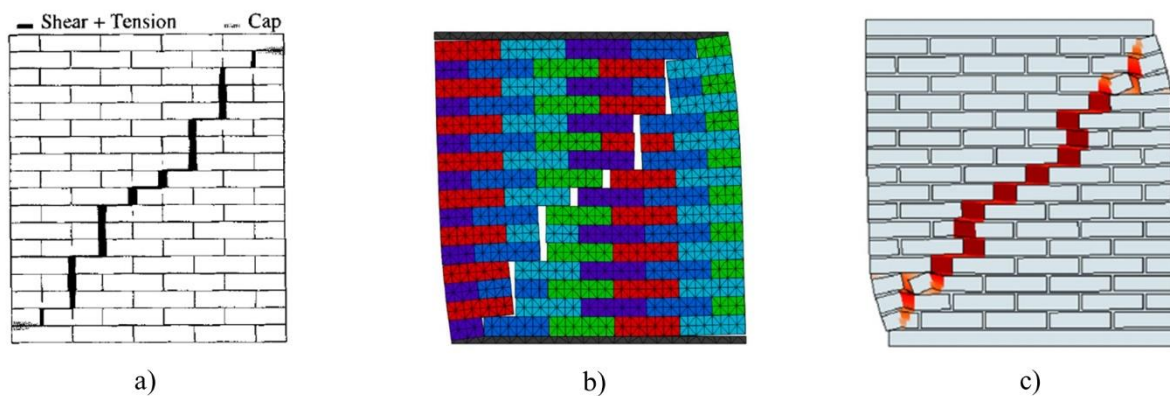


**Figure 9** Examples of block-based models. a) Interface-element-based approach by Lourenço and Rots [29], b) Contact-based approach by Pulatsu et al. [32] c) Textured continuum-based approach by Petracca et al. [31].

Finally, the aforementioned block-based models may be applied to representative volume elements (RVE) of the structure through a homogenization process with the aim of determining

the constitutive law of masonry (at structural-scale) from the properties of the constituents (at material-scale). This constitutive law may be used in continuum-based approaches as the ones described in Section 2.2.1.2.

#### **2.2.1.4. Macroelement models**

The macroelement approach consists in the idealization of the structure into panel-scale structural components, the so-called macroelements (see Figure 10). These macroelements are typically identified either as piers – vertical resisting elements- or as spandrels – horizontal parts over openings that couple the piers. A phenomenological or mechanical-based nonlinear response is assigned to each macroelement. After assembling the individual elements, the macroelement model is able to reproduce the in-plane behaviour of entire masonry walls [33]. The reduced computational effort, the easy definition of the model, and the few required mechanical properties, make the macroelement approach the most widely diffused modelling strategy for common practitioners [3], especially when dealing with the seismic assessment of structures. Nonetheless, a certain expertise of the analyst is essential in the definition of the elements and properties, given the huge simplifications implicit to the method. Among others, the main assumption is that any activation of local (out-of-plane) failure mode is prevented.

Macroelement models can be formulated with an equivalent beam-based approach or a spring-based approach. In both cases, the properties of beam elements and springs are modelled to simulate the different failure modes experienced by masonry members, which were described in Section 2.1.2: axial response, flexure (rocking/toe crushing), joint sliding and diagonal cracking [34]. The common strength criteria defined for these failure modes are based on the following mechanical properties: compressive strength of masonry in the directions perpendicular and parallel to bed joints, cohesion, angle of friction, and diagonal tensile strength

(or tensile strength of units). In addition, Young's modulus and shear modulus of masonry are required to define the stiffness matrix of the model [35].

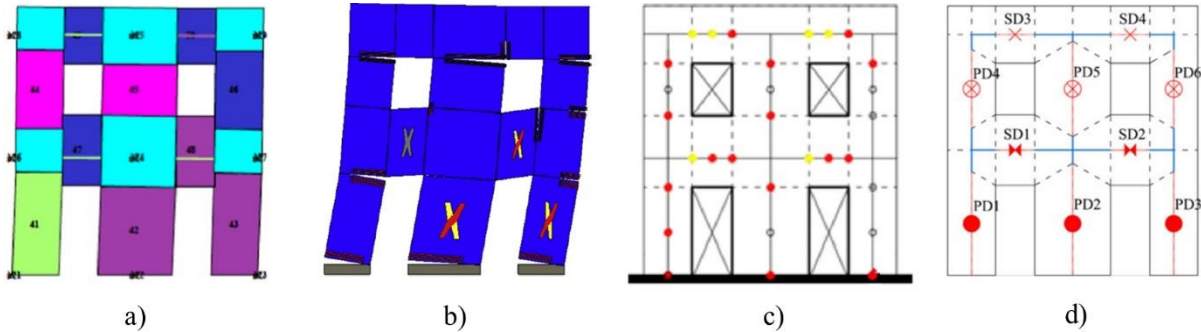


**Figure 10** Examples of macroelement models. a) Lagomarsino et al. [35], b) Calì et al. [36], c) Siano et al. [37], d) Rinaldin et al. [38].

### 2.2.1.5. Inventory of mechanical material properties required for modelling

Table 1 compiles an inventory of the mechanical material properties used in the different modelling strategies reviewed along the previous sections. The table acts as a summary of the most relevant properties. In consequence, it does not include an exhaustive list of all the possible material parameters, which might be very specific of a particular type of model. Parameters such as fracture energies of units and mortar, residual angle of friction, ultimate strains, or the compressive strength of blocks, are not included because they don't belong to general usage. Specific weight of masonry is neither included given that it is needed in all instances. References are indicated as examples to clarify the specific meaning of each parameter.

Table 1 exemplifies the features exposed above. There are two different groups of properties depending on the modelling level of detail: one corresponding to properties of components and their interaction, and one corresponding to properties of masonry as a composite material. Block-based models capture the heterogeneity of masonry and need an extended set of properties. Conversely, the other three approaches apply simplifications at

different level, and do not consider the actual texture of the material. Therefore, these approaches require fewer mechanical properties to be characterised.

**Table 1** Inventory of mechanical material properties used in different modelling strategies. Grey background indicates properties that are typically used in the corresponding strategy. Stripped background stands for properties that could be used within that strategy. HOM indicates that the property is used through a homogenization technique.

Symbol	Mechanical property	Modelling strategy [Examples in brackets]			
		Geometry-based	Continuum	Block-based	Macroelements
$f_c$	Compressive strength of masonry	[15,16]	[23,39–41]	-	[33,36–38,41–46]
$f_t$	Tensile strength of masonry	[16]	[23,39–41,47]	-	[36–38,41–43,45]
$E$	Young's modulus of masonry	-	[23,39–41,47]	-	[33,36–38,41–46]
$\nu$	Poisson's ratio of masonry	-	[23,39–41,47]	-	[37,43]
$G_{ft}$	Fracture energy in tension of masonry	-	[23,39–41,47]	-	[41]
$G_{fc}$	Fracture energy in compression of masonry	-	[39–41]	-	[41]
$G$	Elastic shear modulus of masonry	-	-	-	[33,36,38,41,44,45]
$E_b$	Young's modulus of blocks (units, bricks)	-	HOM [48–50]	[29,31,51–56]	-
$E_m$	Young's modulus of mortar	-	HOM [48,49]	[31,53,57]	-
$\nu_b$	Poisson's ratio of blocks (units, bricks)	-	HOM [48–50]	[29,31,51,52,54–56]	-
$\nu_m$	Poisson's ratio of mortar	-	HOM [48,49]	[31]	-
$f_{t,b}$	Tensile strength of blocks (units, bricks)	-	-	[31,52,56]	[35]
$f_{t,m}$	Tensile strength of mortar (also tensile strength of mortar-unit interface)	-	HOM [48]	[29,31,55–57]	-
$f_{c,m}$	Compressive strength of mortar	-	HOM [48]	[54,55]	-
$c$	Cohesion – Shear strength of masonry at zero normal stress (also $f_{vm0}$ , $\tau_0$ )	[16]	[22,58] HOM [48,50]	[29,31,52–56,59]	[33,36,38,41,42,44]
$\phi$	Angle of friction ( $\mu = \tan\phi \equiv$ coefficient of friction)	-	[22,58] HOM [48,50]	[29,31,32,51–54,56,57]	[36,41,42,45]
$\psi$	Angle of dilatancy	-	[22,58]	[29,31,51,54,55]	-
$G_f^I$	Mode I Fracture energy	-	HOM [48,50]	[29,31,32,52,55,56,59]	-
$G_f^{II}$	Mode II Fracture energy	-	HOM [48,50]	[29,31,32,52,54,55,59]	-
$k_n$	Joint normal stiffness	-	-	[29,31,32,51,55,56,59]	-
$k_s$	Joint shear stiffness	-	-	[29,31,32,51,55,56,59]	-

### **2.2.2. Structural assessment in building codes**

Building codes establish a set of common rules that regulates the standards for constructed objects. Any construction or intervention design must conform to the code in order to obtain the official permit. From antiquity, societies have adopted this type of codes to protect public health, safety and general welfare.

With regard to structural assessment, and in general terms, modern building codes stipulate certain strength criteria that must be fulfilled. The assessment consists then in the verification of the structural members by confronting the actions on the structure with the prescribed strength criteria. As the main load-bearing elements in a masonry building, codes devote special attention to walls.

This section briefly reviews some of the strength criteria established by common codes, with the aim of identifying the material properties that are involved. The focus of the review is placed on these properties, and the rationale behind each limit and equation is not included here. Further information can be found in the corresponding code. In the following, Eurocode 6-1 [60], Eurocode 8-3 [10], and ASCE/SEI 41-17 [61] are reviewed, because these are codes of international diffusion, easily available and which have inspired other national codes. The Italian code Norme Tecniche per le Costruzioni [11] is also considered given its special emphasis on existing buildings.

#### **2.2.2.1. Eurocode 6 – Design of masonry structures. Part 1: General rules**

Eurocode 6 [60] applies to the design of buildings and civil engineering works in unreinforced, reinforced, prestressed and confined masonry. Its Section 6 deals with the definition of the Ultimate Limit State and the corresponding verifications. Within this

framework, design values of applied loads shall be less than or equal to the design values of the resistances.

When a wall is subjected to mainly vertical loading, the design value of the vertical resistance,  $N_{Rd}$ , is given by Equation 1:

$$N_{Rd} = \Phi t f_d \quad (1)$$

where  $\phi$  is a capacity reduction factor that accounts for the effects of slenderness and eccentricity of loading,  $t$  is the thickness of the wall, and  $f_d$  is the design compressive strength of the masonry.

In a wall subjected to shear loading, the design value of the shear resistance,  $V_{Rd}$ , is given by Equation 2:

$$V_{Rd} = f_{vd} t l_c \quad (2)$$

where  $l_c$  is the length of the compressed part of the wall, ignoring any part of the wall that is in tension, and  $f_{vd}$  is the design value of the shear strength which depends on its characteristic value.

In absence of tests, the characteristic shear strength of masonry,  $f_{vk}$ , according to Eurocode 6 [60], may be taken from Equation 3:

$$f_{vk} = f_{vk0} + 0.4\sigma_d \quad (3)$$

where  $f_{vk0}$  is the characteristic initial shear strength, at zero compressive stress, and  $\sigma_d$  is the design compressive stress perpendicular to the shear in the member at the level under consideration.

### 2.2.2.2. Eurocode 8 – Design of structures for earthquake resistance. Part 3:

#### Assessment and retrofitting of buildings

Eurocode 6 [60] does not cover the special requirements of seismic design. Provisions on seismic verifications are given in Eurocode 8 [10]. Its Part 3 is devoted to the evaluation of existing individual building structures. According to Annex C, which is dedicated to masonry buildings, the shear force capacity of an unreinforced masonry wall controlled by flexure,  $V_{f,flex}$ , under an axial load  $N$ , may be given by Equation 4:

$$V_{f,flex} = \frac{DN}{2H_0} \left(1 - 1.15 \frac{N}{Dtf_d}\right) \quad (4)$$

where  $D$  is the in-plane horizontal dimension of the wall (depth),  $H_0$  is the distance between the section where the flexural capacity is attained and the point of zero moment, and  $f_d$  is again the design compressive strength of masonry.

The equation proposed in Eurocode 8 [10] for the shear force capacity of an unreinforced masonry wall controlled by shear under an axial load  $N$ , is the same as Equation 2 proposed in Eurocode 6.

### 2.2.2.3. Norme Tecniche per le Costruzioni

The Norme Tecniche per le Costruzioni, NTC, [11], issued by the Italian Government, constitutes the official building code in Italy. Although it is consistent with Eurocodes, this code reflects the particularities and common practices of the country. As a result of Italian seismicity and abundance of historical constructions, the NTC stands out for paying special attention to seismic assessment and the evaluation of existing buildings.

Other than former Equations 1, 2 and 4, which are transcribed literally in the NTC, the novelty appears in a second document, the Circolare [62], which includes instructions for the

application of the NTC. The Circolare [62] recommends three additional expressions for the verification of the shear capacity. In the case of irregular masonry, the shear resistance of a wall,  $V_t$ , may be given by Equation 5:

$$V_t = lt \frac{f_{td}}{b} \sqrt{1 + \frac{\sigma_0}{f_{td}}} \quad (5)$$

where  $b$  is a correction factor related to the stress distribution within the section,  $\sigma_0$  is the average normal stress, and  $f_{td}$  is the design value of the tensile strength of masonry by diagonal cracking.

In the case of regular masonry, the shear resistance of a wall,  $V_t$ , may be taken as the minimum of the values computed with the former Equation 5 and Equations 6 and 7:

$$V_t = \frac{lt}{b} \left( \frac{f_{v0d}}{1 + \mu\phi} + \frac{\mu}{1 + \mu\phi} \sigma_0 \right) \quad (6)$$

$$V_t = lt \frac{f_{btd}}{2.3b} \sqrt{1 + \frac{\sigma_0}{f_{btd}}} \quad (7)$$

where  $f_{v0d}$  is the shear strength at zero compressive stress,  $\mu$  is the coefficient of friction,  $\phi$  is a parameter describing the interlocking of masonry pattern,  $\sigma_0$  is the acting normal stress, and  $f_{btd}$  is the tensile strength of the blocks.

#### 2.2.2.4. ASCE/SEI 41-17 Seismic evaluation and retrofit of existing buildings

American ASCE/SEI 41-17 specifies provisions for the seismic evaluation and retrofit of existing buildings. Its Section 11 is devoted to masonry. This code defines five primary in-plane actions which masonry walls may be subjected to, and proposes the corresponding five strength criteria.

Expected rocking strength,  $V_r$ , may be calculated with Equation 8:

$$V_r = 0.9(\alpha P_D + 0.5P_w)l/h_{eff} \quad (8)$$

where  $h_{eff}$  is the height to resultant of seismic force,  $P_D$  is the superimposed dead load at the top of the wall under consideration,  $P_w$  is the self-weight of the wall, and  $\alpha$  is a factor equal to 0.5 for fixed-free cantilever walls, or equal to 1.0 for fixed-fixed walls.

Expected bed joint sliding strength,  $V_{bjs}$ , shall be given by Equation 9:

$$V_{bjs} = v_{me}A_n \quad (9)$$

where  $A_n$  is the area of net mortared section of a wall, and  $v_{me}$  is the expected bed joint sliding shear strength.

Lower-bound toe-crushing strength,  $V_{tc}$ , is given by Equation 10:

$$V_{tc} = (\alpha P_D + 0.5P_w)l/h_{eff} \left(1 - \frac{f_a}{0.7f'_m}\right) \quad (10)$$

where  $f_a$  is the axial compression stress caused by gravity loads, and  $f'_m$  is the lower-bound masonry compressive strength.

Diagonal tension strength,  $V_{dt}$ , shall be based in Equation 11, which is equivalent to Equation 5:

$$V_{dt} = f'_{dt}A_n\beta \sqrt{1 + \frac{f_a}{f'_{dt}}} \quad (11)$$

where  $\beta$  is a correction factor depending on the ratio length/height, and  $f'_{dt}$  is the lower-bound masonry diagonal tension strength.

Finally, lower-bound compressive strength of a masonry wall,  $P_{cl}$ , is given by Equation 12:

$$P_{cl} = 0.80(0.85f'_m A_n) \quad (12)$$

where  $f'_m$  is the lower-bound compressive strength.

Overall, the reviewed building codes propose simplified strength criteria that would require the characterisation of the following mechanical properties: compressive strength, shear strength at zero normal stress, diagonal tension strength, tensile strength of blocks and friction coefficient. In addition, all codes consider in their formulations the Young's modulus and the elastic shear modulus of masonry. Table 2 compiles the different material properties included in the strength criteria proposed by the reviewed building codes.

**Table 2** Mechanical properties involved in building codes strength criteria.

Symbol	Mechanical property	Building code			
		Eurocode 6 [60]	Eurocode 8 [10]	NTC [11]	ASCE/SEI 41-17 [61]
$f_c$	Compressive strength of masonry	x	x	x	x
$f_t$	Tensile strength of masonry			x	x
$f_{t,b}$	Tensile strength of blocks (units, bricks)			x	
$c$	Cohesion – Shear strength of masonry at zero normal stress (also $f_{vm0}$ , $\tau_0$ )	x	x	x	x
$\phi$	Angle of friction ( $\mu = \tan\phi \equiv$ coefficient of friction)			x	

### 2.2.3. Summary of characterisation needs

The two previous sections have explored the mechanical characterisation needs that a practitioner would face when analysing a masonry building. These needs depend basically on the modelling strategy selected to perform the analyses. Two groups of properties could be easily identified. Block-based approaches require the complete mechanical characterisation of the masonry components and the interface between them. Geometry-based models, continuum models, and macroelement models, make different assumptions and consider masonry as a simpler composite material. The latter consideration concerns also the simplified strength criteria proposed by common building codes.

Block-based approaches may provide the most detailed and precise simulation of the masonry structural response. However, their high computational cost, together with the

difficulties to determine all the required mechanical properties, and the time-consuming preparation of the model, restrict their applicability to either the research field or reduced structural elements. Even if this situation might change in the future thanks to the increasing power of computers, the other approaches are preferred in common practice by engineers and architects. In consequence, this thesis will be focused on the characterisation of masonry as a composite material, because the potential contributions might have a greater impact in real practice.

From the point of view of masonry as a composite material, the most relevant mechanical properties detected in the previous sections were: compressive strength, tensile strength, Young's modulus, Poisson's ratio, compressive and tensile fracture energies, shear elastic modulus, cohesion or shear strength at zero compressive stress, and angle of friction. Section 4.5.3. of the NTC code [11] reduces the fundamental mechanical properties of masonry to only four parameters: compressive strength, shear strength at zero compressive stress, Young's modulus and shear elastic modulus. A similar list of properties is proposed by Krzan et al. [63] as the fundamental mechanical parameters necessary to define and interpret the behaviour of a masonry assemblage: compressive strength, initial shear strength, coefficient of friction, Young's modulus, shear elastic modulus, and diagonal tensile strength.

The determination of the former mechanical properties will be analysed and discussed within the thesis. The common distinction between masonry loaded in compression and masonry loaded in shear has been applied in this work to organise the chapters and sections.

## **2.3. Mechanical characterisation procedures**

This section delves into the existing procedures for the mechanical characterisation of masonry. It is reminded that each of the papers presented later in Chapters 4, 5 and 6, include a specific and detailed literature review. The section is divided into three parts. Part 2.3.1. discusses general aspects on the characterisation of masonry such as the approaches and challenges normally encountered. It also presents some basic definitions about testing procedures that will contribute to a better exposition of ideas along the thesis. Part 2.3.2. covers the characterisation techniques for masonry loaded in compression, while Part 2.3.3. is devoted to masonry loaded in shear.

According to the literature review presented in the previous Section 2.2., the discussion of this Section 2.3. deals exclusively with six properties of masonry as a composite material: compressive strength and Young's modulus in Section 2.3.2., and initial shear strength, shear elastic modulus and diagonal tensile strength of masonry in Section 2.3.3. Note that this thesis does not cover the following aspects of the characterisation of masonry: fatigue, shrinkage, creep, dilatation, durability, damage limits or hysteretical response.

### **2.3.1. General aspects**

#### **2.3.1.1. Approaches and challenges**

The complex mechanical behaviour of masonry described in Section 2.1.2., which is the result of its composite nature, influences significantly the process of characterisation. Hendry distinguishes three categories of tests depending on the considered scale [1]: a) tests on components, i.e. units and mortar, which are afterwards correlated with properties of the composite material; b) tests on small specimens of masonry, such as prisms and wallettes, which

provide a direct determination of the properties of the composite material; and c) tests on complete masonry elements, which are intended to evaluate global effects.

The major issue in relation with the characterisation of masonry is therefore that of representativeness, the dilemma between local and global behaviour, the quandary about whether the tested specimen and the boundary conditions are able to represent the actual behaviour of masonry.

The former issue applies to any type of masonry. However, in the case of existing historical masonry, the lack of representativeness becomes a multifaceted problem given the high level of heterogeneity found within historical buildings. To obtain significant results, a sufficient amount of tests in different parts of the building should be done to improve their statistical reliability. Nevertheless, this necessity is in contradiction with the impossibility of causing damage to the building in the case of cultural heritage assets.

In the last decades, a vast effort has been devoted to the development of non-destructive tests (NDT) for the characterisation of masonry [64]. Among others, techniques such as thermography, sonic tests, or georadar, are helpful in the definition of hidden characteristics, the overall knowledge of the structural elements, or construction details. More precisely, they offer the possibility to evaluate the quality of the masonry element and can be used with a comparative purpose, to identify parts of the building that have similar physical properties.

Yet, either minor destructive tests (MDT) or destructive tests (DT) are required for the determination of mechanical properties. These type of tests are the ones covered in this thesis, together with standard laboratory tests. The different options are briefly discussed in Section 2.3.2. and 2.3.3. The reader is referred to complete state-of-the-art references for further information [1,63–65].

Lastly, it is relevant to highlight in these general-aspects section, the importance of a sustained research effort to improve the characterisation procedures. In some instances, new methodologies have not been supported by a standard yet, in the lack of extensive and comprehensive experimental campaigns. Conversely, standards and building codes are continuously updated, and usually incorporate new research findings that have been conveniently proven [61,66].

### **2.3.1.2. Requirements for characterisation tests**

When designing a characterisation test, different aspects should be taken into account. Other than the specific mechanical property that is pursued, Hendry considers two additional criteria [1]: a) the cost, considered in relation with the purpose of the test, and b), the practicability of the proposed test. This practicability refers to several features: the time required to perform the test and to obtain the results, the specificity of the required equipment, the levels of skill required to the technicians performing the test, the reproducibility of the test, and, most importantly, the accuracy of the obtained results.

More precisely, different features should be addressed in the definition of a characterisation test: the geometry of the specimen, the boundary conditions, the loading protocol, the instrumentation, and the post-processing of the results [67]. These aspects are discussed in the following in general terms for the case of masonry. The goal is to set a framework for the discussion of the different tests in the next sections.

- Geometry of the specimen.

The geometry of the specimen, i.e. size and configuration, is directly related to the aforementioned issue of representativeness. The testing procedure should define the number of joints to be considered, and the proportions of the specimen with respect to the dimensions of the units. A sufficiently large specimen is also

required to guarantee a proper distribution of stresses and to avoid spurious effects related to the loading system. In the case of existing masonry, the size of the specimen should be chosen with the aim of reducing the damage to the minimum extent.

- Boundary conditions.

Boundary conditions refer to the testing setup and how the load is transferred to the specimen. The testing setup should guarantee the stability of the specimen and provide satisfactory conditions in terms of both loads and restricted displacements. The system should provide enough force capacity to apply the required loads. Attention should be paid also to the contact surfaces between the masonry specimen and the setup.

- Loading protocol.

The loading protocol defines how the load is applied, and covers the rates of loading (under force or displacement control). Loading rates are important to properly capture the studied phenomenon and to allow the comparison of results among researches. The loading protocol establishes also if the load is applied monotonically or cyclically. The latter is important to represent the effect of cyclic actions, but it also has influence in the procedures to determine elastic parameters. An additional issue is related with the moment to stop the test. The determination of postpeak parameters would require the continuation of the test beyond the peak but maintaining the safety of the process.

- Instrumentation.

Different instruments are used to measure displacements, deformations and forces on the specimen. Defining the data that should be measured is a capital question within a test. The design of the instrumentation involves deciding which instruments should be used and their required precision and range, the number of instruments and their position –e.g. with respect to the mortar joints-, and the sampling frequency.

- Post-processing.

The test outcomes are generally expressed in terms of forces and displacements. A post-processing procedure of the data is required to convert the quantities measured during the test into the desired mechanical properties. These procedures, which usually involve simple analytical expressions, should be defined carefully.

### **2.3.2. Characterisation of masonry in compression**

This section reviews the characterisation techniques available for the determination of the two most relevant properties of masonry in compression: the compressive strength and the Young's modulus.

#### **2.3.2.1. Compressive strength of masonry**

The compressive strength is the most relevant mechanical property of masonry [68], and it justifies the traditional way of designing masonry structures. Furthermore, in the lack of other characterisation tests, this parameter is used as a reference to compute the rest of the properties: e.g. by means of common or standard values assumed for the ratios relating tensile strength,

Young's modulus or compressive fracture energy with the compressive strength of masonry [69].

This review on the characterisation of the compressive strength is divided into three parts: a) methods to apply in laboratory, b) methods to apply in situ, and c) derivation from components' properties.

#### **a) Laboratory methods**

In the case of new masonry, the characterisation consists in testing small specimens of masonry under compression [70–72]. The basic procedure considered by all standards involves the construction of the specimen, the storage in convenient conditions to guarantee the hardening of the mortar, the testing under prescribed loading rates, and the computation of the strength as the maximum attained load divided by the net area of the specimen cross section.

The main differences among standards lie on the type of specimen being tested. The American standard ASTM C1314 [70] specifies the testing of masonry prisms built with single units laid one on top of another. From now on, this type of specimen is called stack bond prism (SBP). The European norm EN 1052-1 [72], conversely, prescribes the use of small running bond walls, also called wallettes, to determine the compressive strength. Old versions of some standards recommended to test other types of specimen, such as bigger walls [1] or stack bond prisms composed by two units per row [73].

As discussed in the previous section, the representativeness of the chosen specimen is in conflict with other criteria such as practicability. The American approach [70] results in a more economic test, because prisms are easier to build, to handle, and to test, but they do not consider the likely influence of head joints in the masonry response. In literature, it is possible to find multiple examples of both approaches, either on prisms [74–78] or on wallettes [79–82], as shown in Figure 11.



**Figure 11** a) and b) Examples of compressive tests on stack bond prisms, from Drougkas et al. [75] and Pelà et al. [83], respectively. c) and d) Examples of compressive tests on wallettes, from Parisi et al. [84] and Gumaste et al. [79], respectively.

Although the target of the standards is new masonry, American provisions in building codes [61,66] allow two options for existing masonry: I. constructing the specimens with recovered units and a replicated mortar; and II. cutting specimens from the existing walls. Nevertheless, given the dimensions of the required specimens, the latter option is not often considered as it inflicts heavy damage on the structure and the reliability of the results is uncertain. During the sampling, transport, and handling operations, these specimens could easily dismantle.

With regard to load application, standards recommend the application of monotonically increasing load. However, cyclic actions are present in actual buildings, not only in the extreme case of an earthquake, but because of wind or temperature changes. Very few experiences have dealt with the cyclic behaviour of masonry in compression [85–94].

**b) In situ methods**

Two are the main techniques to determine the compressive strength of existing masonry: double flat jack tests and core testing.

The double flat jack test is specifically designed to evaluate the deformability of masonry [95,96], as explained in Section 2.3.2.2. However, if extended damage is allowed within the masonry wall, and flat jacks offer sufficient pressure, the test can be continued until the failure of the masonry panel is attained [97,98]. This approach affects the integrity of the loaded area, which should be repaired, and presents some accuracy issues. The latter are due to the need of specific calibration required by these instruments. If this test is performed in combination with a single flat jack test to determine the acting stresses within the wall [99,100], the value of strength found with the double flat jack approach could at least provide an estimation of a safety factor for the masonry member being investigated [98].

The core testing consists in testing in laboratory masonry cylinders that have been previously core-drilled from the existing masonry wall. This technique is recommended by the International Union of Railways (UIC) [101] for the inspection of bridges. It has been calibrated and validated during the last decades by different authors [83,102–106]. The UIC recommends this technique for brickwork and establishes the minimum size of the cylinders in 150 mm diameter. This type of cylinders includes at least two bed mortar joints and one head joint (see Figure 12a, b and c). Further experiences on smaller cylinders have been also published [107–109] (see Figure 12d).

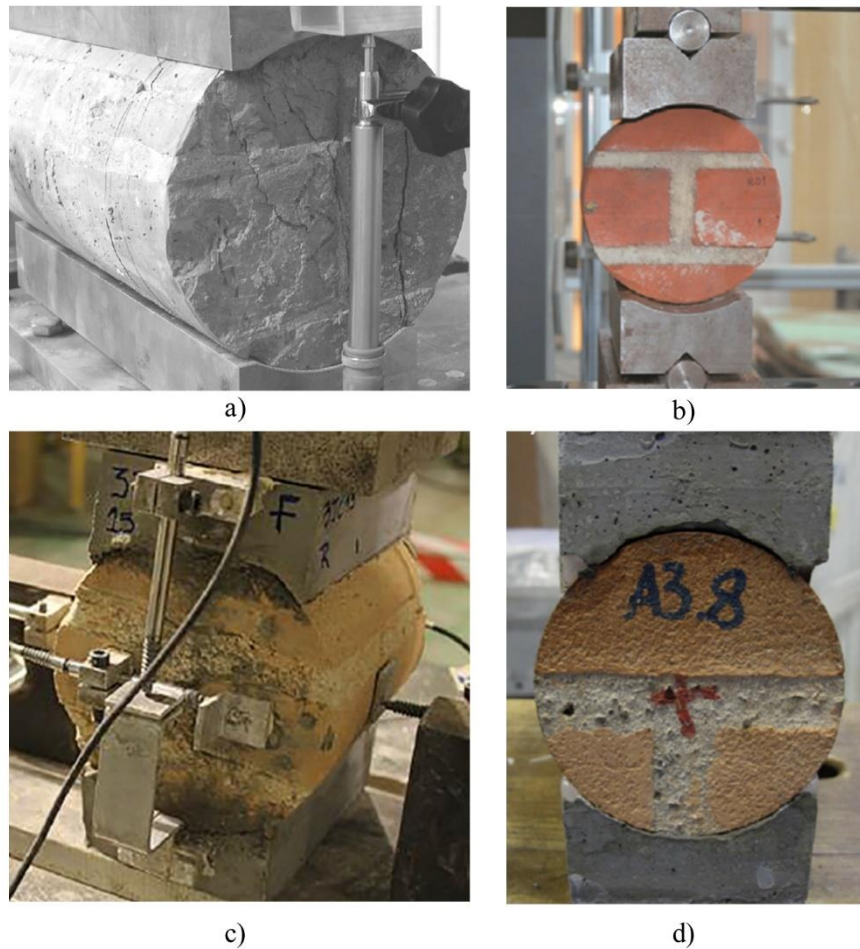


**Figure 12** a), b) and c) Examples of tests on 150 mm cylinders, from Brencich and Sterpi [102], Matysek [104], and Pelà et al. [110] respectively. D) Example of test on 100 mm cylinders, from Sassoni et al. [107].

### c) Derivation from components' properties

A last approach to determine the compressive strength of masonry as a composite material is its derivation from the properties of the components. This approach can be divided into two categories: I. Empirical expressions obtained by statistical methods from experimental databases; and II. Phenomenological expressions that attempt to describe analytically the failure behaviour of masonry under compression.

The first category is recommended by several building codes in the lack of direct experimental results. Eurocode 6 [60] proposes the following Equation 13 to determine the

characteristic compressive strength of masonry  $f_k$  from the normalised mean compressive strength of the units,  $f_b$ , and the compressive strength of the mortar,  $f_m$ :

$$f_k = K f_b^\alpha f_m^\beta \quad (13)$$

where  $\alpha$ ,  $\beta$ , and  $K$  are constants. For masonry made with general purpose mortar and lightweight mortar,  $\alpha$  and  $\beta$  are given values of 0.7 and 0.3 respectively. The value of  $K$  depends on the type of unit and the mortar joint thickness. National building codes from several European countries [11,111] propose the same expression with slight modifications of the coefficients to account for the specificities of each country.

The American code ACI 530.1 [112] recommends the use of the following Equation 14 which depends only on the average compressive strength of the units,  $f_{b,c}$ :

$$f_{c,ACI} = A(400 + B f_{b,c}) \quad (14)$$

where A and B are constants that depend on the type of masonry and type of mortar respectively. This method is known as unit strength method. The experimental database used for the calibration of the former expression is included in the code. Bricks with compressive strengths spanning from 40 to 125 MPa were considered. The compressive strengths of the associated masonry prisms ranged from 15 to 50 MPa.

Different authors have derived equations that belong to the category of phenomenological expressions. Among others, Hilsdorf [113–115], Khoo and Hendry, and Ohler, proposed expressions that incorporate the properties of units (compressive and tensile strengths), mortar, and the geometry of the masonry arrangement (through factors relating the thicknesses of joints and units).

The former empirical and phenomenological approaches deal, however, with the added difficulty of determining the strengths of units and mortar [116–118].

### **2.3.2.2. Young's modulus of masonry**

Young's modulus is the mechanical property that defines the deformability of the material under uniaxial stress. It is capital in the definition of the stiffness of a structural member. This section is organized in parallel with the previous one given that the measurement of this parameter in compression involves the same tests as before.

#### **a) Laboratory methods**

Compression tests are used to determine the Young's modulus of masonry. There are no specific standards that cover the determination of this parameter, although standards for the determination of the compressive strength provide some recommendations. While the maximum attained load was the only test outcome that was required to be measured for the determination of compressive strength, the evaluation of Young's modulus requires the measurement of deformations within the specimen at different stress levels. The differences between standards are found in the definition of Young's modulus and the loading protocol.

The European norm EN1052-1 [72] prescribes the application of the vertical load in three increasing steps until half the possible maximum forces is attained. No unloading cycles are planned. Once the test is finished after the maximum load is reached, the Young's modulus is computed as the secant modulus at a stress equal to one third the maximum stress.

The American standard ASTM C1314 [70] refers to standard ASTM E111 [119] to define the loading protocol. ASTM E111 is a standard that gives specific provisions for the determination of elastic modulus. It recommends the application of at least three loading cycles, without exceeding the proportional or elastic limit. ASTM C1314 defines the Young's modulus as the chord modulus of elasticity between 5% and 33% of the maximum stress reached.

The building code ACI 530-11 [66] admits that further standardization on this subject is needed. It refers that differences in procedures between one research investigation and another may hinder the comparison of results. Also, it admits that the definition of the moduli as secant, tangent or chord modulus is not unanimous among researchers.

#### **b) In situ methods**

Double flat jack tests intend to reproduce within an existing wall a standard compressive test [97,98]. They are regulated by the American standard ASTM C1197 [95] and the recommendations MDT.D.5 by RILEM [120].

Jurina [98], and Gregorczyk and Lourenço [97], offer a comprehensive review on this method. Two horizontal parallel slots are cut in a wall and create an isolated part of masonry between them. Flat jacks are then introduced into the slots and pressurized. The acting stresses are calculated from the pressure of the jacks and corrected by means of calibration factors that depend on the type of jack being used and the section of the slot. The masonry area between the jacks is instrumented and measurements are taken for different levels of pressure (see Figure 13). The resulting deformations allow computing the Young's modulus of masonry.

This test is powerful and versatile, and has been applied successfully to different types of masonry [97,121–124]. Nevertheless, it presents some drawbacks that may hinder its interpretation [98,121]. Among them, difficulties in calibration, and misleading measurements due to stress concentrations or to the confinement effect exerted by the lateral parts of the wall that were not isolated. Practical issues concern the applicability in low rise buildings where the upper masonry does not offer the necessary contrast, or the irreversibility of the inflicted damage. In consequence, users need to be skilled and experienced, not only to precisely interpret the test results, but to perform the tests in conditions of safety and health [125].

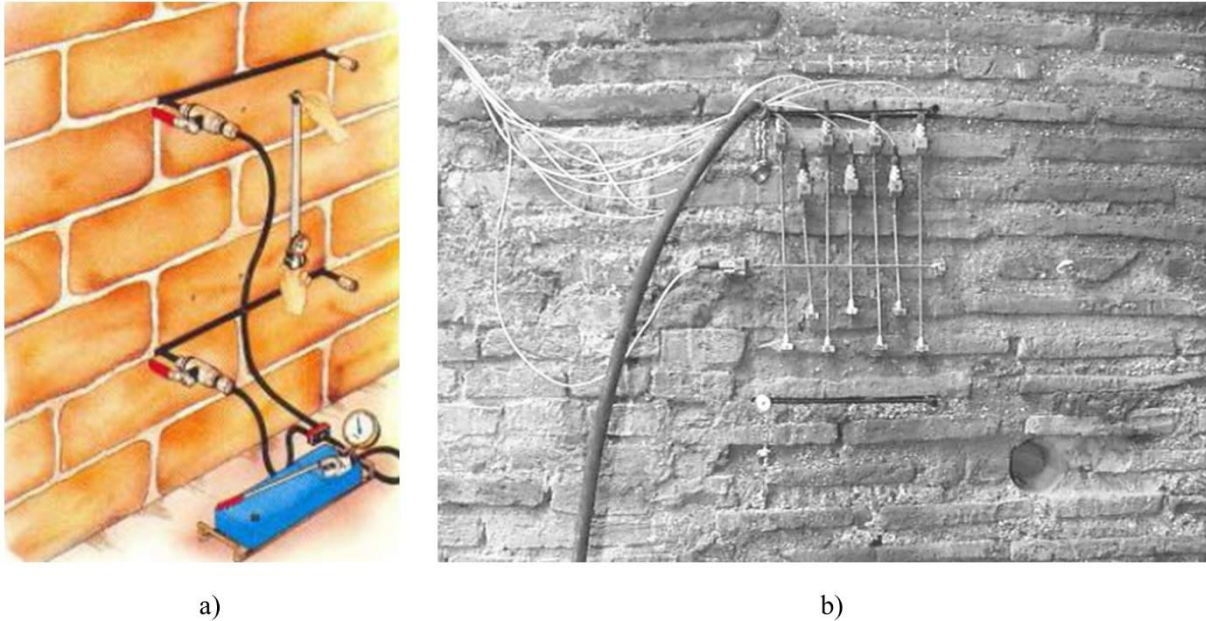


**Figure 13** a) Scheme of double flat jack test, from Jurina [98]. b) Application example on existing building by Binda and Tiraboschi [121].

The technique consisting in coring cylinders from the existing walls and testing them in laboratory may be also of application to the determination of the Young's modulus of masonry. Although the aforementioned UIC leaflet [126] does not recommend the use of these cylinders to evaluate elastic properties, some authors have attempted to find a direct correlation between the Young's moduli determined on prismatic standard compression tests and the ones found from cylinders [105,106].

### c) Derivation from other properties

In the lack of specific measurements, building codes recommend to determine the Young's modulus of masonry proportionally to the compressive strength. Nevertheless, the reliability of such approach is uncertain, given the variability in the testing procedures for Young's modulus mentioned above.

Eurocode 6 and other national European codes recommend a constant of proportionality equal to 1000 between the Young's modulus and the characteristic compressive strength [11,60,111]. Experimental researches have shown that a value of 1000 is probably too high for

existing or low strength types of masonry [127,128]. American codes have adapted this constant progressively. Older versions of codes proposed a value of 1000 [66]. ACI 530-11 recommends a ratio equal to 700 for clay masonry and equal to 900 for concrete masonry [66]. A value of 550 is suggested in FEMA 356 [129]. Furthermore, recent updates of New Zealand Guidelines for seismic assessment prescribe a ratio of 300 [130]. The latter examples show how experimental research plays a capital role in the advance of standards.

Other than in relation with the compressive strength, the Young's modulus of masonry may be derived from the elastic properties of the components [82,131]. For regularly arranged types of masonry, a one-dimensional homogenization method can be applied to estimate the Young's modulus. This type of models consider masonry as a system of series-parallel uniaxial springs that account for the interaction of units with bed and head mortar joints. Other than the severe simplification implicit within the model, this approach deals with the practical difficulties encountered to determine the Young's modulus of both units and mortar joints [132,133].

### **2.3.3. Characterisation of masonry in shear**

This section reviews the characterisation techniques available for the determination of four mechanical properties of masonry in shear: the initial shear strength and the coefficient of friction, the diagonal tensile strength of masonry, and the shear elastic modulus of masonry.

#### **2.3.3.1. Initial shear strength and coefficient of friction**

As described in Section 2.1.2, the shear response of masonry depends on multiple factors. Nevertheless, it is accepted that a key parameter in the shear resistance of a wall is the shear strength of the bed joints. It is traditionally assumed that the joint shear failure at low precompression levels can be adequately described by the Mohr-Coulomb criterion [134], as expressed in the following Equation 15:

$$\tau_u = c + \sigma \times \tan\varphi \quad (15)$$

where the ultimate joint shear strength  $\tau_u$  and the normal compressive stress  $\sigma$  are related by means of the cohesion  $c$  and the internal friction angle  $\varphi$ . In the common case of failure through the unit-mortar interface, the cohesion can be interpreted as the initial bond at zero precompression or initial shear strength  $\tau_0$ , while the tangent of the angle of friction represents the coefficient of friction  $\mu$ .

Different testing methods deal with the characterisation of the former shear parameters: initial shear strength and coefficient of friction. These methods can be classified into laboratory and in situ methods.

#### **a) Laboratory methods**

The most widespread method for determining the shear parameters of bed joints is the test of triplet specimens in shear. This method is specified by the European standard EN 1052-3 [135]. Similar methods on triplets are also recommended by RILEM [136], and other national committees (e.g. New Zealand [137]).

This method consists in testing at least nine triplet specimens in shear under four-point load, with precompression perpendicular to the mortar joints. The specimens consist of three units bonded by two mortar joints. At least three different levels of precompression are considered, with three specimens per level. The specimens are tested to failure, and the maximum shear load and the precompression load are registered. These values are used to calculate couples of data for each specimen: the individual shear strength and the normal compressive stress, which are then plotted in a graph. The line determined from a linear regression of the points provides the shear parameters: the intercept of the line with the vertical axis is the initial shear strength at zero normal stress, while the slope of the line gives the angle of internal friction [135].

The use of triplets is recommended by the standards because it is a compromise solution for a difficult challenge. Riddington et al. defined five criteria to define an adequate testing setup for shear parameters [138]. Among others, these criteria included the need of ensuring uniform distributions of normal and shear stresses along the joints, avoiding tensile stresses at any point, and keeping the setup as simple as possible. Different authors have proposed a plethora of alternatives to the triplet test [134], which presents some drawbacks that originate from the fact of having two joints that might not fail simultaneously [139–141]. Among these alternatives, testing couplet specimens seem to be more suitable to the study of the post-peak behaviour of the joints [69]. The couplet testing setups usually require however complex and very specific equipment [142–144].

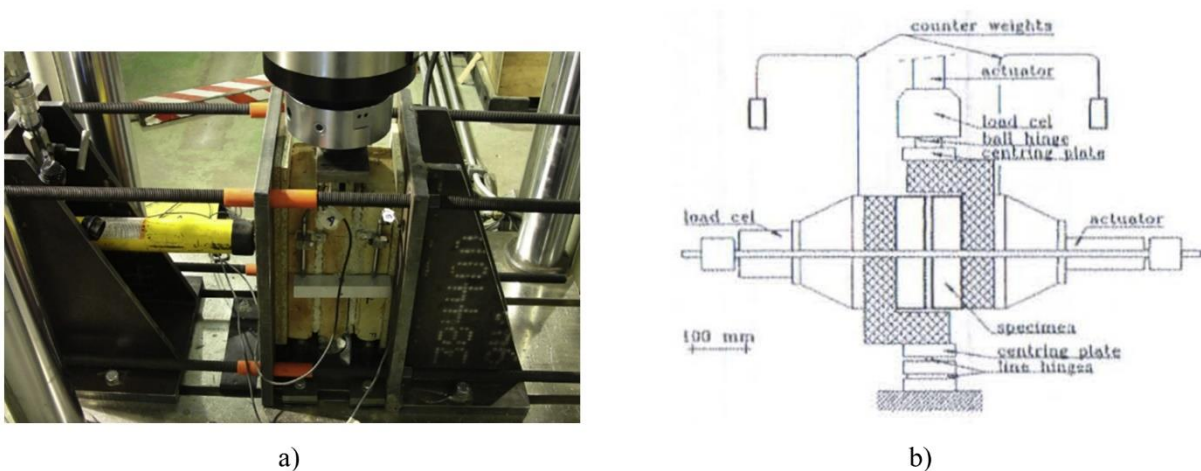


**Figure 14** a) Example of test on standard triplet specimen, from Pelà et al. [145], b) Example of complex setup for testing couplet specimens, from Van der Pluijm [144].

### b) In situ methods

Two main approaches stand as possible solutions for the shear characterisation of existing masonry: the shove test, and the core-testing method. Other secondary approaches are still under development, such as the derivation of the shear parameters from the results of diagonal tests as proposed by Calderini et al [146].

The shove test is supported by the American standard ASTM C1531-16 [147]. RILEM also published a recommendation more than two decades ago, the MS-D.6 [148], on the in situ measurement of masonry bed joint shear strength. Nevertheless, few examples of real applications can be found in literature.

Basically, the shove test consists of pushing (shoving) a brick unit that had been previously isolated by removing the two adjacent bricks. The load is applied horizontally by a jack or ram placed on one side of the brick (see Figure 15a). Before pushing, two flat jacks located above and below the selected brick impose a vertical stress to the surrounding masonry area. With the repetition of the tests under different vertical stresses, a Coulomb-type frictional relationship can be derived [149] to obtain the shear parameters. Recent works have been carried out by different authors to delve into the procedure and interpretation of this type of test [149,150]. These works aimed to better understand some uncertainties related to the shove test, such as the actual vertical compressive stress acting on the tested brick, or the role played by dilatancy.

The core-testing method proposes to drill masonry cylinders from the existing walls and test them in laboratory. The differences with the tests in uniaxial compression described in previous sections are the load application, and the orientation of the cylinders with respect to the load. In this case, cylinders are subjected to Brazilian or splitting tests, and bed joints are not oriented horizontally. Instead, cylinders are rotated and tested with different inclinations with respect to the load (see Figure 15b and c). The vertical load can be then decomposed into normal and tangential components with regard to the bed joint, and used to calculate the normal compression stress and the tangential shear stress in the joint. These couples of values allow the derivation of the shear properties by application of the Mohr-Coulomb failure criterion. Pelà et al. [145,151,152], and Mazzotti et al. [153], have investigated the correlation between this approach and laboratory standard tests. More recently, Jafari et al. evaluated the possibilities of

these tests to assess the nonlinear shear-sliding behaviour of the interface after failure [154]. No specific standard covers this inspection method, except of a recommendation in the New Zealand guidelines that includes a simplified version of this test among the available characterisation methods [137].

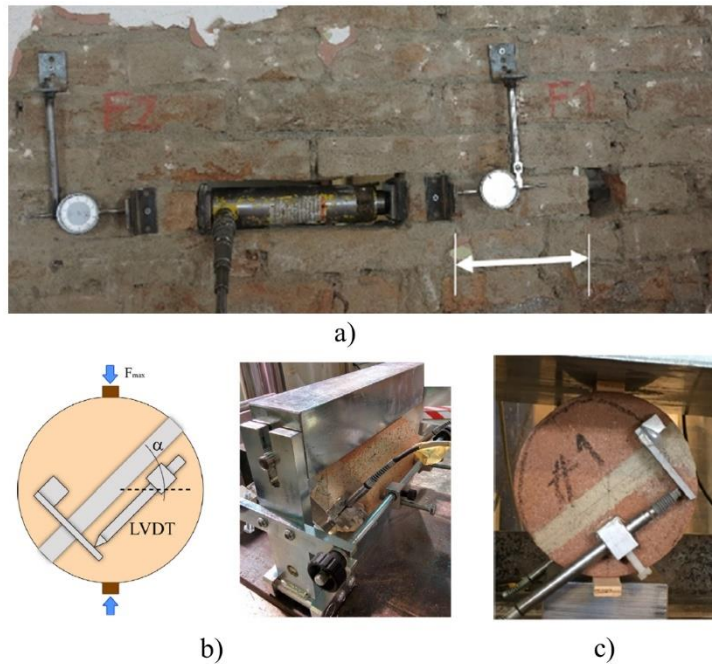


**Figure 15** a) Example of in situ shove test from Ferretti et al. [155]. b) Scheme and example of Brazilian test on cylinders from Marastoni et al. [151]. c) Example of test on cylinder from Jafari et al. [154].

### 2.3.3.2. Diagonal tensile strength of masonry

Section 2.1.2. described diagonal cracking as one of the possible failure modes of masonry walls subjected to shear. This failure is a recurrent response found after seismic events. Diagonal compression tests constitute an attempt to replicate this type of loading in laboratory or in situ.

The American standard ASTM E519 [156] is the main reference that regulates the procedure and interpretation of the diagonal compression test. RILEM also issued a recommendation, LUMB6 [157], which gives very similar provisions. Some other national

standards are direct translations of the ASTM E519, such as the one from Guatemala [158], or incorporate specific details as the Chilean norm NCh 2123 [159].

The procedure consists in applying a compression load to a square panel at two diagonally opposite corners. This load eventually causes the panel to split by tensile stresses around the centre of the panel, and to open through a diagonal crack that tends to connect the loaded corners. The common procedure suggested by ASTM E519 is to place the panel in vertical position inside a test machine (Figure 16a). An alternative consists in placing the wall with one of its sides supported horizontally, and apply the diagonal load by means of a system of tensed bars and jacks. The latter is suitable to be applied in situ to characterise existing masonry walls (Figure 16b and c). With regard to the panels size, ASTM E519 [156] recommends to use panels at least 1200 mm wide, while NCh 2123 [159] allows using smaller panels at least 600 mm wide. RILEM recommendation LUMB6 [157] sets the panel size in relation to the length of the units. It prescribes to use panels at least four units wide.

The main outcome of these tests is the maximum diagonal load attained before failure. This load can be related with the dimensions of the panels to determine the diagonal tensile strength of masonry. Nevertheless, the interpretation of this result is not univocal yet. ASTM E519 defines this parameter as shear strength of masonry, and proposes its calculation under the assumption of considering a pure shear stress state within the panel [156]. Other authors, based on the seminal works by Frocht on photoelasticity [160], have dismissed this assumption, and propose other formulae for the interpretation of the diagonal test results [161,162]. Regardless of this disagreement, the diagonal compression test is widely used in real inspections [163,164] and in research [165–168], notably in the assessment of strengthening solutions (Figure 16d). In addition, it is especially suitable for the characterisation of the behaviour of irregular

masonry walls, which do not present evident sliding planes through regular horizontal bed joints [146].

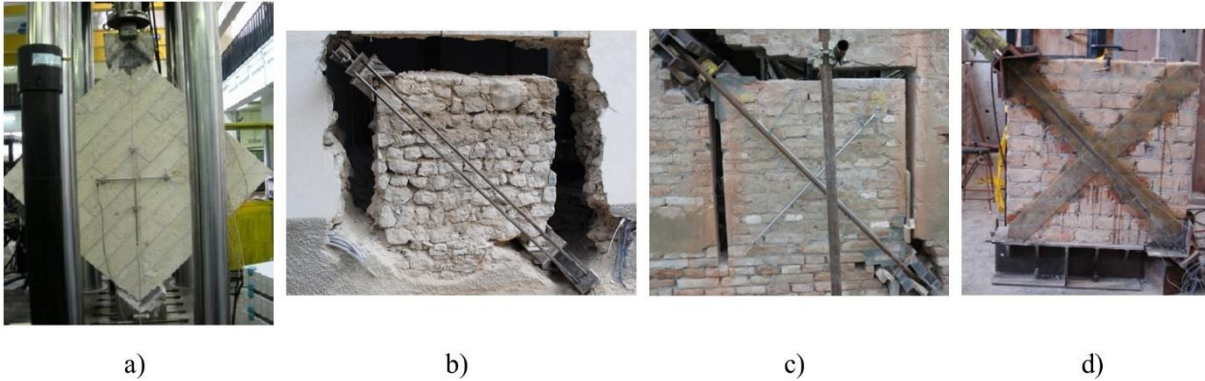


**Figure 16** Examples of diagonal compression tests. a) Test in vertical position by Parisi et al. [169] b) and c) In situ tests, from Borri et al. [164] and Ferretti et al. [155], respectively. d) Test on a strengthened wall by Mahmood and Ingham [165].

Another test that allows the determination of the diagonal tensile strength of masonry is the shear compression test or racking test. Within this test, a vertical load is constantly applied to introduce a precompression into the wall, which is also fixed to the ground. Then, the wall is pushed or pulled at its top and is subjected to shear. Turnšek and Čačovič defined a criterion that correlates the failure shear stress with the precompression stress by means of the diagonal tensile strength of masonry [170]. The drawbacks of this type of test are the lack of regulations or standard procedures, the difficulties encountered to properly apply the loads and the boundary conditions [171], and the difficulties to control the actual mode of failure [165].

### 2.3.3.3. Shear elastic modulus of masonry

The shear elastic modulus is defined as the ratio of shear stress to shear strain, and it is a key parameter in the derivation of the structural stiffness of masonry elements. Being a parameter that describes the deformability of the structural element, its definition is greatly affected by the anisotropy of the material. However, all the existing current characterisation methods rely on the application of simple analytical expressions that are based on an isotropic

behaviour of the material. Furthermore, no standardized method exists for the determination of this parameter. In the following, three available methods are described [172,173]: one of them provides a direct estimation of the shear modulus while the other two can provide only an indirect estimation.

The diagonal compression test presented in the previous section according to ASTM E519 [156] is also used to determine the shear elastic modulus together with the diagonal tensile strength. The loads applied within this test subject the masonry panel to a shear stress state. Within this state, it is possible to directly determine the acting shear stresses and the corresponding shear strains. The shear strains can be calculated from the uniaxial strains measured along the compressed and the tensed diagonals of the wall [156,157]. Consequently, the shear elastic modulus can be directly evaluated from the shear stress – strain curves obtained with these tests. The drawbacks of this procedure are the initial assumption of isotropy to define the state of stresses, and the disparity within the research community about the best procedure to determine the acting stresses.

The two alternative methods are based on higher simplifications. The first possibility is using the results of compression tests to determine the shear elastic modulus. With a compression test, either a standard one in laboratory on prismatic samples, or the double flat jack test applied in situ, the Young's modulus  $E$  and the Poisson's ratio  $\nu$  of masonry can be obtained. These two elastic parameters may be correlated with the shear elastic modulus  $G$  by means of the following relationship presented in Equation 16:

$$G = \frac{E}{2(1 + \nu)} \quad (16)$$

Other than the assumption of isotropy necessary to apply the former equation, this method is influenced by the possible inconsistencies in the determination of the Young's modulus, and,

especially, of the Poisson's ratio. The transversal strains needed to compute the Poisson's ratio usually require highly precise instruments to be measured. Further issues, as the proper location of these instruments, may also affect the results [172].

The second possible alternative is using shear compression tests on masonry panels. These tests, also described in the previous section, provide as main outcomes the shear force at the top of the wall and the corresponding horizontal displacement at the top of the wall. These two results allow the experimental computation of the elastic stiffness of the structural element,  $K_e$ . This stiffness depends, according to the theory of elasticity, on the mechanical properties of the material, the geometry of the element, and the boundary restraints [172]. Equation 17 displays the relationship of the elastic stiffness with the rest of parameters:

$$K_e = \frac{GA}{1.2h \left[ 1 + k' \frac{G}{E} \left( \frac{h}{l} \right)^2 \right]} \quad (17)$$

where  $k'$  is a coefficient which accounts for the applied restraint conditions,  $h$  and  $l$  are the height and length of the wall respectively, and  $A$  is the area of the wall section [172]. The derivation of the shear elastic modulus with this approach faces the inaccuracy associated to the testing setup, the determination of the Young's modulus, and the simplification of Equation 17.

Croce et al. [173] compiled a database of shear elastic modulus values for different types of masonry, which included results from the three types of tests described above. They found a huge variability within the distinct methods and highlighted the need of proposing a harmonized method.

### 2.3.4. Summary of characterisation procedures

The previous sections have briefly compiled the existing methods to characterise the selected properties. Table 3 summarizes the existing tests for each mechanical property, and indicates the main encountered needs for each them. In this thesis' context, a need refers to a test feature that presents uncertainties or inconsistencies, and probably requires further investigation to be better defined. In general, the encountered issues are related to the size of the specimen and the boundary conditions in the case of strength properties, and related to the loading protocol and instrumentation in the case of elastic properties. In most cases, uncertainties with regard to the interpretation and post-processing of results have been detected. Table 3 also includes the corresponding standards and norms that regulate each test, and highlights the lack of standardization in some instances.

**Table 3** Main encountered needs for the different types of test investigated, classified by mechanical property and by test feature. Last column indicates the corresponding standard if applicable.

Property and test	Test features					Standard
	Geometry of specimen	Boundary conditions	Loading protocol	Instrumentation	Post-processing	
<b>Compressive strength</b>						
- Tests on prismatic specimens	1	--	--	--	--	ASTM C1314, EN 1052-1
- Flat jack test	--	--	--	--	2	3
- Core testing	4	--	--	--	5	UIC Leaflet 778
<b>Young's modulus</b>						
- Tests on prismatic specimens	--	--	6	7	8	ASTM C1314, EN 1052-1
- Flat jack test	--	9	--	10	11	ASTM C1197, RILEM MDT D.5
- Core testing	12	--	13	14	15	16
<b>Initial shear strength and coefficient of friction</b>						
- Standard triplet	17	18	--	--	19	EN 1052-3, RILEM MS B4
- Shove test	--	20	--	--	21	ASTM C1531, RILEM MD-D6
- Core testing	--	22	23	--	--	24
<b>Diagonal tensile strength</b>						
-Diagonal compression test	25	--	--	--	26	ASTM E519, RILEM LUMB6
- Racking test	--	27	--	--	28	29
<b>Shear elastic modulus</b>						
- Diagonal compression test	--	--	30	31	32	33
- Compression tests	34	--	--	35	36	37
- Racking test	--	38	--	--	39	40

## Notes:

1. Possibility of testing stack bond prisms and small running wallettes.
2. Difficulties in the interpretation of the actual stresses.

3. Existing standards cover the determination of the stress level and of Young's modulus, but are not specific to compressive strength.
4. Possibility of testing cylinders of different diameters.
5. Doubts in the area to be considered to compute the actual stresses.
6. Inconsistencies between standards about the cycles to be performed.
7. For elastic parameters, the decision of how many joints have to be covered by the instruments is capital.
8. Inconsistencies in the definition of the type of modulus: secant or tangent.
9. Results affected by the surrounding masonry conditions.
10. See Note 7.
11. Difficulties in the interpretation of the actual stresses.
12. Possibility of testing cylinders of different diameters.
13. Need to define the loading cycles to be performed.
14. See Note 7. Doubts on instruments placement.
15. See Note 5.
16. Existing UIC Recommendations do not consider the determination of Young's modulus.
17. Some authors propose to use couplets.
18. Difficulties to ensure an adequate distribution of stresses.
19. Interpretation issues when joints do not fail simultaneously.
20. Uncertainties with regard to the acting stresses.
21. Difficulties in the interpretation of the actual stresses.
22. Need to have cylinders with intact joint to study the initial shear strength.
23. Number of specimens and different orientations to be investigated have not been defined yet.
24. Other than a recommendation in the New Zealand guidelines, there is no official standard.
25. Possibility of testing panels of different sizes.
26. Uncertainties in the definition of the acting stresses.
27. Difficulties to control the actual boundary conditions.
28. Indirect determination through the Turnšek and Čačovič criterion.
29. No standard is available.
30. See Note 13.
31. See Note 7.
32. See Note 26.
33. See Note 3.
34. See Note 1.
35. See Note 7.
36. Doubts in the applicability of the elastic relationship with Young's modulus and Poisson's ratio.
37. No standard is available.
38. See Note 27.
39. Doubts in the applicability of the elastic relationship with the geometrical and material properties of the panel.
40. No standard is available.

## 2.4. Replication of historical-like masonry in laboratory

### 2.4.1. General aspects

As continuously highlighted along the previous sections, the diagnostic activity and characterisation of mechanical properties in existing masonry structures are not exempt of difficulties. Furthermore, in some cases, the inspection procedures may be not compatible with the conservation status of the cultural asset. In other cases, the budget may be limited and could be better devoted to the retrofitting intervention.

At these instances, it is essential to have available reference parameters to be adopted for different masonry types [63]. Building codes attempt nowadays to provide reference values for the characteristics of different masonry typologies, and adapt these values to their regional or local features. A well-known example is the table C8.5.I included in the Italian Circolare [62]. This table provides reference ranges of the basic mechanical parameters for different types of masonry, such as regular stone masonry, solid clay brick masonry or rubble masonry, among others. Similar tables may be found in other codes. In the case of European norms, individual countries may undertake characterisation campaigns to define their own regional values.

In view of the impossibility of performing extensive campaigns on real buildings, research groups investigate the behaviour of historical-like types of masonry that have been reproduced or replicated in laboratory. Usually, this approach combines the aim of investigating local types of masonry, with a primary or secondary scientific goal related, for instance, with strengthening techniques, testing procedures, or analytical considerations.

The approach of investigating replicated historical-like masonry may be a debatable issue, especially because of the effects of ageing and decay that are difficult to be taken into account. Nevertheless, studies on replicated historical-like masonry are very common and cover a great range of possible material combinations. As a matter of fact, research examples span from attempts to reproduce ancient Roman masonry [174] to studies on modern Dutch walls [175], from tests on regional varieties of Spanish masonry [176] to India [79] and New Zealand [177], or from irregular stone multi-leaf masonry used to build houses [178] to regular brick masonry used to build bridges [179].

The replication of historical-like masonry requires the careful choice of the material components. This choice is easy in the case of the units, given that recycled units can be used obtained directly from existing buildings or demolition stocks [180]. E.g. the research group of

the University of Auckland is experienced in recover vintage solid clay bricks to perform experimental campaigns [165,177,181]. Otherwise, stone units can be obtained from the same or similar local quarries from where the historical blocks were cut [176,178]. In the case of bricks, local manufacturers can produce them with manual procedures that imitate the traditional ones [179]. Regarding mortars, the choice of the material is not straightforward. Nowadays, it might be technically possible to determine the mineralogical, chemical and physical properties of a given existing mortar [182–184]. However, the strength of the mortar, as well as the bond between the units and the mortar, require time to develop. This fact is especially true in the case of lime-based mortars, which would need years to harden. Given that time is a limited resource for researchers, mortars that incorporate small amounts of cement or hydraulic lime in their compositions are preferred [176].

#### **2.4.2. Structural masonry in the city of Barcelona**

Similarly to the examples exposed in the previous paragraphs, this thesis also combines the main scientific goal of improving the characterisation techniques of masonry with the investigation on a local type of masonry. The experimental campaigns required to fulfil the main goal are performed on a type of masonry that is common of the city of Barcelona: solid clay brickwork, built with lime-based mortar.

This section describes the general features of this masonry typology. The need of this investigation is justified in the light of the several works and theses that have been published during the last two decades on the seismic performance of typical buildings of Barcelona [185–194]. These works applied advanced analysis tools to assess the seismic vulnerability, which resulted to be high for certain instances. As the city is located in a low to moderate seismic hazard area, its buildings were built traditionally without any seismic consideration. The values

of material properties found during the present thesis would contribute to increase the accuracy of future studies about the buildings of Barcelona.

#### **2.4.2.1. Historical perspective**

Given the availability of local stone from surrounding quarries, the traditional architecture of Barcelona consisted of buildings that combined stone masonry with timber elements [195], while ceramic pieces were only used for vaults. By the end of the 18th century, clay bricks started to be used also in load bearing walls. Progressively, its use increased along the 19th century to become the prevailing building material in the city [196], as the low old stone houses of Ciutat Vella district transformed into the tall new buildings of the Eixample district. These buildings, which according to Paricio constitute the defining construction system of Barcelona [197], consisted mainly of load bearing walls made of brickwork combined with other elements: stone foundations, metallic supports in the ground floors, and beams with ceramic tile vaults in between to create the slabs (see Figure 17a). The beams material changed along the years from timber to steel to concrete.

This evolution is not an exclusive feature of Barcelona. The replacement of stone by bricks is profusely reflected in historical books and construction manuals consulted for this thesis [198–203]. These books, dating from 1763 to 1927, highlight the use of bricks from the Babylonian and Roman antiquities to their time, and praise their advantages where stone quarries are not available. In 1859, Espinosa underlines the extensive use of bricks in Spain, but also in England, Belgium, France, Germany and Italy. Espinosa also mentions the appearance of certain machines in the USA that facilitate the production of bricks [200]. This feature, the possibility of being produced at will in bulk quantities, was key in the spreading of bricks as building material, because it allowed satisfying the huge need of building factories and inexpensive housing encountered in the industrialised countries [204].

In Barcelona, the rise of bricks goes also hand by hand with the city's evolution. The demolition of the medieval walls, and the subsequent development programme by Cerdà in the second half of the 19<sup>th</sup> century, motivated the creation of the Eixample district. As mentioned, load bearing walls made of brickwork were the distinctive elements of the new buildings. In addition, brick masonry was also used in singular constructions and, especially, in factories (Figure 17b, c, d), the industrial facilities that symbolised the progress of the city [205,206]. As a result of the massive use of clay bricks and lime during those years, 70 % of all the current buildings of the Eixample district of Barcelona are made of unreinforced masonry [188].

#### **2.4.2.2. Materials and bond**

Paricio made a thorough study about the construction system in the Eixample of Barcelona from an architectural point of view [197,207]. With respect to the bricks, Paricio provided two important data. The standard dimensions of the typical solid bricks used in Barcelona were 300 (length) × 150 (width) × 50 (thickness) mm<sup>3</sup>, with slight variations depending on the manufacturer. The local industries producing bricks were called 'bòbiles', and were located within the boundaries of the city but also in the surrounding areas. The demand of material was so high, that, for instance, up to 20 bòbiles existed simultaneously only in the Corts district [208]. The second relevant data provided by Paricio is the year 1920 as the approximated date that limits the production of bricks into two types: before 1920, manual production with traditional kiln, resulting in heterogeneous dimensions and qualities; and, after 1920, mechanical production with the introduction of extrusion and Hoffman kilns, resulting in more homogeneous products.

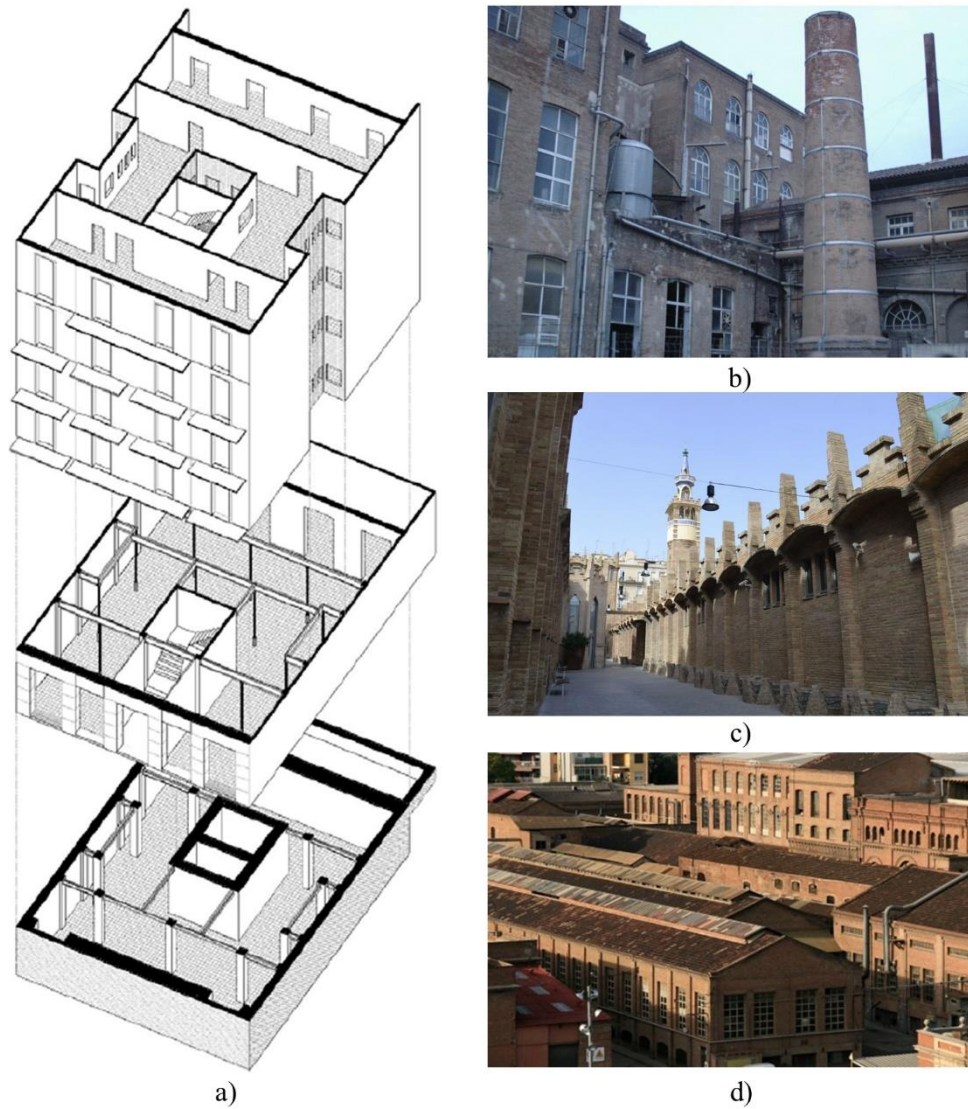


**Figure 17** a) Axonometry by Paricio [197] of a typical rectangular building of the Eixample district in Barcelona. b), c) and d) Singular examples of industrial facilities of Barcelona made of brickwork: Fabra i Coats factory, Casaramona factory, and Can Batlló complex, respectively.

It is important to note the dimensions of the bricks as a peculiarity of the historical masonry of Barcelona and Catalonia. In a comprehensive thesis about the architecture in Barcelona at the end of the 18th century, Rosell [195] includes details of personal documents written by an architect of the city, Josep Renart. In one of these manuscripts, Renart describes the bricks in the year 1810 as being of dimensions  $1\frac{1}{2} \times \frac{3}{4} \times \frac{1}{4}$  palms. Given that the Catalan palm measures approximately 200 mm, these dimensions are consistent with the ones described by Paricio

[197]. These bricks were consistently larger than those used in other parts of Spain and Europe [200,203]. This peculiarity is even reflected in the first Spanish code devoted to masonry, PIET-70 [73], that differentiated two basic types of bricks: Castilian bricks of  $240 \times 115 \times 52.5 \text{ mm}^3$  and Catalan bricks of  $290 \times 140 \times 65 \text{ mm}^3$ .

With respect to mortar, Paricio describes an extensive use of the traditional aerial lime up to approximately 1910 [197]. Depending on the finality, the mortar proportioning varied from two to three parts of sand to one part of lime [207]. From 1910 on, hydraulic binders such as hydraulic lime and Portland cement started to be used. The appearance of hydraulic limes constituted a qualitative advance, although workers were reluctant to abandon their tradition in aerial limes. Hydraulic limes seem however to have been preferred for ground and first floors. The prevailing use of aerial lime mortar described by Paricio is consistent with the common practice reflected in the historical manuals [198–203].

One last aspect should be considered to define the features of the typical historical brickwork of Barcelona. According to Paricio [197], no bond pattern was preferred, provided that workers followed “good practice rules”. In the aforementioned books, different bond patterns were included as general possibilities: English bond pattern, Flemish bond pattern, Spanish bond pattern... To our knowledge, no study has been made yet to define the prevailing bond patterns in the city of Barcelona.

### **2.4.2.3. Mechanical properties**

Up to date, the work presented by Cornadó constitutes the most comprehensive attempt to study the mechanical behaviour of the historical buildings in Barcelona [196]. With regard to the load bearing brickwork, Cornadó provides data from two interesting and different sources.

The first source are the tests performed before 1950 by the architect Joan Bergós, in the laboratory of the Universitat Industrial de Barcelona. This laboratory had been inaugurated

around 1920, and constituted a powerful novelty in the emerging science of materials characterisation. Bergós tested different types of masonry with different mortars. Results are included in the following Table 4. Nevertheless, they are hardly comparable to results obtained with current standards.

**Table 4** Results obtained by Bergós in the laboratory of the Universitat Industrial de Barcelona before 1950 [196].

Material	Compressive strength (MPa)
Brickwork made of hydraulic lime mortar 1:3	6.42
Brickwork made of gypsum mortar	7.87
Brickwork made of fast hardening cement 1:3	8.32
Brickwork made of slow hardening cement 1:3	8.36
Brickwork made of Portland cement 1:3	11.7

The second source provided by Cornadó are the results from tests performed on masonry specimens extracted from 15 real buildings in Barcelona [196]. These tests were carried out between 1995 and 2015 at the Laboratory of Materials of the Escola d'Edificació of the Universitat Politècnica de Catalunya. Cornadó proposed an average value for the compressive strength of 6.5 MPa. No more relevant data are given, except two isolated measurements of Young's modulus, which averaged around 1200 MPa.

The rest of works mentioned at the beginning of 2.4.2. did not provide experimental data. These works directly presented the values used in their models, which are displayed in Table 5. The values in the table come from undefined technical reports and the engineers' expertise.

**Table 5** Summary of mechanical properties used by different authors in the seismic assessment of Barcelona buildings.

References	Mechanical properties
Bonett [185]	$E = 2100 \text{ MPa}$ , $G = 700 \text{ MPa}$ , $\tau = 0.1 \text{ MPa}$
Moreno-González [186]	$E = 1800 \text{ MPa}$ , $G = 300 \text{ MPa}$ , $\tau = 0.12 \text{ MPa}$ , $f_c = 4 \text{ MPa}$
González-Drigo et al. [190,191]	$E = 2650 \text{ MPa}$ , $G = 589 \text{ MPa}$ , $\tau = 0.08 \text{ MPa}$ , $f_c = 2.65 \text{ MPa}$
Pujades et al. [189,193]	$E = 1800 \text{ MPa}$ , $G = 300 \text{ MPa}$ , $\tau = 0.2 \text{ MPa}$ , $f_c = 1.8 \text{ MPa}$

## 2.5. Summary

This chapter has presented the framework of this thesis. By means of short reviews on different aspects, this literature review has served to narrow the scope and set the main objectives described in the following Chapter 3.

First, the mechanical behaviour of masonry has been briefly described. Masonry is a composite and complex material, whose behaviour is influenced by the individual properties of the components and their interaction, but also their relative dimensions, arrangement, and the loading and boundary conditions. Relevant features of masonry are its ability to withstand compression, its anisotropy, its complex response to shear actions, and its variability.

Section 2.2. has covered the mechanical characterisation needs encountered in the structural analysis of masonry. This section has reviewed the different modelling strategies and the building code provisions. Overall, two levels of detail define the required mechanical properties: strategies that consider the microscale and require to know the properties of components and their interaction, and strategies that consider the macroscale and consider masonry as a composite and homogeneous material. The latter is reflected in the strength criteria provided in common building codes. Six mechanical properties of the composite material have been identified as the most relevant to perform structural analysis of masonry:

the compressive strength, the Young's modulus, the initial shear strength, the coefficient of friction, the diagonal tensile strength, and the shear elastic modulus.

Section 2.3. has reviewed the possibilities of experimental characterisation procedures that apply for the aforementioned properties, both in laboratory and in situ. The main issue with respect to the characterisation of masonry is that of representativeness. This section has defined a series of features to be analysed for each testing procedure: geometry of the specimen, boundary conditions, loading protocol, instrumentation, and post-processing. Research needs have been identified for the different tests. In general, tests characterising strength properties present issues related to the size of the specimen and the boundary conditions. The loading protocol and the instrumentation are more relevant in the case of determining elastic properties. Uncertainties related to the interpretation and post-processing of results have been detected in most cases.

Finally, Section 2.4. has investigated the traditional and most relevant type of masonry of the city of Barcelona, which has been identified as solid clay brick masonry made of lime mortar. One of its particularities is the size of the bricks, which are of dimensions  $300 \times 150 \times 50 \text{ mm}^3$ . This type of masonry is in need of further and comprehensive characterisation, given that only partial studies have been performed until now. A better understanding of the mechanical properties would increase the reliability of the structural assessments carried out on existing buildings of the city.

*This page is intentionally left blank.*

**Objectives and methodology**

*This page is intentionally left blank.*

### 3.1. Objectives

As defined in Chapter 1 Introduction, the global scope of this thesis is the critical analysis of the current procedures for the characterisation of masonry, and the contribution with possible improvements applicable to a specific type of masonry.

In agreement with the research needs described in Chapter 2 and summarised in Table 3, a set of specific objectives have been defined for the thesis. These objectives are:

- To critically analyse the following testing techniques:
  - Standard tests on masonry prisms for the determination of compressive strength and Young's modulus.
  - Tests on cylinders extracted from masonry walls for the determination of compressive strength and Young's modulus.
  - Standard tests for the determination of the shear mechanical properties of the bed joints.
  - Standard test for the determination of the diagonal tensile strength of masonry.
- To investigate the size and shape effect of the tested specimens on the results of the abovementioned testing techniques.
- To investigate the influence of the performance of loading cycles on the determination of compressive strength. To study the suitability of performing initial loading cycles to determine elastic properties.
- To carry out experimental campaigns on real buildings to characterize the mechanical behaviour of the typical brickwork of Barcelona.

- To select the appropriate material components for the replication of historical-like masonry in laboratory. To compare the results obtained in the replicated masonry with those obtained in real existing masonry.
- To check the accuracy of available analytical and empirical expressions for the determination of the mechanical properties of masonry.

## **3.2. Methodology**

The methodology applied to fulfil the objectives of the thesis has been as follows:

- An initial literature review –presented in Chapter 2- allowed detecting the potential needs of research with respect to the mechanical characterisation of masonry. This review served to select the testing techniques to be analysed and to select the type of masonry that was going to be used during the experimental campaigns.
- The first experimental step consisted of defining the masonry to be used, with the choice of suitable bricks and an appropriate mortar. The selection of the mortar motivated a whole and independent experimental campaign that studied the influence of limestone filler additions on the behaviour of hydraulic lime mortars. This investigation had as a result the Paper I included in Chapter 4.
- The type of masonry previously defined was used to carry out the experimental campaigns that investigated the individual testing techniques. Three independent campaigns were performed: one in relation with the standard compression tests on prismatic specimens, one in relation with the standard shear test on triplets, and one in relation with the standard test under diagonal compression. These campaigns resulted in Papers II, IV and V, respectively. These papers are included in Chapters 5 and 6.

- An additional experimental programme was performed on existing buildings of the city of Barcelona. The campaign investigated the nonstandard compression tests on cylinders, and also served to characterise examples of real existing masonry. The results were organised in Paper III included in Chapter 5.
- The phases that constituted each one of the former four experimental campaigns consisted of:
  - Preparation of a specific state of the art review to detect the research needs.
  - Design of the individual campaign according to the needs.
  - Performance of the laboratory tests. These tests were performed on specimens built in the laboratory in all cases, and on specimens extracted from real buildings in the case of Paper III.
  - Analysis of the results.
  - Comparison of the results with databases and analytical expressions.
  - Drawing of conclusions.
- Once all the experimental campaigns were completed and the papers were prepared, they were organised into this document. Papers dealing with compression were included in Chapter 5, while papers dealing with shear were included in Chapter 6. Each chapter incorporated also a brief section to discuss the ensemble of results.
- Finally, global conclusions are drawn, with respect to the mortar used to replicate the historical-like type of masonry, to the new findings on the characterisation tests, and to the mechanical properties of the traditional brickwork of Barcelona.
- The last step of this research was the proposal of future lines of work, in the light of the overall results.

*This page is intentionally left blank.*

**4**

**Materials**

*This page is intentionally left blank.*

## **4.1. Introduction**

This chapter briefly presents the different materials used during the experimental campaigns of Chapters 5 and 6.

Section 4.2 and Section 4.3 describe the units and the types of mortar, respectively, which constitute the investigated masonry specimens. Section 4.4 presents additional materials that have been used on the contact surfaces between masonry specimens and the loading machines.

The definition of the mortar to be used for building the masonry specimens required a preliminary research on commercial hydraulic lime mortars. This research explored the possibilities of reducing their strengths by adding limestone filler. It is the base of the first paper of this thesis, Paper I, which is reproduced in Section 4.5.

## **4.2. Units**

### **4.2.1. Units used to replicate historical-like brickwork**

As described in Section 2.4.2.2., units that were characteristic of the brickwork used in Barcelona during the 19<sup>th</sup> century and the beginning of the 20<sup>th</sup> century were handmade solid clay fired bricks, with approximate dimensions of  $300 \times 150 \times 50 \text{ mm}^3$ .

With the aim of replicating in laboratory this type of historical masonry, different brick manufacturers were contacted to obtain bricks of similar characteristics. Bricks produced by the company Terra Cuita Piñol Pallarés SL were finally selected. These bricks have average dimensions of  $311 \times 149 \times 45 \text{ mm}^3$ .

This company, settled in the province of Tarragona, Spain, has kept the traditional way of producing bricks for generations. The only mechanized process in the whole production

sequence is the mixing of the raw materials. After that, bricks are moulded one by one by pouring the clay paste into a wooden mould. This process is carried out in a big protected area with no walls, which favours air circulation and the first stage of drying. The floor in this area is covered with sand to avoid bricks getting stuck. This sand eventually remains on the surface of the bricks. Then, bricks are handled individually and placed carefully inside a traditional kiln that still burns firewood.

The manual process reflects into at least three important features of these bricks:

1. Dimensions among bricks are not constant, especially with regard to thickness. Within the individual brick, thickness is neither constant and it is greater towards the edges.
2. Even if all the brick faces are rough, the face that was casted against the sand of the floor presents a rougher surface.
3. The firing of the bricks depends on their position within the kiln. Some of them may be overbunt, while the ones far from the fire will be less burnt. This fact is reflected in the colouring of the bricks and was well known by ancient masons. It was common practice to devote the imperfect bricks to non-structural parts of the buildings. Within this research, imperfect bricks were disregarded.

The three former features contribute to increase the variability in the properties of these bricks. This fact could be not desirable for a scientific research given that the experimental results reflect the variability and may hinder the drawing of conclusions. However, this variability contributes to increase the representativeness of the obtained results as they better simulate the scattering found in real existing masonry structures.

Bricks from Terra Cuita Piñol Pallarés SL have been used for building masonry specimens in the four experimental campaigns presented in Papers II, III, IV and V. Their mechanical properties are described within those papers, including values of compressive strength, flexural

strength, tensile strength and Young's modulus. Additional information about their physical and chemical properties will be available soon from an ongoing research that is carried out by the research group of Escola de Camins at UPC and performed by Albert Cabané and coworkers.

#### **4.2.2. Other units**

Other units used in this thesis are described in the following paragraphs.

In Paper III (see Section 5.3), three existing buildings of the city of Barcelona were inspected, including two residential buildings from 1840 and 1930, and one textile factory built in 1910-1920. Bricks and masonry cylinders were extracted. In all cases, the bricks belonged to the investigated type: handmade solid clay fired bricks, with dimensions close to the standard  $300 \times 150 \times 50 \text{ mm}^3$ .

Paper IV (see Section 6.2) studies the determination of the cohesion and friction of bed joints. Other than the type of masonry built with handmade bricks provided by Terra Cuita, a second type of masonry was studied to duplicate the available results and increase the research significance. This second type of masonry was built with modern solid bricks, obtained by extrusion. The aim was to compare the results obtained on these bricks with smooth faces, with the results from the handmade bricks that had rough faces. The dimensions of these bricks are  $270 \times 127 \times 51 \text{ mm}^3$ .

## 4.3. Mortars

### 4.3.1. Mortar used to replicate historical-like brickwork

As described in Section 2.4.2.2., historical mortars in Barcelona were produced with aerial lime, sand, and water. From 1910 on, hydraulic lime and Portland cement started to be used as well.

When planning an experimental programme in laboratory, it is essential to count on the time that mortars need to set and harden. This time is especially long in the case of aerial lime, and it explains why research on masonry built with aerial lime in laboratory is so scarce [75,145,180]. In the context of this work, it was preferred to use a hydraulic lime based mortar that would reduce the hardening times and would reduce the global times of the programme. In current research projects, it is common to rely on the support of different material suppliers that provide industrially prepared commercial products. These products present the advantage of having less variable properties, and they are easy to prepare on site. Nevertheless, these products may reach strengths higher than the ones supposed for historical mortars. This issue has been encountered in several occasions by other researchers [209,210], and motivated a preliminary research that is presented as Paper I in Section 4.5.

The practical justification of Paper I is to find a hydraulic lime based mortar that hardens sufficiently fast but keeps a low strength. This objective was achieved by adding limestone filler to the commercial premix. The scientific goal was therefore to investigate the influence of limestone filler additions on the mechanical behaviour of commercial premixed hydraulic lime mortars. It was found that strengths could be maximized with a certain amount of filler. Beyond that point, strengths decreased as required for this thesis. More interestingly, the strengths seemed to be kept constant as the hardening reactions stopped after 28 days. This fact

is very convenient for research purposes. It allows having more freedom in planning experimental campaigns as a greater time window is available.

The finally used mortar consists of a mix of water, limestone filler, and a commercial premix containing NHL 3.5 hydraulic lime and inert aggregates provided by the company Kerakoll. This mortar corresponds with the mix defined in Paper I as mortar MD. The proportioning is 1:1:0.65 in volume – premix to filler to water. Samples of this mortar are characterised along Papers II, IV and V. Average mechanical properties after 28 days are 0.71 MPa and 1.93 MPa for flexural and compressive strengths respectively.

#### **4.3.2. Other mortars**

Other than the main type of mortar used in the experimental programmes of Papers II, IV and V, two additional types of mortar were used to build masonry specimens for this thesis.

In Paper III, masonry cylinders extracted from walls built in laboratory were tested. These walls were built with the handmade Terra Cuita bricks but with an aerial lime based mortar. The walls had been built in the context of an experimental programme previous to the work of this thesis by Kasioumi et al. [106,145]. It is important to note that Kasioumi et al. investigated the compressive strength of the mortar by means of double punch tests (DPT). They obtained an average strength of 0.91 MPa after one year from the construction of the walls. In Paper III, the investigated mortar was tested after two years from the construction of the walls, yielding an average strength by DPT tests of 1.61 MPa. This is further evidence of the low rates of hardening experienced by aerial lime based mortars. The examples of historical masonry studied in Paper III were also constituted by aerial lime based mortars.

In Paper IV, a mortar including modern Portland cement as binder was used to build the specimens of the second type of masonry investigated. It was combined with the modern solid extruded bricks described in the above Section 4.2.2. The mortar consisted of a M7.5 Portland

cement based commercial mortar mixed with water in a ratio 1 to 0.25. Average mechanical properties after 28 days are 1.03 MPa and 2.53 MPa for flexural and compressive strength respectively.

#### **4.4. Additional materials**

Besides the material components –units and mortar- used to build the masonry specimens, additional materials were required to carry out the characterisation tests studied within this thesis. More specifically, all tests needed additional elements to be placed between the masonry specimens and the loading machines. These elements are necessary to ensure a satisfactory contact surface, to guarantee an adequate transmission of loads, and to avoid spurious effects related to the boundary conditions.

In Paper II (Section 5.2), the top and bottom surfaces of masonry prisms and wallettes were regularized with a Portland cement based mortar. These thin mortar layers provided plane and horizontal surfaces, and avoided any concentration of stresses motivated by the rough surfaces of the handmade bricks.

In Paper III (Section 5.3), high strength mortar caps were casted on the top and bottom of the masonry cylinders. These caps allowed having horizontal and plane surfaces to properly apply the compression load into the specimens. This mortar was a premixed commercial especially designed for fast reparation works. It reached 30 MPa of compressive strength after 28 hours.

In Paper IV (Section 6.2), soft board sheets were placed between the external faces of the bricks and the loading machine plates. These sheets served to avoid any concentration of stresses. Furthermore, the sheets were rubbed with Vaseline. The aim of Vaseline was to reduce

as much as possible the friction between the soft board sheets and the loading machine plates in order to avoid spurious measurements of resisting load.

Finally, in Paper V (Section 6.3), the two opposite corners where the diagonal compression loads were applied were regularized with a layer of epoxy resin. The resin created a fast hardening flat and smooth surface appropriate for the subsequent load application. Additional soft board sheets were placed between the resin cap and the metallic shoe to ensure a proper distribution of the load.

*This page is intentionally left blank.*

## **4.5. Paper I – Influence of recycled limestone filler additions on the mechanical behaviour of commercial premixed hydraulic lime mortars**

J. Segura, D. Aponte, L. Pelà, P. Roca, *Constr. Build. Mater.* 238 (2020),

<https://doi.org/10.1016/j.conbuildmat.2019.117722>

*Abstract: This paper presents an experimental programme aimed at investigating the use of limestone filler additions to modify the mechanical properties of commercial premixed hydraulic lime based mortars. The influence of adding recycled limestone filler was evaluated from the mechanical point of view, i.e. by comparing the experimental compressive and flexural strengths of five different mortar mixes with variable filler contents. The comparison of results shows that, up to a certain amount, the addition of filler provides an improvement of the mortar's mechanical properties. Beyond this optimum limit, strengths tend to decrease and eventually stabilize. Hence, mortars tested as part of this experimental campaign covered a range of strengths. Consequently, adding limestone filler can serve to adapt the applicability of hydraulic lime mortars to different practical applications, from the conservation of historical buildings to laboratory research on masonry.*

*This page is intentionally left blank.*

## I.1 Introduction

Masonry buildings making use of hydraulic lime mortar as a constituent material represent a significant part of the architectural heritage [211], which includes structures built during the 19<sup>th</sup> and the beginning of the 20<sup>th</sup> centuries as well as older ones. In fact, after the findings of Smeaton in the 18<sup>th</sup> century, hydraulic lime mortars were systematically used as building material [211–213].

The modern restoration philosophy recommends the use of repair products that are as compatible as possible with the substrate historical materials [214–216]. Therefore, the use of hydraulic lime mortars should be preferred in interventions on the aforementioned buildings. When compared to aerial lime mortars, hydraulic ones present a faster development of strengths and are able to harden under water, thanks to their double hardening mechanism that combines carbonation and hydration reactions [211]. In consequence, the use of hydraulic lime mortars is also encouraged to repair aerial lime-based masonry in cases where a quick hardening is needed or in structures exposed to severe environments [213,214,217–221].

Given the rise in the use of hydraulic lime mortar for restoration purposes [217], the research on this material has increased in the past two decades, with studies on the influence of the type of aggregates, the binder to water ratios and curing conditions on its properties [211,216,218,221,222]. The knowledge gathered through these and other experiences has allowed commercial companies to produce hydraulic lime based ready-mixed mortars that constitute an alternative to traditionally prepared ones [216]. Although these mortars have many advantages, two of them are particularly noteworthy. On one hand, their ease of use makes them available to less-skilled workers [223–225] since they only require adding water to the powder

**PAPER I**

materials. On the other hand, their industrial preparation provides a certain standardization [221,226] that increases the on-site homogeneity.

The research effort has continued in recent years with the double objective of producing enhanced mortars while incorporating different materials into the mix to reduce landfill waste [227,228]. Metakaolin [229], zeolite [230], diatomite [231] or fly ash [231] were added to hydraulic lime mortars to favour pozzolanic reactions and increase the mortar strengths. Barbero-Barrera et al. [232] studied the influence of graphite powder additions, which eventually improved the mortar's mechanical properties by filler and nucleation effects. The incorporation of organic additions, such as herbal [233] or cactus extracts [234], proved to have a beneficial impact on the overall properties thanks to the formation of side compounds. Some of the former mortars were specially designed to be used under severe environmental conditions of rain and freeze-and-thaw cycles, in high humidity and high temperature environments, or against acid erosion and salt crystallization.

Calcareous fines up to 100  $\mu\text{m}$ , hereafter called limestone filler, may be also considered as a possible addition to hydraulic lime mortars. This material is an industrial by-product obtained in great quantities from limestone crushing and grinding [235–238]. Besides its application in asphalt mixes, limestone filler can be incorporated into concrete as well, not only when self-compaction is desired [239,240], but also in common concretes as replacement of either cement or sand. This replacement results in at least three environmental advantages: a) reduction of waste to be landfilled [241], b) decrease of carbon dioxide ( $\text{CO}_2$ ) emissions from the binder production [241,242], and c) reduction of natural or river sand needs in countries with a shortage in this material [243,244].

The influence of limestone filler additions on concrete has been studied for decades [245–247]. Benachour et al. [235] and Wang et al. [248] offer a comprehensive review on the main

mechanisms related to the incorporation of calcareous fines. A filler effect occurs because the fine particles fill the voids and increase the packing density of the material. The nucleation effect relates to the precipitation of hydration products by using the filler particles as nucleation sites. This fact accelerates the hydration reaction and improves the overall hydration of the paste. A limited chemical effect [248] takes place during the cement hydration, when the calcite ( $\text{CaCO}_3$ ) from filler reacts with the aluminate ( $\text{C}_3\text{A}$ ) and ferrite ( $\text{C}_4\text{AF}$ ) minerals of the paste to form carboaluminate. Finally, the dilution effect corresponds to the decrease within the mix of the cement content with respect to the other components. The positive or negative influence of the limestone filler on the global properties of the material would depend on the amount of filler and the combination of the former effects. A critical amount could be determined to optimise the concrete strength [235,242,243,249,250].

A certain influence of limestone filler additions on non-hydraulic products has been identified as well. Fragata and Veiga [251] found higher strengths in aerial lime mortars prepared with two different types of aggregate when calcareous fines were added. Skoulidis et al. [252] found an optimal content of calcite that improved the mechanical behaviour of hydrated lime pastes used for the consolidation of stones. As the rate of carbonation of the calcium hydroxide (portlandite -  $\text{Ca}(\text{OH})_2$ ) was also increased, they suggested that the calcareous particles could act as crystallization seeds for the carbonation process.

It may be assumed that effects similar to those described above for concrete and aerial lime mortars would take place in hydraulic lime mortars given their double hardening mechanism by carbonation and hydration. However, the duality of hydraulic limes also makes them more complex. Furthermore, their hydration products differ from those of cement [211]. More precisely, the major hydraulic phase in hydraulic limes is larnite (belite -  $\text{C}_2\text{S}$ ) instead of alite ( $\text{C}_3\text{S}$ ), and  $\text{C}_3\text{A}$  and  $\text{C}_4\text{AF}$  could be present but in very small amounts. In consequence, the

**PAPER I**

influence of limestone filler on the hydraulic lime mortar properties may also be different and needs to be investigated. Two experiences have recently dealt with this topic. Forster et al. [253] analysed the influence of calcite additions in the form of oyster shells, limestone chippings and precipitated calcium carbonate. They found an increase on the mechanical strengths as result of these additions. Faria and Silva [221] studied the filler incorporation but combined with different aggregates and curing conditions. Besides the impact on the strengths, they found the calcareous filler to be advantageous, particularly with regard to water absorption and drying capability.

The present research is motivated by two related considerations. On one hand, there is an increase in the use of hydraulic lime mortars and commercial ready-to-use premixes for restoration purposes, together with a growing research on different material additions to improve the performance of these mortars. On the other hand, a lack of results has been detected about the influence of limestone filler additions on the mechanical behaviour of hydraulic lime mortars, while this addition, which is an abundant industrial by-product, has proven to be beneficial for both concrete and non-hydraulic lime mixes. With these considerations in mind, the present paper combines both research trends and explores the possibility of modifying the mechanical properties of hydraulic lime based mortars by incorporating limestone filler into their formulation. The influence of this addition has been evaluated from a mechanical point of view, i.e. in terms of changes in the compressive and flexural strengths of the mixture. The research involved five varied contents of filler, with the aim of covering a wide range of final applications.

## I.2 Materials and methods

### I.2.1 Materials

The experimental programme was carried out at the Laboratory of Technology of Structures and Building Materials of the Technical University of Catalonia (UPC – BarcelonaTech).

The mortars of this research were prepared by combining a hydraulic lime based commercial premix (HP) with limestone filler (LF) and water (W). The commercial product was a ready-to-use powder mix of binder and aggregates. A natural hydraulic lime NHL-3.5 as defined by EN 459-1 [254] acted as binder. The aggregates consisted of two types of washed river silica sand ( $0.1 \div 0.5$  mm and  $0.1 \div 1$  mm) and pure white marble powder ( $0 \div 2.5$  mm). The unit weight of this blend was determined to be 1740 kg/m<sup>3</sup>.

The manufacturer supplied the former premix in 25 kg bags. The content of one bag was studied. First, it was conveniently reduced by means of a quartering device to obtain a representative sample. This sample was divided into two fractions, one being the material passing through the 0.063 mm sieve and the other the material retained in the 0.063 mm sieve. Both fractions were analysed by X-ray diffraction with a PANalytical X'Pert PRO MPD Alpha 1 diffractometer using Cu K $\alpha$  radiation ( $\lambda = 1.5406$  Å (45 kV – 40 mA)). Figure I.1 presents those results. The diffractogram of the finer fraction (Figure I.1a) indicates the presence of the binding compounds, namely the hydraulic phases Iarnite and alite with a predominance of the former, as well as portlandite. This composition is in agreement with that of any hydraulic lime based binder [211,216]. The diffractogram of the coarser fraction (Figure I.1b) shows calcite as the main mineralogical phase, together with a reduced presence of quartz. This is consistent with the base materials defined in the former paragraph, silica sand and marble powder. Given

## PAPER I

the nature of the aggregates and both diffractograms, and according to a similar procedure adopted in [216] for the study of commercial NHL mortars, it could be assumed that the material passing the 0.063 mm sieve corresponded to the binder while the material retained in the 0.063 mm corresponded to the aggregates. This assumption was applied to compute an approximate binder to aggregates weight ratio of the hydraulic commercial premix that was 1:3.22. Lastly, the particle size distribution of the aggregates fraction was determined by sieving according to the standard EN 933-1 [255]. Figure I.2 displays the resulting chart, which corresponded to a well-graded fine aggregate.

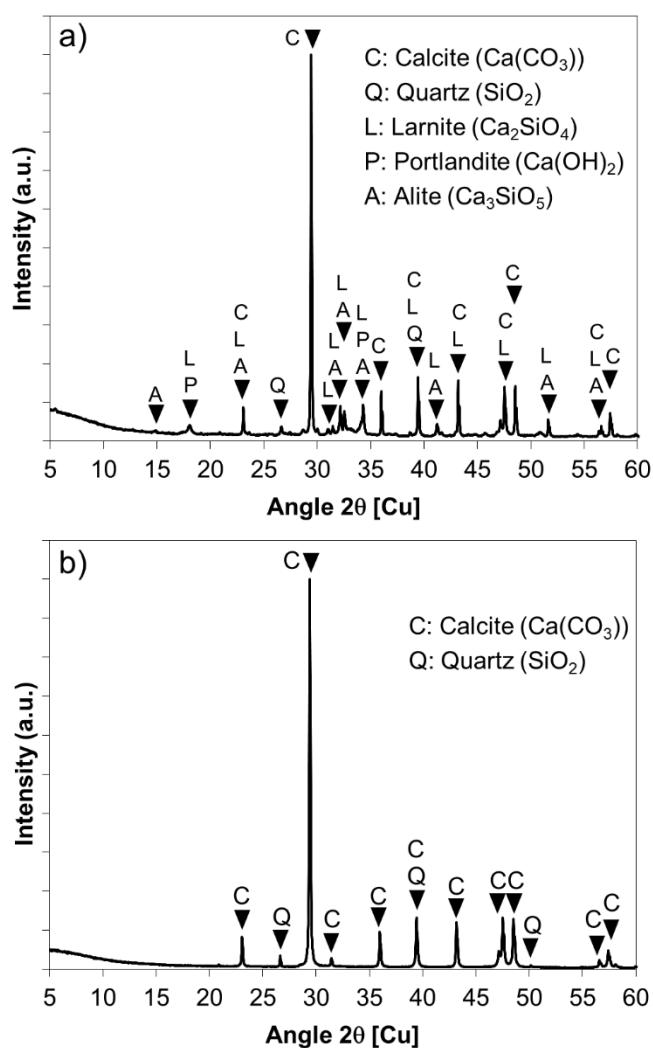


**Figure I.1** XRD diffractograms in the 5 – 60°  $2\theta$  angular region of the anhydrous premix. a) Fraction passing the 0.063 mm sieve, b) fraction retained in the 0.063 mm.

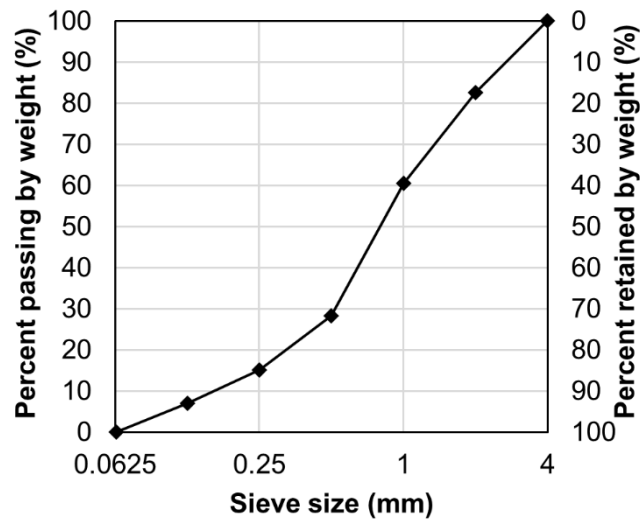


**Figure I.2** Determination of the particle size distribution chart of the premix aggregates.

The limestone filler incorporated into the mortars was supplied by a company that obtained it as a by-product of limestone grinding. A representative sample was studied. First, the unit weight of the filler was determined to be  $1120 \text{ kg/m}^3$  and its fineness was confirmed since 100% of the material passed through the 0.063 mm sieve. The particle size was analysed in more detail by means of a polarized light microscope JenaPol. Figure I.3 includes microscope images with a magnification of 100X of limestone filler particles that had been previously dispersed in oil. These images show that all particles were smaller than  $50 \text{ }\mu\text{m}$  and presented variability of shapes. Finally, Figure I.4 displays the results of an X-ray diffraction of the filler that indicate, as should be expected, the total predominance of calcite as main mineralogical phase. The presence of kaolinite, quartz and muscovite was incidental and could be originated in clays present during the initial extraction of the material. Therefore, the incorporation of the recovered limestone powder into the mortars did not add any harmful substance.

## PAPER I

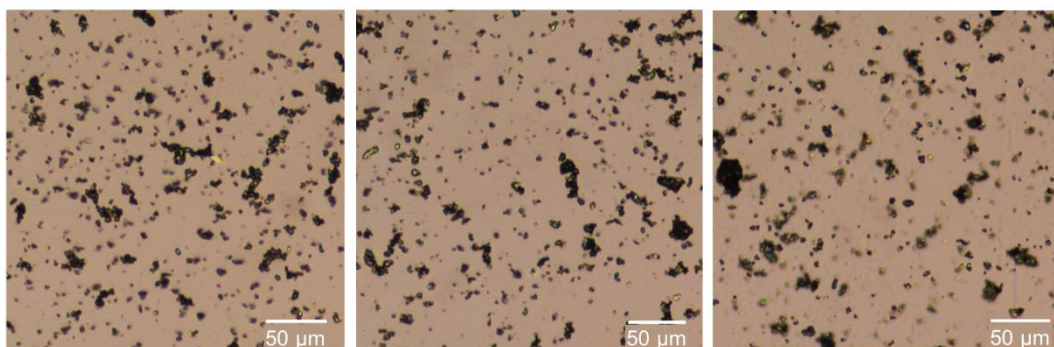


Figure I.3 Polarized light microscope images of limestone filler particles dispersed in oil. Magnification 100X.

Scale 50  $\mu\text{m}$ .

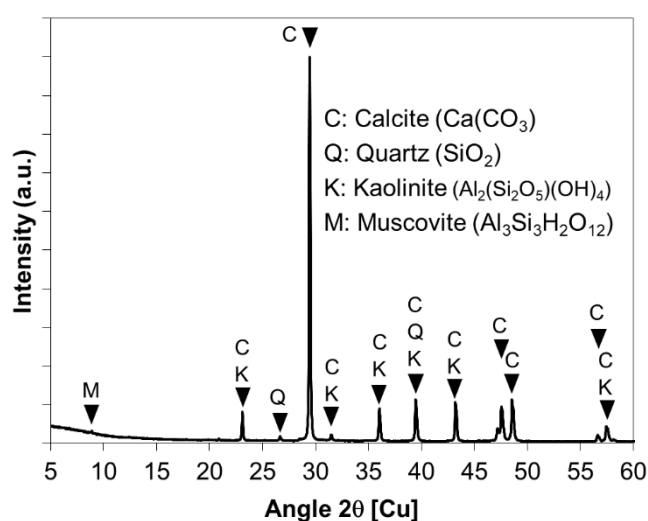


Figure I.4 XRD diffractogram in the 5 – 60°  $2\theta$  angular region of limestone filler.

## I.2.2 Mortars design

The reference mortar, here identified as mix M0, consisted only of hydraulic commercial premix and water. To investigate the influence of the limestone filler additions, four mortars with increasing filler content were defined. Table I.1 indicates the content of the two different constituents for the reference mix M0 and the modified mixes MA, MB, MC and MD. This content is indicated as a percentage of the total powder volume. Figure I.5a shows graphically the mortars definition, which ranged from MA, with a substitution by filler of only 12.5% of the total powder volume, to MD, where half the volume was substituted by filler. The weight proportions of the powder materials displayed in Figure I.5b were calculated with the bulk

densities and the binder to aggregate ratio found in the previous section I.2.1. The chart shows how the proportion of binder decreased with the progressive addition of filler.

**Table I.1** Mortars definition in terms of total powder volume by replaced by limestone filler.

Mortar	Powder volume (%)	
	Hydraulic premix (HP)	Limestone filler (LF)
M0	100	0
MA	87.5	12.5
MB	75	25
MC	62.5	37.5
MD	50	50

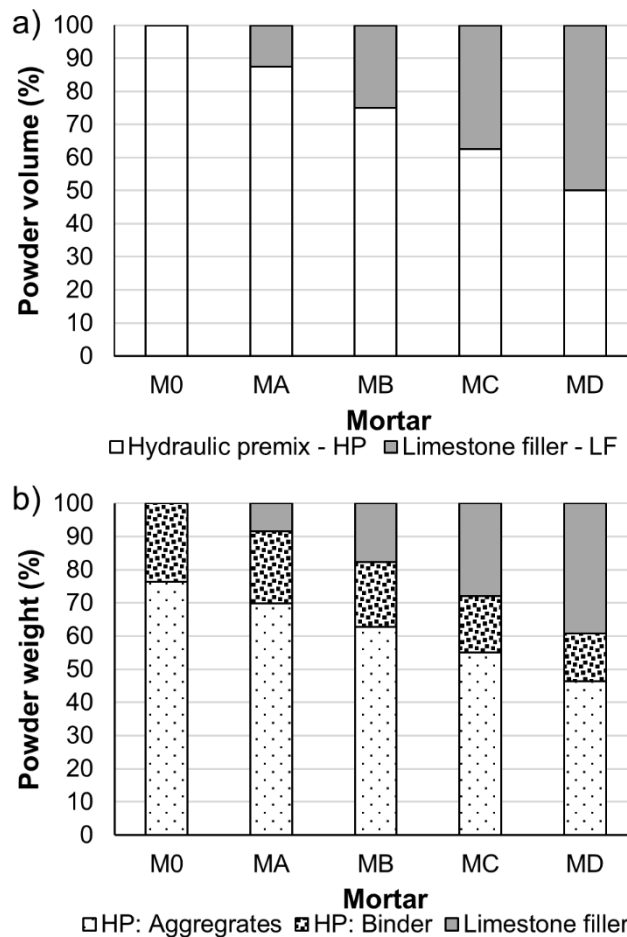


**Figure I.5** Graphical representation of mortars proportioning, a) by percentage of total powder volume and b) by percentage of total powder weight.

## PAPER I

The mortars design was completed by determining the water content of each mix. A batch of reference mix M0 was prepared according to the prescriptions of the manufacturer, i.e. 4.5 l of water every 25 kg of hydraulic commercial premix. The consistence of the fresh mortar was evaluated by means of the flow table test described in the standard EN 1015-3 [256]. A metallic mould was filled with two compacted layers of fresh mortar. After removing the mould and jolting the table 15 times, the result of the test was obtained as the mean diameter of the spread mortar measured in two directions at right angles. The flow value of 168.5 mm measured for mix M0 was considered acceptable in terms of workability [222] and was selected as a target consistence for the rest of the mortars. The water content of the other mixes was determined by a trial-error process until obtaining the required consistence. Table I.2 indicates the water contents and flow values for all the mixes, and the complete proportioning by volume and by weight as well.

**Table I.2** Mortars proportioning by volume and by weight, and flow measured according to EN 1015-3 [256].

Mortar	Proportions by volume			Proportions by weight				Flow (mm)
	Hydraulic premix (HP)	Limestone filler (LF)	Water (W)	HP: Aggregates	HP: Binder	Limestone filler	Water	
M0	1	0	0.312	0.763	0.237	0	0.180	168.5
MA	1	0.143	0.357	0.763	0.237	0.092	0.206	169.3
MB	1	0.333	0.416	0.763	0.237	0.215	0.240	167.8
MC	1	0.600	0.499	0.763	0.237	0.387	0.288	165.5
MD	1	1	0.650	0.763	0.237	0.645	0.375	167.1

### I.2.3 Specimens preparation and testing

The influence of the limestone filler additions on the mechanical behaviour of hydraulic mortars was investigated by means of the evaluation and comparison of two mechanical properties, namely the flexural and compressive strengths of the material. The European

standard EN 1015-11 [257] covers the testing of these two properties on hardened mortars. The experimental work presented herein followed the specifications of the standard.

A set of nine test specimens was built for each mortar. The specimens were  $160 \times 40 \times 40$  mm<sup>3</sup> (length  $\times$  width  $\times$  depth) prisms casted in metallic moulds. The mix of the three constituents, i.e. commercial hydraulic lime based premix, filler and water, was carried out for each mortar type with a mixer following the times prescribed by EN 196-1 [258]. After mixing, the fresh mortars were poured into the moulds in two approximately equal layers. Each layer was compacted by 25 strokes of a standard tamper. A palette knife was used to skim off the excess mortar to ensure surfaces plane and levelled with the top of the moulds. Each mould was then placed in an individual sealed polyethylene bag. Although the standard EN 1015-11 [257] recommends to remove the prisms from the mould after 48 h, the prisms were demoulded after 72 h because it was found preferable due to the slower hardening of the less strong mixes. After the demoulding, the prisms were kept again inside the bags for four additional days. Once extracted, they were stored in laboratory conditions until the age of testing ( $15 \pm 5$  °C and RH  $65 \pm 10\%$ ).

The mortar prisms were tested, in sets of three specimens, at 14, 28 and 56 days. Testing at different ages was important to investigate the evolution of the properties with time. An age of 56 days was considered a sufficient time to carry out the comparison among mixes given the faster hardening of hydraulic lime compared to aerial lime mortars, which are usually tested after 90 days [217,251,259]. The flexural strength of the prisms ( $f_{flex}$ ) was determined by means of three-point bending tests (Figure I.6a) and evaluated according to the following expression (Eq. I.1):

$$f_{flex} = 1.5 * \frac{Fl}{bd^2} \quad \text{I.1}$$

## PAPER I

where  $F$  is the maximum load applied to the specimen,  $l$  is the distance between the axis of the support rollers, which is equal to 100 mm, and  $b$  and  $d$  are the width and depth of the specimen respectively.

The two halves of the prisms broken during the bending tests were kept and tested under compression. A specific laboratory jig (Figure I.6b) ensured that the loaded area ( $A$ ) was a  $40 \times 40 \text{ mm}^2$  square. The compressive strength of the mortar ( $f_{comp}$ ) was evaluated with the following expression (Eq. I.2):

$$f_{comp} = \frac{F}{A} \quad \text{I.2}$$

Both types of test were carried out with a 10 kN capacity compression machine. No additional measuring devices were placed to capture the displacements during the tests. In all cases, the loading rates were selected so that failure occurred after 30 seconds.

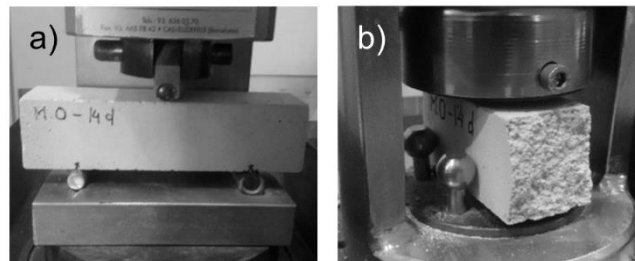


**Figure I.6** Mortar testing setup. A) Three-point bending and b) compression tests.

### I.3 Results and discussion

Table I.3 and Table I.4 present the average 14, 28 and 56-day flexural and compressive strengths of all mortar types. The associated coefficients of variation are included in brackets. Figure I.7 and Figure I.8 plot the development of strengths over curing time. The results show the influence of limestone filler on the mechanical behaviour of hydraulic lime mortar and how it was dependent, as could be expected, on the amount of filler. However, the results also show

that the trend of this influence varied with the curing time and slightly differed depending on the mechanical property investigated.

At 14 days, mortar MD (50% LF) was the weakest in both flexion and compression. M0 (0% LF) was the strongest mortar in compression but MA (12.5% LF) and MB (25% LF) were stronger in flexion. Yet, differences between mixes were minor at this early age. At 28 days, the influence of filler additions was reflected in a reduction of the flexural and compressive strengths, which decreased as the amount of filler increased. At 56 days, conversely, M0 (0% LF) was not the strongest mortar. After two months of curing, the flexural strength of mortar MA (12.5% LF) was 8% higher than the reference one (M0) and 128% higher than the weakest mortar one (MD), while mortar MB (25% LF) was 35% stronger than the reference mortar M0 and 177% stronger than the weakest mortar MD in compression.

Among the 30 average results presented in Table I.3 and Table I.4, only three exhibited a high variability with coefficients of variation “CV” around 15%. The latter is often found for lime-based mortars [260]. Furthermore, one third of the average results had a coefficient of variation lower than 5%. The strength decrease captured for certain mixes between 28 and 56-day tests has been also registered in previous research works available in the relevant literature [118,211,218,222,229,251,253,259]. Some authors pointed out that this behaviour could be attributed to the development of microcracking [218] or changes within the pore structure [253].

**Table I.3** Flexural strength of mortars ( $f_{flex}$ ). Average values at 14, 28 and 56 days for each mortar. Coefficients of variation shown in brackets.

Mortar	$f_{flex}$ (MPa)					
	14 days		28 days		56 days	
M0 - 0% LF	0.94	(10.4%)	1.93	(7.6%)	1.64	(5.1%)
MA - 12.5% LF	1.19	(1.7%)	1.83	(3.1%)	1.76	(3.8%)
MB - 25% LF	1.10	(3.9%)	1.64	(9.1%)	1.55	(11.0%)
MC - 37.5% LF	0.81	(15.9%)	1.03	(4.5%)	1.22	(8.5%)

## PAPER I

MD - 50% LF	0.65	(15.1%)	0.68	(9.9%)	0.77	(2.2%)
-------------	------	---------	------	--------	------	--------

**Table I.4** Compressive strength of mortars ( $f_{comp}$ ). Average values at 14, 28 and 56 days for each mortar. Coefficients of variation shown in brackets.

Mortar	$f_{comp}$ (MPa)					
	14 days		28 days		56 days	
M0 - 0% LF	2.89	(12.8%)	4.47	(7.5%)	3.78	(9.1%)
MA - 12.5% LF	2.58	(3.4%)	4.35	(5.4%)	4.82	(5.1%)
MB - 25% LF	2.39	(3.5%)	4.00	(4.1%)	5.09	(15.2%)
MC - 37.5% LF	2.11	(8.9%)	3.15	(8.3%)	3.60	(8.3%)
MD - 50% LF	1.64	(5.3%)	1.91	(6.4%)	1.83	(4.2%)

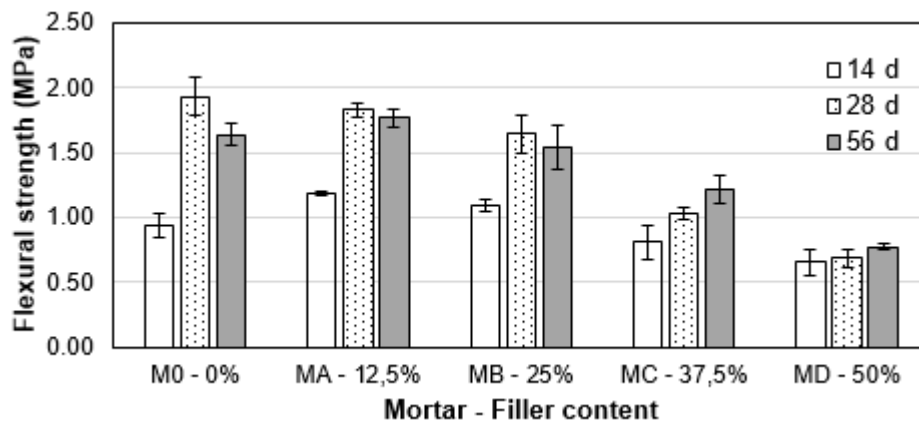


**Figure I.7** Flexural strength of mortars ( $f_{flex}$ ). Bars represent the average values at 14, 28 and 56 days for each mortar. Whiskers indicate the average values  $\pm 1$  standard deviation.

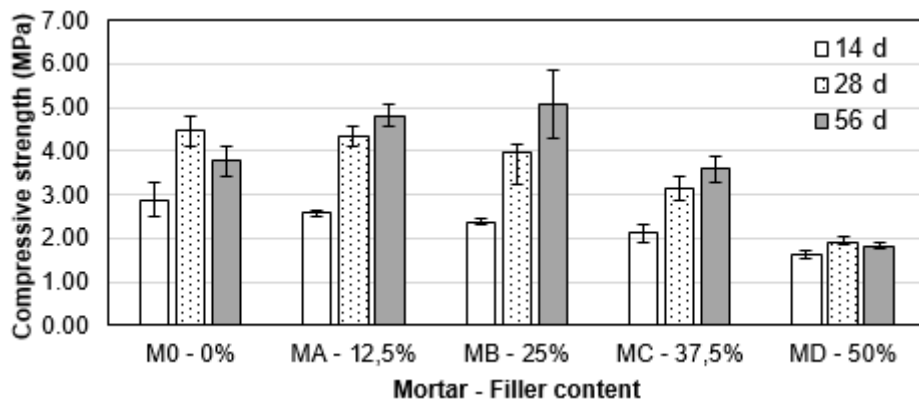


**Figure I.8** Compressive strength of mortars ( $f_{comp}$ ). Bars represent the average values at 14, 28 and 56 days for each mortar. Whiskers indicate the average values  $\pm 1$  standard deviation.

As discussed in Section I.1, the incorporation of calcareous fines may have different effects on the strength development of mortars. Namely, the filler effect that increases the packing density, the nucleation effect that favours the hydration and carbonation reactions, and the dilution effect acting when the binder is not able to coat all the particles. As the two former tend to oppose the latter, the global observed influence would depend, among others, on the amount of filler added. The combination of the three main effects can explain the experimental results presented in this paper. At 14 days, the dilution effect motivated the progressive reduction of compressive strength registered for increasing amounts of filler. Conversely, the greater packing density provided by the filler effect was sufficiently important in flexion in the cases of mortars MA (12.5% LF) and MB (25% LF) to counteract the dilution and both mortars reached higher flexural strengths compared to the reference M0 (0% LF). At 28 days, the dilution effect seemed to prevail over the rest as mortar M0 consistently exhibited higher strengths in both flexion and compression. However, at 56 days, a positive influence in both compressive and flexural strengths was observed that might be attributed to the nucleation effect. This mechanism is related to the hardening reactions of mortar, the hydration of C2S – which is slower than the hydration of C3S in cement mortars- and the carbonation of Ca(OH)<sub>2</sub>. Therefore, it required a certain time to be detected. With regard to the mortar MD incorporating 50% of limestone filler, the dilution effect predominated in such extent that the strength evolution was stopped even at 14 days. For this mix, the mechanical strengths showed almost constant values during the three ages of testing.

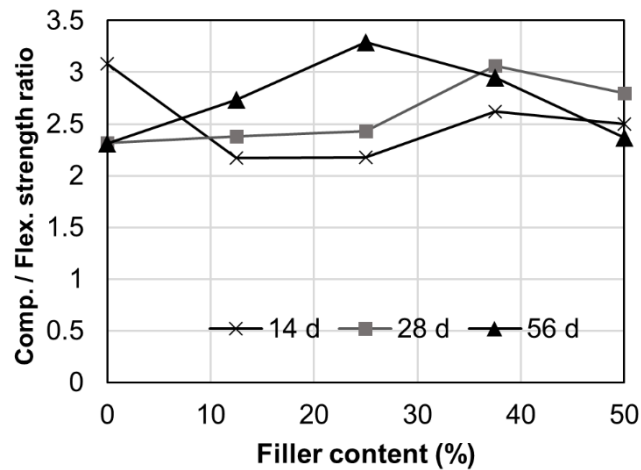
The objective of this work was to study the incorporation of limestone filler into commercial hydraulic lime based mixes to design modified mortars. From that point of view, the research provided a variety of results. At 28 days, mortar MA with a replacement with filler of 12.5% reached strengths similar to those of the reference mortar M0. At 56 days, an optimum

**PAPER I**

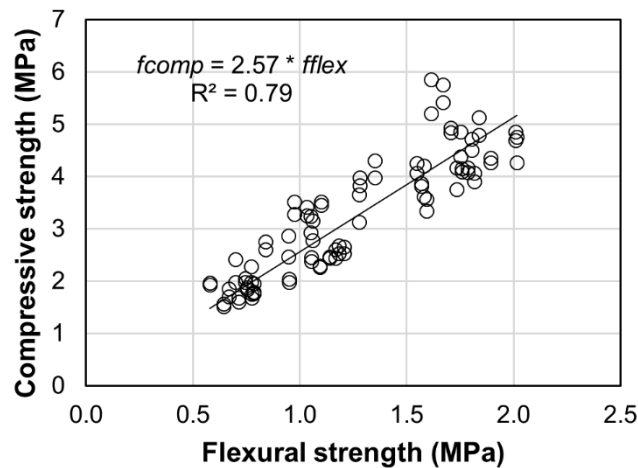
could be found between MA (12.5% LF) and MB (25% LF) to produce the mortar with the highest flexural and compressive strengths. The strength of 5 MPa exhibited by these two mixes in compression compares well with the results of Xu et al. [231] who added diatomite, Grilo et al. [229] who investigated metakaolin additions or Lanas et al. [211] who started from a stronger hydraulic lime. Those mortars might be suitable for restoration of structures in severe environments [229]. Additionally, mortar MD (50% LF) presented certain features that might be suitable for research purposes as discussed in Section I.4.

Figure I.9 plots the compressive ( $f_{comp}$ ) to flexural ( $f_{flex}$ ) strength ratios ( $f_{comp}/f_{flex}$ ) computed for all mortar types and grouped for the different ages. The graphs did not allow identifying any regular trend but showed that all the values ranged between 2.1 and 3.3. Figure I.10 was elaborated thanks to the great number of available test data, as it compares the total 180 results in compression to the 90 results in flexion regardless of the age and the filler content. Even if the coefficient of determination  $R^2$  was 79%, the ratio of 2.57 may be considered as representative of the types of mortar studied herein.

Allen [261] indicated that the compressive to flexural strengths ratio relates inversely to the brittleness and directly to the plasticity of the material. Kalagri et al. [218] found this ratio to be proportional to the dynamic modulus of elasticity. The 2.57 estimated ratio is similar to the ratios found in other researches with hydraulic and aerial lime mortars [215,218,221,259,262] on the same type of tested specimen.



**Figure I.9** Ratio between compressive ( $f_{comp}$ ) and flexural strength ( $f_{flex}$ ) of mortars for each filler content at 14, 28 and 56 days.



**Figure I.10** Correlation between compressive ( $f_{comp}$ ) and flexural strength ( $f_{flex}$ ) by combining the available data from all types of mortar and ages.

#### I.4 Example of application of mortar with limestone filler replacement of 50%

The previous section has shown that replacing the 50% of powder volume by limestone filler (mortar MD) leads to a strength reduction of the commercial premixed hydraulic lime based mortar down to 2 MPa. This strength value can be considered representative of a historical mortar [217,221,263,264] and makes mortar MD suitable to satisfy a need encountered in the research field.

**PAPER I**

Research on historical masonry usually involves building structures or structural elements in laboratory that try to replicate the properties of the real ones [265–267]. This implies the use of low strength mortars, but preferably with a certain hydraulicity to guarantee a fast hardening and to reduce the curing time needed before testing. Some researchers may choose the option of commercially available hydraulic lime premixes because of the homogeneity and easy use offered by an industrial product as exposed in section I.1. In some cases, however, these materials develop a too high compressive strength and may not be adequate to replicate a historical mortar. In fact, as investigated by Gulotta et al. [216], some of these mortars may reach strengths much higher than the strength-resistance classes of the initial binders.

In order to address this issue, some authors have incorporated additions into the commercial premixes to combine the advantages of the latter with a convenient strength level. Magenes et al. [209] modified a hydraulic lime based commercial mortar by replacing 22% of the volume with sand. More recently, Guerrini et al. [210] added EPS beads up to 28% of the volume. Both cases achieved an appropriate strength reduction.

During recent years, the mortar mix MD has been used in the Laboratory of Technology of Structures and Building Materials of the Technical University of Catalonia (UPC) in different experimental campaigns that aimed to study historical-like masonry elements [132,268]. Figure I.11 shows the results of bending and compression characterisation tests on prisms of mortar MD corresponding to the last campaigns carried out at UPC. A total amount of 60 and 120 results are displayed for flexural and compressive strengths respectively. The charts cover different ages from 7 to 112 days. As discussed in the previous section, the incorporation of such amount of filler seemed to stop the strength development of the mortar at an early age. The average flexural and compressive strengths after 28 days were 0.71 and 1.93 MPa respectively and the individual test results exhibited a close oscillation around those values.

The related coefficients of variation, computed with all the data after 28 days, were 16.8% and 12.9%. Taking into account the variability within the material, the differences in curing conditions and the inherent scattering of the experimental tests, those coefficients of variation allow considering the strengths as constant over time. The overall ratio  $f_{comp}/f_{flex}$  was 2.72, which is consistent with the values displayed in Figure I.9.

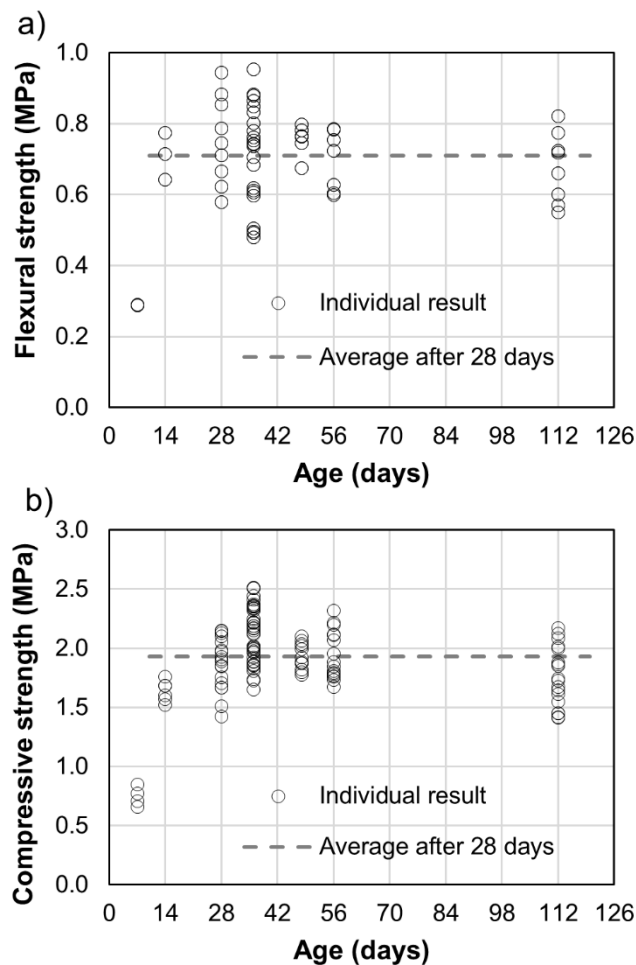


**Figure I.11** Strength evolution of mortar MD with age. The dashed lines indicate the average value of the strengths considering all the individual results after 28 days. a) Flexural strength, b) compressive strength.

The characterisation of this mortar MD was completed with two additional tests. On one hand, Figure I.12 shows three images of mortar joint sections obtained with a stereo microscope Leica using incident light. These pictures, with a magnification of 10X, illustrate the macrostructure of the hardened mortar at 56 days and reveal a porous material, with pores

**PAPER I**

occasionally bigger than 2 mm. The incorporation of filler did not saturate the pore structure and in consequence the mortar could be able to breath and carbonate easily. On the other hand, Figure I.13a displays the X-ray diffractogram of a sample of hardened mortar MD at 56 days after crushing and mechanical sieving. The results show that, at that time, there was a very limited amount of binding compounds (larnite, portlandite) left. Figure I.13b clarifies this aspect as it compares the diffractogram of the hardened mortar to that of the anhydrous original premix. The absence or reduction of the peaks related to the binding phases is especially noted in the 18, 30 – 35, 40 – 45  $2\theta$  angular regions. This fact involves a limited evolution of strengths after 56 days, consistently with the mechanical tests previously presented in Figure I.11 that yielded constant strengths between 56 and 112 days. It is also remarkable that the final products in the hardened mortar, namely calcite and traces of quartz, are the same of those of any hydraulic lime based mortar. This result together with the favourable pore structure imply that mortar MD, in case of being used in restoration works, would not present any compatibility issues with the traditional old substrate materials. Given that mortar MD was the mix with the highest amount of limestone filler, the former conclusions related to final resulting products, pore structure and compatibility would be also applicable to the rest of mixes studied in Section I.3.



**Figure I.12** Stereo microscope images of hardened mortar MD joint sections after 56 days. Magnification 10X.

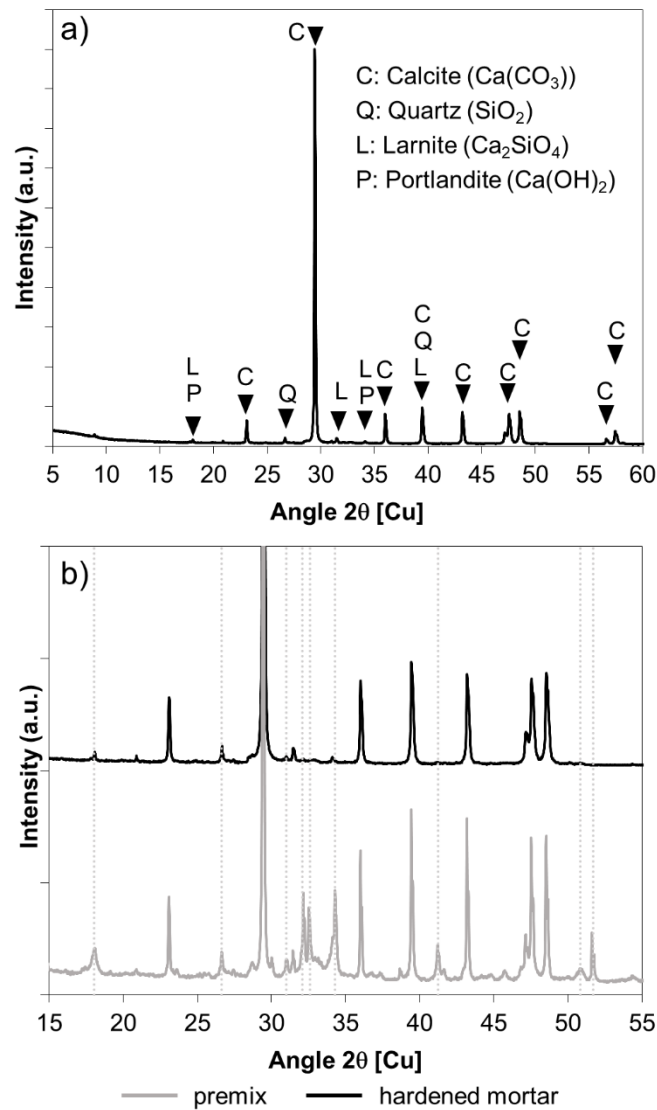


**Figure I.13** a) XRD diffractogram in the 5 – 60°  $2\theta$  angular region of hardened mortar MD at 56 days after crushing and mechanical sieving; b) comparison of XRD diffractograms in the 15 – 55°  $2\theta$  angular region of anhydrous premix (see Figure I.1a) and hardened mortar MD at 56 days.

Additionally, mortar MD was used to build small masonry specimens with handmade solid clay bricks by the authors [268]. Bricks had average dimensions of 311 x 149 x 45 mm<sup>3</sup> and a normalized compressive strength of 18 MPa. Running bond walls and stack bond prisms were tested in compression providing average compressive strengths of 6.51 MPa and 6.75 MPa respectively. These values may be representative of historical masonry elements as they compare well with laboratory campaigns studying this type of materials [105,269], inspection campaigns on real structures [104,270] or studies on historical buildings [196].

**PAPER I**

Therefore, mortar MD combines different features that might be interesting for researchers:

1) it provides a convenient strength value and, when used to build brickwork specimens, the strength values compare well with those of historical masonry elements; 2) it is based on an already premixed material, which is produced industrially and offers a controlled variability; 3) the replacement material, limestone filler, is easily available as an industrial by-product at a low cost; 4) it attains the required strength at or before 28 days, in contrast with aerial lime mortars that require much more time to harden; 5) the constant value of strength over time makes it especially suitable for the experimental research in the laboratory.

**I.5 Conclusions**

This paper has presented an experimental investigation on the influence of limestone filler additions on the compressive and flexural strengths of hydraulic lime mortar. The filler was added to a commercial premix in varying amounts of 12.5%, 25%, 37.5% and 50% of powder volume. Mechanical tests were carried out at 14, 28 and 56 days. The following conclusions can be drawn from these experiments:

- Limestone filler, which is an easily available industrial by-product, was successfully incorporated into mortar mixes. Mortars workability was maintained even for high amounts of material replacement.
- The influence of limestone filler depended notably on the added amount. Yet, the trend of this influence varied with the curing time and the mechanical property evaluated. The effects of filler incorporation described by previous authors for cement and aerial lime mortars could explain the observed results.
- With the amounts of filler studied herein, a positive impact on the mechanical strengths was not consistently registered until 56 days. By that age, the nucleation effect that

favours the slow reactions of hydration and carbonation was sufficiently important as to show its influence. At earlier ages, the dilution effect prevailed.

- An optimum amount of filler between 12.5% and 25% could be found to maximize the compressive and flexural strengths of NHL 3.5 based mortars. At 56 days, the mortar incorporating 25% of filler was 35% stronger than the reference mortar without filler.
- The replacement by filler of 50% powder volume provided a mortar of almost constant mechanical strengths over time for potential applications in the research field.
- The incorporation of limestone filler, which is an inert material, doesn't affect the nature of the resulting products in the hardened mortar if compared with other hydraulic lime based mortars. Therefore, these modified mortars would be compatible with traditional old materials.

*This page is intentionally left blank.*

**5**

**Characterisation of masonry in  
compression**

*This page is intentionally left blank.*

## 5.1. Introduction

This chapter presents two experimental researches that deal with the characterisation of masonry in compression. Based on the findings of the literature review presented in Section 2, these researches address some of the needs encountered in relation with the size and shape effect of the specimens and the type of loading.

Section 5.2 reproduces Paper II, devoted to the characterisation of masonry in laboratory. It explains an experimental campaign on two types of standard specimen -stack bond prisms and running bond walls, and compares the results obtained through monotonic loading with results obtained after the performance of some loading cycles. Paper II pays also attention to different analytical and empirical expressions derived to predict the mechanical behaviour of masonry.

Section 5.3 reproduces Paper III, devoted to the characterisation of masonry in existing buildings. It explains an experimental programme that consists of four campaigns on four different masonry examples, three of them from real buildings of Barcelona. The programme's aim is to compare the results obtained by means of testing cylinders of 150 mm diameter, as recommended by the UIC Leaflet [101], with those obtained from smaller specimens, of only 90 mm diameter, which would reduce the damage to the existing structure during the coring phase.

Section 5.4 discusses some aspects of Paper II and Paper III as a whole and relates the obtained results. Conclusions of the individual papers are not restated here but in Chapter 7.

*This page is intentionally left blank.*

## **5.2. Paper II – Monotonic and cyclic testing of clay brick and lime mortar masonry in compression**

J. Segura, L. Pelà, P. Roca, *Constr. Build. Mater.* 193 (2018) 453-466,

<https://doi.org/10.1016/j.conbuildmat.2018.10.198>

*Abstract: This research presents an experimental programme on the mechanical characterisation of masonry under monotonic and cyclic uniaxial compression. Two different types of standard specimens, running bond walls and stack bond prisms, were built using handmade clay bricks and hydraulic lime mortar. The experimental results are compared and discussed in terms of strength, stiffness and deformability. It was observed that the two specimen types provided very similar results on both strength and stiffness. Cyclic loading tests carried out on a set of samples provided new experimental evidence on the stiffness degradation, loss of load carrying capacity for increasing irreversible compressive strains and energy dissipation. The paper presents eventually a thorough discussion about the comparison between the obtained experimental results with available predictive models for strength, stiffness and fracture energy of masonry under monotonic and cyclic compression loading*

*This page is intentionally left blank.*

## II.1 Introduction

Brick masonry has been largely used for structural purposes up to mid-20th c when, due to the increasing labour costs, it became less attractive than other more modern materials such as concrete and steel [271,272]. Due to its long historical prevalence, masonry consisting of clay bricks and lime mortar is abundant all over the world. Still today, a significant part of the building stock includes structural masonry members such as load-bearing walls [272–278]. Due to changes in regulations and uses, masonry buildings are often in need of structural re-evaluation and, eventually, of possible retrofitting interventions. Within this context, the response of masonry in compression has a critical role in the evaluation of the strength capacity of masonry buildings against both vertical actions and the vertical load effects caused by horizontal actions. Characterising the response of masonry in compression involves the determination of parameters such as the compressive strength of the composite material, its modulus of elasticity and the overall stress-strain curves in compression under both static and cyclic loading.

Traditionally, the characterisation of the mechanical behaviour of masonry in compression has been carried out by means of tests performed on two different types of composite specimens, namely stack bond prisms and small walls. Three recent references [128,279,280], including inventories of past researches on clay brick masonry, refer examples of tests done on either specimen type, although with preference for prisms. The predilection to carry tests on prisms can be explained because they are easier and cheaper to build and the experimental setup needed in the laboratory is simpler.

The possibility of testing two different types of specimen is also reflected in the standards that regulate the experimental determination of the compressive strength of masonry ( $f_c$ ). The

## PAPER II

European standard EN 1052-1 [72] prescribes the use of small running bond walls with certain geometric constraints (Figure II.1a). These samples are supposed to provide a fair estimation of the strength taking into account the possible detrimental influence of head mortar joints. In addition, they are sufficiently slender as to keep the centre of the specimen free from the influence of possible 3D confinement effects caused by the contact between the specimen and the press platens. Conversely, the American ASTM C1314 [70] proposes the possibility of testing simpler stack bond prisms consisting of a sufficient number of stacked units. The standard specifies the recommended height to thickness ratios of the prisms (Figure II.1b). In turn, both types of specimens are considered in the RILEM [71] recommendations.

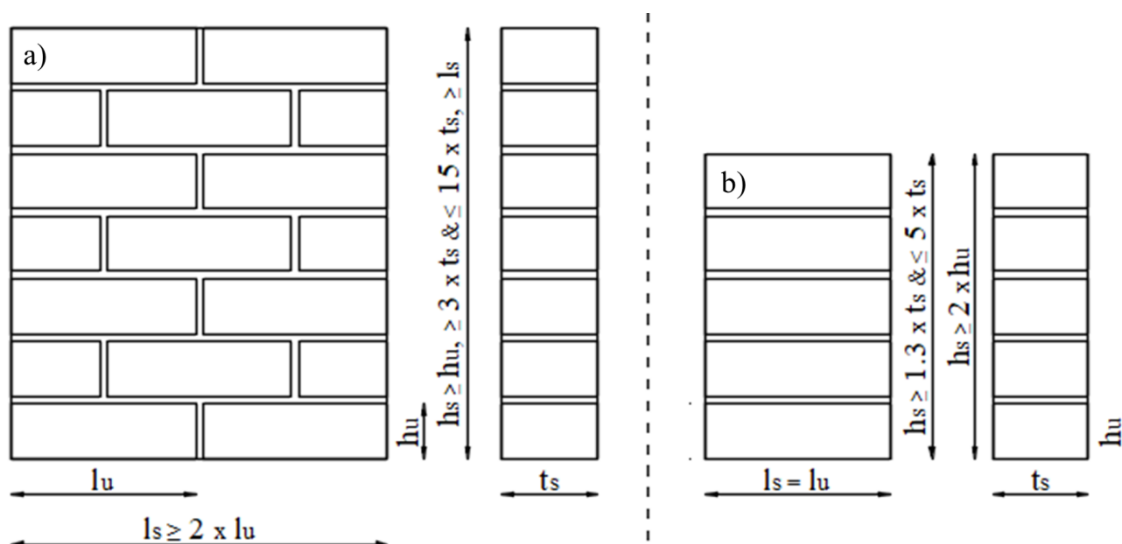


**Figure II.1** Masonry specimens for compression strength tests according to a) EN 1052-1 [72], b) ASTM C1314 [70].

So far, no empirical criterion has been proposed to correlate the experimental results obtained with both specimen types. However, this issue has motivated some research in the past. Several authors [281–283] have compared the results on prisms with those obtained for wall-like samples. Mann & Betzler [284] and Gumaste et al. [79] investigated the effect of the sample shape on the compressive strength. Among other specimen types, they analysed the case of non-standardized both stack bond prisms and running bond walls. They showed that the

comparison between the specimens' results is influenced by the mechanical properties of the constituents, as well as by the specimens' relative slenderness.

Many real structures are subjected to cyclic loading caused by variable loads such as thermal effects, the passing of trains on railway bridges, or seismic actions. However, most of the research effort on the compressive behaviour of masonry has only focused on monotonic loading [75]. A few works can be found on cyclically loaded stone [85–87] and concrete block masonry [88]. With regard to brick masonry, [89,90] carried out pioneering researches on frogged clay and sand-plast brick masonry specimens. These authors developed the concepts of common and stability points to characterise the intersections among unloading-reloading branches in masonry. More recently, [91,92] contributed with more laboratory results, and [87] explored the possibility of performing and registering cycles in the softening range. Two more researches [93,277] dealt with samples obtained from historical buildings, while [94] is the only study including masonry built in the laboratory with solid clay bricks and hydraulic lime based mortar without cement.

This paper aims to provide new experimental data on the static and cyclic response of brick masonry in compression. The paper focuses on the case of masonry built with solid clay bricks and hydraulic lime based mortar, on which there is still limited experimental evidence although being the traditional typology in historical masonry in many countries [81,93,196]. The research on the static response includes a comparison of results on the masonry compressive strength and elastic modulus for two different types of standardized specimens, corresponding to stack bond prisms and running bond walls. In turn, the research on the cyclic response includes cyclic tests up to and beyond the peak load on stack bond prisms. The performance of different criteria and models for the estimation of the masonry compressive properties and the simulation of its cyclic response has been evaluated by comparison with the experimental results.

**PAPER II****II.2 Experimental programme**

The experiments were carried out at the Laboratory of Technology of Structures and Materials of the Technical University of Catalonia (UPC – BarcelonaTech). As mentioned, the experimental programme included compression tests on two different types of specimens (running bond walls and stack bond prisms), under monotonic and cyclic loading.

**II.2.1 Materials**

The masonry specimens were built with materials similar to those existing in historical masonry walls, including handmade solid clay bricks and a low mechanical performance lime mortar.

Handmade fired solid clay bricks were chosen, with average dimensions of 311 (length) × 149 (width) × 45 (height) mm<sup>3</sup> and density of 1700 kg/m<sup>3</sup>. Given their manual way of manufacturing, these bricks presented a moderate compressive strength, rough surfaces and slightly variable dimensions. A commercial premixed lime mortar based on NHL 3.5 natural hydraulic lime was selected. Its strength category was M5, which was considered to be too high to reproduce the expected compressive strength of lime mortar in historical masonry. Hence, a new mix was studied and prepared in laboratory by adding an amount of non-reactive material (in this case, limestone filler) to reduce the strength of the mortar. The volume ratio of premixed mortar to filler to water was 1 : 1 : 0.65.

The standard EN 772-1 [285] was considered as reference to obtain the normalized compressive strength of the bricks ( $f_b$ ). Their faces were polished until getting a constant height of 40 mm to obtain flat surfaces. Pieces of 100 x 100 mm<sup>2</sup> were cut to fulfil the minimum height to width ratio of 0.4 required by the standard and then tested. The measured strength values were corrected by applying a shape factor of 0.7 in compliance with the standard. The bending

tensile strength of the units ( $f_{b,fl}$ ) was determined by three-point-bending tests on full bricks. In the lack of a specific standard for the determination of the bending tensile strength of clay units, the tests were carried out according to EN 772-6 [286] for aggregate concrete masonry units. Similarly, and since there are no available standards on the determination of the elastic modulus of bricks, EN 12390-13 [287] on the determination of the modulus of elasticity for hardened concrete was used as a reference. Brick prisms measuring  $40 \times 40 \times 80 \text{ mm}^3$  were cut both in longitudinal and transverse directions of the unit. It should be noted that measuring the modulus of the bricks in the direction parallel to the load is hardly feasible due to their very small height. Three loading-unloading compressive cycles, with minimum and maximum loads equal to 10% and 30% of the estimated peak load, were applied to the specimens. The moduli of elasticity in the two directions ( $E_{b,long}$  and  $E_{b,trans}$ ) were evaluated as the slope of the last reloading branches as suggested in the standard [287]. The results of this characterisation are presented in Table II.1. The considerably high coefficients of variation found in the determination of the elastic modulus may be explained by the heterogeneity of the handmade bricks. In addition to the scattering related to the raw materials, the manual process adds variability during the casting of the bricks and the curing inside the traditional furnace.

**Table II.1** Mechanical parameters of bricks

	$f_b$ [MPa]	$f_{b,fl}$ [MPa]	$E_{b,long}$ [MPa]	$E_{b,trans}$ [MPa]
Average	17.99	2.44	3718	3331
Number of samples	20	10	12	17
CV	8.3%	20.0%	28.0%	51.4%

The compressive strength ( $f_m$ ) and the bending tensile strength ( $f_{m,fl}$ ) of the mortar were evaluated according to EN 1015-11 [257], by using prisms with dimensions of  $160 \times 40 \times 40 \text{ mm}^3$  that were casted with mortar obtained from the mason's batch during the construction of the masonry specimens. As for the evaluation of bricks elastic modulus, EN 12390-13 [287] was adopted as reference. The estimation of the mortar elastic modulus ( $E_m$ ) was carried out on

## PAPER II

mortar cylinders 200 mm high with a diameter of 100 mm. These cylinders were tested under cyclic loading similarly to the brick prisms. A summary of the results is presented in Table II.2

**Table II.2** Mechanical parameters of mortar

	$f_m$ [MPa]	$f_{m,fl}$ [MPa]	$E_m$ [MPa]
Average	1.91	0.72	948
Number of samples	36	18	6
CV	10.1%	10.9%	18.4%

### II.2.2 Masonry specimens

Two different sets of masonry specimens were built and tested. The first set consisted of 4 standard running bond walls (RBW) fulfilling the requirements of EN 1052-1 [72]. The second set consisted of 7 stack bond prisms (SBP) built according to the geometric prescriptions of ASTM C 1314 [70]. As previously indicated, one of the aims of the present research lays in the comparison of the strength and elasticity parameters measured by means of these two types of standardized specimens. The average dimensions of both types of samples are 639 (length,  $l_s$ ) x 148 (thickness,  $t_s$ ) x 658 (height,  $h_s$ ) mm<sup>3</sup> for walls, with aspect ratio ( $h_s/t_s$ ) of 4.45, and 312 x 148 x 288 mm<sup>3</sup> for prisms, with aspect ratio ( $h_s/t_s$ ) of 1.95 (Figure II. 2). The samples were built with 15 mm thick mortar joints. This thickness, which is often observed in historical clay brick masonry, allowed a sufficiently regular laying of bricks despite of the geometrical irregularities of their faces.

The building and storing of the specimens were carried out according to EN 1052-1 [72]. The bricks were wetted for one minute before being laid. The samples were all built during the same day, by the same highly qualified mason, and stored under the same environmental conditions until the performance of the tests. After construction, they were covered with polyethylene sheets in order to prevent the dry-out of the mortar. After 3 days, they were uncovered and stored in the laboratory at 15 °C and 65 % of relative humidity.

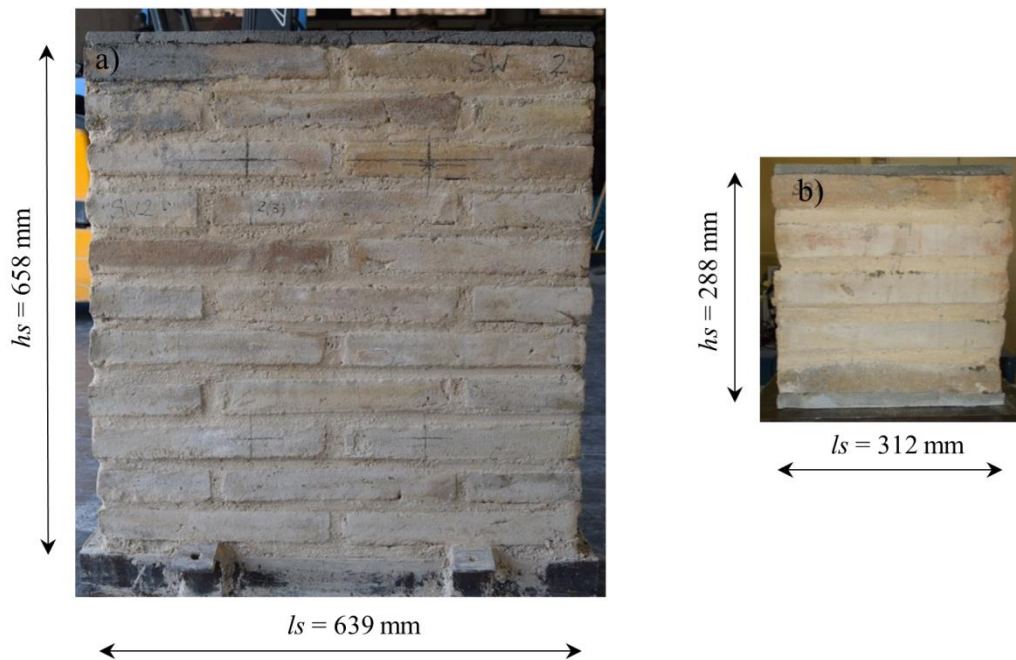


**Figure II. 2** Masonry samples, average dimensions. a) Running bond walls, b) Stack bond prisms. Common average thickness  $t_s = 148$  mm.

With the aim of facilitating the handling of the RBW wall specimens, they were built and tested on top of metallic beams filled with concrete. Some days before testing, the top face of the RBWs, as well as the bottom and top faces of the SBPs, were capped with a layer of high strength cement mortar in order to ascertain a smooth contact between the samples and the loading machine plates.

### II.2.3 Test procedures

The wall and prism masonry samples were tested in compression after 28 days from their construction, following EN 1052-1 [72] recommendations. The prisms SBP were tested in a general-purpose loading machine with a capacity of 3000 kN (Figure II.3a). The walls RBW had to be tested inside a steel reaction frame due to their larger dimensions. In the reaction frame, the load was applied by means of a double effect hydraulic jack with capacity of 1000 kN (Figure II.3b). A combination of instruments was placed on the specimens' faces in order to capture vertical displacements. Four LVDTs (with a displacement range of  $\pm 5$  mm and a

## PAPER II

precision of 5  $\mu\text{m}$ ) were glued between the second and fourth bricks of the SBPs. They allowed having a reference length longer than one third of the sample height while avoiding possible boundary effects. The same distance was also monitored in the case of RBWs with a vertical LVDT placed on each face. This allowed obtaining comparable measurements in the two specimen types, with the difference that a head mortar joint was included in the walls.

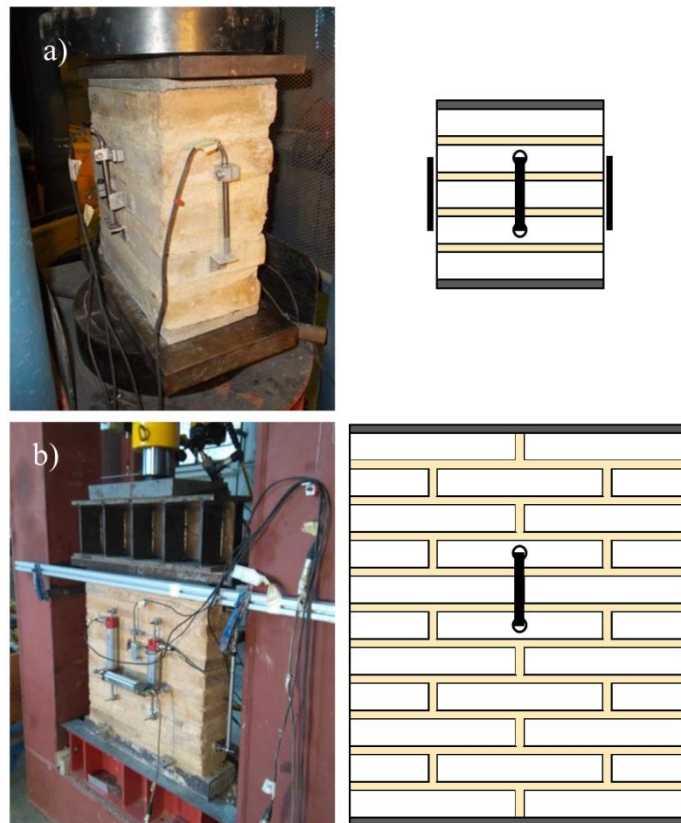


**Figure II.3** Experimental setups: a) Stack bond prisms, b) Running bond walls.

The tests were carried out in two stages (Figure II.4), the first one was aimed to facilitate the measurement of the elastic modulus of masonry and the second one investigated its ultimate capacity. In the lack of a specific standard on the measurement of the elastic modulus of masonry, the procedure adopted during the first stage was based on standards for the determination of the elastic modulus in other materials such as concrete (EN 12390-13 [287], ASTM C 469-02 [288]) and stone (EN 14580 [289]), and also on methods applied in former researches [75,105,283].

The first stage was common to all the specimens and included three loading-unloading cycles performed under load control. The lower and higher load levels applied during the cycles were set to 5% and 30% of a supposed maximum load ( $P_0$ ) that had been estimated before the tests. In the case of the walls, these limits were taken as 26 and 150 kN, while for the prisms the limits were 14 and 83 kN. Rates of loading of 2 kN/s and 1 kN/s were selected for walls and prisms respectively to keep the duration of the loading/unloading branches around 1 minute. After each loading/unloading branch, the load level was maintained also for 1 minute. As stated by the general standard ASTM E111 [119], the lower load was used to minimize the errors due to initial effects of backlash and specimen irregularities while the upper load was selected so as to keep the specimen within the elastic range of the material.

The second stage of the tests explored the strength and non-linear behaviour of the specimens under either monotonic or cyclic loading. A displacement controlled loading procedure (at a rate of 0.6 mm/s) was used during this stage with the intention of capturing the post-peak response. This phase was undertaken under monotonically increasing displacement for the 4 running bond walls (identified as RBW1, RBW2, RBW3, RBW4) and for 4 stack bond prisms (SBP1, SBP2, SBP3, SBP4).

In the remaining three stack bond prisms (SBP5, SBP6, SBP7), the displacement was imposed cyclically. The aim of these tests was not to represent any example of real structures, which may be subjected to cyclic loads characterised by very different frequencies and amplitudes, but to study a generic case. The type and number of cycles was decided as to have comparable results with former researches [87]. The system was programmed to apply increasing load up to vertical displacement values of 2.5, 4, 5.5, 7, and 8.5 mm. These values were defined based on the results of the previous monotonic tests. Once those displacements were reached, the specimens were unloaded under force control until the previously set level of

## PAPER II

5% of the estimated maximum load. The vertical displacement was controlled by the loading machine's internal transducer.

With regard to the elastic moduli, they were evaluated for all the specimens as the chord modulus between the 5% and 30% of the actual maximum load ( $P_{max}$ ) (Figure II.4), of the stress-strain curves obtained during the second testing stage.

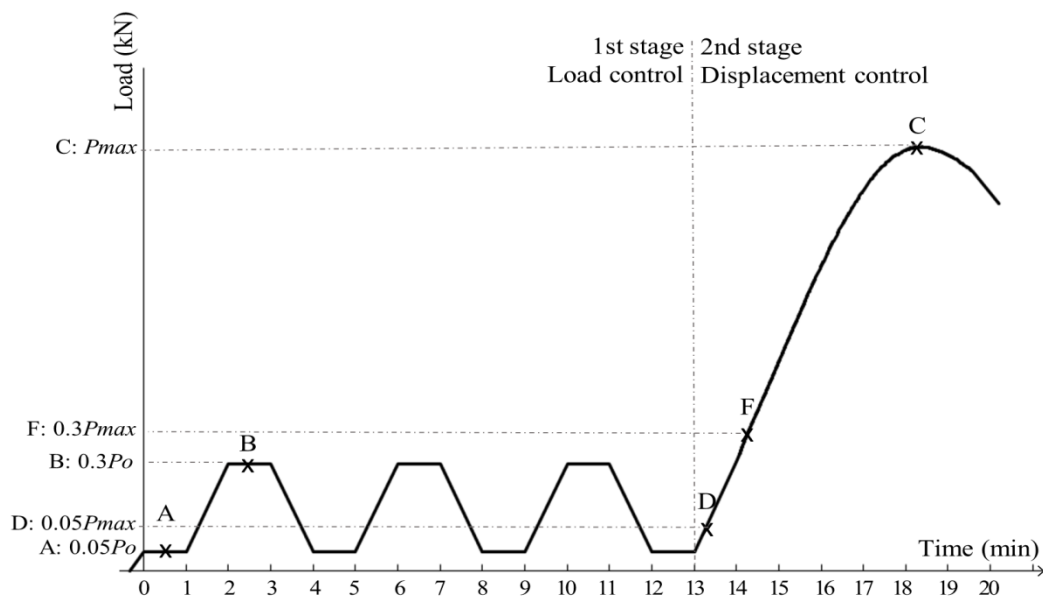


**Figure II.4** Generic load (kN) vs. time (min) curve describing the adopted loading history. Load levels: A - 5% of an estimated maximum load ( $P_o$ ). B - 30% of an estimated maximum load ( $P_o$ ). C - Actual maximum load registered during the test ( $P_{max}$ ). D and F - Loads corresponding to 5% and 30% of the actual maximum load ( $P_{max}$ ), used as limits to compute the elastic modulus on the stress-strain curves.

### II.3 Experimental results

This section presents the results of the experimental campaign for each type of specimen and loading protocol. Compressive stresses acting on the samples were computed as the ratio between the applied load and the area of the cross section. LVDT readings were divided by their reference lengths and averaged to obtain axial strains. In some cases, anomalous individual deviations of one LVDT were omitted. Full stress-strain curves, considering both stages of

testing, are plotted for all the tests. As for the post-peak branches, they are only shown for the cases in which it was possible to obtain meaningful results.

### II.3.1 Running bond walls

The stress-strain curves resulting for both stages are shown in Figure II.5, for the RBW specimens. The effect of the application of the three cycles is illustrated in Figure II.5a. The unloading-reloading branches have higher stiffness than the original monotonic loading one. The elastic moduli ( $E_c$ ) reported in Table II.3 were evaluated according to the procedure indicated in section II.2.3. The average value is 2744 MPa. However, the result associated to sample RBW3 is anomalously high compared to the other specimens. This high value may be explained by a possible better manufacture or by an unexpected localization of better quality materials within the length captured by the measuring instruments. Due to the significant deviation of this value with respect to the remaining set of values, it has been deemed preferable to also calculate the average value of the elastic modulus without taking it into account. The value of this second calculated average is 2318 MPa. This has been the value considered in the discussions presented in sections II.4 and II.5. Other RBW3 results, such as the compressive strength and the strain at peak stress, are considered sufficiently representative and have not been disregarded in the calculation of the corresponding averages. Globally, the curves depicted in Figure II.5b continue to be linear up to around 2 MPa and then experience a progressive reduction of the stiffness until the peak stress. Table II.3 presents the values of the compressive strengths ( $f_c$ ) and the strains at the peak stresses ( $\varepsilon_p$ ). The average strength is 6.51 MPa and the average strain at peak stress is 0.98%.

## PAPER II

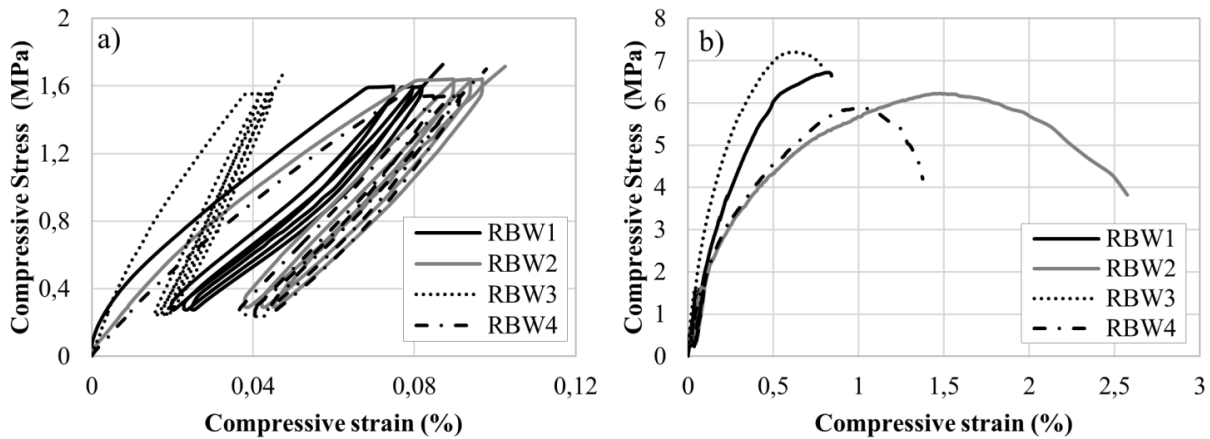


**Figure II.5** Stress vs. strain experimental curves for running bond walls. a) Detail of the three loading/unloading cycles, b) Full curves until failure.

**Table II.3** Compressive strength, stiffness and strain at peak stress of running bond walls.

RBW	$f_c$ (MPa)	$E_c$ (MPa)	$\varepsilon_p$ (%)
RBW 1	6.72	2205	0.82
RBW 2	6.22	2227	1.48
RBW 3	7.20	4023	0.62
RBW 4	5.88	2521	1.00
Average	6.51	2744	0.98
CV	8.9%	31.5%	37.6%
Average		2318*	
CV		7.6%*	

\* The value of  $E_c$  for RBW3 is not considered in the average.

The failure mode of the RBWs was qualitatively similar for the 4 samples. The first visible cracks appeared at about 75% of the maximum load. These cracks were thin and vertical, initially only visible in the bricks and mostly located in the external thirds of the front faces of the specimens. At the peak load, the cracks were wider and visibly affected both bricks and mortar (Figure II.6a). After the peak, degradation continued, with further opening of the cracks and sudden spalling of mortar and brick portions. In two samples, sudden transverse splitting, visible from the lateral faces, was produced (Figure II.6b). Once dismantled (Figure II.6c), the specimens exhibited a typical sandglass failure, characterised by the presence of a remaining core.

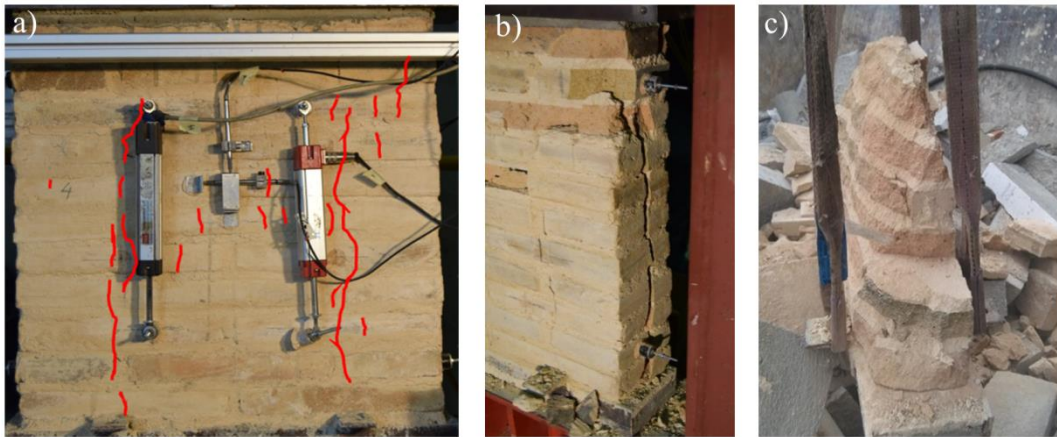


**Figure II.6** Failure of running bond walls. a) Crack pattern at peak load, b) State at the end of the test, c) Dismantled specimen.

### II.3.2 Stack bond prisms – Monotonic loading

Among the 7 stack bond prisms prepared, 4 were tested following the same procedure applied to the running bond walls. After the first stage, involving three cycles under load control, they were subjected to a steadily increasing imposed displacement. The experimental stress-strain curves are displayed in Figure II.7. Although SBP3 presents a longer linear branch, all 4 specimens have a noticeable non-linear behaviour. Significant deformability is observed after 65% of the maximum load, particularly for specimens SBP1 and SBP2. Table II.4 reports a summary of the experimental results, which yielded an average elastic modulus of 2494 MPa, compressive strength of 6.49 MPa, and strain at peak stress of 1.2%.

The mechanical behaviour and failure of the stack bond prisms are illustrated in Figure II.8. Before the peak load, vertical cracks developed in the bricks, mainly on the three central ones and near the edges of the faces. After the peak load, these cracks propagated and opened leading to the spalling of some brick and mortar portions. A remaining core forming a sandglass shape could be observed for some of the specimens (Figure II.8c).

## PAPER II

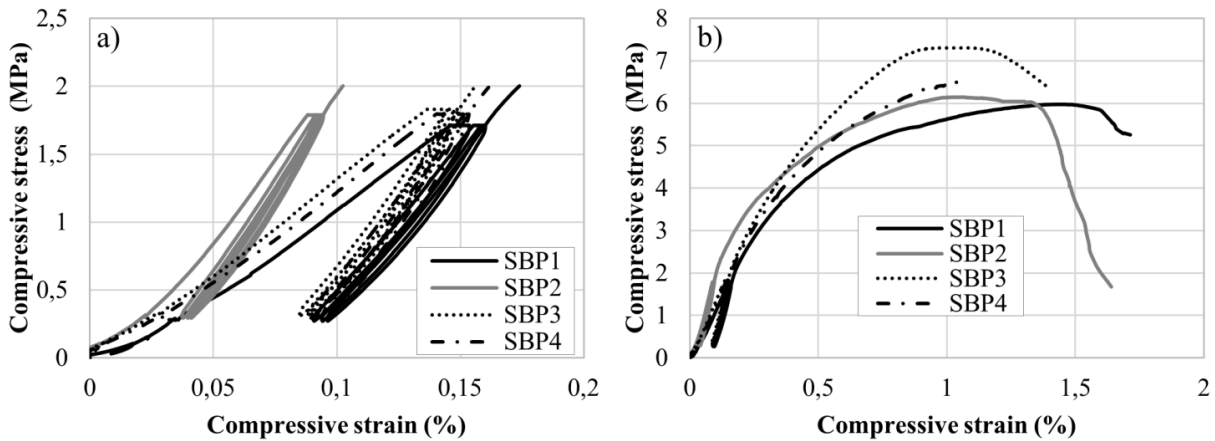


**Figure II.7** Stress vs. strain experimental curves of the stack bond prisms with monotonic loading. a) Detail of the three loading/unloading cycles and beginning of the second stage, b) Full curves until failure.

**Table II.4** Compressive results of stack bond prisms.

SBP mono	$f_c$ (MPa)	$E_c$ (MPa)	$\varepsilon_p$ (%)	SBP cyclic	$f_c$ (MPa)	$E_c$ (MPa)	$\varepsilon_p$ (%)
SBP 1	5.98	2249	1.45	SBP 5	6.91	1957	0.90
SBP 2	6.15	2782	1.05	SBP 6	7.34	2549	1.09
SBP 3	7.31	2443	1.10	SBP 7	7.03	2634	1.00
SBP 4	6.52	2502	1.05				
Average	6.49	2494	1.16	Average	7.10	2380	1.00
CV	9.1%	8.8%	16.4%	CV	3.1%	15.5%	9.4%

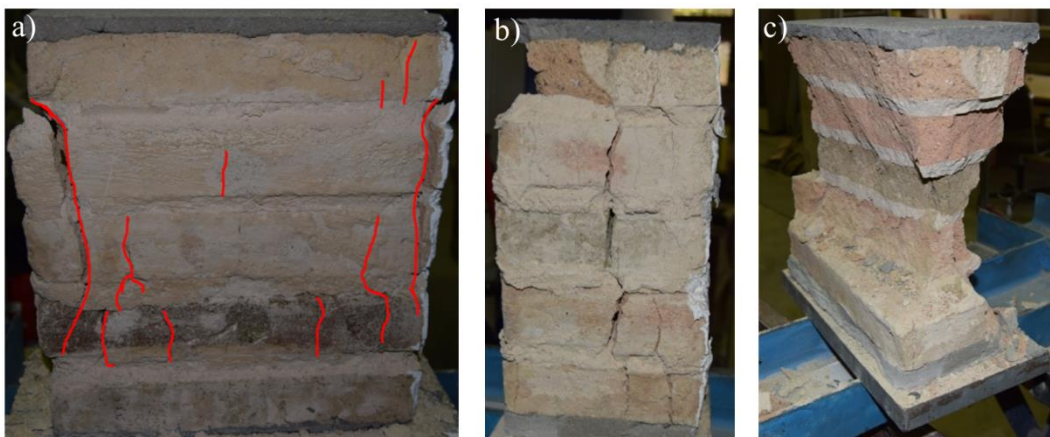


**Figure II.8** Stack bond prisms after failure. a) Front view, b) Lateral view, c) Dismantled specimen.

### II.3.3 Stack bond prisms – Cyclic loading

As explained in section II.2.3, three stack bond prisms were tested cyclically at the second loading stage until displacement controlled failure. As shown in Figure II.9, the stress-strain

curves of specimens SBP5 and SBP6 present a complete set of 8 cycles, composed of the three initial ones corresponding to the first stage, two more cycles on the pre-peak range and three additional cycles after the peak load. The post-peak response of specimen SBP7 could not be plotted since it was not properly captured by the LVDTs.

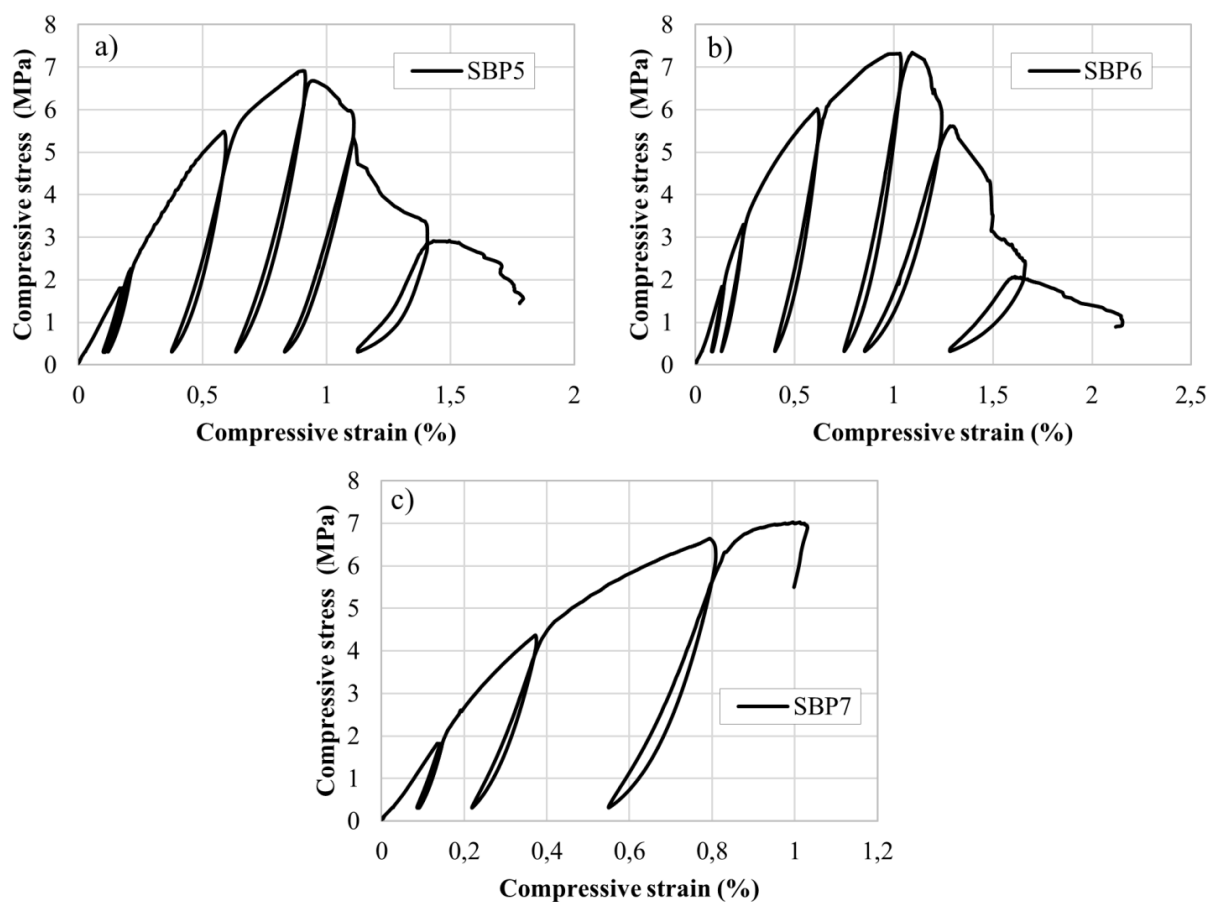


**Figure II.9** Stress vs. strain experimental curves of the stack bond prisms with cyclic loading until failure. a) SBP5, b) SBP6, c) SBP7.

The displayed curves clearly reveal the non-linear behaviour, the accumulation of non-reversible strains and the stiffness degradation experienced by masonry under cyclic loading. As stated by former researches [89,91,277,290], the cyclic behaviour is characterised by the presence of intersecting points between the reloading branches and the unloading branches of previous cycles, the so-called ‘common points’. In the tests here presented, the reloading branches are almost straight lines for cycles before the peak load, while after the peak load they

## PAPER II

present a more complex shape. This is consistent with the findings of similar experimental campaigns, e.g. Naraine et al. [290].

One important feature shown by the experimental curves is the stiffness degradation experienced at each cycle, which is accentuated after the peak load. Figure II.10 illustrates the evolution of the elastic modulus as a function of strain by means of normalized values. The normalized elastic modulus is calculated as the ratio between the elastic modulus of each reloading branch ( $E_{c,i}$ ) and the maximum elastic modulus found for that specimen ( $E_{c,max}$ ). The normalized compressive strain used here for each reloading branch is the ratio between the strain at the end of the branch ( $\varepsilon_{r,i}$ ) and the strain at peak stress ( $\varepsilon_p$ ) reported in Table II.4. As can be observed, values of  $E_c$  are maximum and almost constant for the first cycles, corresponding to strains below 25% of the strain at peak stress. At peak stress, the stiffness degradation attains 20 to 40% of the initial one. After the peak load, the decrease of the elastic modulus is very significant due to the damage experienced by the material.

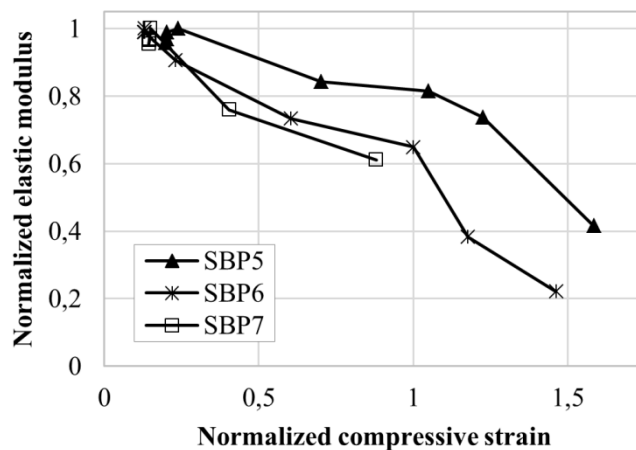


**Figure II.10** Normalized elastic modulus ( $E_{c,i}/E_{c,max}$ ) of the reloading branches vs. normalized compressive strain ( $\varepsilon_{r,i}/\varepsilon_p$ ), for the stack bond prisms tested under cyclic loading.

The crack patterns and mechanical behaviour of the prisms under cyclic loading were essentially the same as the ones reported for the monotonically loaded prisms in section II.3.2. The resulting experimental values are included in Table II.4 and are characterised by an average

elastic modulus of 2380 MPa, compressive strength of 6.95 MPa, and strain at peak stress of 1.0%.

Additionally, an estimation of the compressive fracture energy ( $G_{fc}$ ) could be done for specimens SBP5 and SBP6 since their post-peak response was captured until low values of residual load. It was calculated as the area below the envelope stress-displacement curve through a Riemann sum. Results are 8700 N/m for SBP5 and 10800 N/m for SBP6.

## II.4 Analytical studies

The aim of this section is to investigate the validity of existing predictive equations and models for the estimation of the compressive strength and the elastic modulus of masonry and the simulation of its compressive behaviour. The experimental results are compared with analytical and empirical expressions.

### II.4.1 Masonry compressive strength

In the absence of experimental evidence obtained through standardized tests, such as the ones described in EN 1052-1 [72] or ASTM C1314-09 [70], building codes propose the use of some expressions for the determination of the masonry compressive strength from the properties of the component materials. Eurocode 6 [60] allows the use of an equation (Appendix. Eq. A1) that relates the characteristic compressive strength of masonry with the compressive strengths of brick and mortar. Similarly, the American ACI, ASTM and TMS, on a Commentary on the Specification for Masonry Structures ACI 530.1-02 [112], proposes the use of an empirical expression (Appendix. Eq. A2) that relates the compressive strength of masonry to the compressive strength of the units only.

## PAPER II

Several authors have derived analytical models or closed form expressions to estimate the compressive strength of masonry. Among others, Hilsdorf [113], Khoo & Hendry [114], and Ohler [115], developed models based on equilibrium and the multiaxial stress states experienced by the masonry components at failure. The proposed formulations (Appendix. Eq. A3 to A5) depend on the relative thicknesses of the components, the compressive strength of mortar, and both the compressive and tensile strength of the units. The reader is referred to [128,291] for details about these models and the standards' expressions.

The compressive strength of masonry was evaluated for the different equations aforementioned. A specific investigation has been carried out on the sensitivity of the models to the variation of the material properties. For that purpose, a virtual sample of data normally distributed was created for each of the material properties reported in Table II.1 and Table II.2. The tensile strength of the bricks was determined from the bending tensile one by applying the conversion formula proposed by Eurocode 2 [292]. This formula (Appendix. Eq. A6) was used in the lack of a more specific one available for clay bricks. Each virtual sample was composed of 5000 data and characterised by the mean and the standard deviation of each property. 5000 strength estimations were obtained for each equation. A summary of the results indicating the mean value and the coefficient of variation is shown in Table II.5. All the predictions can be compared with the average experimental values ( $f_{c,exp}$ ). To convert the characteristic value provided by the European code [60] to the average one, the former was multiplied by a factor equal to 1.2 as proposed by the EN 1052-1 [72]. In the table,  $f_{c,EC6}$  and  $f_{c,ACI}$  refer to the values calculated with Eurocode 6 [60] or ACI 530.1-02 [112], while  $f_{c,Hilsdorf}$ ,  $f_{c,K\&H}$  and  $f_{c,Ohler}$  correspond to those calculated according to [113], [114] and [115] respectively. All the analytical predictions present reasonable estimations of the compressive strength of masonry, being  $f_{c,EC6}$  and  $f_{c,K\&H}$  the lower and upper bounds respectively.

**Table II.5** Experimental and analytical compressive strength values (MPa). The coefficient of variation is indicated in brackets.

Sample	$f_{c,exp}$	$f_{c,EC6}$	$f_{c,ACI}$	$f_{c,Hilsdorf}$	$f_{c,K\&H}$	$f_{c,Ohler}$
RBW	6,51 (8.9%)					
SBP,mono	6,49 (9.1%)	6,06 (6.7%)	6,36 (4.8%)	6,80 (9.3%)	7,14 (10.0%)	6,47 (9.8%)
SBP,cyclic	7,1 (3.1%)					

## II.4.2 Masonry stiffness

In the case of the elastic modulus of masonry, building codes also propose some simple relationships to estimate this parameter in the lack of experimental results. Eurocode 6 [60] proposes to evaluate the elastic modulus ( $E_{c,EC6}$ ) through a linear relationship with the masonry characteristic compressive strength. The recommended constant of proportionality is 1000. The American Requirements for Masonry Structures [66] follow a similar approach and suggest to estimate the elastic modulus ( $E_{c,ACI}$ ) as 700 times the compressive strength. These criteria were applied to the masonry herein investigated by using the strength estimates obtained in the previous section II.4.1. The comparison with the experimental results ( $E_{c,exp}$ ) is included in Table II.6. The experimental value shown for the SBPs is an average of all the static and cyclic tests on prisms (7 tests) since they do not differ in the procedure used for the measurement of the elastic modulus.

Based on the findings of Pande et al. [131], Pelà et al. [105] proposed a very simple one-dimensional homogenization method for the estimation of the elastic modulus of masonry. This model considers the interaction of units with bed and head mortar joints as a system of series-parallel uniaxial springs, by incorporating the elastic moduli of the material components. It allows using different expressions for the different testing specimens such as stack bond prisms -without head joints-, and running bond walls -with head joints. The model (Appendix. Eq. A7 and A8) was applied with the material properties specified in Table II.1 and Table II.2. In the lack of a specific measurement, the elastic modulus of the bricks in the direction parallel to the

## PAPER II

load was estimated as the average of the values of the other two perpendicular directions. Table II.6 presents the results of the homogenization method ( $E_{c,1D}$ ) that provides more accurate Young's moduli estimations than the expressions provided by the aforementioned standards.

**Table II.6** Experimental and analytical elastic modulus values (MPa).

Sample	$E_{c,exp}$	$E_{c,1D}$	$E_{c,EC6}$	$E_{c,ACI}$
RBW	2318	2075	5050	4445
SBP, all	2445	2098		

### II.4.3 Stress-strain relationships under cyclic loading

The literature review presented in section II.1 reported a limited number of references dealing with the experimental testing of masonry under cyclic compression. The number of references studying the constitutive stress-strain laws of the masonry cyclic compressive response is even more reduced. Naraine & Sinha [290] proposed a simple mathematical model to predict the unloading and reloading curves of brick masonry. It consisted of exponential stress-strain relationships, which were calibrated to fit previous experimental data obtained by them [89]. The same data were used by Eibl et al. [293] to define another simple model, which proposed exponential unloading curves and linear reloading curves. Similar formulations, representing the curves with exponential or polynomial functions are also included in [294–296] for different types of masonry. None of the former models considered the case of partial unloading-reloading.

Sima et al. [297] proposed a more complex constitutive model based on a damage parameter. The model was also calibrated using experimental results of Naraine and Sinha [89]. The newest available approach is the one formulated by Facconi et al. [92], which is partially based on the work of Crisafulli [298]. Its equations were calibrated for different types of masonry tested by different authors [89,92,277,295,299,300].

The latter two models are able to also predict the case of partial unloading-full reloading. In addition to their larger generality, these two models have been selected for the present investigation because of their ability to model cyclic loading processes not reaching zero stress as in the case of the experiments presented in section II.3.3.

The two investigated models consider the strain at the onset of unloading as the internal variable that completely defines a whole cycle of unloading-reloading. The rest of parameters controlling the cycle are obtained from this strain by means of relationships adjusted from experimental data. The parameters of the model of Sima et al. [297] have been recalibrated in this work by using the experimental results of tests SBP5, SBP6 and SBP7 as reference data. The new calibration is displayed in Figure II.13 in terms of relationships between unloading strain to plastic strain ratio ( $r$ ) and the unloading damage ( $\delta_{un}$ ), between the final unloading stiffness to initial stiffness ratio ( $R$ ) and the unloading damage ( $\delta_{un}$ ), and between the reloading damage ( $\delta_{re}$ ) and the unloading damage ( $\delta_{un}$ ).

The model of Sima et al. [297] defines the envelope curve based on the modulus of the initial linear branch ( $E_o$ ), the strain value limiting the initial branch ( $\varepsilon_o$ ), the compressive strength ( $f_c$ ) and the strain at the peak stress ( $\varepsilon_p$ ). The model of Facconi et al. [92] considers the same parameters with the exception of the strain limiting the initial branch. Instead, their model uses the ultimate strain at zero stress ( $\varepsilon_u$ ) to also delimit the post-peak response.

In both cases, unloading branches are defined via nonlinear equations. Sima et al. [297] proposes straight reloading branches. Conversely, Facconi et al. [92] implements a more refined double-curvature law for the reloading response, although the limits of the resulting curves are also based on a linear relationship. In addition, the model of Facconi et al. offers the possibility to modify the value of some parameters to obtain a better adjustment of the curves and specifically the parameter  $\gamma_{un}$ , which governs the initial slope of the unloading curves.

## PAPER II

Both models have been used to simulate the tests on specimens SBP5 and SBP6, with the input data indicated in Table II.7. Figure II.11a and Figure II.12a show the comparison between the experimental stress-strain curves of specimens SBP5 and SBP6, respectively, and the analytical curves obtained through the direct application of Facconi et al. model [92]. Figure II.11b and Figure II.12b display the comparison with the model of Sima et al. [297] with the new calibration previously indicated.

**Table II.7** Model input data for comparison with the experimental results of specimens SBP5 and SBP6.

Specimen	Model	$E_o$ (MPa)	$\varepsilon_o$ (%)	$f_c$ (MPa)	$\varepsilon_p$ (%)	$\varepsilon_u$ (%)	$\gamma_{un}$ (-)
SBP 5	Facconi et al. [92]	1100	-	6.91	0.90	1.60	3
	Sima et al. [297]	1030	0.5	6.91	0.90	-	-
SBP 6	Facconi et al. [92]	1600	-	7.34	1.09	2.00	3
	Sima et al. [297]	1463	0.2	7.34	1.09	-	-

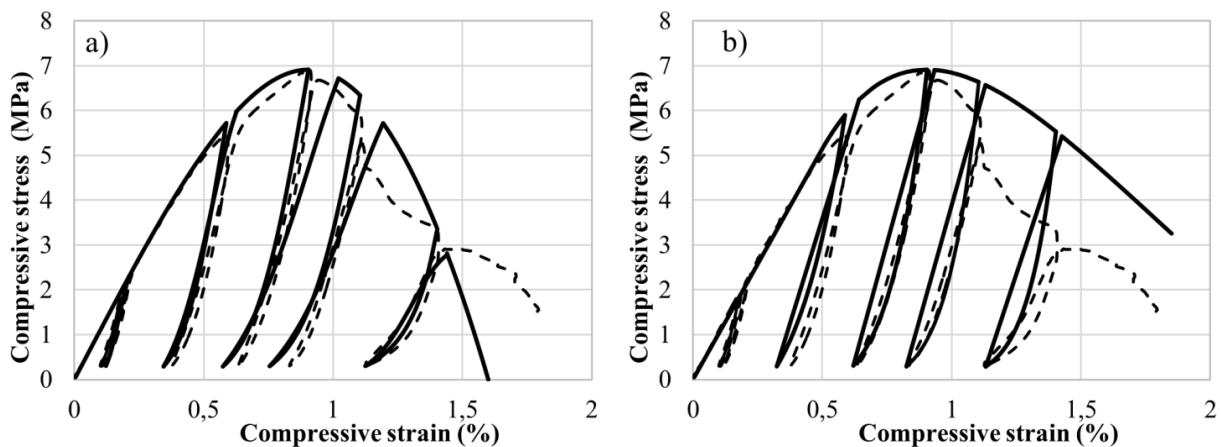


**Figure II.11** Experimental (dashed) and analytical (solid) stress-strain curves for specimen SBP5. a) Analytical model by Facconi et al. [92], b) Analytical model by Sima et al. [297], with new calibration.

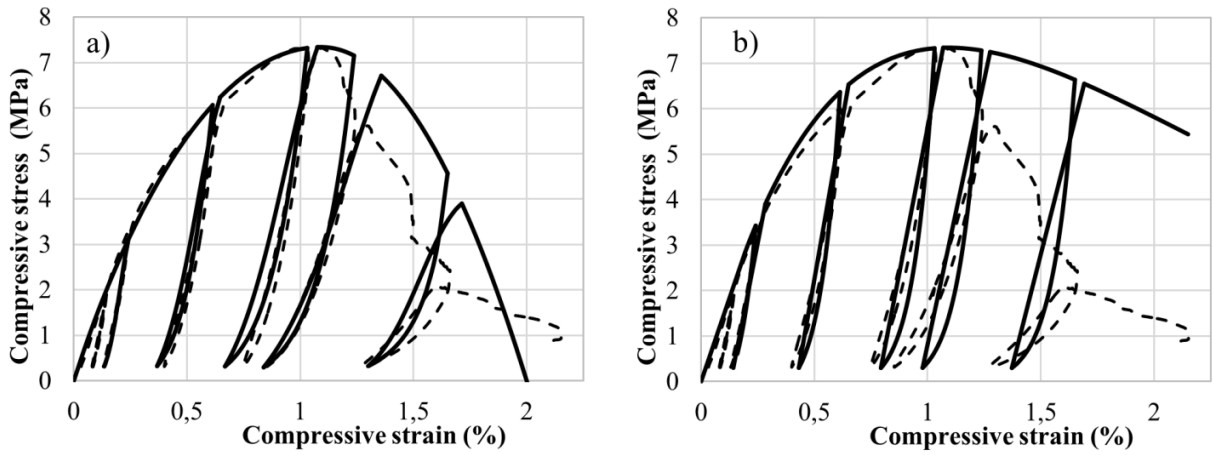


**Figure II.12** Experimental (dashed) and analytical (solid) stress-strain curves for specimen SBP6. a) Analytical model by Facconi et al. [92], b) Analytical model by Sima et al. [297], with new calibration.

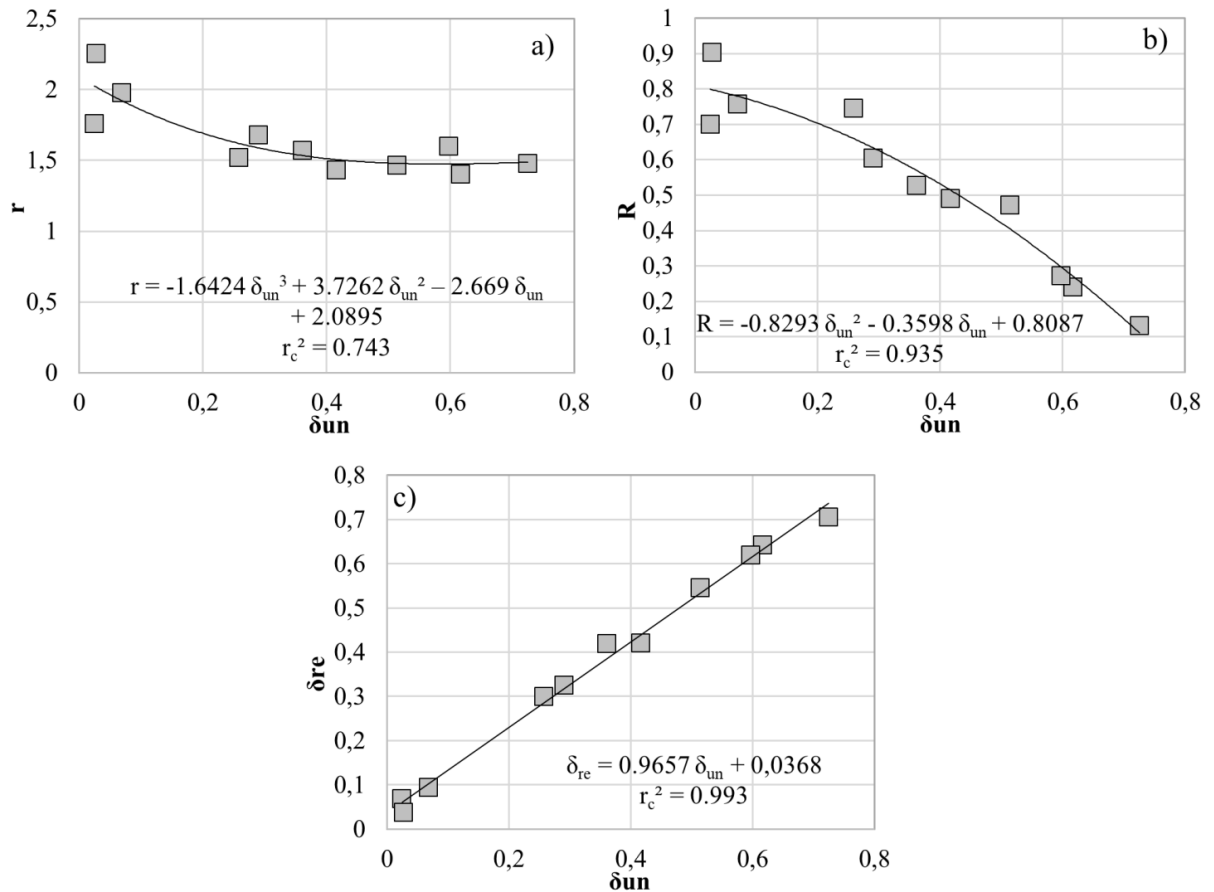


**Figure II.13** New relationships for the model proposed by Sima et al. [297], obtained by curve fitting of the present work's experimental data. Notation according to [297]. a) Relationship between unloading strain – plastic strain ratio ( $r$ ) and the unloading damage ( $\delta_{un}$ ), b) Relationship between the final unloading stiffness – initial stiffness ratio ( $R$ ) and the unloading damage ( $\delta_{un}$ ), c) Relationship between the reloading damage ( $\delta_{re}$ ) and the unloading damage ( $\delta_{un}$ ). In the above,  $r_c^2$  is the coefficient of determination R squared.

**PAPER II****II.5 Discussion**

Masonry specimens of two different configurations, consisting in running bond walls (RBWs) built according to EN 1052-1 [72] and stack bond prisms (SBPs) built following ASTM C1314 [70], have been tested under uniaxial compression. The failure modes observed during the tests have been very similar for both sets of samples. The response of both types of specimen was characterised by an initial crack pattern consisting of thin vertical cracks in the bricks, appearing mainly near the specimens' edges. With the increase of load, these cracks become later apparent across the mortar joints and propagated over the whole height of the specimens. Additional vertical cracks affected the central part of the faces after the peak load. A final remaining core was observed showing a sandglass shape, as typically obtained in compression tests. Due to their similar failure mode, both types of sample can be considered able to represent the complex mechanism of the compressive response of masonry.

The average value of the compressive strength obtained for stack bond prisms tested under cyclic loading is 7.10 MPa, which is slightly higher than the strength obtained for monotonically loaded prisms, equal to 6.49 MPa. The associated variabilities, the scattering of the materials (see Table II.1 and Table II.2), and the limited amount of specimens tested might justify such a difference derived from monotonic and cyclic testing. The monotonic curves seem to provide, however, a good estimate of the peaks' envelope of cyclic curves, as also seen by [89,91,277].

The strength obtained for the stack bond prisms is very similar to that obtained for the running bond walls, equal to 6.51 MPa. The difference is very small and may be only due to the scattering of the material properties. The almost null influence of the head joints in the wall specimens may be explained as the consequence of a careful construction in laboratory involving the accurate filling of all joints with mortar. It should be noted that the presence of head joints could have a more detrimental effect in not-so-carefully built masonries.

Very moderate coefficients of variation, of 9.1% for SBP under monotonic load, 3.1% for SBP under cyclic load and 8.9% for RBW, have been obtained. These coefficients are lower than the ones obtained for the material properties. It can be said that, as shown in the experiments, the scattering of the results on composite specimens is smaller than that shown by the component materials.

The equations available in the standards for the prediction of the compressive strength have provided satisfactory estimations of the strengths measured experimentally, as reported in Table II.5. In the case of the ACI equation [112], a satisfactory estimation has been obtained in spite of the fact that it was originally adjusted for more resistant masonry types than the one studied herein [112].

Table II.5 also includes the results of the application of three closed form expressions to predict the compressive strength. The three equations yield very accurate values fully comprised within the limits of the experimental ones taking into account the obtained scattering. Nevertheless, former researches such as [105,291] have found that these formulas may in some cases overestimate the experimental strength. A possible explanation for this overestimation can be found in the fact that the three equations, based on equilibrium considerations, are very sensitive to the value of the tensile strength of the units. The latter is a mechanical parameter of difficult determination whose measurement is not covered by any available standard. Due to it, these equations or similar closed form ones should only be used when reliable values of the material properties have been made available through accurate experimental tests.

Table II.5 also presents the coefficients of variation obtained for the simulations. In a way consistent with the experimental results, the 5 studied equations provide coefficients of variation lower than the ones of the component material properties.

**PAPER II**

The elastic modulus of masonry has been evaluated as the chord modulus of the stress-strain curves between the 5% and 30% of the maximum compressive load obtained after three initial loading cycles. The execution of the cycles is done, among other reasons, to cancel possible effects related to the first contact between the specimens and the loading machine platens. As shown in Figure II.5a and Figure II.7a, and highlighted in [94], the performance of cycles introduces irreversible strains in the specimen, which leads to an increase in the stiffness of the reloading branches. In addition to the platen-specimen contact effects, these irreversible strains might be due to an initial compaction of the material motivated by the closing of micro-cracks in the unit-mortar interface and voids within the mortar joints [75]. The elastic moduli computed following this approach, after the application of cycles, are considered to be more realistic than the very low ones that would be obtained from the initial curves.

A very similar value of the elastic modulus has been obtained for both types of specimen (RBW and SBP), with a difference of only 5%. The average elastic modulus obtained for running bond walls is 2318 MPa, while for all stack bond prisms is 2445 MPa. The latter value has been obtained as an average for the 7 SBPs, since there is no difference between monotonic and cyclic tests at this test stage. The similitude of the values for both specimen types was expected since the LVDTs were placed considering the same reference lengths, which included two bed joints and one full brick.

The small difference between the elastic modulus obtained in the two specimen types may be explained as due to the scattering of the material properties. It might be also explained by the presence of the head joint in the case of the RBWs. In fact, the applied spring model detects a certain influence of the head joint, as shown by the results included in Table II.6 for the simple 1-D homogenization, with a slightly lower value for the case of RBWs. In both cases, this simple method has provided a very satisfactory estimation of the experimental values. The

relative errors, from -10% to -15%, are of the same magnitude of those found by [105]. However, it is worth mentioning that this method is based on mechanical parameters (the elastic modulus of both units and mortar) that are difficult to be accurately measured in laboratory.

Compared to the compressive strengths,  $E_c/f_c$  ratios equal to 356 and 362 are obtained respectively for running bond walls and stack bond prisms. The ratios proposed by the building codes, equal to 1000 in the case of the European Eurocode 6 [60] and to 700 in the American requirements [66], clearly overestimate the measured elastic modulus. This provides further evidence on the fact that these expressions, derived mainly for new masonry, don't apply for historical or existing masonry made of solid clay bricks and lime mortar. Previous researches on clay brick masonry have also obtained  $E_c/f_c$  ratios significantly below those indicated by the codes, as for instance [77] with a ratio of 550, [127] with a ratio of 422, or the inventory presented in [128] with an average ratio of 356. In any case, the ratios obtained herein are very similar for both types of specimen. Additionally, the coefficients of variation associated to the estimation of the elastic modulus are moderately low (7.6% for RBWs, and 8.8% and 15.5% for SBPs). The performance of initial load cycles during the tests may have contributed to reduce the scattering obtained in the measurement of this mechanical property.

A much higher scattering, with a variation coefficient between 9.4% for stack bond prisms under cyclic loading and 37.6% for running bond walls, has been obtained for the values of the strain at peak stress. However, the average values attained for the different samples are similar and equal to 1.2% and 1% for SBPs tested monotonically and cyclically respectively and to 0.98% for RBWs. The strain at peak stress shows a strong dependence on the compressive strength, and tends to decrease as the strength increases.

In the case of the cyclic tests performed on stack bond prisms it has been possible to record the evolution of stiffness along the full tests and its progressive reduction with the accumulation

**PAPER II**

of damage, as shown in Figure II.10. Additionally, it has been possible to capture a significant fraction of the post-peak response, as in the researches made by Oliveira et al. [87] and De Felice [94]. The tests here presented have confirmed the loss of load-carrying capacity with increasing strains, but also the ability of the specimens to resist full unloading-reloading cycles after the peak load. In tests SBP5 and SBP6 the reloading branches recovered the stresses level attained before the unloading.

Taking advantage of the almost complete curves obtained for SBP5 and SBP6 specimens, the compressive fracture energy was evaluated. Lourenço [301] introduced the concept of ductility index as the ratio between the compressive fracture energy and the compressive strength. The experimental ductility indices computed for this campaign are 1.24 mm for test SBP5 and 1.47 mm for test SBP6. These values are close to the recommendation of 1.6 mm found in literature [301] for masonry with compressive strength lower than 12 MPa.

The two cyclic constitutive models studied are in good agreement with the experimental results obtained for specimens SBP5 and SBP6. Sima et al. model [297] is simpler and requires a lesser number of input parameters. However, in order to obtain a satisfactory agreement with the experimental results it has been necessary to recalibrate the parameters of the model based on the current tests. Conversely, Facconi et al. [92] model has provided a satisfactory agreement by directly applying the parameter values originally recommended by the authors, which were adjusted based on a set of different experimental campaigns. Compared to Sima et al model [46], the envelope curve formulated by Facconi et al. [92] has provided a better fit to the test results. The nonlinear shape proposed for the reloading branches is also more realistic. The prediction of the intersection of the reloading branches with the envelope curve for post-peak cycles, however, could be improved with an expanded series of experimental results.

## II.6 Conclusions

This paper has presented an experimental programme with new insights on the mechanical behaviour of brick masonry under compression. Two different sets of specimens were tested consisting of running bond walls built according to the geometric prescriptions of EN 1052-1 and stack bond prisms built according to ASTM C1314. They were tested in the laboratory under uniaxial compression to evaluate their compressive strength, elastic modulus and post-peak behaviour. A set of three stack bond prisms was tested under cyclic loading. The following conclusions can be drawn from these experiments:

- For the specific combination of materials studied, the tests on the two types of standard specimens have provided similar results in terms of compressive strength and deformability. Additional research should be carried out to extend this conclusion to other types of masonry.
- New experimental evidence on the behaviour of masonry under uniaxial cyclic loading has been obtained. Consistently with previous researches, the tests have shown the stiffness degradation of masonry for increasing strains. They have also shown that the static strain-stress curves can be used as a satisfactory estimation of the peak envelope of cyclic tests.
- The evaluation of the elastic modulus of masonry has been done after the application of three initial loading-unloading cycles. This approach is consistent with the recommendations of standards on other materials specifically devoted to the determination of this parameter. Given the consistency of the experimental results obtained herein, it is recommended to measure the elastic modulus of masonry, as a general rule, after the application of several cycles.

**PAPER II**

- The expressions provided by the European and American standards and some authors for the evaluation of the compressive strength of masonry have provided values in agreement with the experimental ones. Conversely, the criteria proposed by these standards for the calculation of elastic modulus have strongly overestimated the experimental corresponding values. The elastic modulus has been satisfactorily estimated, however, by means of a simple one-dimensional homogenization model. Two cyclic constitutive models investigated, proposed by different authors, have shown their ability to satisfactorily simulate the cyclic response obtained in the experimental tests. As opposite to Facconi et al. model, the use of Sima et al. model has required significant previous calibration.

### **5.3. Paper III – Experimental analysis of the size effect on the compressive behaviour of cylindrical samples core-drilled from existing brick masonry**

J. Segura, L. Pelà, P. Roca, A. Cabané, *Constr. Build. Mater.* 228 (2019),

<https://doi.org/10.1016/j.conbuildmat.2019.116759>

Abstract: This paper presents the results of an experimental programme about the evaluation of the size effect on the compressive behaviour of cylindrical samples of existing masonry. The study focuses on the in-situ coring and experimental testing of core specimens with 150 mm and 90 mm diameter. The 150 mm cylinder, recurrent in minor destructive evaluation of the compressive strength of existing masonry, includes four brick pieces, two mortar beds and one head joint. The 90 mm specimen includes one mortar bed and two segments of brick, and inflicts less damage on the inspected structural member due to its lower invasivity. The experimental research investigates the size effect on four different types of clay brick masonry. The first type was built in the laboratory using historical-like materials. The other three types of masonry belong to structural walls of existing historical buildings. The combination of experimental results from laboratory controlled materials and existing historical members shows that the size of the cylindrical specimen has regular effect on the compressive strength and the Young's modulus. The consistent relationship found between the compressive strengths of the 150 mm and 90 mm core samples allows the use of the latter specimen for a more respectful inspection of existing structural masonry.

*This page is intentionally left blank.*

### III.1 Introduction

The use of masonry as building material is abundant all over the world, including many major examples of architectural heritage. Many of these buildings are in need of structural assessment because of structural damage or material decay experienced over the years. Additionally, their structural condition often requires careful evaluations due to the adaptation to new uses. The knowledge on the mechanical behaviour of this material and its most influential parameters, such as compressive strength and Young's modulus, is of paramount importance for this kind of structural evaluations.

The experimental determination of the mechanical properties of existing masonry is a challenging task. The in-situ sampling and subsequent testing of masonry specimens in the laboratory provide a suitable approach to the problem, since it is possible to obtain direct measurements of the mechanical parameters that describe the elastic and strength behaviour. However, the composite character of masonry requires laboratory tests on sufficiently large samples, able to represent the complexity of the material texture, and therefore including both units and mortar joints. Yet, the in-situ sampling of large prismatic specimens of masonry, e.g. extracted from existing walls, may encounter important difficulties. In addition, sampling procedures should always be minimal in the case of historical buildings due to their cultural heritage value.

A possible solution to the aforementioned limitations in the case of brickwork is offered by the minor destructive testing (MDT) technique consisting in extracting masonry core samples from the existing structure to be tested in the laboratory. This technique was proposed by the UIC Leaflet [126] on the inspection of brick masonry arch bridges, which suggests to core drill cylinders with a diameter of at least 150 mm including four brick segments, two

**PAPER III**

mortar beds and one head joint. The cylindrical specimen is then tested under compression along the direction perpendicular to the mortar beds. Recent researches have shown that tests on such samples are able to reproduce the complex failure mechanisms of brickwork in compression. The calibration of this technique by comparison with tests on other non-standard [102–104] and standard [83,105,106] masonry specimens has shown its ability to provide reliable estimations of the compressive strength of the material. Pelà et al. [105] investigated also the possibility of estimating the Young's modulus of masonry by means of compression tests on this type of specimen.

The use of cylindrical samples smaller than those suggested by the UIC Leaflet might constitute a possible alternative to reduce the damage inflicted to the building. This may reveal to be necessary in case of protected heritage constructions requiring minimum invasivity of the in-situ inspection. The use of smaller cylinders may provide also additional practical advantages, besides the reduction of damage grade during sampling. A larger amount of cylindrical cores could be extracted, allowing an increase of the statistical significance of the results. Also, finding convenient spots where to drill smaller cores is easier than for 150 mm diameter cylinders, especially in the case of plastered walls. Moreover, the reduced size of the cores makes the transport, storage and testing operations easier.

A suitable cylindrical sample with dimensions smaller than the 150 mm diameter specimen of the UIC Leaflet should still include both the brick and mortar components in order to be able to represent realistically the composite character of the masonry material. The smallest core sample with these characteristics is composed of one diametric mortar joint and two cylindrical segments of brick. The diameter of this type of specimen should be around 90 mm and 100 mm in order to ensure a proper cutting of the two bricks without affecting the integrity of the interposed mortar joint. The use of cylinders with a diameter of 100 mm to determine the

masonry compression parameters has been already investigated in [107,108] with satisfactory results.

Previous experimental and analytical studies available in the scientific literature have already addressed the size dependence on the strength of different types of brick masonry samples. The research by Carpinteri et al. [302] focused on size dependence on fracture properties, such as strength and toughness, by testing different samples under three-point bending. The authors highlighted the important effect of constitutive heterogeneity on the size effect, especially when the specimen size is small. The numerical study by Lourenço [303] also showed the effect on tensile and compressive failures of the geometrical relationship between masonry units and the structural size.

This paper presents an experimental research aimed at evaluating the size effect on the compressive strength and elasticity of cylindrical samples of existing brick masonry of 150 mm and 90 mm diameter. The adequacy of the 150 mm diameter masonry cores to assess the mechanical behaviour of masonry in compression has been already investigated and validated in [83,102–106]. This research pays special attention to the use of the smaller 90 mm diameter core samples, with the following specific objectives: (1) exploring the possibility to reproduce the mechanical behaviour of brick masonry in compression by means of tests carried out on them; (2) analysing the consistency and reliability of the results obtained and, specifically, investigating whether the scattering obtained is sufficiently moderate; (3) determining size-effect correlations for compressive strength and Young's modulus based on the comparison with experimental results obtained from the 150 mm diameter cylinders.

The comparison between the tests on the two types of cylindrical cores has been carried out for four different types of masonry, all of them made of solid clay bricks and lime mortar but characterised by different brick and mortar compressive strengths.

**PAPER III**

The paper includes five sections. After an introduction about the purpose and objectives of the study, Section III.2 presents the first experimental campaign performed on masonry walls built in the laboratory with historical-like materials. The extraction, preparation and testing of two sets of cylinders, with 90 mm and 150 mm diameter, were carried out in a laboratory controlled environment. Section III.3 presents a second stage of the research, with three different experimental campaigns on different masonry typologies obtained from three real existing buildings. All field campaigns considered the in-situ sampling and subsequent laboratory testing of 90 mm and 150 mm cylindrical specimens. The results from the experimental programmes are discussed in Section III.4, in terms of failure modes, stability of experimental measurements, and size effect correlations of the compressive strengths and Young's moduli of the 90 mm and 150 mm core samples. Section III.4 presents also a comparison with predictive expressions from building codes. The paper ends with the concluding Section III.5.

**III.2 Experimental programme on masonry built in the laboratory**

The first stage of the research considered core samples extracted from masonry walls built in the laboratory with historical-like material components. The samples of this campaign were identified with code "MA". The experimental programme was carried out at the Laboratory of Technology of Structures and Building Materials of the Technical University of Catalonia (UPC – BarcelonaTech).

**III.2.1 Materials and construction of walls**

As stated before, the proposed MDT technique aims to study the compressive behaviour of existing brick masonry structures, with special focus on the case of historical buildings.

Therefore, the masonry built in the laboratory was designed to represent as much as possible a typical historical masonry with solid clay bricks and low-strength lime mortar in joints.

The bricks were handmade and presented rough surfaces and slightly variable dimensions. The nominal dimensions were  $305 \times 145 \times 45 \text{ mm}^3$ . A set of bricks was polished and cut into pieces of dimensions  $100 \times 100 \text{ mm}^2$  to be tested in compression according to EN 772-1 [285]. Table III. 1 reports the normalized compressive strength ( $f_b$ ), obtained by multiplying the experimental value by the shape factor proposed by the standard.

Two single-leaf walls with dimensions  $1.6 \times 0.8 \times 0.145 \text{ m}^3$  were built in the laboratory by using the aforementioned bricks (Figure III.1a). A qualified mason built the walls in running bond using a pure aerial lime mortar, classified as CL90 according to EN 459-1 [254]. The joint thickness varied between 15 mm and 20 mm. The walls were stored in laboratory conditions for more than one year until the coring process. This long time was necessary for a sufficient hardening of the aerial lime mortar.

At the time of the coring process for obtaining the masonry cylinders, some mortar joints were dismantled. These portions of mortar were cut into slabs with approximate dimensions of  $50 \times 50 \text{ mm}^2$ . After regularization with a little amount of gypsum powder, these pieces were subjected to the double punch test (DPT) by following DIN 18555-9 [304]. More detailed information on DPT can be found in [118,145,151]. As can be seen in Table III. 1, the average compressive strength value measured by means of this test ( $f_{m,DPT}$ ) was equal to 1.61 MPa. It is worth mentioning that this compressive strength value for the aerial lime mortar was obtained after two years from the construction of the wall. The DPT technique, suitable for the mechanical characterisation of the mortar joints in existing buildings, was considered in campaign “MA” as well as in the three case studies that will be described in Section III.3. The

## PAPER III

DPT results from the four campaigns will allow direct comparisons of the actual compressive strength of mortar inside the joints.

**Table III. 1** Experimental compressive strength of bricks ( $f_b$ ) and mortar joints ( $f_{m,DPT}$ ) in campaign “MA” executed on masonry built in the laboratory.

“MA”	$f_b$	$f_{m,DPT}$
Average (MPa)	17.44	1.61
Number of specimens	14	32
CV	8.3%	20.1%

### III.2.2 Core drilling and preparation of masonry specimens

Before the extraction of masonry cylindrical samples, a low vertical compression was applied to the walls with the aim of ascertaining their stability during the transportation inside the laboratory and the coring process.

The extraction of the cores was done by horizontal drilling using the dry coring technology proposed, among others, in [104] and [105]. Two types of cylinders were extracted (Figure III.1b). First, 150 mm diameter core samples (actual diameter of 152.5 mm), including one vertical and two horizontal mortar joints and four brick portions. Second, 90 mm diameter core samples (actual diameter of 92 mm), including a single diametric mortar joint and two brick portions. All the cores had an approximate depth of 145 mm. Six cylindrical specimens of each diameter were extracted from the walls. Additional cores were extracted and used for other parallel researches carried out by the authors [145].

After extraction, two high strength mortar caps were casted on the cylindrical specimens (Figure III.2). These caps were used to create two flat surfaces allowing the application of an evenly distributed load. This approach was already proposed in [83,105,145] and differs from the UIC leaflet [126] where it is recommended to apply the load through steel concave loading plates and to make use of lead sheets in contact with the sample. The high strength mortar caps

match the irregular curved perimeter of the cores and avoid any stress concentration during the tests. The widths of the caps were about 110 mm for the 150 mm cores, and about 70 mm for the 90 mm cores. These dimensions were chosen to maintain similar width to diameter ratios for the two different types of cylinder.

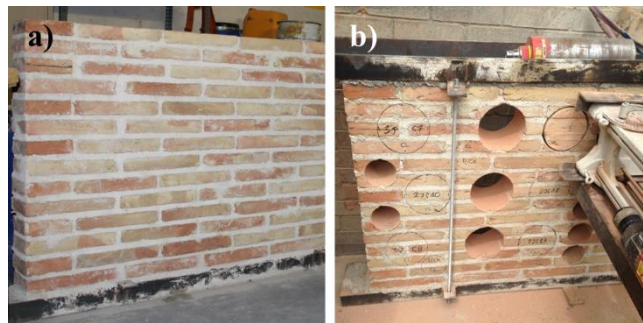


**Figure III.1** a) Masonry wall built in the laboratory for the campaign “MA”, and b) core drilling of 150 mm and 90 mm cylindrical samples.

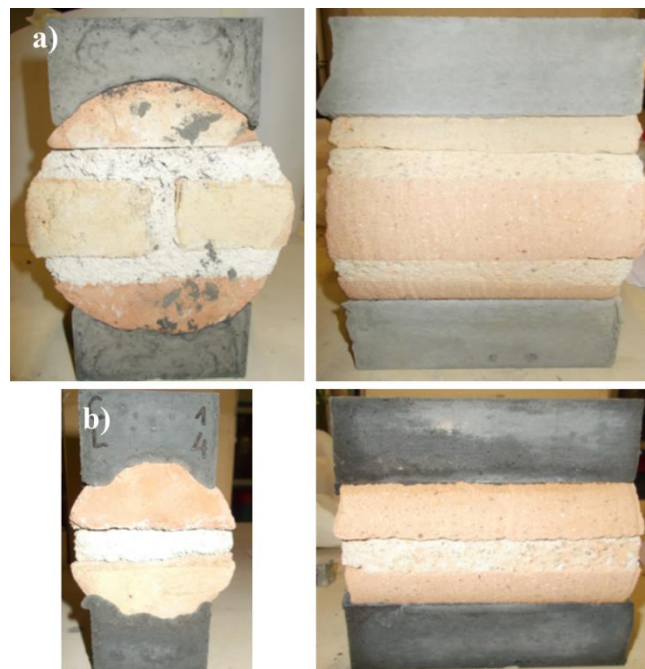


**Figure III.2** Front and lateral views of regularized core samples of campaign “MA”: a) 150 mm cylinder and b) 90 mm cylinder.

**PAPER III****III.2.3 Testing procedures**

Both 150 mm and 90 mm cores were tested in a general-purpose compression machine with load capacity of 3000 kN (Figure III.3) after two years from the construction of the walls. Thanks to the mortar caps, uniaxial compression could be applied perpendicularly to the horizontal joints.

The tests were carried out in two consecutive stages. The first one was aimed to study the elastic behaviour of the material and consisted in the application of three loading/unloading cycles under load control. These cycles ranged from 5% to 20% of a supposed maximum load that had been estimated before the tests. In the lack of a specific standard for these tests, the first stage was planned taking as reference some standards on the measurement of the Young's modulus for other materials [119,287–289], as well as former researches [75,105]. The Young's modulus was calculated for the loading branch of the third cycle. The second stage aimed to investigate the nonlinear behaviour of the material and to measure its compressive strength. The cylinders were tested under displacement control, at a rate of 0.004 mm/s. The tests were stopped after registering part of the post-peak softening response.

Linear variable differential transformers (LVDTs) were used to record the displacements experienced during the tests. Two vertical LVDTs of  $\pm 5$  mm range and 5  $\mu\text{m}$  precision were attached to the mortar caps to capture the vertical displacements. The vertical strains in compression were calculated as the ratio of the displacement experienced by the LVDTs and the cylinder's diameter, as the high strength mortar caps had negligible deformation in comparison with that of the masonry.

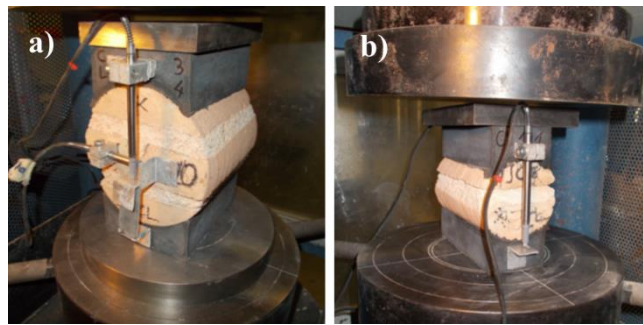


**Figure III.3** Experimental setups of campaign “MA” for a) 150 mm cylinder and b) 90 mm cylinder.

### III.2.4 Results

Figure III.4 shows the stress-strain curves obtained during the second stage for the 150 mm and 90 mm cylindrical samples. All the curves present an initial linear branch. The end of this branch corresponds to the maximum stress reached in the previous loading/unloading cycles. After that, all the specimens present another linear branch with lower slope.

In the case of the 150 mm core samples (Figure III.4a), the linear branch continues up to 80÷90% of the maximum load, when a sudden reduction is registered in the slope for the majority of the specimens. This point usually corresponds to the appearance of the first crack, and indicates the start of a noticeable nonlinear behaviour until the peak stress. Then, a softening response follows with decreasing stresses under increasing strains. The curves of the 90 mm core samples (Figure III.4b) are similar. However, the nonlinear behaviour before the failure begins at an earlier point corresponding to 50÷60% of the maximum load. The softening is more accentuated, showing a faster loss of load-carrying capacity under increasing strains.

The failure mechanism observed in the 150 mm core samples started with a crack arising next to one of the edges of the mortar caps, either within the top or bottom brick of the specimen (Figure III.5a). The crack first appeared at one side of the specimen, possibly corresponding to the weakest of the two bricks. With increasing load, this crack propagated further by splitting the intermediate brick, and then a symmetrical crack appeared at the other lateral side (Figure

## PAPER III

III.5b). Additional distributed thinner vertical cracks appeared through the entire specimen, both at the front and rear faces, as well as on the lateral faces. At failure (Figure III.5c), the two main cracks developed also through the mortar until fully connecting the top and bottom caps. This caused the detachment of the external parts, with a characteristic sandglass shape failure.

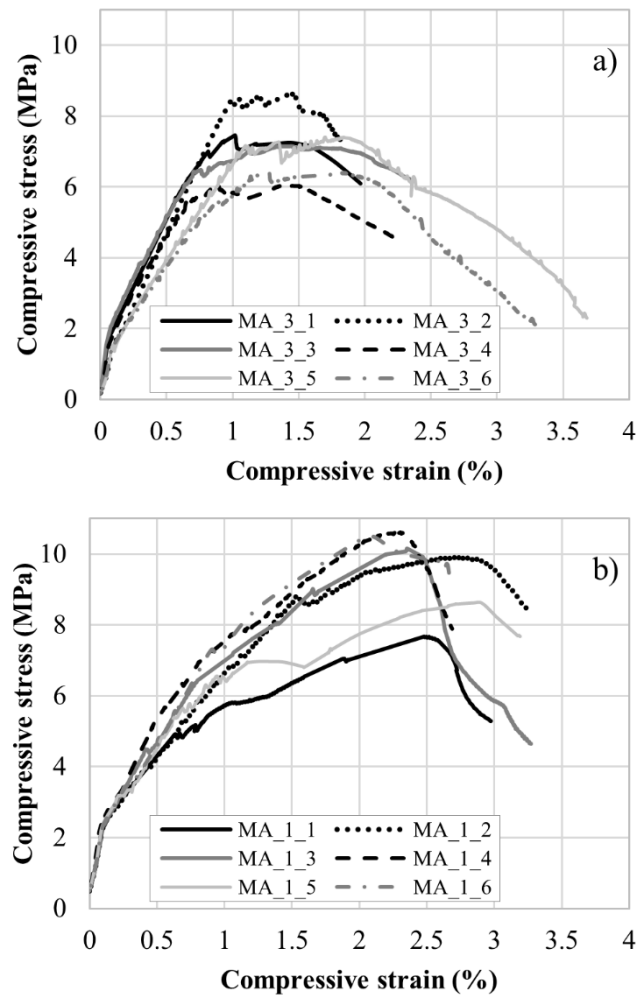


**Figure III.4** Compressive stress-strain curves of core samples of campaign “MA”: a) 150 mm cylinders and b) 90 mm cylinders.

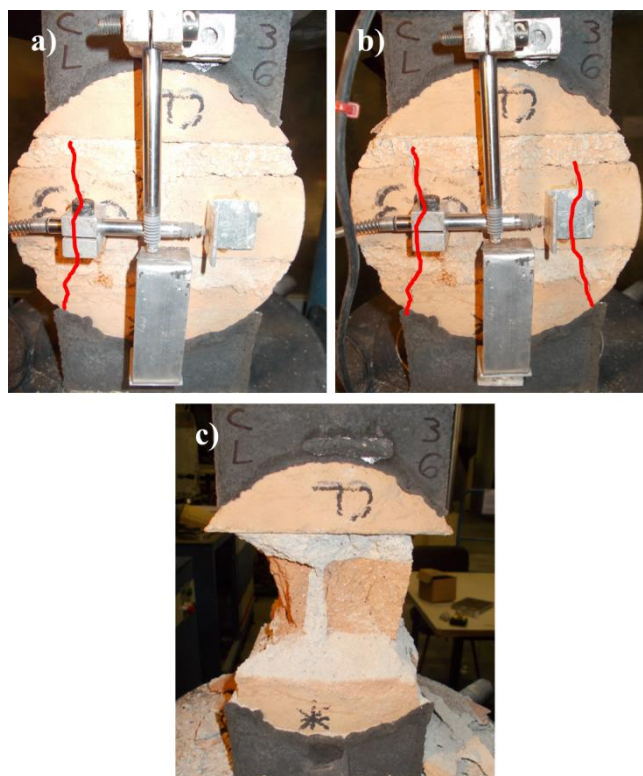


**Figure III.5** Typical failure of 150 mm cylinders in compression tests of campaign “MA”: a) appearance of the first crack at one side, b) further opening of the first crack and development of a second crack at the other side, and c) final sandglass failure.

The cracking process was similar in the 90 mm cylinders (Figure III.6a). The first initial vertical crack appeared in one of the two bricks, near the cap edge. A second crack appeared either in the same brick near the opposite edge or in the other brick by creating a longer crack at the same side. The lateral vertical cracks propagated also through the diametric mortar joint. At failure (Figure III.6b), the lateral cracks crossed the entire specimen from the top to the bottom caps causing the detachment of the external parts and the sandglass shape failure. Additional thinner vertical cracks appeared at the mid-section of the bricks.

As described above, a similar failure mode was obtained for both 150 mm and 90 mm cylinders, producing a sandglass shaped remaining core. At the peak load, the external parts of the cylinders were already separated from the central core by vertical cracks. This suggests that the effective resisting cross-section at failure corresponded to the width of the mortar caps.

## PAPER III

Taking into account this mechanical response, the compressive stresses acting on the specimen were calculated as the ratio between the load and the cross section determined by the width of the mortar caps. This is in agreement with the findings of [83,106,109]. Table III.2 presents the summary of the experimental results of campaign “MA”, including the compressive strength ( $f_c$ ) and the Young’s modulus ( $E$ ) of masonry.

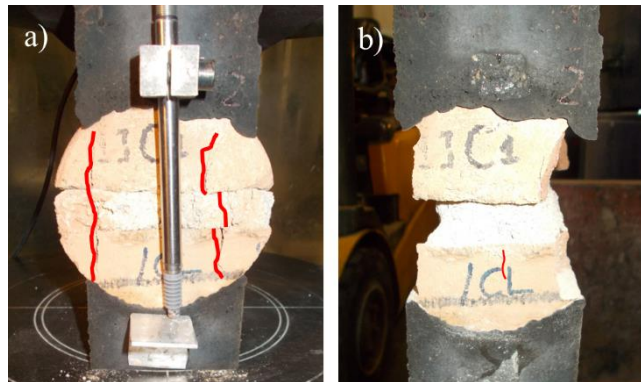


**Figure III.6** Typical failure of 90 mm cylinders in compression tests of campaign “MA”: a) vertical cracks crossing the core from the top to the bottom mortar caps, and b) final sandglass failure.

**Table III.2** Compressive strength ( $f_c$ ) and Young’s modulus ( $E$ ) of 150 mm and 90 mm masonry cylinders in campaign “MA”.

“MA” 150 mm cylinders			“MA” 90 mm cylinders		
ID	$f_{c,150mm}$ (MPa)	$E_{150mm}$ (MPa)	ID	$f_{c,90mm}$ (MPa)	$E_{90mm}$ (MPa)
MA_3_1	7.46	--	MA_1_1	7.67	1771
MA_3_2	8.64	1328	MA_1_2	9.93	1739
MA_3_3	7.15	--	MA_1_3	10.16	1806
MA_3_4	6.05	1900	MA_1_4	10.62	2253
MA_3_5	7.41	1282	MA_1_5	8.63	1863
MA_3_6	6.45	1390	MA_1_6	10.51	1823
Average	7.19	1475	Average	9.59	1876
CV	12.5%	19.4%	CV	12.3%	10.1%

The values of compressive strength obtained from the 150 mm samples are lower than those from the 90 mm cylinders. The average  $f_c$  values are equal to 7.19 MPa and 9.59 MPa respectively. This is a direct consequence of the size effect related to the two different geometries. The strength of the 150 mm samples is particularly affected by the presence of two mortar beds and the central head joint. The ratio between the strengths of the 150 mm and 90

mm samples is 0.75. The scattering obtained in the measurement of the compressive strength is very similar in the two types of cylinders, with a coefficient of variation around 12%. This scattering can be considered moderate taking into account the nature of the historical-like masonry investigated and the fact that it is built with handmade bricks. It is interesting to note that, in spite of their smaller size, the use of the 90 mm samples has not increased the scattering of the results with respect to that of the 150 mm.

The value of the Young's modulus obtained from the 150 mm samples is also lower than that estimated from the 90 mm specimens. In specific,  $E$  is equal to 1475 MPa and 1876 MPa respectively. This can be explained partly by the different size of the samples and also by the presence of two mortar beds in the 150 mm core. The ratio between the Young's moduli of the 150 mm and 90 mm samples is 0.79. The coefficient of variation is almost 20% in the case of the 150 mm specimens, which is still acceptable for the type of masonry tested. Again, the low scattering found for the tests of the 90 mm cylinders (CV 10%) confirms that the use of a smaller diameter is not introducing significant sources of variability.

The ratios relating the Young's modulus to the compressive strength ( $E/f_c$ ) are also very similar for the two types of specimen. They are equal to 214 for the 150 mm samples, and 198 for the 90 mm ones.

### **III.3 Experimental programmes on existing masonry buildings**

This section presents three experimental campaigns on real case studies intended to provide more results about the size effect on the masonry compression parameters for 90 mm and 150 mm core samples. Three different examples of urban architecture of Barcelona, Spain, were inspected in the context of on-going renovation works. In all cases, samples of constituents (bricks and mortar joints), and cylinders (90 mm and 150 mm cores) were extracted and then

**PAPER III**

tested in the Laboratory of Technology of Structures and Building Materials of the Technical University of Catalonia (UPC – BarcelonaTech).

The campaign with code “MB” dealt with one emblematic example of Catalanian industrial heritage (Figure III.7a), namely the textile factory “Fabra i Coats” built in 1910-1920 in Barcelona. The main 4-storey building consists of floors made of steel beams with small ceramic vaults in between supported by load bearing masonry walls. Its industrial activity decayed during the 1970s and the municipality recently converted the complex into a new cultural facility. Some works refurbished the building and adapted it to hold public exhibitions according to modern regulations. A structural assessment was required to design and verify these works. The project foresaw the opening of some new windows and doors in one façade wall. The cylinders tested within the present research were extracted from the same wall portions that were going to be eventually removed to make room to new openings.

The campaign with code “MC” studied a residential building located in Rambla de Catalunya, one of the main streets of Barcelona (Figure III.7b). This construction was built in 1930 in Noucentist style, and stands as a good example of bourgeois architecture of Barcelona’s Eixample neighbourhood. The load bearing masonry wall structure supports floors made of steel beams with small ceramic vaults in between. The building originally hosted 6-storeys, and two additional floors were added at the top in the second half of the 20th century, as in many other constructions of this area. This modification changed the loading conditions envisaged in the original project. Recently and prior to the execution of some renovation works, a structural assessment of the masonry structure was carried out. The assessment included inspection works to characterise the masonry mechanical properties. Again, the cylinders were extracted from wall portions to be demolished as part of the on-going renovation works.

The campaign with code “MD” involved a historical building in the district of Ciutat Vella (Figure III.7c). Built in the first half of the 19<sup>th</sup> century in Neoclassical style, this housing complex reflects the specific economical context of the time. The building stands out by the high-quality materials used, the stone masonry elements of the facades and the overall size of the construction. Brick masonry walls constitute the load bearing structure, which supports the floors made of timber beams with ceramic vaults in between. As in the former cases, the on-going renovation works motivated and allowed the extraction of the cylinders.

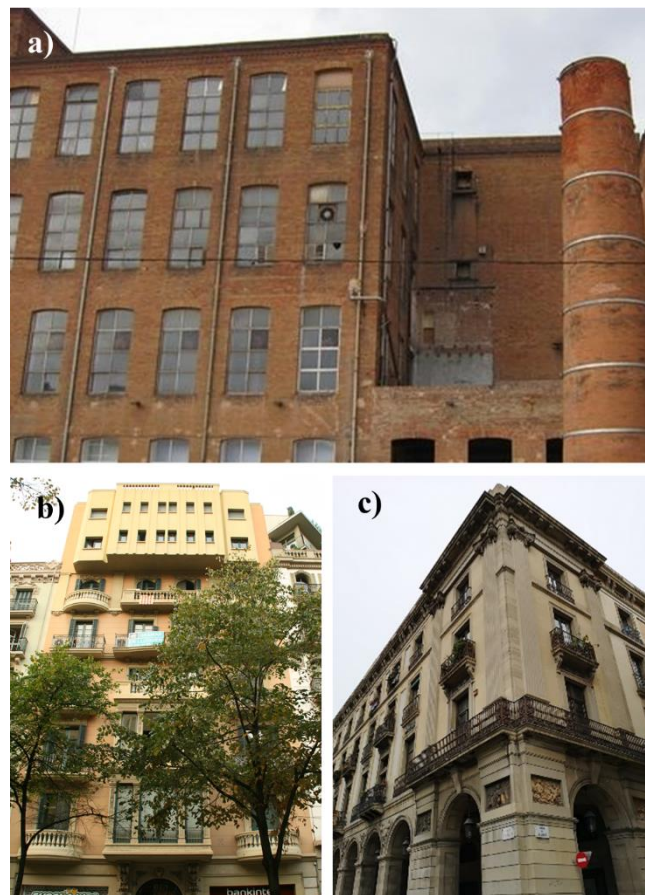


**Figure III.7** a) View of the building of the “Fabra i Coats” industrial complex in Barcelona studied in campaign “MB”, b) main façade of the residential building at Rambla de Catalunya Street in Barcelona studied in campaign “MC”, c) façade of the housing complex in the district of Ciutat Vella in Barcelona studied in campaign “MD”.

During the visits to the three buildings, sets of bricks and fragments of mortar joints were extracted. Bricks had average dimensions of  $291 \times 140.5 \times 52 \text{ mm}^3$  in campaign “MB”,  $294 \times$

### PAPER III

145 × 49 mm<sup>3</sup> in campaign “MC” and 294 × 145 × 45 mm<sup>3</sup> in campaign “MD”. The three sets of bricks showed variability in grain size and colour. Brick pieces of 140 × 140 mm<sup>2</sup> and 100 × 100 mm<sup>2</sup> were cut respectively for campaign “MB” and campaigns “MC” and “MD”. These brick pieces and mortar fragments were prepared and tested in compression following the procedures described in Section III.2.1 for campaign “MA”. Table III. 3 shows the corresponding results. The variability observed by visual inspection was also reflected in the compressive strength of bricks ( $f_b$ ), particularly in the case of campaign “MC”. Bricks of campaign “MD” were twice stronger than those of campaigns “MB” and “MA”, and three times stronger than the bricks of campaign “MC”.

**Table III. 3** Experimental compressive strengths of bricks ( $f_b$ ) and mortar ( $f_{m\_DPT}$ ) of campaigns “MB”, “MC” and “MD”.

“MB”	$f_b$	$f_{m\_DPT}$	“MC”	$f_b$	$f_{m\_DPT}$	“MD”	$f_b$	$f_{m\_DPT}$
Average (MPa)	18.80	0.62	Average (MPa)	10.74	1.52	Average (MPa)	35.45	3.1
No. of specimens	6	12	No. of specimens	12	28	No. of specimens	10	32
CV	12.4%	16.0%	CV	28.0%	35.0%	CV	14.8%	55.4%

The masonry walls investigated in campaign “MB” were 600 mm thick, built in English bond with variable mortar joint thickness between 10 mm and 15 mm (Figure III.8a). The walls investigated in campaigns “MC” and “MD” were interior single leaf walls 145 mm thick built in running bond (Figure III.8c and e). The mortar joint thickness varied between 14 mm and 17 mm in the former and between 10 and 15 mm in the latter. The quality of workmanship was better in the types of masonry “MB” and “MD” in terms of regularity and complete filling of mortar joints.

Up to seven specimens of each cylinder type, 90 mm and 150 mm, were extracted in the three campaigns (Figure III.8b, d and f). Two additional specimens of 150 mm were extracted in campaign “MD”. The coring followed the same dry procedure mentioned in III.Section 2.2.

It is worth to remark the advantages of this technique, as already reported in [105,145]. The total absence of water protected the integrity of the weak mortar joints and guaranteed the efficiency of the full process. Only two operators could easily handle the equipment and a half working day was enough to extract the required amount of cores. The extraction of 90 mm cylinders was easier than for the 150 mm cores. Once the core-drilling machine was fixed to the masonry wall, the coring bit could be moved and the samples extracted along a circumferential path. Within a wall, finding an adequate spot to extract a 90 mm sample resulted easier than for a 150 mm core. Additionally, the specimens of campaign “MB”, which were extracted from 600 mm thick walls, were sawn to adjust their depth to the width of the constituent bricks ( $\approx 145$  mm).

The extracted specimens of the three campaigns were regularized with mortar caps and tested in compression, as described in Sections III.2.2 and III.2.3 for campaign “MA”. Figure III.9, Figure III.10 and Figure III.11 show the stress-strain curves of the tests for the three campaigns. The trends are similar to those discussed in Section III.2 for the campaign “MA”. The cracking sequences, which are illustrated by the failure examples shown in Figure III.12, resulted very similarly to those of campaign “MA”.

## PAPER III



**Figure III.8** a) Façade wall investigated in “Fabra i Coats” factory and b) in-situ core drilling for campaign “MB”, c) inner wall of the analysed building in Rambla Catalunya street and d) in-situ core drilling for campaign “MC”, e) inner wall of the building in Ciutat Vella and f) in-situ core drilling for campaign “MD”.

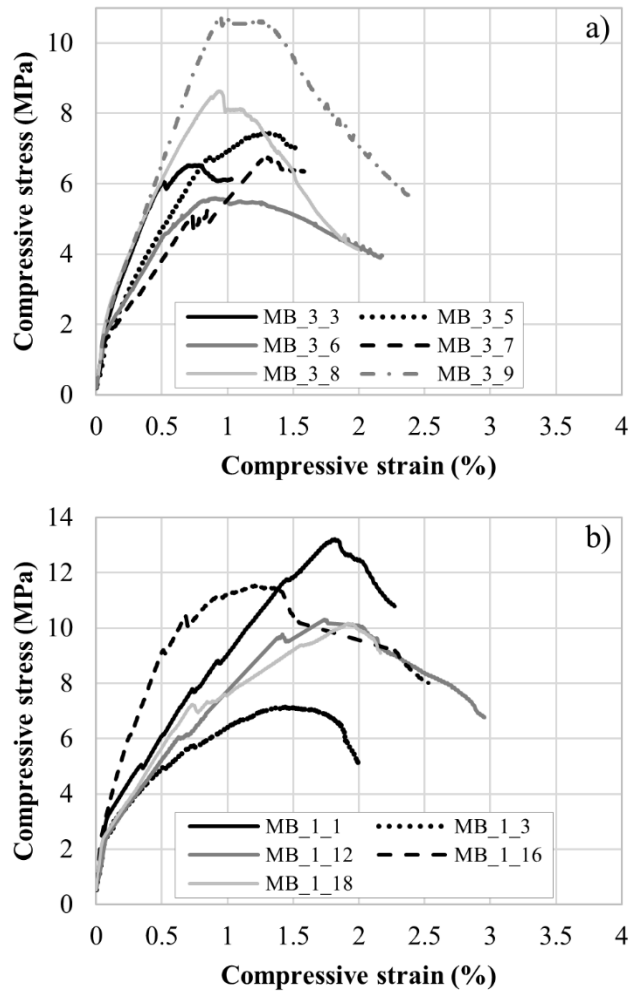


**Figure III.9** Compressive stress-strain curves of campaign “MB”: a) 150 mm samples and b) 90 mm samples.

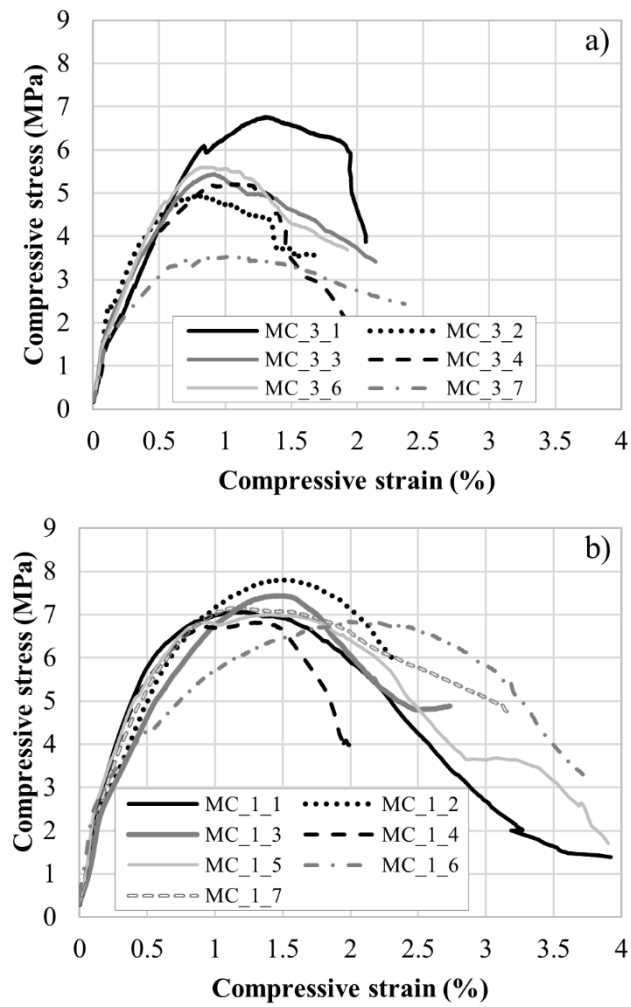


Figure III.10 Compressive stress-strain curves of campaign "MC": a) 150 mm samples and b) 90 mm samples.

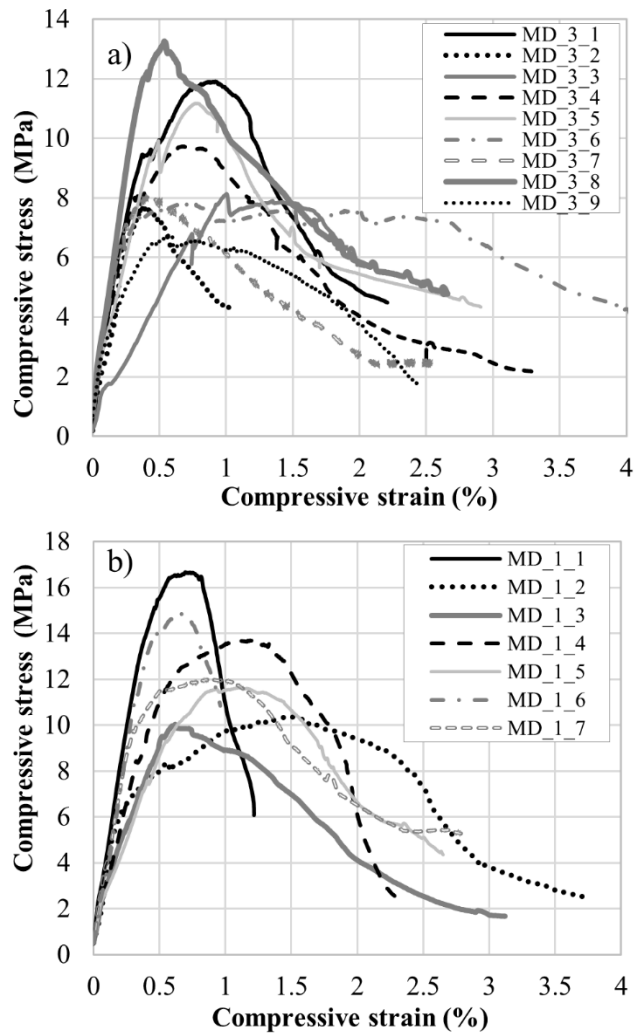
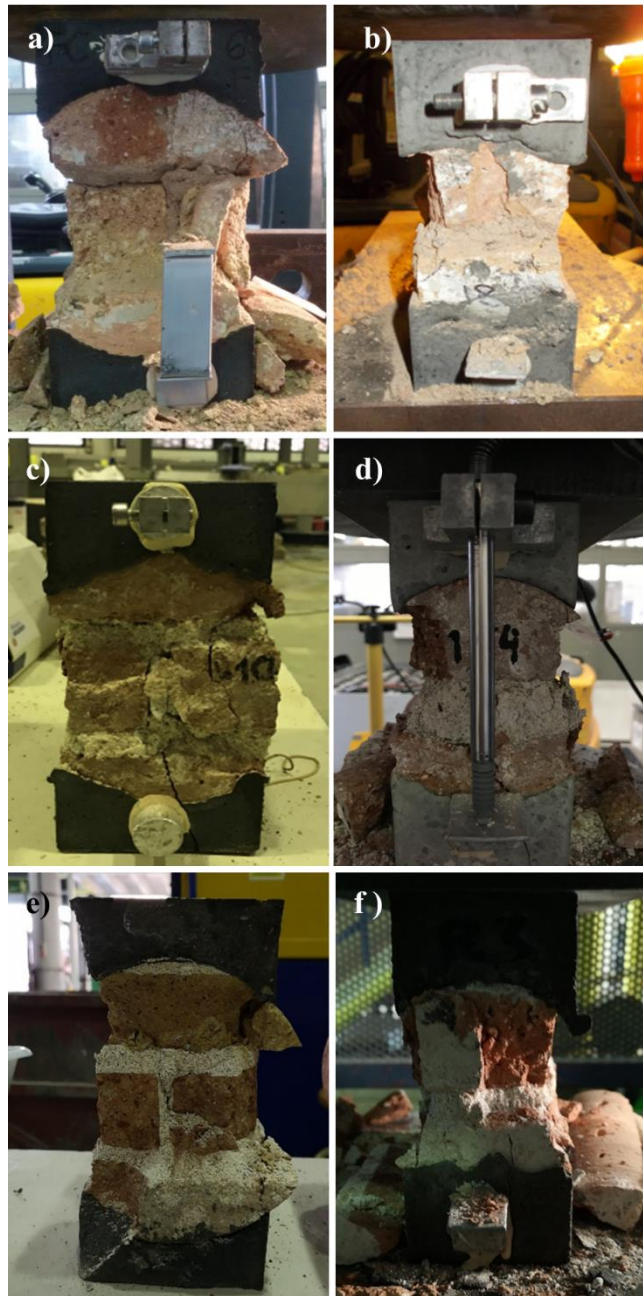


Figure III.11 Compressive stress-strain curves of campaign “MD”: a) 150 mm samples and b) 90 mm samples.

## PAPER III



**Figure III.12** Modes of failure in the 150 mm (left) and 90 mm (right) core samples extracted from existing masonry buildings: a) and b) campaign “MB”, c) and d) campaign “MC”, e) and f) campaign “MD”.

Table III.4, Table III.5 and Table III.6 present the compressive strength and Young’s modulus results obtained from both types of cylindrical specimen for the campaigns “MB”, “MC” and “MD” respectively. The discussion of the results is included in Section III.4.1.

**Table III.4** Compressive strengths ( $f_c$ ) and Young's moduli ( $E$ ) of 150 mm and 90 mm masonry cylinders of campaign "MB".

"MB" 150 mm cylinders			"MB" 90 mm cylinders		
ID	$f_{c,150mm}$ (MPa)	$E_{150mm}$ (MPa)	ID	$f_{c,90mm}$ (MPa)	$E_{90mm}$ (MPa)
MB_3_0	9.13	--	MB_1_0	8.26	--
MB_3_3	6.53	2580	MB_1_1	13.22	3027
MB_3_5	7.45	1663	MB_1_3	7.14	2551
MB_3_6	5.60	2019	MB_1_6	8.51	--
MB_3_7	6.75	1992	MB_1_12	10.31	2430
MB_3_8	8.64	2902	MB_1_16	11.55	3727
MB_3_9	10.74	2665	MB_1_18	10.17	3719
Average	7.83	2304	Average	9.88	3091
CV	22.6%	20.9%	CV	21.2%	20.0%

**Table III.5** Compressive strengths ( $f_c$ ) and Young's moduli ( $E$ ) of 150 mm and 90 mm masonry cylinders of campaign "MC".

"MC" 150 mm cylinders			"MC" 90 mm cylinders		
ID	$f_{c,150mm}$ (MPa)	$E_{150mm}$ (MPa)	ID	$f_{c,90mm}$ (MPa)	$E_{90mm}$ (MPa)
MC_3_1	6.76	1416	MC_1_1	7.06	1797
MC_3_2	4.94	1830	MC_1_2	7.81	1490
MC_3_3	5.44	1827	MC_1_3	7.44	1290
MC_3_4	5.20	1291	MC_1_4	6.82	1840
MC_3_5	5.47	--	MC_1_5	7.01	1956
MC_3_6	5.61	1688	MC_1_6	6.84	1906
MC_3_7	3.55	1360	MC_1_7	7.18	1495
Average	5.28	1569	Average	7.16	1682
CV	18.1%	15.4%	CV	4.9%	15.1%

**Table III.6** Compressive strengths ( $f_c$ ) and Young's moduli ( $E$ ) of 150 mm and 90 mm masonry cylinders of campaign "MD".

"MD" 150 mm cylinders			"MD" 90 mm cylinders		
ID	$f_{c,150mm}$ (MPa)	$E_{150mm}$ (MPa)	ID	$f_{c,90mm}$ (MPa)	$E_{90mm}$ (MPa)
MD_3_1	11.91	4258	MD_1_1	16.67	5265
MD_3_2	7.68	3362	MD_1_2	10.36	3157
MD_3_3	8.14	1783	MD_1_3	10.04	2958
MD_3_4	9.73	3927	MD_1_4	13.72	3598
MD_3_5	11.18	2948	MD_1_5	11.66	3278
MD_3_6	7.80	4157	MD_1_6	14.86	3590
MD_3_7	8.05	3951	MD_1_7	12.02	4498
MD_3_8	13.26	3614			
MD_3_9	6.75	3035			
Average	9.39	3448	Average	12.76	3763
CV	23.9%	22.6%	CV	19.1%	22.0%

**PAPER III****III.4 Discussion****III.4.1 Comparison among the four experimental campaigns**

The experimental programme described in Section III.2 consisted in testing samples extracted from masonry walls built in the laboratory. Useful remarks were drawn from the comparison between the results of the more novel MDT technique consisting in tests on 90 mm masonry cylinders with one mortar joint and the results of the relatively well-studied technique involving tests on 150 mm cylinders with two horizontal and one vertical mortar joints. Section III.3 described three additional campaigns on samples extracted from real historical buildings that aimed to confirm the aforementioned findings for the case of real existing masonry.

The comparison of the stress-strain curves depicted in Figure III.4, Figure III.9, Figure III.10 and Figure III.11 shows similar recognizable trends for the two types of specimen studied. The first branch observed in all the curves up to low values of stress is related to the specific testing protocol adopted in this research, which included the performance of initial loading/unloading cycles. Then, the curves can be generally divided into three sections: a linear branch, a non-linear behaviour before the peak stress and a softening response after the peak stress. Some differences are observed, however, in the stress-strain curves. Longer linear branches are generally observed in the case of the 150 mm specimens that, in some cases, develop up to almost the peak stress. For the 90 mm samples, usually higher values of the strain at peak stress are detected. These observations apply for the four types of masonry investigated.

The examples of tested specimens shown in Figure III.12 for campaigns “MB”, “MC” and “MD” confirm the failure mechanisms reported for the masonry of campaign “MA”. The 56 cylinders tested in the context of this research failed in a very similar way. The failures were characterised by pseudo-vertical cracks appearing firstly on the bricks that caused eventually

the detachment of the external parts, leaving a final sandglass shaped core. These features are in agreement with the findings described by former researches on 150 mm cores [83,102–105] and 100 mm cores [108].

The failure is consistent with the common understanding of the mechanical behaviour of masonry in compression [1,2]. Because of the different elastic properties of the two constituents, i.e. stiff bricks and soft mortar in the types of masonry studied in this research, different stress states develop within the sample. Due to the mortar's trend to experience a much higher lateral expansion than the bricks, units experience horizontal tensile stresses causing vertical splitting cracks in them. The sandglass shape results from the confinement exerted by the caps, which is more pronounced in the top and bottom sections of the cylinders than in the mid-section.

Additional evidence that supports the use of core samples to characterise masonry may be found in the possible parallelism between the tests investigated herein and the tests on standard prismatic specimens for masonry [268]. EN 1052-1 [72] proposes the use of small walls to estimate the compressive strength of new masonry. These specimens include both bed and head joints and might be compared to the 150 mm cylinders, which also include a head joint. Conversely, ASTM C1314 [70] recommends the use of simpler stack bond prisms, without head joints, like the 90 mm cylinder investigated herein.

The results on the compressive strength and the Young's modulus reported in Table III.2, Table III.4, Table III.5 and Table III.6 for the four experimental campaigns are summarized in Figure III.13 and Figure III.14. As in campaign "MA", the rest of campaigns confirm that tests on the 90 mm samples provide higher values of the compressive strength (Figure III.13). This was explained in Section III.2 as due to the size effect related to the different geometries. The presence of more mortar joints in the 150 mm samples may be especially relevant as they

**PAPER III**

introduce more weak points. Additionally, vertical stresses may be better distributed in the 90 mm cylinders thanks to the absence of head joints. However, the ratio of the strengths obtained for the two types of specimen, calculated as  $R_c = f_{c,150mm} / f_{c,90mm}$ , is very similar for the four campaigns. The ratios obtained are 0.75, 0.79, 0.74 and 0.74 for campaigns “MA”, “MB”, “MC” and “MD” respectively.

The coefficients of variation found for the compressive strength in the campaigns on real buildings are still moderate, and they can be fully explained by the variability of the materials. In campaigns “MB” and “MD”, the scattering for the two types of cylinder is very similar. This confirms that testing smaller cylinders does not introduce further variability into the results. Furthermore, a remarkably low value of the coefficient of variation, below 5%, was obtained in the case of 90 mm samples of campaign “MC”.

With regard to the determination of the Young’s modulus, the values obtained with 90 mm specimens are higher than the results derived from 150 mm samples in the four experimental campaigns (Figure III.14). This outcome was explained in Section III.2 as due to the presence of one additional horizontal mortar joint in the 150 mm cores. The higher values of Young’s modulus and strain at peak stress in 90 mm cores are not contradictory, since the latter can be explained by the higher strengths reached by 90 mm specimens. The ratio of Young’s moduli ( $R_E = E_{150mm} / E_{90mm}$ ) between the two types of specimen presented a certain scatter. The values ranged from 0.79 and 0.75 for campaigns “MA” and “MB” to 0.93 and 0.92 for campaigns “MC” and “MD”.

The scattering observed in the estimation of the Young’s modulus is also moderate and similar to that observed for the compressive strength. The variability is consistent between the two types of cylinder in the three campaigns on real buildings. As occurred in campaign “MA”, no additional scattering may be attributable to the use of smaller cylinders. It is also significant

that both types of specimen provide similar values of the ratio relating the Young’s modulus to the compressive strength ( $E/f_c$ ) for each type of masonry investigated. These ratios range approximately from 200 to 350 in all the cases. These values are realistic for historical lime mortar brickwork [128,305].

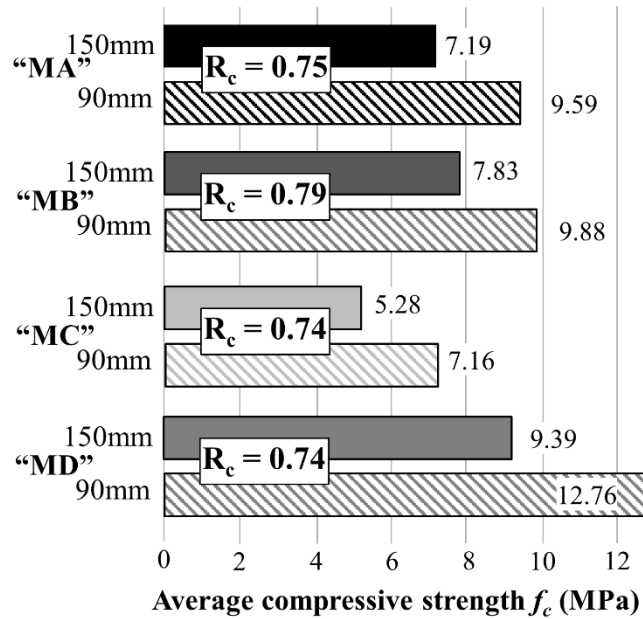


Figure III.13 Comparison of compressive strengths ( $f_c$ ) results obtained for 150 mm and 90 mm cylinders for the four types of masonry investigated.

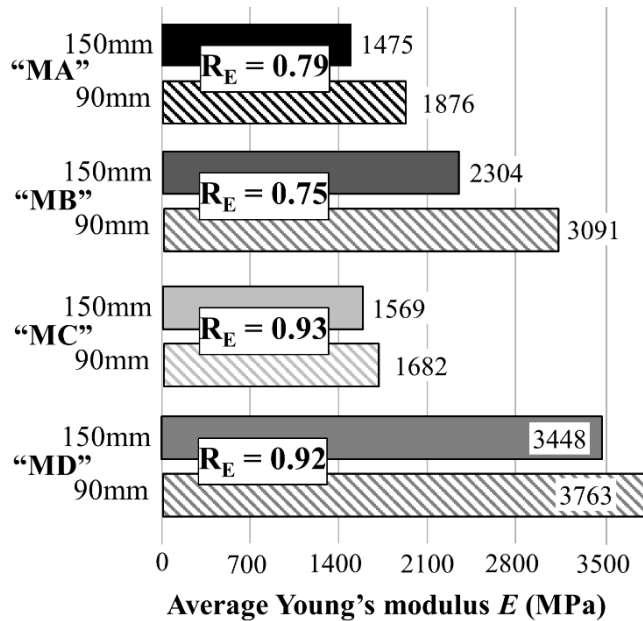


Figure III.14 Comparison of Young’s moduli ( $E$ ) results obtained for 150 mm and 90 mm cylinders for the four types of masonry investigated.

**PAPER III**

Figure III.13 and Figure III.14 allow also analysing the consistency of the results in terms of the relative values obtained for each type of masonry. The highest values of the compressive strength (Figure III.13) correspond to the masonry of Ciutat Vella building (campaign “MD”) that was constituted with the strongest materials (Table III. 3). The masonry of Fabra i Coats factory (campaign “MB”) is the second strongest. The weakness of its mortar (Table III. 3) is compensated with the combination of strong bricks and reduced thickness of the joints. Slightly lower values were obtained for the masonry built in the laboratory (campaign “MA”). The lowest masonry strength was found in the building in Rambla de Catalunya Street (campaign “MC”). This may be related to the weaker bricks used for its construction (Table III. 3). Both types of cylinder are able to predict the same trends.

The Young’s modulus of the masonry of campaign “MD” is consistently characterised as the highest one by the two types of specimen. These highest values of Young’s moduli may be due to the combination of thin joints and strong mortar that characterises this masonry. The thinness of the mortar joints as well as the thickness of the bricks also explain the high values of Young’s moduli obtained in campaign “MB”. A simple 1-D homogenization model [105,131] to estimate the Young’s modulus can justify the former conclusions. Conversely, similar values of Young’s moduli have been obtained for the other two types of masonry, whose constituents have thicknesses that are more similar.

With the exception of the compressive strength of campaign “MC” obtained by 90 mm specimens, which presented a remarkably low variability, the scattering found in the determination of both compressive strength and Young’s modulus presents also an expected trend. Campaigns “MB”, “MC” and “MD” present more variable results than campaign “MA”. This is related to the higher variability of historical masonry, which is intrinsic to its traditional constructive techniques and materials, in addition to a possible decay (not evident in the

materials analysed) and the possible influence of the experienced load histories. This variability contrasts with the more controlled processes used to build the walls in the laboratory.

### III.4.2 Size effect on the compressive strength and Young's modulus of cylindrical specimens

As presented in the Section III.4.1, the 90 mm specimens provide higher values of both the compressive strength and the Young's modulus than the 150 mm ones. Figure III.15 shows graphically the size effect relationships on both properties. They are calculated as the linear regressions of the ratios  $R_c$  and  $R_E$  between the 150 mm and 90 mm core samples for the four experimental campaigns considered in this research.

The constant of proportionality is 0.75 for the four pairs of compressive strength values derived from the 150 mm cylinders ( $f_{c,150mm}$ ) and the 90 mm cores ( $f_{c,90mm}$ ). The approach followed in this research, which combines experimental results from laboratory controlled materials and real historical members spanning different levels of strength, allows obtaining a regression with a satisfactory coefficient of determination  $r^2$  equal to 0.975. The increase of the compressive strength with the reduction of the specimen's size is consistent with the trends obtained in previous experimental and analytical studies on prismatic masonry samples [303,306,307].

Based on the aforementioned results, the size-effect relationship on compressive strength of masonry cylindrical specimens can be written as follows (Eq. III.1):

$$f_{c,150mm} \cong 0.75 f_{c,90mm} \quad (\text{III.1})$$

The constant of proportionality is 0.85 for the four pairs of Young's modulus values derived from the 150 mm cylinders ( $E_{150}$ ) and the 90 mm cores ( $E_{90}$ ). Although the ratios  $R_E$

## PAPER III

present a larger scattering than those of the compressive strengths  $R_c$ , the obtained coefficient of determination  $r^2$  is still higher than 0.9 and equal to 0.92.

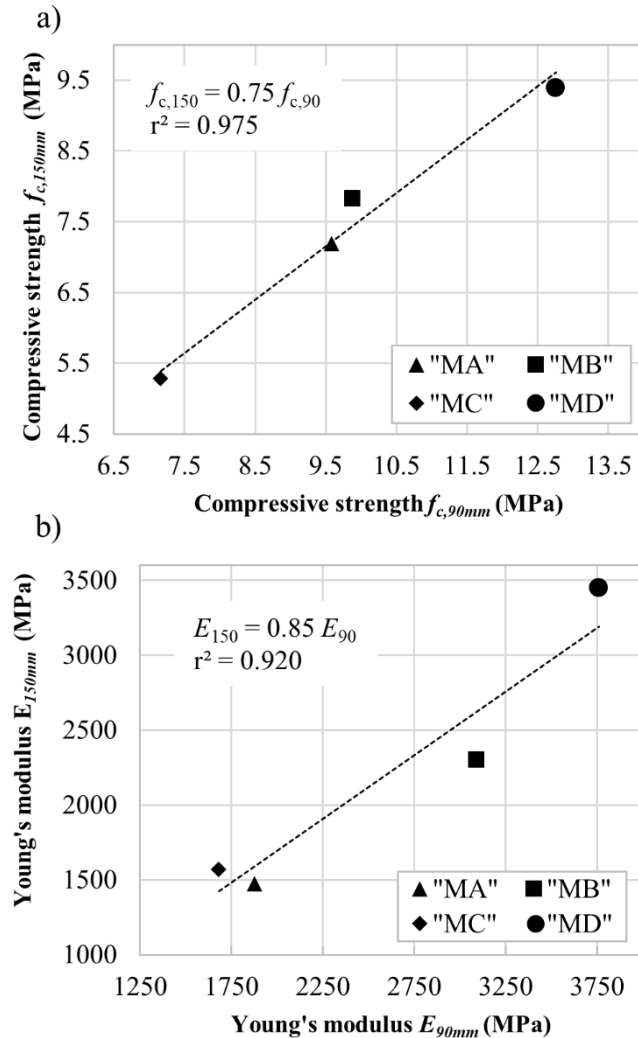


**Figure III.15** Size effect on a) compressive strength and b) Young's modulus obtained from 150 mm and 90 mm cylinders for the four types of masonry investigated in this research.

### III.4.3 Estimation of the compressive strength of masonry and comparison with available predictive expressions

As stated in Section III.1, the 150 mm specimens have been shown suitable for a direct evaluation of the masonry compressive strength by previous researches [83,106,109]. Eq. III.2 expresses this approximate evaluation as:

$$f_c^* \cong f_{c,150mm} \quad (\text{III.2})$$

where  $f_c^*$  is the compressive strength of the masonry being inspected. Other references [102,104] include in the former relationship a correction factor because they consider the diametrical section to calculate the acting stresses and the load is applied differently as described in Section III.2.2. Taking into account this latter remark, all the aforementioned references [83,102,104,106,109] propose equivalent expressions.

Combining the former Equations III.1 and III.2, a new practical approach can be proposed consisting in the extraction and testing of 90 mm specimens and the estimation of the compressive strength of masonry through the application of the following expression (Eq. III.3):

$$f_c^* \cong 0.75 f_{c,90mm} \quad (\text{III.3})$$

Table III.7 presents the application of Equation III.3 to the four types of masonry investigated herein. The estimations of the compressive strength are compared to the predictions provided by the application of other approaches. Among the available possibilities, one consists in testing the individual components, i.e. bricks and mortar, and applying empirical or analytical correlations to estimate the mechanical properties of the composite material from those of the components [128,279,280]. This approach faces several difficulties. One of them stems from the applicability of the equations available in literature. The expressions with an empirical basis, like those proposed by some available standards for the design of new masonry structures, are in principle only adequate for the new construction materials for which they were calibrated and show limitations in the applicability to historical masonry. Another major difficulty lays in the characterisation of the existing mortar [117,118], which is hindered by the impossibility of extracting non-disturbed or normalized prismatic samples [257]. A possible

### PAPER III

solution to this difficulty is found in extracting joint fragments and testing them under double punch compression, as it is done in the present research and explained in Section III.2.1.

Table III.7 includes the comparison between the experimental estimation of the compressive strength by Equation III.3 and the predictions of two expressions available in building codes [60,112]. The term  $f_{c,ACI}$  represents the compressive strength estimated by the *unit strength method* expression proposed in the Commentary on the Specification for Masonry Structures ACI 530.1-02 [112]. This empirical expression correlates the strength of the masonry with the strength of the units. The term  $f_{c,EC6}$  indicates the value obtained with the expression proposed by Eurocode 6 [60]. In the latter, the characteristic compressive strength of the composite material is correlated with the average compressive strengths of both mortar and units. The values reported in Table III.7 have been previously converted into mean value by multiplying by a factor equal to 1.2 as recommended in EN1052-1 [72]. The mortar strength introduced into the equation is the one obtained via the double punch tests. The columns on the right of the predictions express the difference in percentage terms ( $\Delta$  %) with respect to the experimental estimation.

**Table III.7** Experimental estimation of masonry compressive strength ( $f_c^*$ ) vs. predictions from expressions of ACI [112] ( $f_{c,ACI}$ ) and EC6 [60] ( $f_{c,EC6}$ ).  $\Delta$  % expresses the difference in percentage of the predictions with respect to the experimental estimation.

Masonry	$f_c^*$ (MPa)	$f_{c,ACI}$ (MPa)	$\Delta$ %	$f_{c,EC6}$ (MPa)	$\Delta$ %
"MA" - Lab	7.19	6.24	-13.2%	5.63	-21.7%
"MB" - Fabra	7.41	6.52	-12.0%	4.46	-39.8%
"MC" - Rambla	5.37	4.90	-8.8%	3.94	-26.6%
"MD" C. Vella	9.57	9.84	2.8%	11.26	17.7%

The expression proposed by the ACI Specification [112] provides similar values to the experimental estimations, with a close agreement of 2.8 % in the case of the masonry made with the strongest bricks (campaign "MD"). In the latter, the equation of the Eurocode 6 [60] provides a non-conservative estimation, while it yields more conservative estimations in the

cases of campaigns “MA”, “MB” and “MC”. It is remarkable that the highest difference is found for campaign “MB”, which is the type of masonry with the poorest mortar.

In the cases of low strength materials (campaigns “MA”, “MB” and “MC”), the expressions proposed by the building standards have provided more conservative values of the compressive strength compared with the experimental results. Under the assumption that the values obtained by means of the use of masonry cylinders are closer to the actual compressive strength of masonry, the investigated technique can be regarded as a convenient tool for mechanical characterisation. Since an accurate estimation of the mechanical properties helps to reduce uncertainties during the structural assessment, the design of possible interventions, such as retrofit or strengthening, can be less prominent and thus more respectful of the cultural value of existing heritage buildings.

### **III.5 Conclusions**

This paper has presented an experimental research on the characterisation of the compressive mechanical properties of existing masonry. The laboratory testing of core samples extracted from masonry walls has been investigated as a MDT inspection technique. Two types of core, the already studied and validated three-joint cylinder with diameter of 150 mm and the proposed one-joint cylinder with diameter of 90 mm, have been tested and compared to study the effect associated to the reduction of size. The aim in reducing the cylinder’s size is to limit the damage caused to the structure during the sampling and allowing a more efficient extraction and testing. Tests on the two types of cylinder were investigated on masonry walls built in the laboratory with historical-like materials and then applied to three real case studies of historical buildings in Barcelona.

The following conclusions can be drawn from the analysis of the results:

**PAPER III**

- The dry procedure applied to drill the cores has proved to be a clean and efficient method for the extraction of cylindrical specimens in existing buildings. The extraction of 90 mm cylinders was comparatively easier than the extraction of 150 mm cylinders.
- The experimental evidence confirms the adequacy of the 90 mm samples to reproduce the expected mechanical behaviour of masonry in compression. Similar failure mechanisms were found for the two cylinder types. It has been observed that tests on both cylinder types adequately represent the complex interaction between bricks and mortar that characterises the masonry response in compression.
- The size of the core sample has been found to have significant effect on the compressive strength and the Young's modulus. The comparison of the four experimental campaigns has shown that the tests on the two types of specimen provide consistent results and the same logical trends for the compressive strength and the Young's modulus of masonry. The moderate scattering obtained in the tests can be fully explained by the variability found in the constituents' material properties.
- The comparison of the compressive strength results obtained from 150 mm and 90 mm specimens has provided an almost uniform relation for the four different experimental campaigns. A linear regression of the results has yielded a proportionality constant of 0.75. This coefficient may be considered applicable to masonry types similar to the ones investigated, i.e. made of solid clay bricks –with normalized compressive strengths from 10 to 35 MPa- and joints made of lime mortar –with compressive strengths from 0.60 to 3 MPa.
- Testing small 90 mm diameter cores has proved to be an advantageous and promising technique for the evaluation of the resisting properties of masonry in compression. A suggested set of 6 specimens extracted from an existing structural member may provide

a reliable estimation of the compressive strength and an acceptable estimation of the Young's modulus.

*This page is intentionally left blank.*

## 5.4. Discussion

The two previous sections have presented Papers II and III on the characterisation of masonry in compression. This section develops some remarks that can be drawn from the comparison of both papers. The individual conclusions of each paper are restated in Chapter 7.

The tests performed on prismatic specimens in Paper II are acknowledged by the standards as being representative of the mechanical behaviour of masonry. Both specimens -running bond walls and stack bond prisms- behaved in a similar way, with compatible stress-strain curves and sandglass-like failures. The cylindrical specimens studied in Paper III, which are investigated as an alternative to be applied on existing buildings, behaved similarly. The comparison of failure modes and stress-strain curves between standard prismatic specimens and cylindrical specimens allows stating that the latter are also able to replicate the mechanical behaviour of masonry satisfactorily.

The origin itself of the investigation included in Paper III was born from the research of Paper II. The fact of having a standard specimen that consists of only bed joints -the stack bond prism- motivated the possibility of studying the small cylinders that included only one bed joint. Therefore, the parallelism between both papers can be traced: big cylinders of 150 mm and three joints correspond to running bond walls, while small cylinders of 90 mm and one single joint correspond to stack bond prisms.

In both papers, the study of smaller specimens is justified by practical reasons. These smaller specimens are easier to handle and require more reduced equipment for testing. In addition, in the case of cylinders, the smaller ones inflict less damage into the structure and are easier to extract.

With regard to the evaluation of the compressive strength of masonry, the size and shape of the specimens had different effects. In Paper II, statistically equal determinations were obtained from running bond walls and from stack bond prisms. This fact was explained in the paper by the careful construction of the specimens and the careful application of the loads during the tests. Recent researches by other authors have shown that, in general, stack bond prisms provide higher estimations, although for some cases results from both types of specimen are similar [308]. This is the case of the masonry studied in the thesis. Conversely, in Paper III, the size and shape effect of cylinders was clear. It was even possible to find a linear correlation with a very good coefficient of determination  $r^2$ .

This different influence of size and shape on the compressive strength found in prismatic and cylindrical specimens may be explained by the different way of applying the compressive load. For the prismatic specimens, the load was applied on the top and bottom flat surfaces, and in both cases the central part of the specimens was free of any platen effect. Even being smaller, the stack bond prisms were still sufficiently large as to properly distribute the compressive loads. For the cylindrical specimens, the mortar caps used to regularise the curved faces exerted a confinement on the sample. Even if the ratio cap width over sample diameter was maintained between the two cylinder sizes, the smaller cylinder seemed to be more affected by the cap confinement.

Contrariwise, both prismatic and cylindrical specimens seem to be affected in a similar way with regard the evaluation of Young's modulus. In Paper II, the influence of the vertical head joint motivated that results obtained with running bond walls were 94% those of stack bond prisms. The simple homogenisation spring model discussed in the paper could justify this difference. In Paper III, estimations of Young's modulus provided by the bigger cylinders were around 75 to 90% the estimations of Young's modulus provided by the smaller cylinders. This

is predictable taking into account that smaller cylinders have only one mortar bed joint and therefore are less deformable than bigger ones, which include two bed joints and one head joint.

Another important remark, related to the objectives of the thesis, is about the performance of initial cycles at low load levels to facilitate the measurement of Young's modulus. This procedure has shown to be especially important in the case of cylinders from existing buildings, where the cycles application helped to stabilize the curves. A further consideration is the definition of Young's modulus. In Paper III, whose experimental campaign was carried out before the campaign of Paper II, the Young's modulus was evaluated between the plateaus of the third loading cycle. In Paper II, the Young's modulus was evaluated on the final stress-strain curve, between the limits defined by the actual maximum load attained for each particular specimen. This method constitutes a way to normalise the results and allows having a better comparison between them. As a consequence of this observation, it is recommended in the future to perform at least three loading cycles and evaluate the Young's modulus as the chord modulus on the stress-strain curve, between two limits calculated according to the actual maximum attained load.

Table 6 compares values of the five different masonry examples studied in Papers II and III. All of them belong to the category of traditional brick masonry in Barcelona, two of them replicated in laboratory, the other three extracted from existing buildings.

The choice of the bricks from Terra Cuita Piñol Pallarés SL has shown to be satisfactory. Their compressive strength lays between the limits of the existing ones. Its value is very close to the one of bricks from the Fabra i Coats factory (masonry MB). Their variability is lower than that of historical bricks but this is explained because the bricks used in laboratory belonged to a single batch, while bricks from existing structures were obtained from different parts of the buildings.

The aerial lime mortar used in masonry MA of Paper III made in laboratory properly represents the values of historical mortars. The compressive strength of the modified hydraulic lime mortar of Paper II also compares satisfactorily. Nevertheless, strength values obtained by means of DPT tests are not directly comparable to values obtained from standard prismatic specimens.

The values of compressive strength for replicated masonry (6.5 MPa in Paper II, 7.19 MPa in Paper III) match the average value of existing masonry considering types of masonry MB (factory) and MC (residential building). The case of masonry MD, which yielded a compressive strength of 9.39 MPa, can be disregarded in this comparison. The building belongs to the historical heritage of the city, and was built by one of the richest businessmen of modern Barcelona. It could be argued that both materials and masons participating in the construction were not representative of the common building practices of the time. Finally, it should be highlighted that the values obtained within this research for the compressive strength are very similar to the average value of 6.5 MPa found by Cornadó [196] (see Section 2.4.2).

With regard to the Young's modulus, the values obtained with replicated masonry also match the values of masonry from existing buildings. Again, the higher values associated to masonry MD could be disregarded for the comparison.

Overall, it has been shown that historical-like masonry can be replicated in laboratory satisfactorily, at least with regard to the ability of replicating compressive parameters. The masonry built in Paper II, with the mortar prepared in Paper I and the selected bricks, has succeeded to provide similar values of Young's modulus and compressive strength to those estimated from real examples of buildings of Barcelona.

**Table 6** Comparison among the types of masonry studied in Paper II and Paper III. Coefficients of variation indicated in brackets.

Type of masonry	Paper II	Paper III MA	Paper III MB	Paper III MC	Paper III MD
Origin	Replicated in laboratory	Replicated in laboratory	Existing building	Existing building	Existing building
Bricks	Terra Cuita handmade solid clay fired bricks	Terra Cuita handmade solid clay fired bricks	Historical handmade solid clay fired bricks	Historical handmade solid clay fired bricks	Historical handmade solid clay fired bricks
Compressive strength of bricks	17.44 MPa (8.3 %)	17.44 MPa (8.3 %)	18.80 MPa (12.4 %)	10.74 MPa (28.0 %)	35.35 MPa (14.8 %)
Mortar	Modified hydraulic lime mortar (see Paper I)	Aerial lime mortar	Historical aerial lime mortar	Historical aerial lime mortar	Historical aerial lime mortar
Compressive strength of mortar	1.91 MPa (10.1 %) Prisms	1.61 MPa (20.1 %) DPT	0.62 MPa (16.0 %) DPT	1.52 MPa (35.0 %) DPT	3.1 MPa (55.4 %) DPT
Compressive strength of masonry	6.51 MPa (8.9 %) RBW	7.19 MPa (12.5 %) 150 mm	7.83 MPa (22.6 %) 150 mm	5.28 MPa (18.1 %) 150 mm	9.39 MPa (23.9 %) 150 mm
Young's modulus of masonry	2318 MPa (7.6 %) RBW	1475 MPa (19.4 %) 150 mm	2304 MPa (20.9 %) 150 mm	1569 MPa (15.4 %) 150 mm	3448 MPa (22.6 %) 150 mm

A last remark on the different expressions for predicting the compressive strength can be done. In general, the unit strength method proposed by American building codes [112] provides better estimations than the expression included in Eurocode 6 [60]. The former only depends on the strength of the bricks while the latter depends on both the bricks and the mortar used. It seems that the expression from Eurocode 6 does not succeed in taking into account the peculiarities of historical and old mortars. This is probably due to Eurocode 6's expression having been calibrated for more modern mortars. A second possibility relates to the difficult estimation of the mortar's compressive strength in the case of existing masonry. A further observation is that masonry studied within the present work lays below the limits considered in the ACI standard, in terms of compressive strength of the units and compressive strength of masonry. The values of this thesis, together with other researches, could allow increasing the scope of the aforementioned standard.

*This page is intentionally left blank.*

# 6

## **Characterisation of masonry in shear**

*This page is intentionally left blank.*

## 6.1. Introduction

This chapter presents two experimental researches that deal with the characterisation of masonry in shear. Based on the findings of the literature review presented in Section 2, these researches address some of the needs encountered in relation with the type of specimen and the uncertainties about interpretation of results.

Section 6.2 reproduces Paper IV, devoted to the characterisation of masonry in laboratory. It explores the possibility of proposing a couplet specimen for the determination of cohesion and friction of brick – mortar interfaces, instead of the standard triplet specimen. The paper includes an experimental campaign on two different types of masonry, which compares the performance of the two types of specimen. Other than cohesion and friction, this work pays also attention to fracture energy and other shear parameters.

Section 6.3 reproduces Paper III, devoted to the characterisation of masonry by means of the diagonal compression test. This versatile test is of common use in laboratory but it has been also usually applied to existing structures. The paper presents an experimental campaign that is used as benchmark for calibrating a numerical model. The numerical investigation delves into the interpretation of the test and eventually proposes coefficients for the determination of the tensile strength of masonry and the shear modulus of masonry.

Section 6.4 discusses some aspects of Paper IV and Paper V as a whole and relates the obtained results among them and with Papers II and III. Conclusions of the individual papers are not restated here but in Chapter 7.

*This page is intentionally left blank.*

## **6.2. Paper IV – Experimental comparison of two testing setups for characterising the shear mechanical properties of masonry**

J. Segura, E. Bernat, V. Mendizábal, L. Pelà, P. Roca, L. Gil. *Under review*

*Abstract: The prediction of the structural capacity of masonry buildings against lateral loads requires an accurate characterisation of the masonry strength and general response under shear stresses. The experimental determination of shear strength parameters typically relies on shear tests on wallettes, or on standard triplets. Aiming to avoid the behavioural interpretation problems related with the existence of two mortar joints in triplets, this paper investigates the alternative possibility of testing simple couplet specimens. A direct experimental comparison was established with tests on the two specimen configurations (triplets and couplets) performed on two different types of masonry, both characterised by low strength mortars (hydraulic lime and cement based). The obtained results include the evaluation of Mohr-Coulomb parameters, residual shear strengths, second mode fracture energy, and secant shear modulus. The findings point out that couplets yield consistent experimental results and provide systematically higher estimations of all parameters compared to triplets.*

*This page is intentionally left blank.*

## IV.1 Introduction

Earthquakes, wind, support settlements or unsymmetrical distributions of vertical loads constitute actions that subject buildings to in-plane shear loading [309]. Under these conditions, the evaluation of the masonry shear strength is of great importance to accurately assess the structural performance of the building [310].

The shear strength of a masonry wall depends on a number of factors [311], such as the wall aspect ratio, the mechanical properties of the components - i.e. units and mortar-, the bond tensile strength of the joints, the boundary conditions, and the compression stress level experienced by the wall. Zhang and Beyer [312] and Malomo et al. [313] have also investigated the role played by the bond pattern. Nevertheless, it is accepted that a key parameter in the shear resistance of a wall is the shear strength of the bed joints. The vast amount of research carried out along the last decades [134] has established as a consensus that the joint shear failure at low precompression levels can be adequately described by the Mohr-Coulomb (MC) criterion, expressed herein by Equation IV.1:

$$\tau_u = c + \sigma \tan \phi \quad (\text{IV.1})$$

where the ultimate joint shear strength  $\tau_u$  and the normal compressive stress  $\sigma$  are related by means of the cohesion  $c$  and the internal friction angle  $\phi$ . In the common case of failure through the unit-mortar interface, the cohesion can be interpreted as the initial bond at zero precompression  $\tau_0$ , while the tangent of the angle of friction represents the coefficient of friction  $\mu$ .

Different testing configurations have been proposed for the experimental determination of the Mohr-Coulomb parameters [314–316]. Riddington et al. [138] identified a series of quality criteria that an ideal testing setup should fulfil: *i*) ensure a uniform distribution of normal and

**PAPER IV**

shear stresses; *ii*) when failure is initiated at one point, the majority of the joint should be close to failure; *iii*) tensile stresses should be avoided along the joint; *iv*) the failure should be initiated away from the edge of the joint, and *v*) the testing setup should be kept as simple as possible. Yet, as stated by Popal and Lissel [317], none of the currently available methods meets the five criteria. In particular, the first criterion on uniformity -that is the basic assumption for the computation of the acting stresses along the joint- has been found nearly impossible to satisfy [318,319].

With the previous considerations in mind, tests on triplet specimens conformed by three units and two bed joints stand as a compromise solution and have been adopted by most of the national and international standards. The European standard EN 1052-3 [135] gives guidance on the preparation of the specimens, the testing machine, the test method and the calculation method. One of the proposed procedures involves testing groups of specimens at different precompression levels and finding the cohesion and the angle of friction by a linear regression.

The triplet test has been largely applied in both the research and the industrial fields and is used to characterise many different materials (e.g. masonry made of solid [145] and hollow bricks [320], stone units [321] or concrete blocks [320]). Nevertheless, even if generally accepted, this method presents certain inconsistencies derived mainly from the fact that the tested specimen includes more than one joint. Indeed, the assumed symmetry of both specimen and setup may be only apparent since several sources of asymmetry arise: imperfections in the geometry of the units and particularly in the thickness of the mortar joints; irregular boundary conditions, especially with regard to the applied precompression; the scattering of the properties of the materials including the variation in the roughness of the units' faces and the possible heterogeneity within the mortar.

In consequence, as reported by a number of authors [139–141], both joints do not fail simultaneously. This circumstance is found experimentally [322–324] in force-displacement curves that present two peaks, each of them representing the failure of one of the two different joints. This ‘two-peak-phenomenon’, as identified by Vermeltoort [319], hinders the interpretation of the results and raises doubts on which area should be considered for the calculation of shear stresses [325]. In addition, Angelillo et al. [69] have highlighted the impossibility to obtain accurate post-peak characteristics, and Riddington and Jukes [326] have pointed out some practical concerns associated to the size, weight and fragility of the triplet specimens.

An alternative to overcome the limitations of tests on triplets can be found in testing specimens with a single bed joint, hereafter called ‘couplets’ [142,327–329]. Many researchers have proposed specific and complex testing setups on couplets [142,143], with the aim of fulfilling the first four of the aforementioned Riddington criteria. Van der Pluijm [144] designed a testing configuration with special metal devices. This latter setup allowed improving the knowledge on the shear behaviour of bed joints and has been successfully and continuously utilised for the calibration of numerical models [141]. However, it has been hardly used in laboratory afterwards given the specificity of the test arrangement, together with some difficulties [134] related to the need of attaching the steel sections to the bricks and the occurrence of a diagonal crack through the centre of the specimen instead of a joint failure for certain types of units.

The research presented herein explores the possibility of testing couplets with the simplest setup, i.e. a simple modification of the standard triplet arrangement, and aims to correlate results obtained with both types of specimen. Although some authors have compiled inventories of shear tests that reported examples from either triplets or couplets [134,330,331], very few

**PAPER IV**

references have dealt with their direct experimental comparison. Lawrence [329] and Schubert and Caballero [332] obtained higher values of cohesion in couplets tests. Conversely, Fouchal et al. [333] found very similar results for both types of specimen. More recently, Zhang et al. [141] presented a numerical evaluation.

This paper presents an experimental programme on triplets and couplets and compares the obtained results in terms of Mohr-Coulomb parameters, i.e. cohesion and angle of friction, but also with regard to fracture energy, deformability and force-displacement curves. Two different material combinations have been considered, both with low strength mortars. The choice of the components of one of the combinations has been intended to represent a historical-like type of masonry. Therefore, the results obtained may contribute to expand the database on shear properties available for this type of material.

**IV.2 Experimental programme****IV.2.1 Materials**

The experimental programme was carried out at the Materials and Structures Laboratory of Innovation Technology of the Technical University of Catalonia in Terrassa, Barcelona (UPC – BarcelonaTech).

As mentioned, the tests involved two different material combinations to carry out the comparison between triplets and couplets. The first combination was chosen to represent a historical-like type of masonry. Given the difficulties to evaluate the shear properties of existing masonry structures [145], this campaign provided an opportunity to contribute with results obtained through standard triplet tests. Handmade fired solid bricks were selected, with average dimensions  $311$  (length)  $\times$   $149$  (width)  $\times$   $45$  (height)  $\text{mm}^3$ . These bricks presented rough

surfaces because of their manual way of manufacturing. A NHL 3.5 natural hydraulic lime based commercial mortar was chosen. The mortar was modified with limestone filler additions to reduce its strength, as explained by the authors in a recent publication [334]. The volume ratio of commercial premixed mortar to filler to water was 1:1:0.65. This material combination has been already studied in compression, with results similar to historical ones [268]. On the other hand, the second type of masonry was designed to have different properties but keeping the low strength of the mortar. Modern materials were used in this case, which included a M7.5 Portland cement based mortar and conventionally extruded solid clay bricks, with smooth surfaces and average dimensions  $270 \times 127 \times 51 \text{ mm}^3$ . The volume ratio of commercial premixed mortar to water was 1:0.25 [335].

The two sets of materials were conveniently characterised according to EN 772-1 [285] and EN 1015-11 [257]. Table IV.1 summarizes the components' strengths. The mortar prisms were casted during the construction of the masonry specimens and were tested at the same age. As planned, strengths were different for the two material combinations, with lower strengths in the case of historical-like materials. Nevertheless, the strength of the cement-based mortar can still be considered as a low strength. The variability found in the strength values, with a coefficient of variation up to 28 % in the case of the flexural strength of extruded bricks, is common in this type of materials [270].

**Table IV.1** Mechanical strengths of masonry components. Number of specimens and coefficients of variation are shown in brackets.

Material	Compressive strength (MPa)	Flexural strength (MPa)
Handmade brick	17.99 (20, 8.3%)	2.44 (10, 20.0%)
Extruded brick	27.93 (30, 19.0%)	5.99 (15, 28.0%)
Hydraulic lime mortar	1.02 (12, 22.1%)	0.33 (6, 25.3%)
Portland cement mortar	2.53 (12, 5.7%)	1.03 (6, 9.9%)

## PAPER IV

## IV.2.2 Specimens preparation

Two types of specimen were built for each material combination: standard triplets consisting of three bonded bricks with two mortar joints, and couplets consisting of two bonded bricks with one mortar joint. Figure IV.1 displays the dimensions of each specimen type.

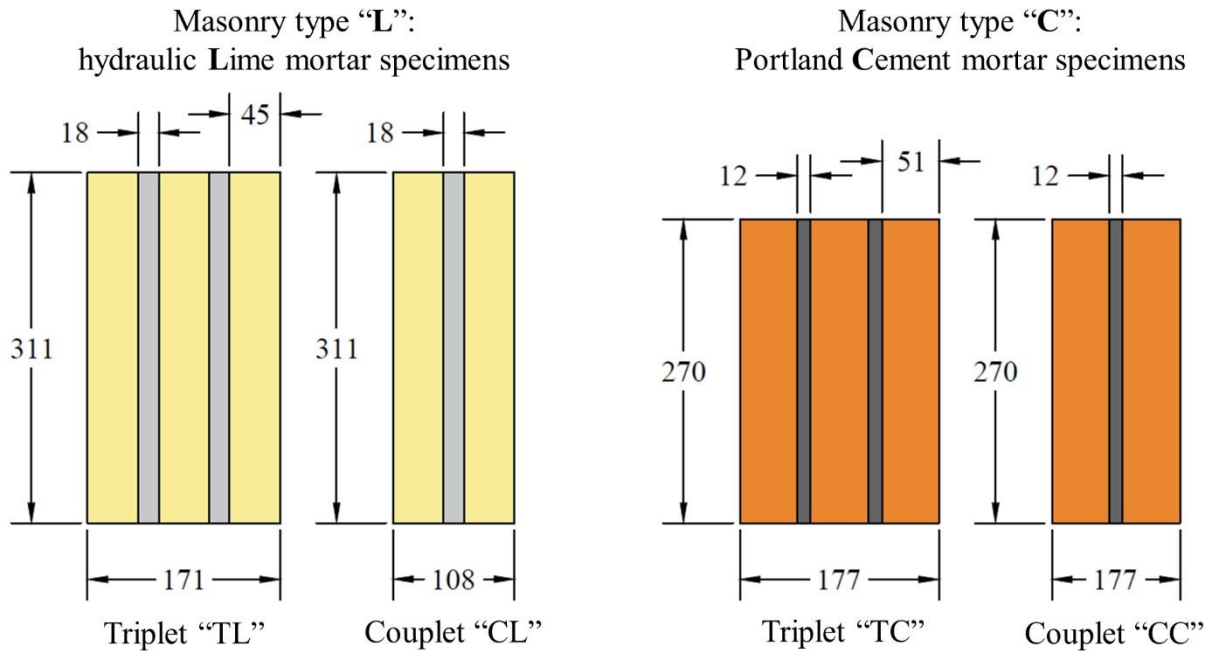
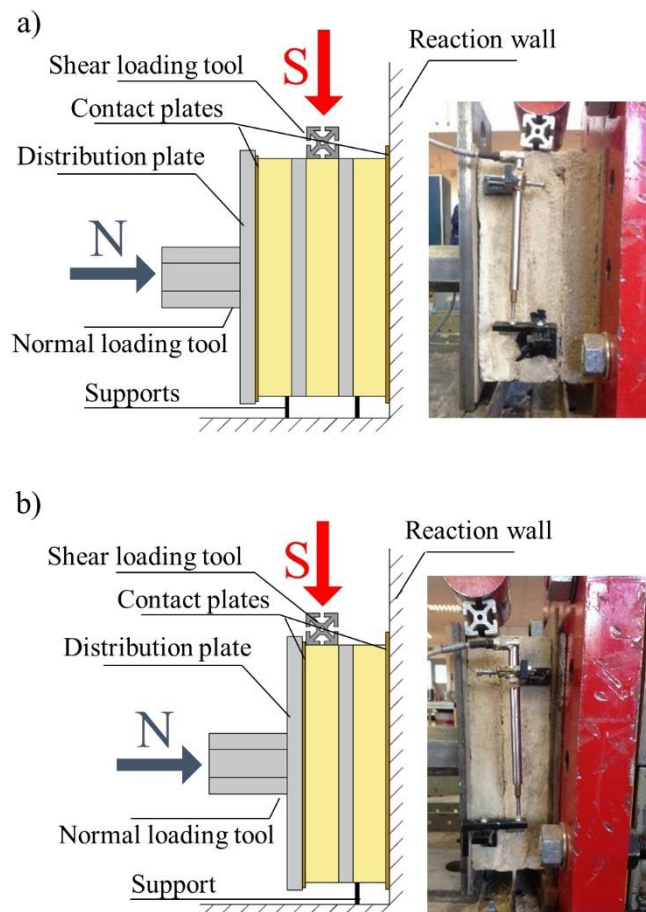


Figure IV.1 Geometric definition of the masonry specimens.

The construction of the specimens included brushing the bricks, especially the handmade ones, wetting them by immersion into water for at least 1 minute, levelling the first brick, which was laid horizontally on its main side, and placing the next brick(s) on top maintaining the specified mortar joint thickness by using wooden mechanical gages. Average joint thicknesses of 18 mm and 12 mm were selected for the hydraulic lime and the cement mortar respectively. The former was necessary to accommodate the irregularities of the handmade brick surfaces, whereas the latter is more representative of real Portland cement joints in modern masonry. All samples were covered with plastic and cured in the same environmental conditions for 28 days.

### IV.2.3 Setup and testing procedure

Figure IV.2 sketches the testing setups for both triplets and couplets. The shear load ( $S$ ) was applied through an aluminium profile 40 mm wide at the top of the corresponding brick. Steel profiles supported the other brick(s). The supporting edges were placed in all cases at 2 mm from the brick-joint interface. The precompression normal load ( $N$ ) was applied through a distribution steel plate 20 mm thick. Contact plates were placed at the external faces of the specimen, against the distribution steel plate and the reaction wall. These plates consisted of soft board sheets rubbed with Vaseline. Their aim was double: avoiding local normal stress concentrations and reducing the friction against the shear load. The latter of the utmost importance in the case of couplets.



**Figure IV.2** Testing arrangements for a) triplets and b) couplets.

## PAPER IV

Once the specimen was placed in its position, two LVDT sensors with 20 mm range and 0.2% linearity were installed according to Figure IV.3 to measure the shear vertical (see Figure IV.2) and normal horizontal deformations. Both sensor support elements and reference contrasting elements were bonded to the brick with cyanoacrylate after convenient polishing and cleaning of the surface.

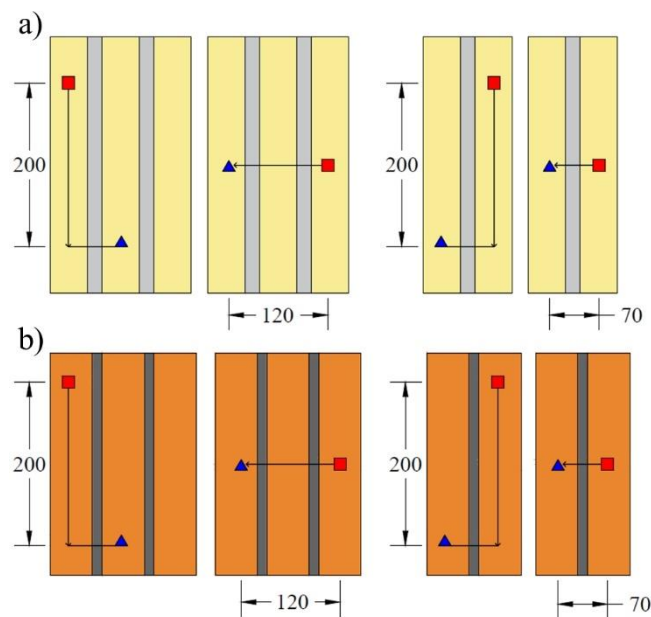


**Figure IV.3** LVDTs position for each specimen type. Red squared dots indicate support of the LVDT, blue triangular dots indicate support of the contrasting element. See Figure IV.2 for an actual picture of the vertical LVDTs.

The tests consisted of two stages. They started with the application of the precompression normal load at a ratio of 10 kN/min. Tests at different levels of normal stress were performed, as indicated in Table IV.2. The horizontal actuator that applied the precompression load had a maximum capacity of 50 kN. When the precompression load was reached, it was maintained constant during the test, whereas the shear load was indirectly applied as an imposed displacement at a ratio of 1 mm/min. The vertical actuator that applied the shear load had a maximum capacity of 100 kN.

The tests finished when the sensor recording the shear deformation reached its maximum elongation (around 15 mm) and the contact with the reference element was lost. In few cases, this sensor fell from its position due to the energy release associated with the joint failure. In these cases, no full information is available and the corresponding curves are not included in the subsequent analyses.

Table IV.2 lists all the tested specimens. The name of the test starts with a letter indicating the type of specimen (“T” for triplets and “C” for couplets), followed by a letter representing the type of masonry (“L” for masonry made of hydraulic lime mortar and handmade bricks and “C” for masonry made of Portland cement mortar and extruded bricks). The combination of these four letters defines the four different sets of samples being tested. The name of the specimens includes also a number that indicates the applied precompression force in kN, and a last number that designates the repetition of the test.

The standard EN1052-3 [135] prescribes to perform tests at three different precompression levels with at least three specimens at each level. For units with compressive strengths higher than 10 MPa, the standard recommends to use precompression loads that give approximately 0.2 MPa, 0.6 MPa and 1 MPa of precompression stress. This approach has been followed in the case of masonry L. However, taking advantage of the greater homogeneity of the industrialized materials used in TC and CC specimens, it was decided to investigate the convenience of including an additional normal-tangential stresses pair while reducing the repeatability of tests from 3 to two repetitions. This approach allowed to obtain additional information for the linear regression while saving one specimen. The new level of load considered for specimens TC and CC aimed to represent a zero normal precompression condition. The actual applied stress was 14.6 kPa, and corresponded to the minimum capacity

## PAPER IV

of the horizontal actuator (0.5 kN). This minimum load was necessary to maintain the overturning stability of the specimens during the tests.

**Table IV.2** List of tested specimens and applied normal stresses.

Specimen	Precompression normal stress (kPa)	# Repetition	Specimen	Precompression normal stress (kPa)	# Repetition
TL13.5_1	291.3	1	TC0.5_1	14.6	1
TL13.5_2	291.3	2	TC0.5_2	14.6	2
TL13.5_3	291.3	3	TC8_1	233.3	1
TL27_1	582.7	1	TC8_2	233.3	2
TL27_2	582.7	2	TC20_1	583.3	1
TL27_3	582.7	3	TC20_2	583.3	2
TL45_1	971.1	1	TC35_1	1020.7	1
TL45_2	971.1	2	TC35_2	1020.7	2
TL45_3	971.1	3	CC0.5_1	14.6	1
CL13.5_1	291.3	1	CC0.5_2	14.6	2
CL13.5_2	291.3	2	CC8_1	233.3	1
CL13.5_3	291.3	3	CC8_2	233.3	2
CL27_1	582.7	1	CC20_1	583.3	1
CL27_2	582.7	2	CC20_2	583.3	2
CL27_3	582.7	3	CC35_1	1020.7	1
CL45_1	971.1	1	CC35_2	1020.7	2
CL45_2	971.1	2			
CL45_3	971.1	3			

### IV.2.4 Results

According to the assumption of uniformity in the stresses distribution made in the EN 1052-3 [135], the shear strength ( $\tau_u$ ) of each specimen was calculated by means of Equations IV.2 and IV.3 for triplets and couplets respectively. The normal acting stresses ( $\sigma$ ) were calculated for both types of specimen with Equation IV.4:

$$\tau_u \text{ (Triplets)} = S_{max} / 2A \quad (\text{IV.2})$$

$$\tau_u \text{ (Couplets)} = S_{max} / A \quad (\text{IV.3})$$

$$\sigma = N / A \quad (\text{IV.4})$$

where  $S_{max}$  is the maximum shear force attained during the test,  $N$  is the precompressive force, and  $A$  is the cross sectional area of the specimen parallel to the bed joints.

The pairs of values of shear strength and compressive stress for all the tests are plotted in Figure IV.4, for the four different sets of samples (TL, CL, TC, CC). Figure IV.4 also indicates the values of cohesion and angle of friction corresponding to the Mohr-Coulomb failure criterion defined by Equation IV.1. These parameters have been calculated as the intercept with the  $\tau$ -axis and the arctangent of the slope, respectively, of a linear regression on the pairs of values.

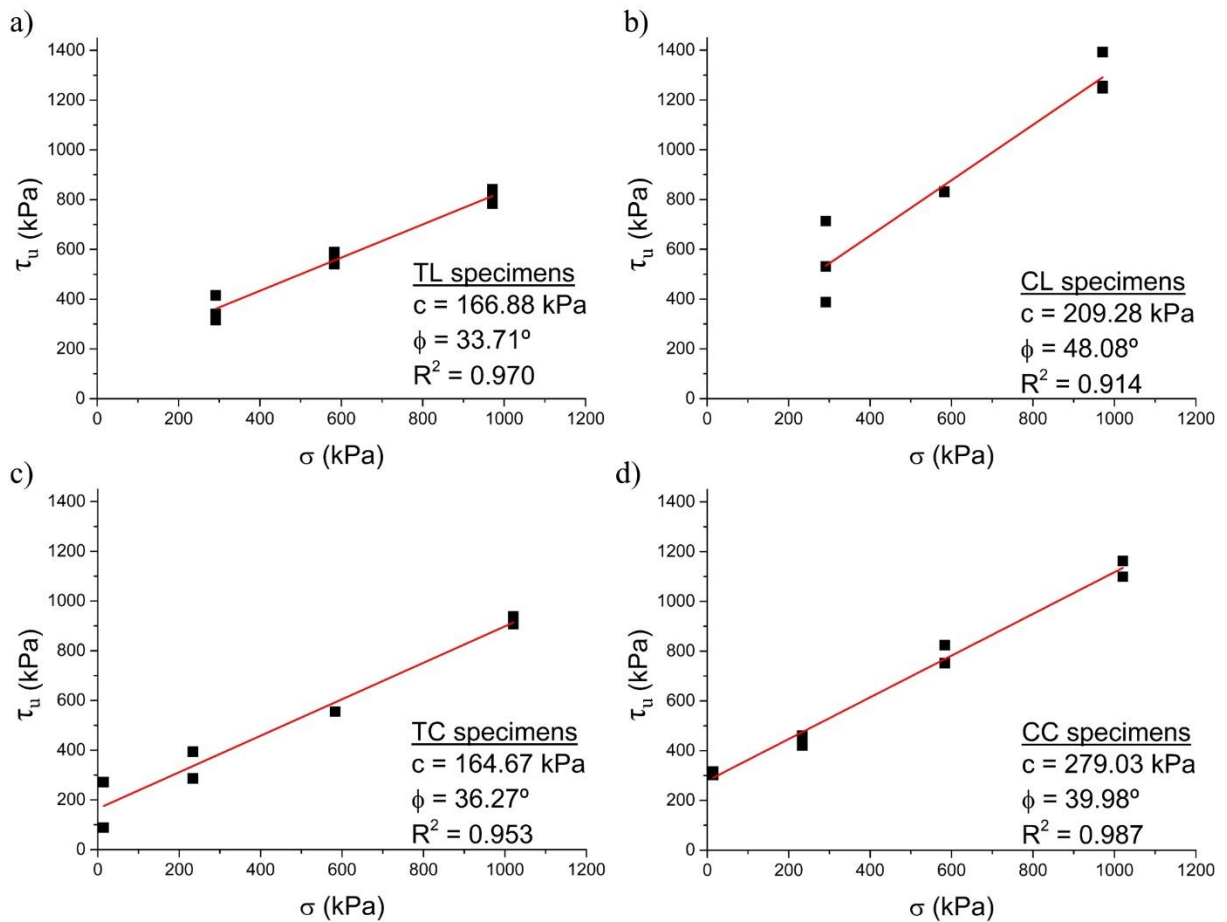


**Figure IV.4** Shear strength  $\tau_u$  vs. normal stress  $\sigma$  plots for a) TL, b) CL, c) TC, and d) CC specimens. Red lines represent the regression corresponding to the Mohr-Coulomb failure criterion, with indication of the cohesion  $c$ , the angle of friction  $\phi$  and the coefficient of determination  $R^2$ .

## PAPER IV

Figure IV.5 and Figure IV.6 display two types of plot for both masonry combinations. The shear stress recordings along each of the tests are plotted against the relative shear displacement. These curves represent the mechanical response of the joints in shear. The shear displacements are also compared to the displacements measured in the direction perpendicular to the joint. This type of plot captures the possible signs of dilatancy. In both figures, curves with inconsistent data associated to measurement issues during the tests are disregarded.

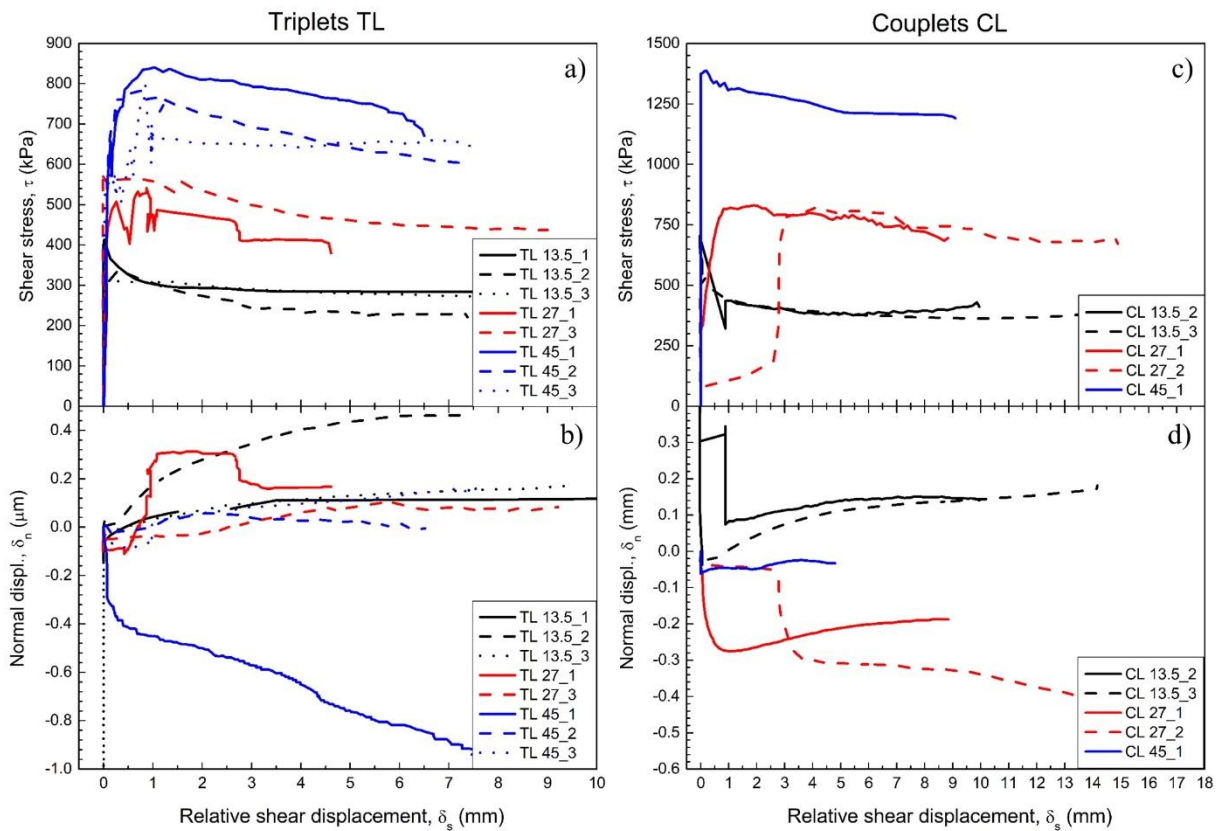


**Figure IV.5** Curves for masonry made of hydraulic lime mortar and handmade bricks. a) Shear stress vs. shear displacement plot for triplets. b) Normal displacement vs. shear displacement plot for triplets. c) Shear stress vs. shear displacement plot for couplets. d) Normal displacement vs. shear displacement plot for couplets.

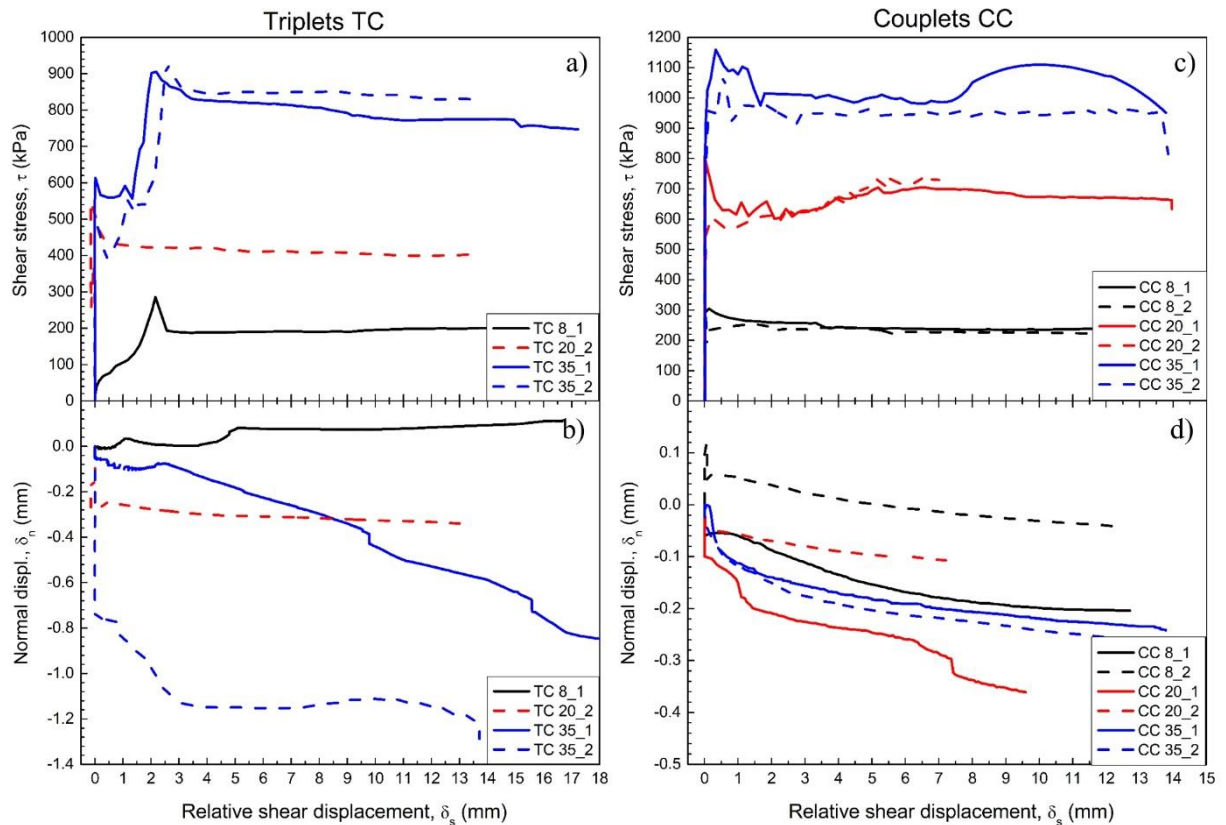


**Figure IV.6** Curves for masonry made of Portland cement mortar and extruded bricks. a) Shear stress vs. shear displacement plot for triplets. b) Normal displacement vs. shear displacement plot for triplets. c) Shear stress vs. shear displacement plot for couplets. d) Normal displacement vs. shear displacement plot for couplets.

Once the peak or ultimate shear strength  $\tau_u$  was reached and after the failure of the joint(s), the specimens submitted to precompression were able to resist against additional shear deformation. In this research, the residual shear strength  $\tau_{res}$  has been computed as the measured shear stress for a shear strain of 2.5%. This value of strain allowed the computation of the parameter  $\tau_{res}$  for most of the tests. The residual strength can be compared to the ultimate strength by means of a strength degradation ratio (SDR) as defined by Augenti and Parisi [331] and the following Equation IV.5. A higher value of SDR corresponds to a lower degradation. Table IV.3 presents the available results of ultimate and residual shear strength and indicates the corresponding strength degradation ratio. The two latter parameters are used here mainly for comparative purposes between the types of specimen, but residual values play an important role in the evaluation of structures after seismic events.

**PAPER IV**

$$\text{SDR} = \tau_{\text{res}} / \tau_u \quad (\text{IV.5})$$

Additionally, Table IV.3 includes the estimated values of the second mode fracture energy. This mechanical property is relevant for the structural analysis of masonry by means of micromodelling approaches [3,29]. Two different procedures have been applied for their calculation. Figure IV.7 schematizes both procedures. The first approach follows the common definition as proposed by Van der Pluijm [144] and Lourenço [336] ( $G_f^H$ , column 6). The fracture energy is estimated as the area below the apex of the shear stress – displacement curves and above the plateau of the residual shear strength. This definition only applies when the shape of the experimental curve is similar to the idealized one of Figure IV.7a. To overcome the impossibility of computing the fracture energy in some cases, a second approach is proposed. The second procedure defines the fracture energy as the area below the shear stress – displacement curves up to a displacement corresponding to a 2.5% of shear strain ( $G_{f\_2.5\%}^H$ , columns 7 and 8). The first approach aims to distinguish frictional energy from cohesive fracture energy [337] and evaluates this latter component, whereas the second proposed method involves all energy associated to the failure process for comparable damage final states. For the sake of clarity, these two parameters are called cohesive fracture energy ( $G_f^H$ ) and cohesive-frictional fracture energy ( $G_{f\_2.5\%}^H$ ) in the following. The combination of both approaches allows having more objective elements for the comparison between types of specimen.

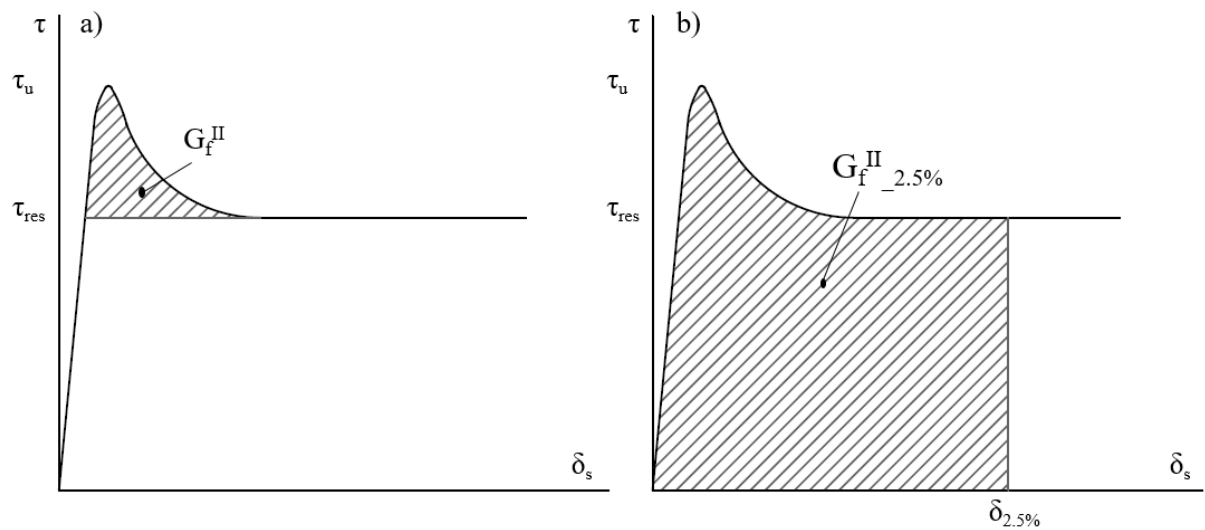


**Figure IV.7** Schematic shear stress  $\tau$  vs. displacement  $\delta_s$  curves that show the corresponding areas for the two approaches to calculate second mode fracture energy: a) Cohesive fracture energy  $G_f^{II}$ , b) Cohesive-frictional fracture energy taking into account the frictional dissipation up to a displacement corresponding to a 2.5% shear strain  $G_f^{II}_{2.5\%}$ .

**Table IV.3** Ultimate shear strength  $\tau_u$ , residual shear strength  $\tau_{res}$ , strength degradation ratio *SDR*, cohesive fracture energy  $G_f^{II}$  and cohesive-frictional fracture energy  $G_f^{II}_{2.5\%}$  for all specimens and precompression levels. The average values for each precompression level of *SDR* and  $G_f^{II}_{2.5\%}$  are indicated in square brackets.

Specimen	$\tau_u$ (kPa)	$\tau_{res}$ (kPa)	SDR	Second mode fracture energy	
				$G_f^{II}$ (N/mm)	$G_f^{II}_{2.5\%}$ (N/mm)
TL13.5_1	414.87	284.77	0.686	0.070	1.566
TL13.5_2	340.66	233.27	0.685	[0.752]	1.364
TL13.5_3	316.12	280.16	0.886	-	1.496
TL27_1	541.26	363.12	0.671	-	2.308
TL27_2	556.60	-	-	[0.737]	-
TL27_3	589.75	473.01	0.802	-	2.704
TL45_1	783.37	628.97	0.803	-	3.842
TL45_2	841.14	756.30	0.899	[0.853]	4.003
TL45_3	810.49	693.63	0.856	-	3.420
CL13.5_1	387.70	-	-	-	-
CL13.5_2	713.40	377.07	0.529	[0.625]	2.231
CL13.5_3	530.97	382.95	0.721	-	2.117
CL27_1	832.03	774.82	0.931	[0.952]	3.861
CL27_2	830.21	808.00	0.973	-	2.115
CL45_1	1393.01	1214.44	0.872	[0.872]	6.573
CL45_2	1247.05	-	-	-	-
TC8_1	286.82	189.55	0.661	[0.446]	0.824
TC8_2	393.87	91.05	0.231	-	0.692
TC20_1	234.45	-	-	[0.747]	-
TC20_2	555.33	414.93	0.747	-	2.220
TC35_1	907.78	822.19	0.906	[0.905]	3.802
TC35_2	938.71	849.90	0.905	-	3.517
CC8_1	460.83	234.12	0.508	[0.515]	1.303

PAPER IV

Specimen	$\tau_u$ (kPa)	$\tau_{res}$ (kPa)	SDR	Second mode fracture energy	
				$G_f^{II}$ (N/mm)	$G_f^{II}_{2.5\%}$ (N/mm)
CC8_2	421.20	219.46	0.521	-	1,204
CC20_1	823.98	672.98	0.817	-	3,311
CC20_2	752.09	718.99	0.956	[0.817]	3,122
CC35_1	1162.75	1014.66	0.873	-	5,327
CC35_2	1099.41	941.64	0.856	[0.873]	5,116

Finally, the secant shear modulus  $G$  at any point can be calculated by means of Equation IV.6:

$$G_i = \tau_i / \gamma_i \tag{IV.6}$$

where  $\gamma$  is the shear strain computed as the ratio between the shear displacement and the reference length of the measuring instrument. Figure IV.8 displays the evolution of the secant shear modulus for the four sets of specimens.

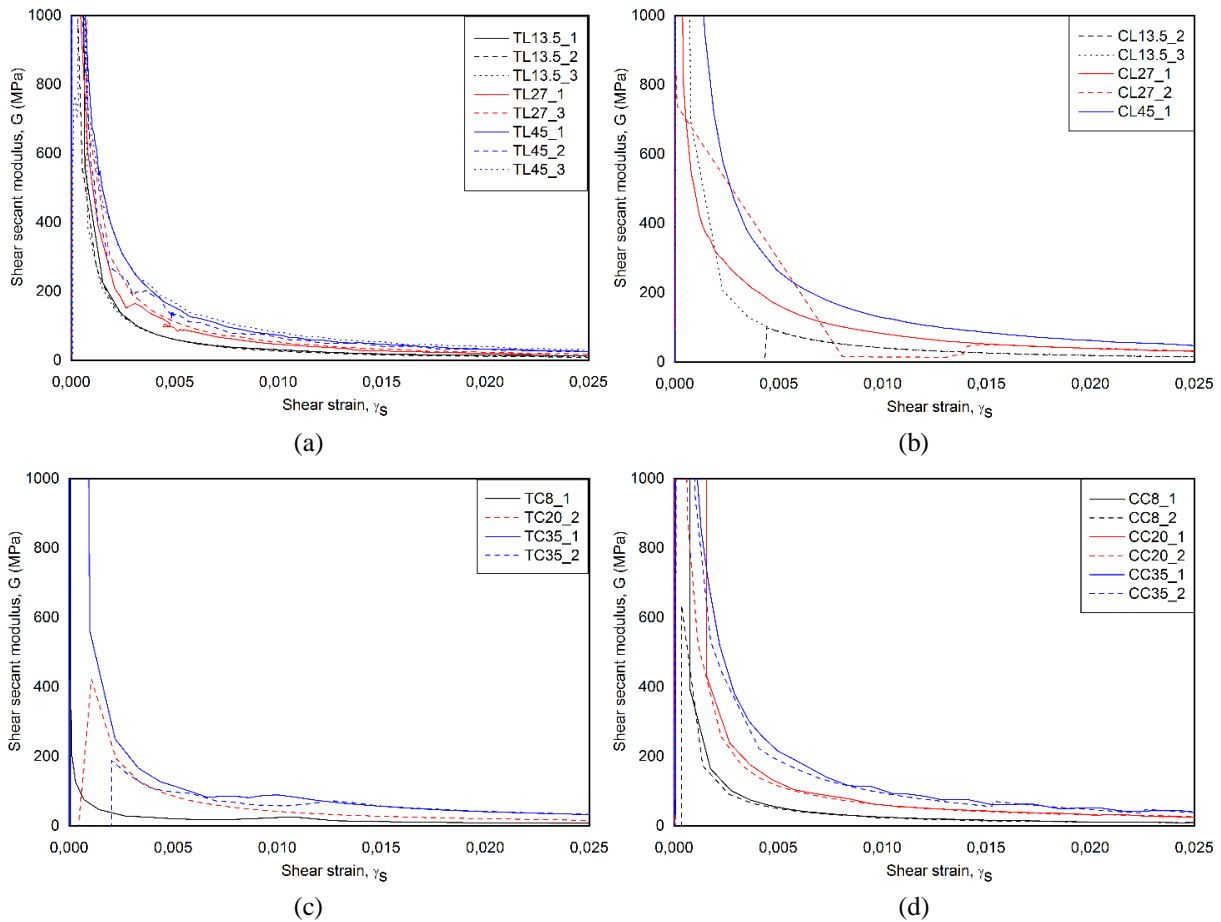


Figure IV.8 Shear secant modulus  $G$  vs. shear strain  $\gamma$  plots for a) TL, b) CL, c) TC, and d) CC specimens.

### IV.3 Discussion

The discussion of the experimental outcomes is organized in four sections. First, the results are studied from a general point of view. The second section analyses the influence of the type of specimen and compares the results of triplets and couplets. The last two sections evaluate the influence of the different materials on the former comparison and present a database of shear mechanical properties for masonry made of low strength mortars.

#### IV.3.1 General

The results of the four sets of samples show dependency on the level of confining normal stress. This dependency applies for all the parameters, not only for the shear strength and residual shear strength values, but also for the strength degradation ratio, the fracture energies and the secant shear modulus. Table IV.3 shows the clear upward trends for each variable. This dependency on the level of confining normal stress was expected due to the frictional behaviour of the material, and has been described by many authors [69,134,331,338].

Figure IV.4 depicts all the pairs  $\sigma$ - $\tau_u$  and the corresponding Mohr-Coulomb envelopes. In three cases (TL, TC and CC) the coefficients of determination  $R^2$  of the regression lines were higher than 0.95. In the single case of couplets made of hydraulic lime mortar and handmade bricks (CL) this coefficient was lower, but still acceptable, with a value higher than 0.9. This can be explained by the inherent variability of the material components, which was evidenced in Table IV.1 by high coefficients of variation in their mechanical properties. Among the individual data, the results of shear strengths for lower levels of normal stress seem to be more scattered. This is consistent with previous works [145] and is explained because at higher confining stresses the specimens are more stable. In this sense, the high scatter encountered in the samples tested at zero precompression, together with the fact that those tests do not allow

**PAPER IV**

the evaluation of postpeak parameters, make advisable to follow the prescriptions of the standard EN1052-3 [135] with regard to the levels of precompression and number of repetitions.

With respect to the stress-displacement curves, Figure IV.5 and Figure IV.6 show in general a very stiff behaviour before reaching the peak shear stress. Shear deformation before failure is so small that it is hardly detectable by the installed instruments. In consequence, the curves present quasi-rigid initial branches, as also found by other researchers, e.g. Mojsilovic et al. [339] and Fouchal et al. [333]. This high stiffness is reflected by the vertical asymptotes depicted in the curves of Figure IV.8, and causes a great difficulty in the measurement of the strain at peak stress. After the peak stress, shear secant modulus is exponentially reduced for all tested cases (see Figure IV.8). Roca and Araiza [143] also reported similar difficulties to measure the strain at peak stress, finding a significant scattering and even randomness. Although not able to capture the initial deformation, the installed instrumentation was able to measure the sliding along the joint and thus the postpeak regions of the curves can be considered as reliable. In spite of the difficulties encountered, the general validity of the results for carrying out the comparison between types of specimen is confirmed.

**IV.3.2 Influence of the type of specimen**

The type of specimen showed to have influence on the determination of all the analysed mechanical properties. The first difference between triplets and couplets is evident when comparing the stress-displacement curves of Figure IV.5a and Figure IV.6a, with Figure IV.5b and Figure IV.6b. This difference is related to the presence of the additional joint in the triplet specimens. Couplets show a much stiffer behaviour that lasts until the peak stress is reached, while triplets are more deformable and present sometimes the two-peak phenomenon already

mentioned in the Introduction section IV.1. The non-simultaneous failure of the two joints is manifest, for instance, in the curve of specimen TL27\_1.

The second and more significant difference is that couplets attained higher shear strengths than triplets for a given level of confining normal stress. Consequently, the estimation of the Mohr-Coulomb parameters was affected. On one hand, the estimated cohesion increased as the shear strength values were higher. On the other hand, the effect of the type of specimen also increased with the confining normal stress, i.e. the greater the confining normal stress, the greater the difference between couplets and triplets. Therefore, the slope of the regression lines changes and so the estimated angle of friction.

These observations partially agree with the few available experimental studies that have previously studied this comparison. Lawrence [329] undertook an experimental campaign on triplet and couplet tests to show up the differences between the two methods. This author found that the shear strength of couplets was higher than the comparative triplet tests. Schubert and Caballero [332] found that the cohesion values estimated in couplet specimens were twice as large the values estimated in triplets. More recently, Fouchal et al. [333] presented an experimental campaign that involved again these two types of specimen. Although they concluded that both test methods provided similar results, a detailed analysis of their individual data show that couplet specimens gave higher values of cohesion than triplets. However, the three former references dealt with tests performed with zero precompression and their conclusions are not fully comparable to the ones presented herein. The work by Zhang et al. [141] considers different levels of confining normal stresses, but their research is only based on numerical simulations. Under idealized boundary conditions, they found that couplets provided lower values of cohesion but slightly higher values of angle of friction than triplets.

**PAPER IV**

Independently of the previous literature considerations, the differences between triplets and couplets reported in the present research can be justified. Firstly, for the case of zero or low confining normal stresses, Lawrence [329] performed finite element linear analyses to confirm his experimental findings. He investigated the influence of the bending moment created by the non-aligned shear forces in both types of specimen. By comparing the stress distributions along the mortar joints, he found that triplet specimens had a larger region subjected to tension than couplets. Under the hypothesis that bond failure is triggered in the tension regions, this would explain why the shear strength in triplets was lower. Similar stress distributions were determined by Ali and Page [340]. Secondly, as stated by Lei [341], it is an established consensus that brittle fracture obeys the weakest-link postulate. This researcher has validated the existence of a specimen size effect for a wide spectrum of quasi-brittle materials and fracture modes, i.e. an inverse relationship between size and strength attributed to the stochastic distribution of microdefects in a material. Given that the brick-mortar interface area in the two-joint specimens is twice larger than in one-joint specimens, the lower strengths obtained with triplets could also be explained from a statistical approach. Lastly, as for the evaluation of the actual stresses along the joints, it is worth highlighting again that triplets usually present a double peak phenomenon. It is possible that, at the higher peak, one of the two joints is contributing with the residual strength while the other one has not failed yet. This could lead to an underestimation of the acting shear stress. Conversely, in the couplet specimens, if the friction along the external surface is not negligible, the measured strength could be an overestimation of the actual one. It is likely that both effects occur, which eventually motivates the difference between the two types of specimen.

### IV.3.3 Influence of the materials on the comparison between types of specimen

With regard to the two sets of materials being investigated, the tests on standard triplet specimens provided very similar values of cohesion (167 kPa for TL specimens and 165 kPa for TC specimens) and angle of friction ( $33.71^\circ$  for TL specimens and  $36.27^\circ$  for TC specimens). The influence of the different physical properties of each material component is difficult to analyse, as the research on the topic is controversial [134,319]. It could be expected that masonry C, made of cement mortar and extruded bricks, would show a better shear performance given the stronger mortar and the thinner mortar joints. However, the rougher surfaces of the handmade bricks and the higher fineness of the lime mortar aggregates used in masonry L compensate those effects.

In both material sets, the change of testing setup from triplets to couplets resulted in higher values of cohesion and angle of friction although the rates of increase were different. For hydraulic lime mortar specimens, cohesion turned from 167 kPa to 209 kPa (+25.1%) and the angle of friction varied from  $33.71^\circ$  to  $48.08^\circ$  (+42.6%). In the case of cement mortar specimens, the variations were from 165 kPa to 279 kPa (+69.1%), and from  $36.27^\circ$  to  $39.98^\circ$  (+10.2%). Even if both variables showed significant increase in both cases, the angle of friction increases more in L specimens, because of the better frictional response due to the roughness of the bricks, while cohesion increases more in C specimens, as they are characterised by better mortar adhesion and smooth surfaces of the bricks. Finally, it has to be remarked that the absence of an evident trend makes it difficult to find a direct correlation between the results of both types of specimen. This asymmetry in the influence of the type of specimen with respect to the materials has also been observed in the results of Fouchal et al. [333], as the increase in the cohesion values was much higher for hollow bricks than for solid bricks.

**PAPER IV**

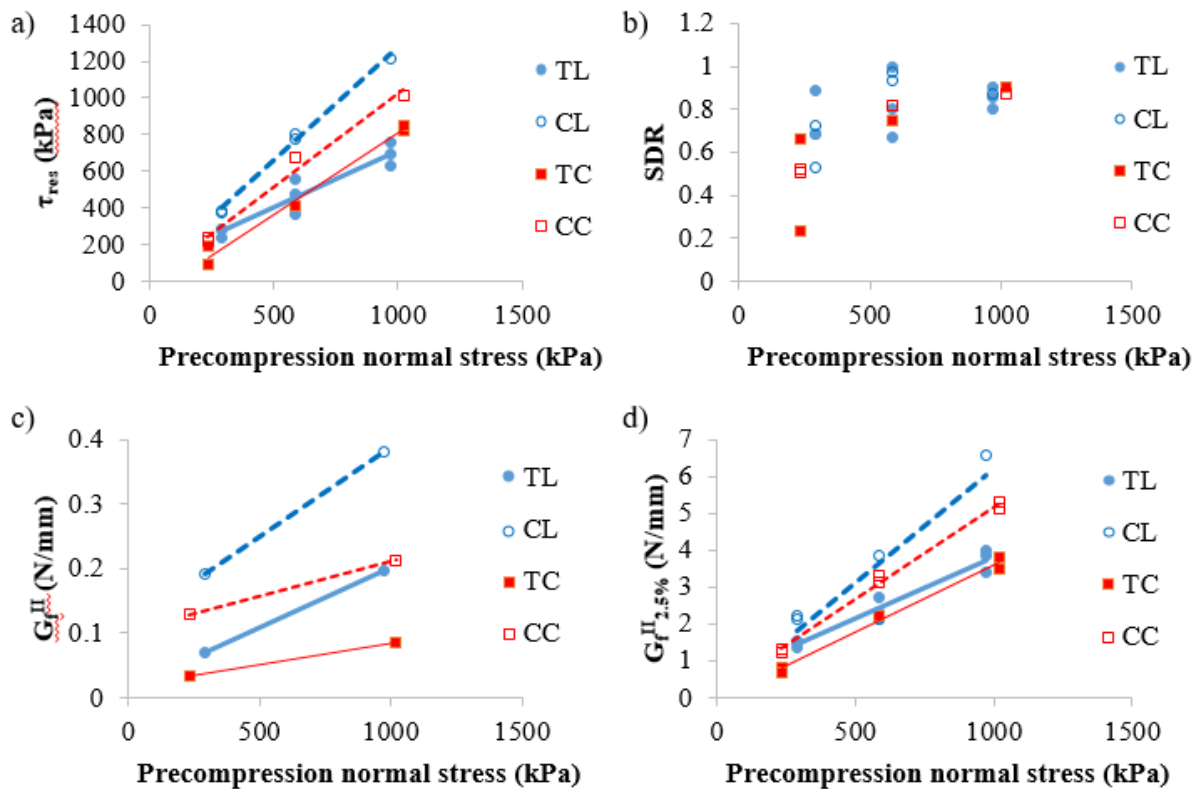
A further difference found between materials is the dilative nature of the hydraulic lime mortar specimens. Dilatancy is the increase of material's volume after crack formation that is associated with the shearing of the joint. The normal vs. shear displacement plots displayed in Figure IV.5b and 5d agree with the common features of dilative materials reported by Shadlou et al. [342]: (1) - dilatancy is prevented at small strains and accelerates after yielding at higher strains, as shown by most of the curves that start with a negative slope but change in correspondence with the peak stresses; and (2) – dilatancy depends on the level of normal precompression, as the curves of specimens subjected to the highest normal stresses do not show dilatancy. In the case of cement mortar, all the curves plotted in Figure IV.6b and Figure IV.6d present a negative slope and therefore no dilatancy effects were captured. This difference between both materials is related again to the roughness of the bricks surfaces. The handmade ones present an irregular surface as result of the fabrication process. One of their faces is especially rough due to the casting on a layer of sand, so dilatancy is really expected. Conversely, the industrially made bricks present a smooth surface as result of the extrusion process that explains why no dilatancy effects were observed. Moreover, with regard to the comparison between types of specimen, it is significant that both triplets and couplets have yielded the same observations with respect to dilatancy.

Figure IV.9 provides comparative plots to ease the data interpretation about residual shear strength, strength degradation ratios, and fracture energies. As aforementioned, all the studied parameters show linear dependency on the level of precompression stress. The estimations from couplet tests are also greater in all cases, except for the strength degradation ratios SDR. With respect to this latter parameter, Figure IV.9b shows that there is an influence of the material for lower and medium precompression stresses. Indeed, masonry L, which relies more on the contribution of friction, presents higher values of SDR. Eventually, the scattering of the results

for higher precompression stresses is significantly reduced and all specimens show similar final SDR, with an average value of 0.87 and a coefficient of variation of 4.2%.

As shown in Figure IV.9c, a very limited collection of cohesive fracture energy ( $G_f^H$ ) values could be calculated following the previously described first approach. Nevertheless, an estimation of the cohesive fracture energy at zero normal stress can still be done by linear regression. The results for the sets TL, CL, TC and CC are 0.0152 N/mm, 0.110 N/mm, 0.0284 N/mm and 0.104 N/mm respectively. These values are similar or of the same magnitude than those provided in the seminal research of Van der Pluijm [144], with 0.026 N/mm for soft mud brick and 0.058 N/mm for wire cut brick. It is important to note that other than the latter reference mentioned, very few comparative values of second mode fracture energy are available in literature for brick masonry, e.g. Ferretti et al. [322] found a value of 0.011 N/mm for calcium silicate bricks and cement mortar. Regarding the cohesive-frictional fracture energy ( $G_{f_{-2.5\%}}^H$ ) computed with the second approach, it is noted that specimens built with handmade bricks and hydraulic lime mortar showed greater fracture energy than those made of Portland cement and extruded bricks. This is again likely related with the superficial roughness of handmade bricks that increase the necessary energy to propagate the crack along an irregular superficial contact.

## PAPER IV



**Figure IV.9** Comparative plots for different tested specimens of a) residual shear strength  $\tau_{res}$ , b) strength degradation ratio SDR, c) cohesive fracture energy  $G_f^{II}$ , and d) cohesive-frictional fracture energy  $G_{f_{2.5\%}}^{II}$ .

#### IV.3.4 Comparison with available experimental values and standards

Table IV.4 presents an updated literature review of experimental campaigns on masonry made with low strength mortars. A mortar compressive strength of 3.5 MPa has been selected as the top bound. Given the limited number of available references on brick masonry, stone specimens have also been considered to increase the database on historical-like materials. The table indicates, ordered by increasing mortar strength, the type of specimen tested, the mortar's binder and compressive strength, the type of unit and its compressive strength, and the shear parameters cohesion and angle of friction. The scarcity of available references is remarkable, which supports the contribution of the work presented herein. Although the majority of data were obtained from standard triplet tests, a non-negligible number of results comes from couplets or small wallettes. This highlights the need of studying the correlation between

different setups or, at least, defining the trends that compare results from one type of specimen to another.

The magnitude of the results of this campaign in terms of cohesion and angle of friction lay within the intervals of the other researches. As already known, there is no univocal correlation between the compressive strength of the mortar and the shear parameters as the latter depends on varied physical properties of the masonry constituents.

**Table IV.4** Cohesion ( $c$ ) and friction ( $\phi$ ) for different types of masonry available in the literature, with compressive strengths of mortar  $f_m$  and of units  $f_b$ .

Source	Mortar	$f_m$ (MPa)	Unit	$f_b$ (MPa)	$c$ (MPa)	$\phi$
Rahgozar and Hosseini [343] – Direct shear couplet	Lime	0.54	Solid clay brick	10.0	0.054	41.08°
Milosevic et al. [321] – Irregular triplet	Aerial lime	0.56	Roughly cut stones	50.0	0.080	29.24°
Rahgozar and Hosseini [343] – Direct shear couplet	Lime	0.71	Solid clay brick	10.0	0.064	41.37°
Alecci et al. [344] – Triplet	Aerial lime	0.96	Solid clay brick	17.0	0.044	-
<i>This research – Couplet</i>	<i>Hydraulic lime</i>	<i>1.02</i>	<i>Solid clay brick</i>	<i>17.99</i>	<i>0.209</i>	<i>48.08°</i>
<i>This research – Triplet</i>	<i>Hydraulic lime</i>	<i>1.02</i>	<i>Solid clay brick</i>	<i>17.99</i>	<i>0.167</i>	<i>33.71°</i>
Milosevic et al. [321] – Irregular triplet	Hydraulic lime	1.47	Roughly cut stones	50.0	0.200	50.88°
Binda et al. [345] - Triplet	Hydraulic lime	1.50	Sandstone blocks	106.0	0.330	36.46°
Binda et al. [345] - Triplet	Hydraulic lime	1.50	Calcareous stone blocks	5.9	0.580	30.12°
Pelà et al. [145] - Triplet	Aerial lime	1.63	Solid clay brick	30.7	0.040	35.65°
Uranjek and Bokan-Bosiljkov [346] – Triplet	Aerial lime + slag	2.47	Solid clay brick	32.2	0.099	43.78°
Augenti and Parisi [331] – Couplet wallette	Pozzolana	2.5	Cut tuff blocks	4.1	0.146	16.44°

**PAPER IV**

Source	Mortar	$f_m$ (MPa)	Unit	$f_b$ (MPa)	$c$ (MPa)	$\phi$
<i>This research – Couplet</i>	<i>Cement</i>	2.53	<i>Solid clay brick</i>	27.93	0.252	41.10°
<i>This research – Triplet</i>	<i>Cement</i>	2.53	<i>Solid clay brick</i>	27.93	0.165	36.27°
Binda et al. [116] – Triplet	Hydraulic lime	2.61	Clay brick	14.25	0.230	30.00°
Alecci et al. [344] – Triplet	Cement-lime	2.75	Solid clay brick	17.0	0.212	-
Uranjek and Bokan-Bosiljkov [346] – Triplet	Aerial lime	2.82	Solid clay brick	32.2	0.121	38.00°
Van der Pluijm [144] – Couplet	Cement lime	3.00	Soft brick	33.00	0.100	47.55°
Van der Pluijm [144] – Couplet	Cement lime	3.00	Sandlime brick	35.00	0.150	57.87°
Alecci et al. [347] – Triplet	Cement-lime	3.22	Solid clay bricks	24.1	0.260	34.38°

Finally, Table IV.5 includes a comparison of the experimental results of cohesion or initial shear strength with the values recommended in two design standards: the Eurocode 6 for masonry structures [60] and the “Circolare” associated to the Italian NTC [62]. The latter is specific for existing and historical structures. Even if conceptually different, since the experimental values refer to the strength of a single joint and the design values refer to the strength of the masonry composite, the codes use the joint results to feed their models. The characteristic values of the cohesion are obtained as the 80% of the experimental results as indicated in EN1052-3 [135]. In the present research, and in the case of the weaker mortar, the characteristic initial strength is underestimated by the Eurocode 6 proposed value, while it is overestimated for the cement mortar masonry. With regard to the Italian recommendations, the experimental values lay within the suggested limits. The triplet tests, although with the associated problems of interpretation, provide values which are safer with regard to design. On the other hand, it could be expected that couplet tests may provide more representative

estimations that could allow more economical and respectful interventions. Nevertheless, their representativeness should be investigated with further theoretical and numerical studies.

**Table IV.5** Comparison of experimental results with design standard values.

Tests	Experimental cohesion $c$ (MPa)	Experimental characteristic cohesion $ck$ (MPa)	Characteristic initial shear strength EC6 [60] $f_{vk0}$ (MPa)	Initial shear strength NTC2018 [62] $f_{v0}$ (MPa)
TL	0.167	0.134	0.1	0.13-0.27
CL	0.209	0.167		
TC	0.165	0.132	0.2	0.13-0.27
CC	0.252	0.202		

#### IV.4 Conclusions

This paper has presented an experimental investigation on the shear characterisation of masonry. A novel contribution is the execution of a direct experimental comparison between two types of specimen, standard triplets and couplets. The testing setup for couplets was a simple modification of the standard setup for triplets. Two different sets of materials were considered, with the aim of duplicating the observations.

Both types of specimen have provided sound experimental results showing the expected dependency with the normal compression stresses. This dependency influenced the values of ultimate and residual shear strengths, as well as the values of fracture energy. The magnitudes of the estimated mechanical parameters, such as cohesion, angle of friction, and cohesive fracture energy at zero precompression, are similar to those found in literature for comparable materials. In addition, both specimens have predicted similar trends with respect to dilatancy.

Couplet specimens provided consistently higher values of cohesion and angle of friction than triplets. For masonry made of handmade bricks and hydraulic lime mortar, the variations were of +25.1% and +42.6% for cohesion and angle of friction respectively. For masonry made of extruded bricks and cement mortar, the rates of increase were +69.1% and +10.2% for

**PAPER IV**

cohesion and angle of friction respectively. This asymmetry in the influence of the type of specimen seems to be related with the dominant response of the materials, which is frictional in the case of the rougher handmade bricks, and cohesive in the case of the smooth extruded bricks. Therefore, a direct univocal correlation could not be found given the limited amount of data and the divergent trends. The type of specimen also influenced the estimations of fracture energy and residual shear strengths.

The differences between standard triplets and couplets could be explained as the result of several causes. First, the stress distributions along the mortar joints are different in both types of specimen. Second, the lower strengths found with triplets could be explained from a statistical approach, given that the brick-mortar interface area is twice larger in triplets than in couplets. Third, the evaluation of the actual stresses along the joints may be biased in both types of specimen, by the double peak phenomenon in the case of triplets, and by the friction of the lateral faces in the case of couplets.

A database of shear parameters for masonry made with low strength mortars has been presented. Besides results on standard triplets, the database included results from couplets and other irregular specimens, which are easily found in literature. It was however difficult to find references with experimental comparisons between the different types of specimen. This is a consideration that should be kept in mind when using parameters from existing databases. It is always necessary to know the conditions under which those parameters were obtained.

One of the studied sets of materials aimed to represent a historical type of masonry built of handmade bricks and hydraulic lime mortar. The standard triplet tests provided a cohesion of 167 kPa and an angle of friction of  $33.71^\circ$ . These new results contribute to complete the available database on similar materials.

### **6.3. Paper V – Experimental and numerical insights on the diagonal compression test for the shear characterisation of masonry**

J. Segura, L. Pelà, S. Saloustros, P. Roca. *Under review*

*Abstract: The masonry tensile strength and shear modulus play a key role in the definition of the shear capacity of masonry structures. These properties are often determined experimentally by means of the diagonal compression test on square walls, which is regulated by the ASTM E519 standard. In spite of its wide use, the interpretation of the test is still controversial and no universal criterion exists on how to derive the masonry mechanical properties from the wall overall strength. Aiming to contribute in the improvement of the test's reliability and interpretation, this paper presents an investigation on the use of the diagonal compression test to characterize the shear properties of masonry. First, an experimental campaign on brickwork walls is described. The walls were built in laboratory in Flemish bond, a pattern that has been scarcely investigated in the available research studies on this type of test. Second, an advanced numerical model is used for the analysis of walls subjected to the diagonal compression test. The adopted numerical model, enhanced by a crack-tracking algorithm to reproduce accurately the tensile damage localization, constitutes a very useful and powerful tool to interpret correctly the behaviour during the test. Finite element analysis was executed to interpret the walls' response in the linear and nonlinear ranges with models properly calibrated by comparison with the experimental results. As a result, a criterion was determined for the calculation of the tensile strength from the outcomes of the diagonal compression test. A sensitivity analysis was carried out with regard to the most influent material*

**PAPER IV**

*properties of the material, the geometrical dimensions of the panel, and the loading conditions of the testing setup. The findings of this research were finally applied and validated by means of simulations of diagonal compression tests from eight experimental campaigns performed by other authors on different masonry typologies.*

## V.1 Introduction

Shear walls resist the seismic effects in masonry buildings mostly through in-plane resisting modes. Being local out-of-plane wall failures prevented by appropriate connections between elements, the resisting mechanism that governs the global behaviour of the structure is the in-plane shear capacity of the walls [348,349], directly depending on the masonry shear strength.

The definition of the shear strength of masonry is not univocal [310]. Because of its complex and composite behaviour, masonry may experience different failure modes under lateral loading, depending on the relative mechanical properties of the constituents, the boundary conditions, the geometry of the panel, and the level of vertical load acting on the structure. Three mechanisms are usually identified as potential failure modes in shear [350]: a) rocking failure involving the overturning of the wall and crushing of the compressed corner, b) shear sliding failure along a horizontal crack in the mortar bed-joints, and c) shear diagonal cracking through bed- and head-joints or also through the units. Different physical models have been adopted to estimate the shear capacity associated to the former mechanisms [310]

In the case of diagonal cracking, which is a recurrent mode observed after past earthquakes [165,310], Turnšek and Čačovič proposed a criterion that predicts the shear capacity of a wall for a given level of compressive stresses [170]. The criterion is based on a triple assumption: a) masonry is considered a homogeneous and isotropic material, b) failure occurs when the maximum principal stresses at the centre of the panel, which can be derived through the Mohr's circle from the acting shear and compressive stresses, exceed a reference value, and c) the reference value is supposed to be constant for walls made of the same material and represents a characteristic property. Turnšek and Čačovič validated these assumptions experimentally and

**PAPER V**

provided the following Equation V.1 for the shear interaction diagram of a wall (presented herein in the more general form published in [351]):

$$\tau_m = \frac{f_t}{b} \sqrt{1 + \frac{\sigma_0}{f_t}} \quad (\text{V.1})$$

where  $\tau_m$  and  $\sigma_0$  are the average shear stress at failure and the compressive stress in the wall due to vertical loading respectively, and  $b$  is a coefficient that accounts for the distribution of stresses within the panel.  $f_t$  is the reference limit strength, defined and adopted as the conventional tensile strength of masonry [310,350]. Although the initial assumptions are drastic [3,350], this criterion is thoroughly diffused [352] as it manages to describe a complex behaviour with a single global parameter. Furthermore, the hypothesis of homogeneity is consistent with the continuum homogeneous models still in use for the analysis of masonry structures [3,12].

The experimental determination of this tensile strength of masonry would require the performance of shear-compression tests in the laboratory and the derivation of  $f_t$  from the inverse of Equation V.1. These tests are however costly in terms of time and equipment as special loading apparatus are necessary to impose the proper boundary conditions and loads [171], and the mode of failure is difficult to control [165]. An alternative test that induces a state of stresses leading to a diagonal cracking failure is the diagonal compression test [146,348,351]. This type of test is considered to be more versatile, simpler, and less expensive [169,353,354], being also applicable to in-situ inspections of real buildings [146].

The diagonal compression test consists of loading a masonry assemblage in compression along one of the diagonals, thus causing a tension failure with the specimen splitting apart parallel to the direction of load [355]. Given its ability to induce a shear diagonal cracking, it has been extensively used recently as a tool for comparing reinforcement products and

techniques [165–168,356,357], as well as to investigate the behaviour of historical buildings [163,164,358]. This test is also recommended as a characterisation tool by several national and international building codes [10,62,129].

The American standard ASTM E519 [355] is the main reference that provides guidance on the features of the masonry specimens required for the test and on the loading conditions and protocols. It regulates the calculation of the acting stresses and the shear modulus of masonry as well. Based on the hypothesis of an isotropic linearly elastic material, the standard assumes a stress state of pure shear at the centre of the panel. Figure V.1b represents the corresponding Mohr's circle. Under the hypothesis of pure shear, the maximum principal stress,  $\sigma_1$ , is equal to the shear stress,  $\tau_{xy}$ , and the standard proposes the following Equation V.2 for their calculation:

$$\sigma_{I,ASTM} = \tau_{xy,ASTM} = 0.707 \frac{P}{A} \quad (V.2)$$

where  $P$  is the diagonal load at a given time and  $A$  is the net area of the specimen computed with Equation V.3:

$$A = t \frac{w + h}{2} \quad (V.3)$$

where  $w$ ,  $h$  and  $t$  are the width, height and thickness of the specimen respectively. Equation V.4 applies for the calculation of the tensile strength assuming that it is equal to the maximum principal stress at failure:

$$f_{t,ASTM} = 0.707 \frac{P_{max}}{A} \quad (V.4)$$

where  $P_{max}$  is the diagonal load value at failure. Additionally, there exists a recommendation by RILEM, LUMB6 [157], that covers also this test and specifies dimensions of specimens and apparatus. The suggested expression to calculate the tensile strength is the same as in ASTM E519 [355].

## PAPER V

However, as soon as in 1931, Frocht found that a square plate made of an elastic isotropic material loaded in diagonal compression does not experience a pure shear state of stresses but a complex non-uniform one, where the normal components are not null [160]. Frocht drew this conclusion both from analytical derivation and by photoelasticity. These findings were confirmed afterwards in several instances by means of modern numerical methods [161,162,359]. Equations V.5 to V.7 show the expressions to calculate the acting stresses following Frocht's approach. Equation V.8 relates the tensile strength of masonry with the maximum principal stress at failure:

$$\sigma_{x,Frocht} = \sigma_{y,Frocht} = -0.58 \frac{P}{A} \quad (V.5)$$

$$\tau_{xy,Frocht} = 1.1 \frac{P}{A} \quad (V.6)$$

$$\sigma_{I,Frocht} = 0.52 \frac{P}{A} \quad (V.7)$$

$$f_{t,Frocht} = 0.52 \frac{P_{max}}{A} \quad (V.8)$$

where  $\sigma_x$  and  $\sigma_y$  are the normal stresses. Figure V.1c depicts the corresponding Mohr's circle. More recently, Brignola et al. [162] performed non-linear numerical analysis that accounted for the redistribution of stresses after failure and proposed new coefficients for Equation V.8, as explained in Section V.4.2.2.

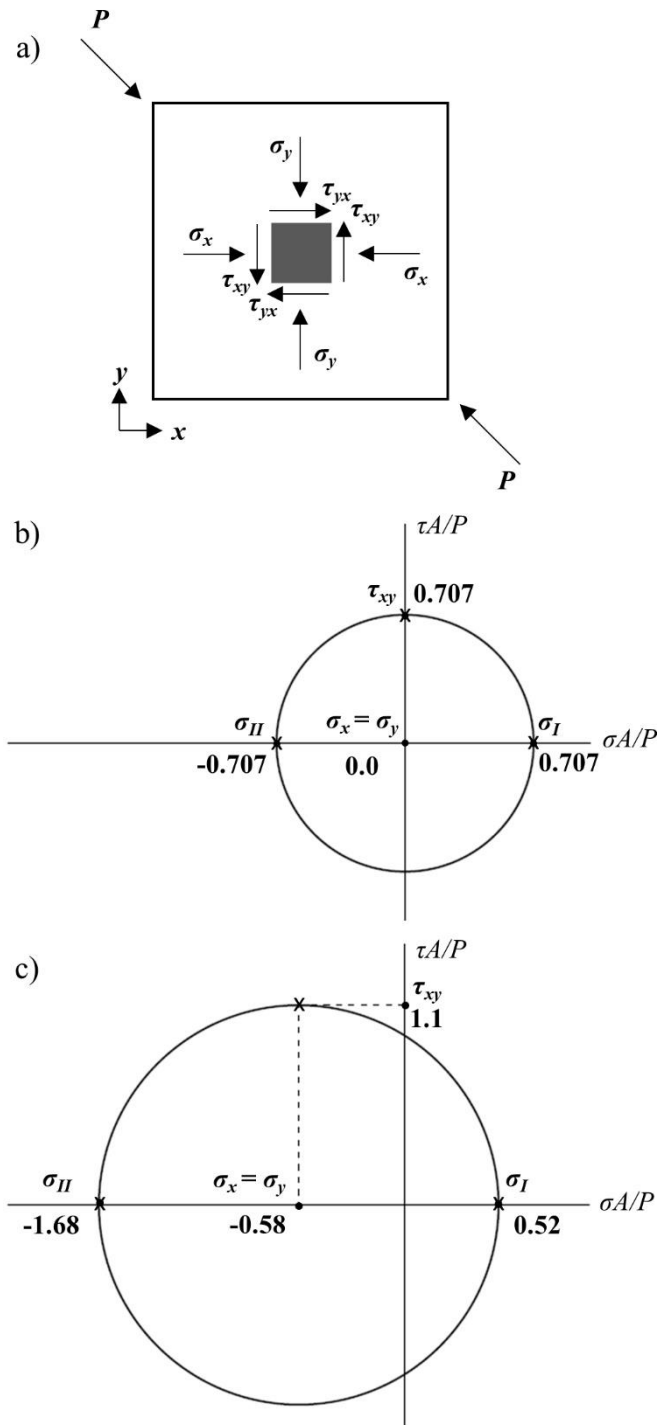


**Figure V.1** a) Coordinate system in the diagonal compressed wall. b) Mohr's circle representations of the stresses at the centre of the panel according to ASTM's and c) Frocht's approaches.

As illustrated in Figure V.1, both approaches, i.e. ASTM's and Frocht's, lead to different estimations of the tensile strength of masonry, but also of the acting shear stresses and the shear strength at zero compressive stress. Several authors have pointed out the controversy around

**PAPER V**

these interpretations of the diagonal tests and have questioned the proposed formulae [163,169,171,344,348]. This open debate hinders the applicability of the test and makes the comparison between researches difficult. Yet, even if the approach of ASTM E519 [355] overestimates the values of tensile strength compared to Frocht's approach, it is still the most spread standard, and Equation V.2 is widely used [167,168,173,356,357,359–363].

The work presented herein provides new insights on the mechanical behaviour of masonry panels under diagonal compression, and investigates the use of this test for the determination of homogenised properties of masonry, specifically the tensile strength and the shear modulus.

The paper starts with two preliminary sections that describe the data and tools used to carry out the investigation. Section V.2 presents an experimental campaign involving diagonal compression tests that will be used as calibration results. This campaign has additional relevance as it deals with tests on masonry walls made of clay bricks and hydraulic lime mortar arranged in Flemish bond. This masonry typology has received little attention until now in the available scientific literature [364], and its investigation constitutes a novel contribution of the paper. Section V.3 describes the numerical tools used for the simulation of the experimental tests. The employed numerical model is based on a standard finite element formulation and includes the accurate description of tensile crack localization through a crack-tracking algorithm.

Section V.4 constitutes the core of the paper. It includes the calibration of a numerical continuum model with the experiments of Section V.2, the interpretation of the stress field within a masonry panel and the proposal of coefficients for the calculation of both the tensile strength and the shear modulus from diagonal tests. It also includes a sensitivity analysis of the proposed coefficients and their validation with cases investigated by other authors. Section V.5 presents the concluding remarks of the research.

## V.2 Experimental programme

The experimental programme presented herein had two main objectives: a) providing experimental data to calibrate the numerical models necessary for the investigation on the interpretation of the diagonal test, and b) characterizing a masonry typology recurrent in existing historical buildings. This section describes briefly the programme, which was carried out at the Laboratory of Technology of Structures and Building Materials of the Technical University of Catalonia (UPC – BarcelonaTech).

### V.2.1 Materials

The masonry walls were built with handmade solid clay bricks and a low mechanical performance lime mortar, aiming to replicate a historical brickwork.

Solid clay bricks, moulded and fired manually, were provided by a local company. Bricks had average dimensions of 311 (length)  $\times$  149 (width)  $\times$  45 (height) mm<sup>3</sup> and presented rough surfaces because of their traditional manufacturing. Table V.1 includes the results of characterisation tests. The brick compressive strength,  $f_{b,c}$ , was estimated according to the standard EN 772-1 [285] on cut pieces of 100  $\times$  100 mm<sup>2</sup>. Two different types of test were carried out to approximate the tensile strength of the bricks: three-point-bending tests on full bricks according to EN 772-6 [286] to evaluate the flexural tensile strength,  $f_{b,f}$ , and Brazilian tests on prismatic pieces of 160  $\times$  40  $\times$  40 mm<sup>3</sup> to estimate the indirect splitting tensile strength,  $f_{b,sp}$ .

A hydraulic lime based commercial mortar was chosen as binding material. This mortar was modified with limestone filler additions to reduce its strength, as explained by the authors in a recent publication [334]. During the construction of each masonry wall, mortar prisms with dimensions 160  $\times$  40  $\times$  40 mm<sup>3</sup> were prepared from the mason's batch. Each set of prisms was

## PAPER V

tested at the same time of its companion wall. Table V.1 presents the average compressive strength,  $f_{m,c}$ , and the average flexural tensile strength,  $f_{m,f}$ , of mortar determined according to EN 1015-11 [257]. Additionally, after the test of each wall, some masonry bed-joints were disassembled with the aim of extracting mortar samples to perform double-punch tests (DPT). Specimens with approximated dimensions of  $50 \times 50 \times 15 \text{ mm}^3$  were tested according to DIN 18555-9 [304] to assess the mortar compressive strength within the joints,  $f_{m,DPT}$ .

Masonry specimens made with these two same components were tested in parallel campaigns [268,365] to evaluate the compressive and shear mechanical properties of the masonry composite (see Table V.1). The compressive strength of masonry,  $f_c$ , was obtained from tests on running bond walls according to EN 1052-1 [72]. Two additional tests on stack bond prisms provided estimations of the compressive fracture energy,  $G_{fc}$ . Triplet specimens were tested by following the standard EN 1052-3 [135] to determine the cohesion,  $c$ , and angle of friction,  $\phi$ , of the masonry bed-joints.

**Table V.1** Mechanical properties of constituent materials (brick and mortar) and of masonry composite.

Brick	$f_{b,c}$ [MPa]	$f_{b,f}$ [MPa]	$f_{b,sp}$ [MPa]	
Average	17.99	2.44	1.44	
Number of specimens	20	10	24	
CV	8.3%	20.0%	13.0%	
Mortar	$f_{m,c}$ [MPa]	$f_{m,f}$ [MPa]	$f_{m,DPT}$ [MPa]	
Average	2.19	0.66	5.11	
Number of specimens	38	76	232	
CV	26.1%	25.4%	23.0%	
Masonry	$f_c$ [MPa]	$G_{fc}$ [N/m]	$c$ [MPa]	$\phi$ [°]
Average	6.51	9750	0.16	33.71
Number of specimens	4	2	-	-
CV	8.9%	15.2%	-	-

### V.2.2 Masonry specimens

Five double-leaf masonry walls with nominal dimensions  $1270 \times 1270 \times 311 \text{ mm}^3$  were built in the laboratory. The specimens were labelled URM\_#, where # is a digit from 1 to 5.

The chosen dimensions allowed to satisfy the geometrical requirements established in the standard ASTM E519 [355] and in the recommendations LUMB6 of RILEM [157], i.e. have a minimum dimension of 1200 mm and be a minimum of four units wide, respectively. The walls were built in Flemish bond, as shown in Figure V.2. This bond pattern is particularly common in historical buildings [358,366] but still few experimental results are available in literature for this typology [358,364]. As reported in [165], there is a lack of experimental evidence on double-wythe masonry.

Professional bricklayers built the walls on metallic C-profiles. This measure facilitated the later handling of the specimens. To avoid any influence of the metallic base during the tests, an interface consisting of one Teflon sheet 3 mm thick and one PVC sheet 3 mm thick was placed on top of the C-profile before laying the first joint of mortar (see Figure V.2). Up to 21 brick courses conformed the walls, with 15 mm thick mortar joints. This thickness was necessary to accommodate the irregularities of the brick surfaces. After the construction, the walls were stored in laboratory conditions during the curing of the mortar and were tested after 28 days.

### **V.2.3 Setup and testing procedure**

The standard ASTM E519 [355] served as reference for the execution of the tests. However, a modification was introduced with respect to the positioning of the walls and they were kept horizontal instead of rotated 45 degrees. This measure avoided any damage during the handling of the specimens due to their low strength and is rather common in research practice [166,367,368]. Furthermore, this setup replicates the same one used for in-situ testing [163,164].

Figure V.2 displays the entire experimental setup for testing a wall. The specimens were placed on top of a metallic bench. Two steel loading-shoes, bolted to two robust beams, were

**PAPER V**

placed at two diagonally opposite corners of the specimens. The two beams were connected by two Dywidag bars, one at each face of the walls. During the test, two hydraulic jacks pulled the bars, thus creating a closed-loop system and introducing the diagonal load into the specimens [367]. The loading depth of the steel shoes at the corners was of 140 mm. The ratio of the loaded depth (140 mm) with respect to the total width of the wall (1270 mm) is equal to  $1/9^{\text{th}}$ . This ratio was chosen as a compromise between the suggestions reported in ASTM E519 [355] and in RILEM LUMB6 [157], which are  $1/8^{\text{th}}$  and  $1/10^{\text{th}}$  respectively.

The loading protocol involved two stages, following the approach applied by the authors in [268]. The first stage aimed to facilitate the measurement of the elastic shear modulus of masonry, and consisted of the application of three loading-unloading cycles, from 10 to 50 kN under load control. The execution of cycles, as reported in [268] and suggested by specific standards for the determination of elastic properties (e.g. [119,287]), minimizes the possible errors due to initial effects of backlash and specimen irregularities. The second stage of the tests investigated its ultimate capacity. The load was applied beyond failure under displacement control at a constant rate of approximately 0.5 mm/min. The tests were stopped when the reduction of the load attained 50% of the registered peak load.

Besides the pressure transducer and the encoder necessary to control the hydraulic jacks, the walls were mainly instrumented with four linear variable differential transducers (LVDTs). The mounted instruments had a displacement range of  $\pm 5$  mm and a precision of 5  $\mu\text{m}$ . Two LVDTs were placed on each face of the specimens along the diagonals, one aimed to measure the shortening of the compressed diagonal and the other aimed to capture the elongation of the diagonal under tension. Redundant instrumentation, including wire sensors and additional displacement transducers, was mounted to assess the global behaviour of the walls during the

tests. Further details on the whole setup and testing procedure are available in [168], which covers a parallel research on strengthened masonry.

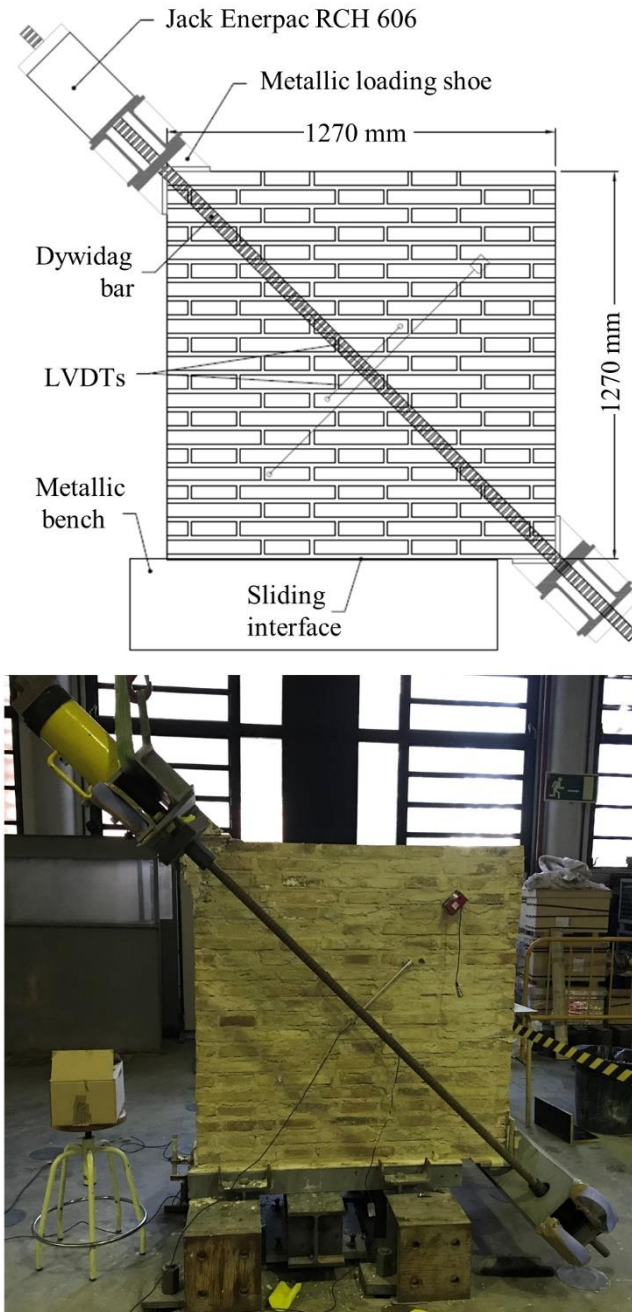


**Figure V.2** Setup of the diagonal compression test.

After the tests, the tensile strengths of each wall were evaluated with Equations V.4 and V.8 corresponding to the different approaches of ASTM E519 [355] and Frocht [160]. The shear strains  $\gamma$  were calculated with the following Equation V.9:

**PAPER V**

$$\gamma = \varepsilon_c + \varepsilon_t \quad (\text{V.9})$$

where  $\varepsilon_c$  and  $\varepsilon_t$  are the compressive and tensile strains along the compressed and tensioned diagonals, obtained as the average of the readings from the LVDTs on both sides of the wall. The shear elastic moduli were evaluated as the chord modulus between the 5% and 30% of the actual maximum load ( $P_{max}$ ) of the shear stress-strain curves. Equations V.10 and V.11 present the expressions to calculate the shear elastic moduli  $G$  for each of the considered approaches, where the shear stresses are evaluated with Equations V.2 and V.6:

$$G_{ASTM} = \frac{0.707 \frac{\Delta P_{5-30\%}}{A}}{\Delta \gamma_{5-30\%}} \quad (\text{V.10})$$

$$G_{Frocht} = \frac{1.1 \frac{\Delta P_{5-30\%}}{A}}{\Delta \gamma_{5-30\%}} \quad (\text{V.11})$$

where  $\Delta P_{5-30\%}$  and  $\Delta \gamma_{5-30\%}$  stand for the increase of load and strain respectively between the 5% and 30% of the maximum load.

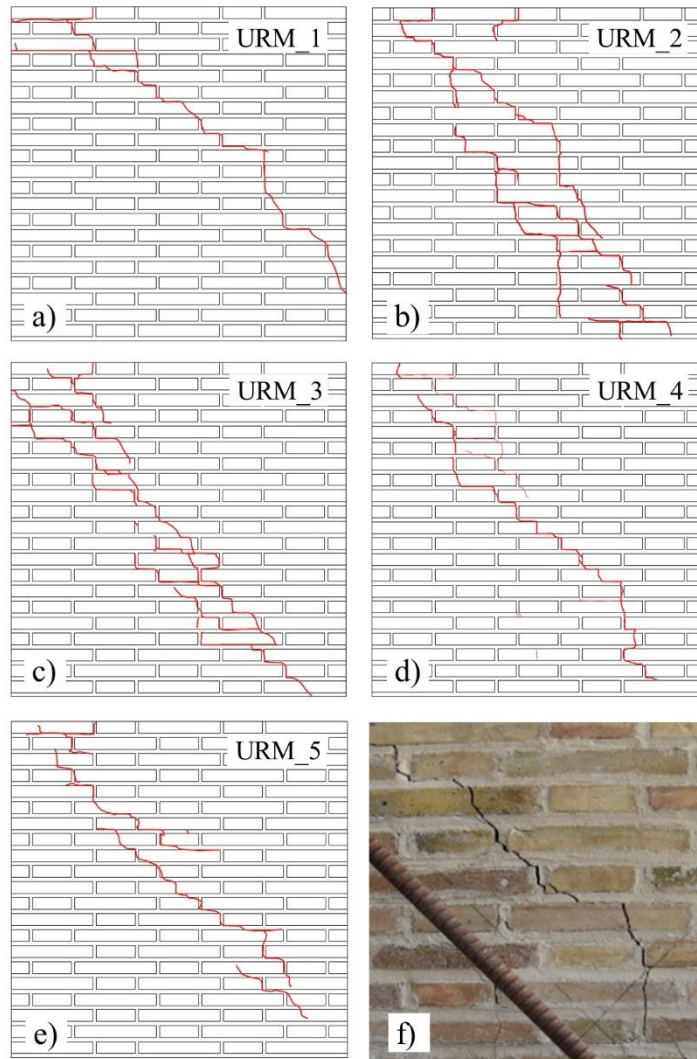
## V.2.4 Experimental results

Figure V.3 displays the crack patterns of the five walls after failure. These patterns were qualitatively similar and, in all cases, a final diagonal main crack connected both loaded corners. The particularity of the Flemish bond used to build the walls reflects in the number of bricks affected by the crack. Contrarily to other bond arrangements such as header bond, where cracks follow the mortar joints and bricks are broken only rarely [166,369], the length of the bricks used herein hindered the formation of a stair-stepped crack and necessarily required the failure of bricks in tension. Figure V.3f includes a detail of URM\_2 that shows cracks involving both bricks and mortar joints.

The five walls presented a relatively brittle behaviour. In all cases, the load increased linearly with the imposed displacement until a change in the slope of the loading curves was noticed. This sudden change would indicate the appearance of initial damage and was detected by both the LVDTs and the redundant instrumentation at a load level around 80 to 90% of the maximum load  $P_{max}$ . At that moment, superficial cracks were not visible to the naked eye. Full cracks connecting the corners appeared at the maximum load or immediately after, and continued to develop and open during the loss of bearing capacity of the wall. Only in the case of specimen URM\_3, cracks started clearly at the centre of the panel and progressed along the diagonal to reach the corners. In the rest of specimens, it was difficult to place the starting point of cracks, as they appeared almost simultaneously along the full length.

Table V.2 presents a summary of the experimental results from diagonal compression tests on the five walls. Table V.2 indicates the registered values of maximum load  $P_{max}$  and the calculated values of tensile strength  $f_t$  and shear modulus  $G$  according to the two approaches and Equations V.4, V.8, V.10 and V.11. No values of shear modulus are given for specimen URM\_2 due to invalid readings of the LVDTs during the test. The need of delving into the interpretation of the diagonal test outcomes is evident in the light of the obtained average results. Compared to the standard procedure of the ASTM E519 [355], the estimations of the tensile strength and shear modulus of masonry with Frocht's approach are 26% lower and 56% higher respectively.

## PAPER V



**Figure V.3** a) to e) Crack patterns at the end of the test for the five specimens. f) Pattern detail of wall URM\_2 with cracks involving both bricks and mortar joints.

The obtained average values of tensile strength compare well with the few published results in literature on Flemish bond walls built with similar components [358].

**Table V.2** Experimental results. Maximum load, tensile strength and shear modulus of each specimen.

Specimen	$P_{max}$ [kN]	$f_{t\_ASTM}$ [MPa]	$f_{t\_Frocht}$ [MPa]	$G_{ASTM}$ [MPa]	$G_{Frocht}$ [MPa]
URM_1	178	0.32	0.24	1536	2389
URM_2	167	0.30	0.22	-	-
URM_3	117	0.21	0.15	1149	1787
URM_4	179	0.32	0.23	1571	2444
URM_5	115	0.21	0.15	883	1375
Average	151	0.27	0.20	1285	1999
CV	21.5%	21.3%	21.3%	25.6%	25.6%

The coefficients of variation of the experimental results range from 20 to 25%. This relatively high variability is common in this type of material and typology of test [348,356,359,370]. According to the coefficients of variation presented for bricks and mortar in Table V.1, the inherent variability of the material constituents can fully explain the scattering found in the diagonal compression tests. In this type of tests, cracks are localized in a narrow band of the wall, as shown in Figure V.3. Given the brittleness of the observed failures, and in agreement with the weakest-link postulate for brittle materials [341], it could be expected that the global results were sensitive to the local properties of the constituents. Another additional source of variability is given by the Flemish bond and the relevant two-brick thickness of the walls, which constitutes a further complexity in the material structure compared with the recurrent tests available in the literature on one brick walls with units laid in a stretcher pattern.

As will be seen in Section V.4.1, this variability is helpful to the aim of this study because the results can be grouped in data sets of similar properties, and they can be used for the calibration of the numerical model in Section V.4. Table V.3 identifies the three proposed data sets, one corresponding to the average values and the other two corresponding to the higher and lower values.

**Table V.3** Experimental data-sets for numerical calibration.

Data-set	Specimens	$P_{max}$ [kN]	$f_{t\_ASTM}$ [MPa]	$f_{t\_Frocht}$ [MPa]	$G_{ASTM}$ [MPa]	$G_{Frocht}$ [MPa]
High-set	URM 1 & 4	178.5	0.32	0.23	1553	2417
Average-set	URM 1 to 5	151	0.27	0.20	1285	1999
Low-set	URM 3 & 5	116	0.21	0.15	1016	1580

### V.3 Numerical tools

This Section V.3 provides the details of the numerical model employed in Section V.4 to interpret the diagonal compression tests. Section V.3.1 presents the modelling approach,

**PAPER V**

Section V.3.2 provides a brief description of the constitutive models used for the materials, and Section V.3.3. reports details on the simulation process.

**V.3.1 Modelling approach**

Different approaches have been adopted in recent years for the numerical simulation of diagonal compression tests. The possibilities span from distinct element models [371] to continuous finite element models, the latter covering a variety of cases depending on the level of discretisation detail: 3D and 2D homogeneous macromodels with a single masonry material [353,371,372], 3D and 2D simplified micromodels with no unit-joint interfaces [373,374], micromodels with simplified interfaces [67], or detailed micromodels [375], with diverse options of material constitutive laws.

This research investigates the use of the diagonal compression test to determine homogenised mechanical properties of masonry considered as a continuous isotropic material. Consistently, and in coherence with the Introduction and the initial hypothesis on which Turnšek and Čačovič based their criterion [170], a macromodelling approach has been applied to simulate the tests. With this approach, only two materials are considered: steel for the loading shoes, and masonry as a whole for the wall. This strategy allows a direct comparison between the experimental outcomes and the material input parameters within the same framework.

**V.3.2 Constitutive model**

The nonlinear behaviour of the masonry material is modelled with a constitutive model based on Continuum-Damage Mechanics [376]. For the sake of simplicity, few aspects are highlighted in the following. The reader is referred to the most recent developments on the model for further details [31,377].

The strain-based continuum damage model uses two scalar damage variables that allow to distinguish between tensile ( $d^+$ ) and compressive ( $d^-$ ) damage. The constitutive law is given in Equation V.12:

$$\boldsymbol{\sigma} = (1 - d^+) \bar{\boldsymbol{\sigma}}^+ + (1 - d^-) \bar{\boldsymbol{\sigma}}^- \quad (\text{V.12})$$

where  $\boldsymbol{\sigma}$  is the stress tensor, and the effective stress tensor  $\bar{\boldsymbol{\sigma}}$  is split in a tensor related to tension stress states  $\bar{\boldsymbol{\sigma}}^+$  and in a tensor related to compression stress states  $\bar{\boldsymbol{\sigma}}^-$ .

Two additional scalar variables,  $\tau^\pm$ , the equivalent stresses, determine the shape of the positive and negative damage surfaces, expressed according to Equations V.13 and V.14:

$$\tau^+ = H[\bar{\sigma}_{max}] \frac{1}{1-a} \left[ \sqrt{3\bar{J}_2} + a\bar{I}_1 + b\langle \bar{\sigma}_{max} \rangle \right] \frac{f^+}{f^-} \quad (\text{V.13})$$

$$\tau^- = H[-\bar{\sigma}_{min}] \frac{1}{1-a} \left[ \sqrt{3\bar{J}_2} + a\bar{I}_1 + \kappa_1 b \langle \bar{\sigma}_{max} \rangle \right] \quad (\text{V.14})$$

with

$$a = \frac{(f_b^- / f^-) - 1}{2(f_b^- / f^-) - 1} \quad (15)$$

$$b = (1 - a) \frac{f^-}{f^+} - (1 + a) \quad (16)$$

In the above,  $\bar{I}_1$  is the first invariant of the effective stress tensor and  $\bar{J}_2$  the second invariant of the deviatoric effective stress tensor.  $f^+$  and  $f^-$  stand for the tensile and compressive strengths respectively and  $f_b^-$  for the biaxial compressive strength.  $\bar{\sigma}_{max}$  and  $\bar{\sigma}_{min}$  denote the maximum and minimum principal effective stresses respectively.  $H[x]$  is the Heaviside step function.

The failure surfaces described above stand for a tension-compression damage model. Within a wall subjected to diagonal compression, the combination of tension and compression leads to a shear stress state. The parameter  $\kappa_1$  introduced in Equation V.14 is a constant

**PAPER V**

proposed by Petracca et al. [31,378] for an enhanced mechanical description of the shear behaviour of masonry structures, as it controls the shape of the failure surface in the shear quadrants. Note that a zero value of  $\kappa_1$  leads to the Drucker-Prager criterion, while a unity value yields a criterion equivalent to the one proposed by Lubliner et al. [379]. Petracca et al. [31,378] have obtained satisfactory results in simulations of shear loading and diagonal cracking when using this model.

The basis of the model also includes the definition of internal variables for the representation of the current damage thresholds, as well as the evolution laws for the damage variables. An exponential softening law is adopted in tension, while a parabolic hardening – exponential softening curve applies in compression. Six material properties are required to define the model input parameters: both tensile,  $f_t$ , and compressive,  $f_c$ , strengths, both tensile,  $G_{ft}$ , and compressive,  $G_{fc}$ , fracture energies, and the elastic properties Young's modulus,  $E$ , and Poisson's ratio,  $\nu$ .

Additionally, the implementation of a local crack-tracking algorithm allows the simulation of localized cracks. This feature is especially convenient to the actual localized cracking found in the diagonal compression experiments, and provides a more realistic representation of the cracks if compared with the common smeared damage approach. This algorithm identifies the elements crossed by propagating cracks at each time/load increment, see references [380–385] for further details and the latest developments on this numerical technique. The use of a nonlinear stress-strain relationship for the elements on the crack path, together with a linear elastic response for the ones outside, allows the simulation of discrete cracks. The parameters of the crack-tracking algorithm have already been calibrated with shear benchmark problems [383,384] and are directly implemented herein.

### V.3.3 Numerical simulation

The diagonal compression test has been analysed under plane stress conditions. The simulation of the load application has been performed through imposed displacements, ( $\delta_u$ ,  $\delta_v$ , see Figure V.4a), with increasing magnitude, in agreement with the testing procedure. Displacements of the same magnitude and opposite direction were imposed at both corners of the wall simultaneously. As shown in Figure V.4a, simplified steel loading shoes have been included to better simulate the load application. The actual geometry of the masonry specimens is modelled with average dimensions.

The discretization of the specimens consists of an unstructured mesh of 2D plane-stress three-noded triangles (see Figure V.4b). The reference mesh contains 8573 nodes, with average mesh size,  $h_e$ , of 13 mm.

The choice of a suitable reference measurement for the comparison between experimental and numerical curves to calibrate the models constituted a crucial point of the study. The use of the overall stroke of the jacks compared to the displacement between corner nodes was not suitable due to spurious readings associated to deformations of the loading devices. The compressive strain computed from the experimental readings of the LVDTs placed along the compressed diagonal was eventually chosen. This magnitude was compared to the numerical compressive strain calculated between two nodes of the compressed diagonal. These two nodes acted as a “virtual LVDT” placed at an equivalent position of the experimental LVDTs (see Figure V.2 and Figure V.4). However, the value of this compressive strain, immediately before and after the peak load, is affected in both the experimental case and numerical cases by the opening of the diagonal crack. Given the randomness of the experimental cracking, it was decided, during the calibration process, to compare the experimental and numerical curves only in terms of initial stiffness and value of the maximum load.

## PAPER V

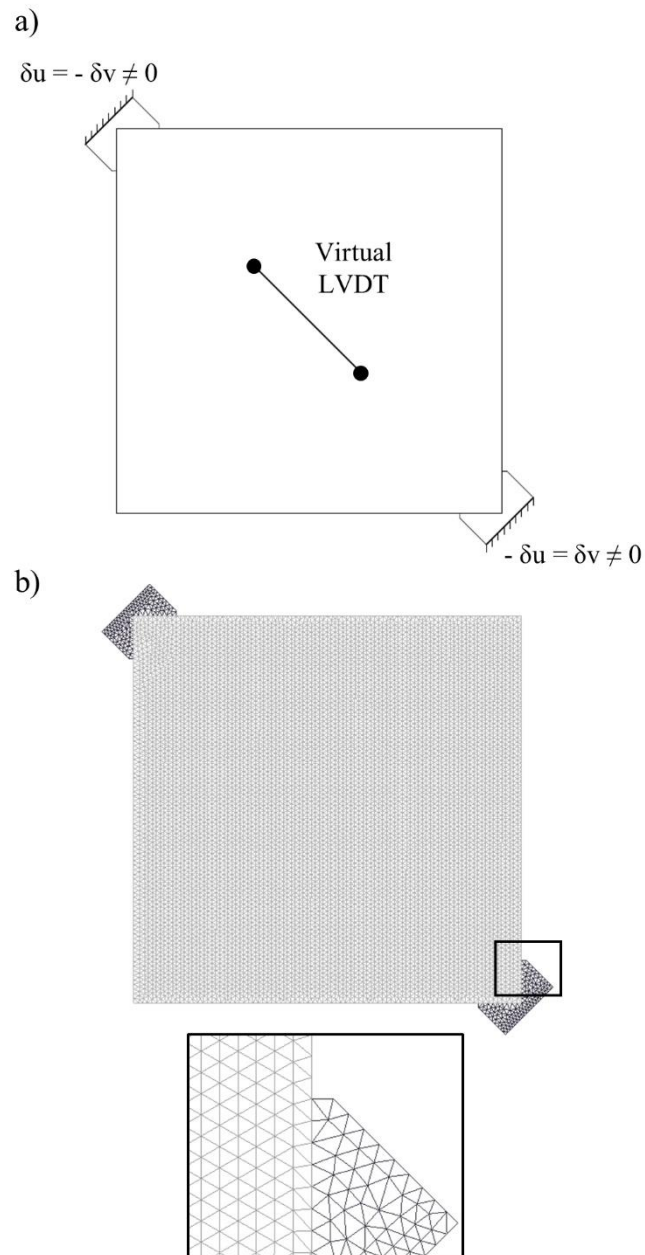


**Figure V.4** a) Boundary conditions on the numerical simulation and position of the virtual LVDT for comparison. b) Discretized domain used for the macromodelling approach.

The numerical solution was carried out in an incremental manner. A modified Newton-Raphson method (using the secant stiffness matrix) together with a line-search procedure were used to solve the corresponding nonlinear equations. To achieve convergence at each step, the maximum value of the ratio between the norm of the iterative residual forces and the norm of the total external forces was set at  $10^{-2}$ . Calculations were performed with an enhanced version

of the finite element software COMET [386], while the software GiD [387] was used for the pre- and post-processing of the model. Both software have been developed at the International Centre for Numerical Methods in Engineering (CIMNE), in Barcelona.

#### **V.4 Study on the diagonal compression test to estimate homogenised properties of masonry**

This section investigates the possibility of using the diagonal compression test experimental outcomes to determine two mechanical properties of masonry: tensile strength and shear modulus. The basic hypothesis is considering masonry as a homogeneous and isotropic material, in correspondence with the assumption of the Turnšek and Čačovič criterion. Thus, the tensile strength and shear modulus are considered as global and intrinsic parameters of the material.

The investigation begins with the calibration of a numerical macromodel with the experimental results exposed in Section V.2. Once the model is calibrated, the state of stresses within a reference panel is interpreted, and a factor is proposed to calculate the tensile strength. A sensitivity analysis evaluates the influence on this factor of the input material properties, the panel size and the dimensions of the loaded corners. Eight different experimental campaigns available in the scientific literature have been used as benchmark problems to validate the findings of this section for different masonry typologies.

##### **V.4.1 Calibration of the macromodel**

The numerical macromodel has been calibrated to fit the experimental curves of the three data sets defined in Table V.3. The calibration process followed a splitting approach, as defined by Chisari et al. [67]. The first stage involved the calibration of the elastic parameters, Young's

**PAPER V**

modulus and Poisson's ratio, to adjust the slopes of the curves. The second stage required the calibration of the tensile strength and the tensile fracture energy to reach the corresponding maximum load.

The initial values of the mechanical properties were chosen as follows. The compressive strength and compressive fracture energy of masonry were always taken equal to the experimental values provided in Table V.1. The experimental shear moduli obtained from both approaches, i.e. ASTM's and Frocht's in Table V.3, were used to determine the Young's moduli by means of the relationship  $E = 2G(1 + \nu)$ . The former expression is valid due the elastic linear behaviour presented by the walls at low load levels. Different values of Poisson's ratio were checked. The experimental values of tensile strength obtained from both approaches (Table V.3) were assumed as starting point. Two different expressions were used to link the tensile fracture energy to the strengths of masonry. Equation V.17 was proposed by Angelillo et al. [69] as an adaptation from Model Code 1990 for concrete structures [388]. Equation V.18 is the proposal of the Model Code 2010 [389].

$$G_{ft} = 0.04 f_t^{0.7} \quad (\text{V.17})$$

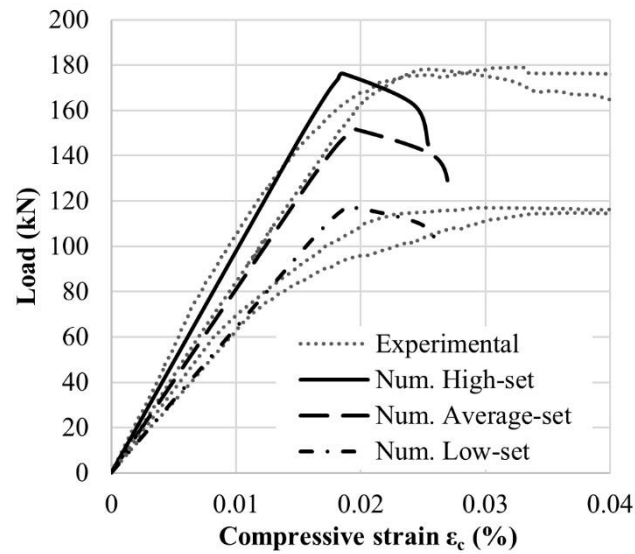
$$G_{ft} = 73 f_c^{0.18} \quad (\text{V.18})$$

Figure V.5 shows the results of the calibration with the comparison between the numerical and the experimental curves. Figure V.6 displays the contour of maximum principal strains in the finite element model for one of the cases after failure. The resulting numerical crack is perfectly diagonal and mesh-independent, proving the high accuracy of the considered computational technique. The adopted numerical approach simulates well the described crack patterns obtained experimentally and shown in Figure V.3. Table V.4 includes the final input parameters for the three different data sets and the comparison between the numerical and experimental maximum loads. The difference is always lower than 2%.

Regarding the input data indicated in Table V.4, the final values of Young's moduli, which best fitted the experimental slopes, corresponded to those obtained from the values of shear moduli given by Frocht's expression (Equation V.6). The input tensile strength was the most relevant parameter affecting the appearance of damage and defining the maximum load. In the three data sets, the values obtained by means of ASTM's and Frocht's approach (Equations V.4 and 8) led to very high values of peak load. In the three data sets, in order to attain the sought load levels, it was necessary to reduce the input tensile strength to a value close to 0.40 times the experimental load  $P_{exp}$  over the area  $A$ . The modified expression from Model Code 1990 for the tensile fracture energy (Equation V.17) worked well also for the three-data sets. These satisfactory results were obtained with a constant value of 0.16 for the numerical parameter  $\kappa_1$  proposed by Petracca et al. [31,378]. The same value was used in [31,377,384] to simulate other shear tests. The calibration process described in this paragraph applied for the three different data sets and led to good simulations of the initial slopes of the experimental curves, the maximum attained loads, and the failure mechanism.

**Table V.4** Calibration of the numerical model with experimental results: Input data for the numerical analyses of the three data-sets, and comparison between experimental and numerical maximum loads.

Data-set	Input data							Comparison exp - num		
	E (MPa)	$\nu$ (-)	$f_t$ (MPa)	$f_c$ (MPa)	$G_{ft}$ (N/m)	$G_{fc}$ (N/m)	$\kappa_1$ (-)	$P_{exp}$ (kN)	$P_{num}$ (kN)	$\Delta_{exp-num}$
High-set	4203	0.15	0.183	6.51	12.17	9750	0.16	178.5	176.3	+ 1.2%
Average-set	3477	0.15	0.155	6.51	10.85	9750	0.16	151	151.8	-0.5%
Low-set	2748	0.15	0.119	6.51	9.03	9750	0.16	116	117.6	-1.4%



**Figure V.5** Comparison between the load-strain curves of the experimental tests and the numerical analyses. No experimental curve is given for specimen URM\_2 due to invalid readings of the LVDTs during the test.

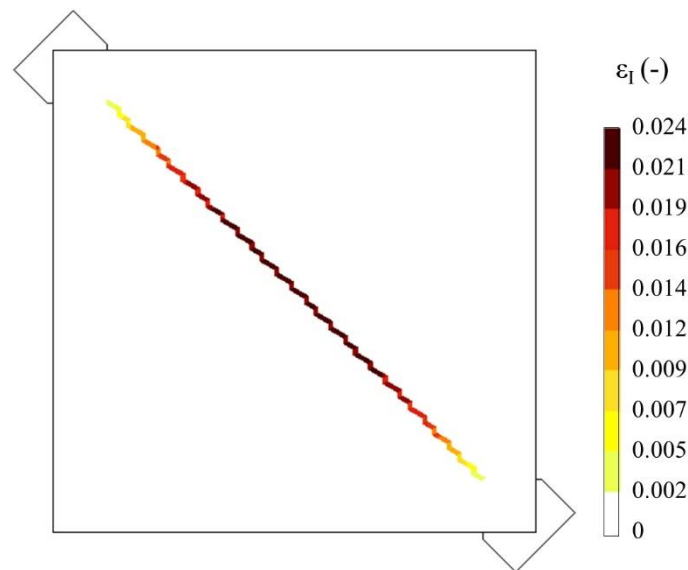


**Figure V.6** Contour of the maximum principal strains,  $\varepsilon_1$ , after the peak load.

#### V.4.2 Interpretation of the diagonal test

The previous section allowed having a properly calibrated numerical model able to simulate satisfactorily the experimental diagonal compression tests. This section seeks to interpret the state of stresses within the panel and to derive conclusions on the use of the

experimental outcomes to determine mechanical properties of masonry. The average data set defined in Table V.3 is used as a reference in the following.

#### V.4.2.1 Linear range

First, the focus is placed in the initial stage of the analysis when the wall still behaves linearly. For the sake of clarity, it is decided to define a series of coefficients alpha  $\alpha$  or normalized stresses for the different stress components, according to the applied load  $P$  over the transversal area  $A$ . For a given time-step ( $i$ ), the coefficients for the different stresses ( $\sigma_x$ ,  $\sigma_y$ ,  $\tau_{xy}$ ,  $\sigma_I$ ) are defined with Equations V.19a to V.19d:

$$\alpha_x(i) = \sigma_x(i) \frac{A}{P(i)} \quad (19a)$$

$$\alpha_y(i) = \sigma_y(i) \frac{A}{P(i)} \quad (19b)$$

$$\alpha_{xy}(i) = \tau_{xy}(i) \frac{A}{P(i)} \quad (19c)$$

$$\alpha_I(i) = \sigma_I(i) \frac{A}{P(i)} \quad (19d)$$

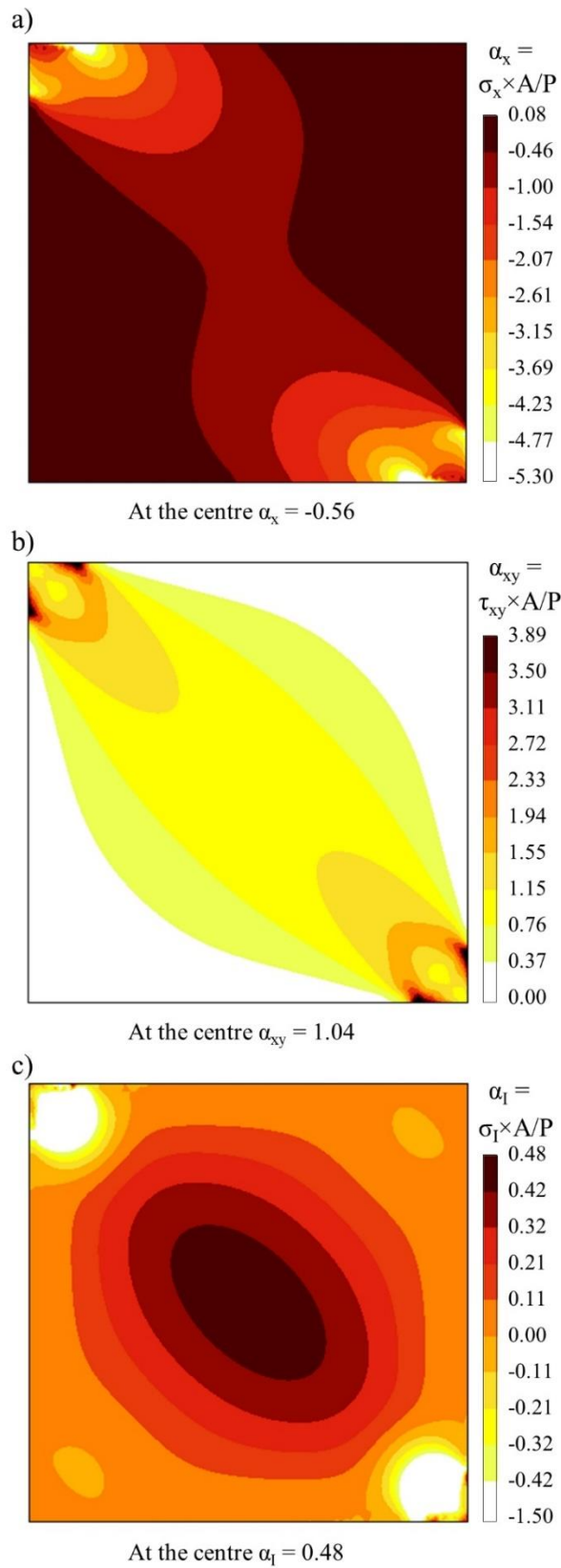
Figure V.7 shows three contour plots that represent the stress state of the wall in the linear range. The coefficient  $\alpha$  corresponding to each stress component at the centre of the panel is indicated below each of the plots. Unlike the hypothesis of pure shear stated in the American standard ASTM E519 [355], Figure V.7a illustrates that the normal stresses along the X-axis (also along Y-axis) are not null. As pointed out by Gabor et al. [374], the stress condition of pure shear would require an additional pair of tensile forces acting at the opposite free corners. Therefore, Equation V.4 as proposed in ASTM E519 [355] is not sufficiently realistic. The coefficients found in the research presented herein ( $\alpha_x = -0.56$ ,  $\alpha_{xy} = 1.04$ ,  $\alpha_I = 0.48$ ) are very

**PAPER V**

similar to those found by Brignola et al. [162], and agree with the elastic solution proposed by Frocht [160]. The slight differences between the values obtained with numerical methods and those found by Frocht may be due in the consideration of Poisson's ratio and the incorporation into the models of the effect of the loading shoes.

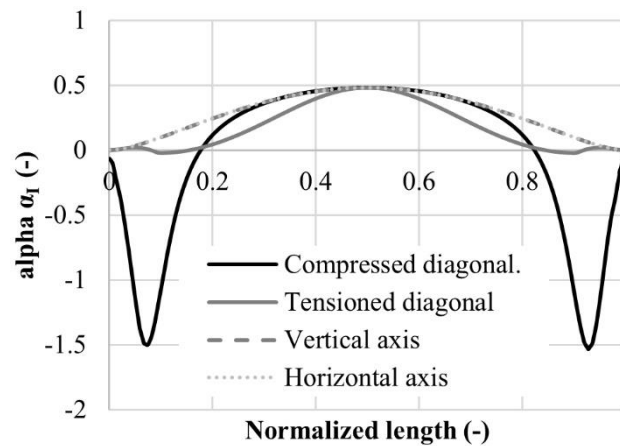
The confining effect exerted by the loading shoes is evident in the three plots of Figure V.7. This effect vanishes towards the centre of the panel, where stresses are more uniform. This fact highlights the need of following the prescriptions of the standards with regard to the size of the panel and length of the loading shoes. Section 4.3 investigates this effect in more detail.

Figure V.7c confirms that the highest values of tensile stress appear at the centre of the panel, and are distributed on a finite region, as shown in Figure V.8. This figure depicts the distribution of maximum principal stresses along the four axes of symmetry of the panel. The central fifth of the wall is subjected to tensile stresses very close to the maximum value, associated with an  $\alpha_t$  of 0.48. This observation implies that the real wall of masonry would not fail at the central point of maximum tensile stresses, but at the weakest point within the material, considering both the high stress level and the local material properties at that specific point. As stated in Section V.2, the diagonal compression test is sensitive to the local properties of the components, and the global scattering in the experimental results would reflect the variability within the constituent materials.



**Figure V.7** Contour of stresses in the linear range, expressed in terms of normalized stress  $\alpha$ . a) Normal stresses  $\sigma_x$  along X-axis [ $\sigma_y$  are not shown due to the problem's symmetry], b) shear stresses  $\tau_{xy}$ , and c) maximum principal stresses  $\sigma_1$ .

## PAPER V



**Figure V.8** Distribution of the maximum principal stresses along the axes of symmetry of the panel. Stresses are normalized and expressed in terms of the coefficient  $\alpha_l$ . The X-axis represents normalized lengths. The centre of the panel corresponds to the coordinate 0.5.

#### V.4.2.2 Non-linear range

The second stage of the study deals with the non-linear range. Figure V.9a shows the numerical evolution of stress components at the central element of the panel with increasing load, while Figure V.9b depicts the counterpart curves in terms of coefficient  $\alpha$  or normalized stresses. The horizontal axes of both figures are normalized with respect to the maximum load. The constant slope of the linear curves for the stresses agrees with the linear behaviour of the walls detected during the tests, and justifies the experimental procedure adopted herein to determine the shear modulus as a slope between load levels of 5 and 30% of the assumed maximum load. Figure V.10 illustrates the tensile crack propagation in the panel with increasing load.

From Figure V.9 and Figure V.10, it is evident that cracking starts when the maximum principal stresses  $\sigma_l$  at the centre of the panel attain the level of the input tensile strength of the material  $f_t$ . Reaching the level of the tensile strength triggers the apparition of damage at the centre of the panel. As shown in Figure V.10, this damage develops from the central region to the corners, and eventually leads to the collapse of the panel with the formation of a complete

diagonal crack. This sequence agrees with the experimental behaviour described in Section V.2. The localization of initial damage within the central region of the wall is in agreement also with the general experimental observations, as reported by Magenes and Calvi [350].

According to Figure V.9 and Figure V.10, the initiation of damage occurs at a level of applied load around 80% the maximum attained load. This value is in agreement with the observations in the experimental curves reported in Section V.2. It also agrees with the results of other researches that also applied a macromodelling approach. Basili et al. [353] used a smeared crack model and the computer code MIDAS-FEA to simulate diagonal compression tests. In their analyses, the level of damage initiation was equal to 78% the maximum attained load.

This finding does not comply with the assumption of the standard [355] that establishes a correspondence between the initiation of damage at the centre of the panel and the failure of the panel. It has been found that the state of stresses of the panel at failure does not correspond to the elastic one, and that a redistribution of stresses occurs after the initiation of damage. The most important implication of this observation is that, although the failure of the panel depends on the tensile strength of the material as it triggers the damage initiation, the subsequent behaviour of the wall is more complex and there is not a direct identification between the maximum attained load  $P_{max}$  and the tensile strength of the material  $f_t$ .

Nevertheless, the experimental outcome provided by a diagonal compression test is the maximum attained load. As mentioned in Section V.2, it is difficult to precisely define in laboratory the exact moment of cracking with common instrumentation. Therefore, in order to allow the use of the diagonal compression test to determine mechanical properties of masonry, it is necessary to define a possible correlation, even if not univocal, between the maximum load and the tensile strength of the material. It is proposed to find the coefficient alpha  $\alpha$  that

## PAPER V

correlates the maximum load with the tensile strength. For a given numerical analysis, the coefficient  $\alpha_{I,calc}$  is back-calculated with Equation 20, which involves the maximum attained load and the tensile strength used as an input parameter in the analysis:

$$\alpha_{I,calc} = \frac{f_{t,input} * A}{P_{max}} \quad (20)$$

In the three cases studied in the calibration section, the coefficient  $\alpha_{I,calc}$  is almost constant. It takes the values of 0.408, 0.402 and 0.400 for the high, average and low data sets respectively. Brignola et al. [162] adopted an equivalent solution and proposed different coefficients  $\alpha$  for different masonry typologies. Their micromechanical model allowed to incorporate further material details into the analyses. More precisely, a coefficient of 0.4 relating the maximum load to the maximum principal stress was found for a ratio of mortar tensile strength to joint cohesion of 0.5. The macroscopic approach used herein is consistent with the diagonal compression test that considers masonry as a macroscopically homogeneous material on which global mechanical properties can be determined. The advantage of the model used in this work is that it includes these global properties, such as the tensile strength, as input parameters. Nevertheless, the coefficient  $\alpha_{I,calc}$  may only apply to the specific material and walls studied in the experimental campaign described in Section V.2. The sensitivity of the coefficient  $\alpha_{I,calc}$  to different parameters is analysed in Section V.4.3, while its use is validated with experimental campaigns carried out by other authors in Section V.4.4.

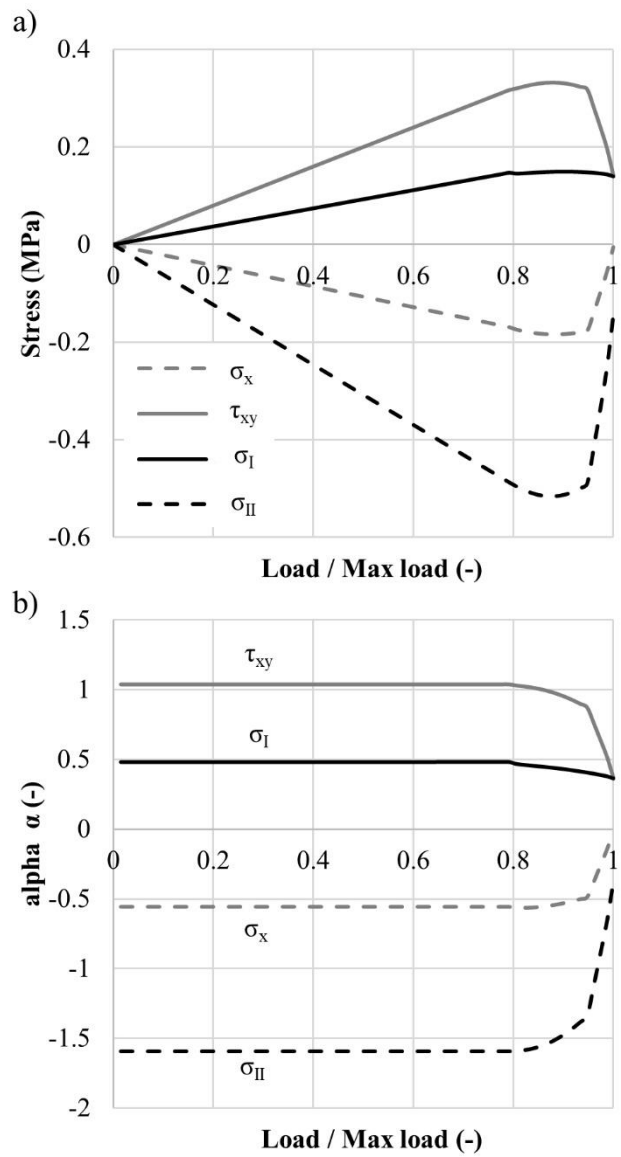


**Figure V.9** a) Evolution of stresses and b) relevant normalized values  $\alpha$  in the centre of the panel with increasing load. The load is normalized with respect to the maximum load attained during the analysis.

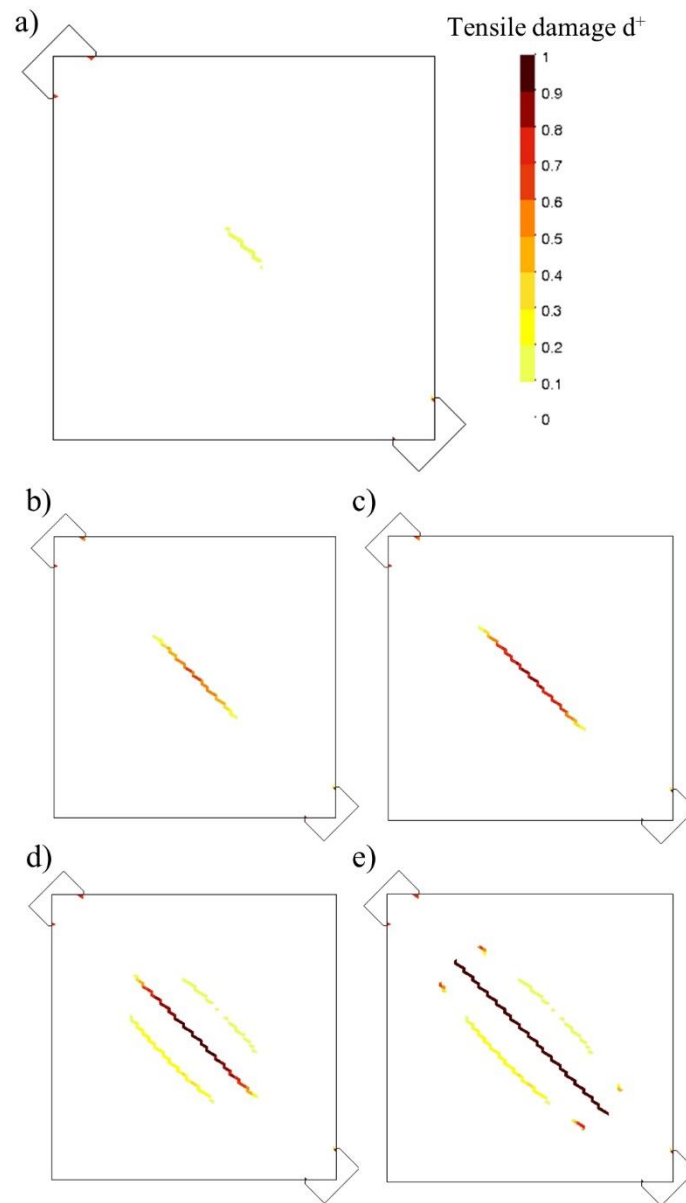


**Figure V.10** Evolution of tensile damage contour for different levels of imposed displacement  $\delta$ . The tensile damage index  $d^+$  ranges from 0 (intact material) to 1 (completely damaged material). a)  $\delta = 0.198$  mm,  $P = 0.82P_{max}$ , b)  $\delta = 0.216$  mm,  $P = 0.89P_{max}$ , c)  $\delta = 0.230$  mm,  $P = 0.95P_{max}$ , d)  $\delta = 0.244$  mm,  $P = P_{max}$ , e)  $\delta = 0.247$  mm,  $P = 0.92P_{max}$

### V.4.3 Sensitivity analysis

This section investigates the sensitivity of the back-calculated coefficient  $\alpha_{I,calc}$  to different input parameters and boundary conditions. In each sensitivity analysis, the parameter investigated was varied, while the rest of properties and conditions were kept constant at the

reference values. The average data set defined in the calibration Section V.4.1 was taken as reference.

### V.4.3.1 Material properties

Given the features of the problem, the compressive parameters, such as the compressive strength and the compressive fracture energy, have little influence in the maximum attained load and the coefficient  $\alpha_{I,calc}$ . The Poisson's ratio has a negligible influence as well. The material properties involved in the sensitivity analysis were the Young's modulus, the tensile strength, and the tensile fracture energy. The influence of the numerical parameter  $\kappa_1$ , which constitutes a special feature of the numerical model that controls the shear response, was also investigated.

Table V.5 reports the values of the parameters that were considered in the sensitivity analyses. Either three or four variations were studied for each parameter, whose values were chosen as follows. The reference value for the Young's modulus,  $E = 3477$  MPa, represents a ratio of 534 with respect to the compressive strength of masonry (Table V.1,  $f_c = 6.5$  MPa). As indicated by Tomazevic [305], the ratio  $E/f_c$  usually ranges between 200 and 1000 in common masonry. The values of Young's modulus reported in Table V.5 correspond to ratios of 200, 400 and 1000. Similarly, the reference value for the tensile strength,  $f_t = 0.155$  MPa, corresponds to a ratio of 2.5% with respect to the compressive strength. Common values for the tensile strength of masonry range from 1 to 10% the compressive strength [69]. The values of tensile strength in Table V.5 stand for 1%, 4% and 5% of the compressive strength. Greater percentages were considered unrealistic in this case. The choice of the values of tensile fracture energy relied on different approaches. The reference value, which allowed a good calibration in Section V.4.1, was obtained by means of Equation V.17 adapted in [69] from the Model

## PAPER V

Code 1990 [388]. The other two higher values correspond to the unmodified expression of Model Code 1990 [388], and to Equation V.18 obtained from the Model Code 2010 [389]. The lowest value corresponds to a ductility index of 0.029 mm suggested for bricks by Angelillo et al. [69]. Last, the parameter  $\kappa_1$  of the constitutive model proposed by Petracca et al. [31,378] was varied within its extreme possible values, 0 and 1.

**Table V.5** Values of the parameters investigated in the sensitivity analyses.

Input parameter	$E$ , Young's modulus (MPa)	$f_t$ , Tensile strength (MPa)	$G_{ft}$ , Tensile fracture energy (N/m)	$\kappa_1$ (-)
<i>Reference value</i>	3477	0.155	10.85	0.16
Variation 1	1302	0.065	4.73	0
Variation 2	2604	0.26	18.5	0.1
Variation 3	6510	0.325	56.2	0.3
Variation 4	-	-	102	1

Figure V.11 shows the results of the sensitivity analyses in terms of load – strain curves and influence on coefficient  $\alpha_{l,calc}$ . The effects were qualitatively predictable. Variations in the Young's modulus changed the stiffness of the curves and affected slightly the maximum attained load (Figure V.11a). Variations in the tensile strength of the material were strongly related to the maximum attained load while the slope of the curves was maintained (Figure V.11b). The influence of varying the tensile fracture energy was restricted to the postpeak range (not shown in Figure V.11c), and the maximum attained load was only slightly affected.

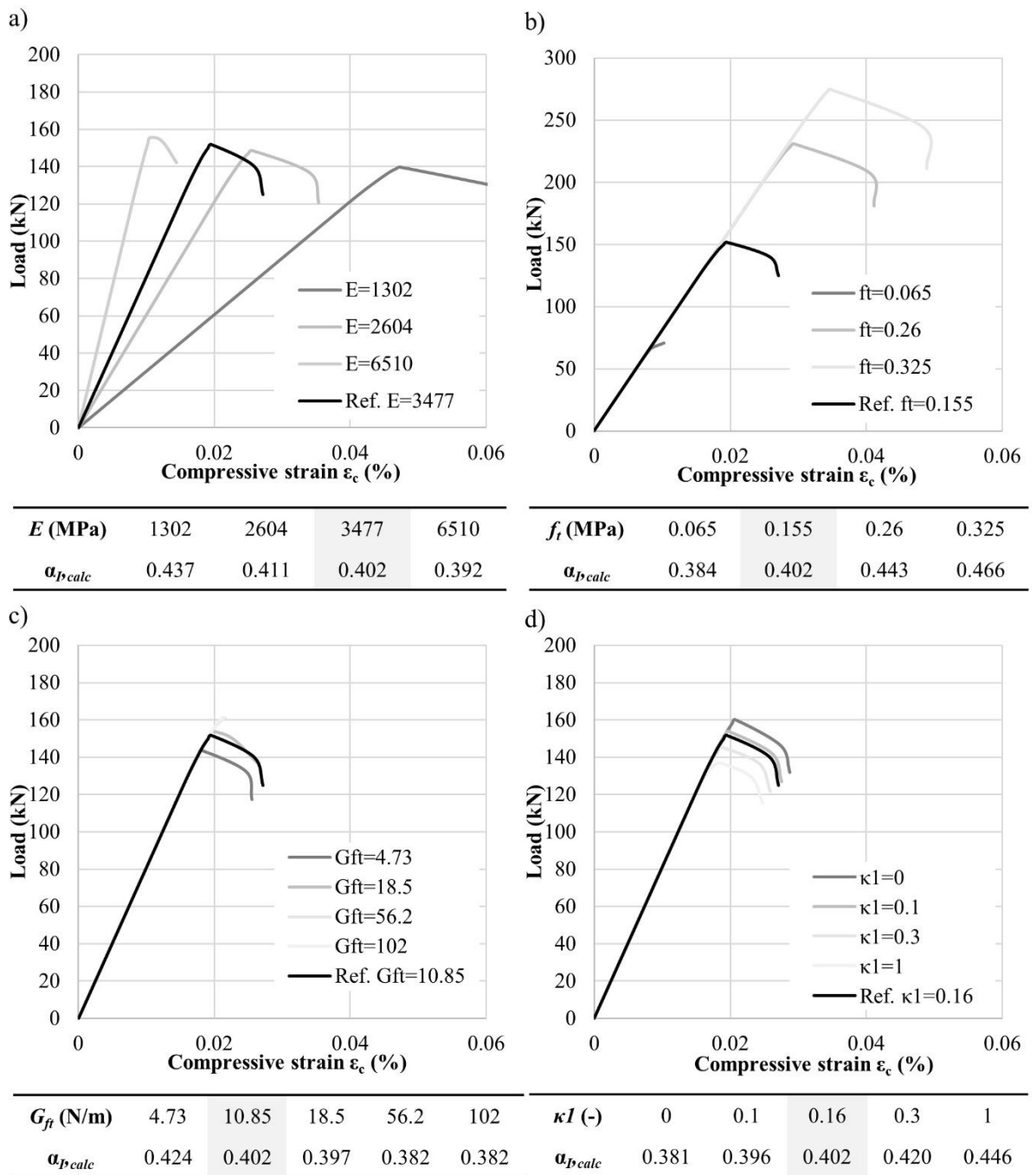


**Figure V.11** Sensitivity of the model to variations of different parameters, in terms of load – strain curves and coefficient  $\alpha_{l,calc}$ . a) Variation of input Young’s modulus,  $E$ . b) Variation of input tensile strength,  $f_t$ . c) Variation of input tensile fracture energy,  $G_{ft}$ . d) Variation of parameter  $\kappa I$ .

Quantitatively, the impact of the properties variation on the value of coefficient  $\alpha_{l,calc}$  was limited, taking into account the wide range of variation investigated. In overall, the coefficient  $\alpha_{l,calc}$  spanned from 0.38 to 0.45, with the exception of the highest value assigned to the tensile

**PAPER V**

strength, and remained always below the value associated to the elastic response (0.48). An increase of 87% in the reference value of Young's modulus produced a decrease of only 2.5% in the coefficient  $\alpha_{I,calc}$ . An increase of 840% in the reference value of tensile fracture energy involved a decrease of 5% in the coefficient  $\alpha_{I,calc}$ . The influence of the tensile strength was greater, as an increase of 110% in the reference value produced an increase of 16% in the value of the coefficient  $\alpha_{I,calc}$ . This is further evidence of the intimate relation between this parameter and the result of the diagonal compression test. For high values of tensile strength, the redistribution of stresses is reduced and the load of initial damage is closer to the maximum attained load. Figure V.11d illustrates the influence of the parameter  $\kappa_1$  of the adopted constitutive model.

**V.4.3.2 Size and confinement effect**

As mentioned in Section 2, the American standard ASTM E519 [355] and the RILEM recommendation LUMB6 [157] differ in the prescriptions of panel size and depth of the loading shoe. Although the minimum size of 1.2 m prescribed by ASTM E519 [355] is generally respected, a number of researches have considered smaller panels, mainly due to economical and practical reasons. In fact, the Chilean norm NCh 2123 [159] allows testing wallets with a minimum length of 0.6 m. Similarly, the depth of the loading shoe also presents a great variability in practice in spite of the recommendations. It is therefore necessary to investigate the effect of the size panel and the loading shoe depth on the maximum attained load and the coefficient  $\alpha_{I,calc}$ . A series of numerical analyses were performed with identical material properties to the average data set defined in the calibration in Section V.4.1, but varying these two dimensions.

Figure V.12 shows the values of the coefficient  $\alpha_{I,calc}$  for the different panel sizes considered: 0.4 m, 0.6 m, 0.8 m, 1 m, 1.1 m, 1.2 m, the reference panel of 1.27 m, 1.3m, and 1.4 m. The influence of the panel size revealed to be negligible and was only significant for very small panels. A constant value of 0.4 would apply for panels from 0.6 to 1.4 m. This numerical finding is consistent with the very limited experimental evidence available in literature. Knox et al. [307] did not find statistically significant differences between the strengths attained in walls 0.6 m and 1.2 m wide. In a seminal research, Fattal [390] investigated walls 1.2 m, 0.8 m, 0.6 m and 0.4 m wide. Only the smallest walls 0.4 m wide showed an evident size effect in the results.

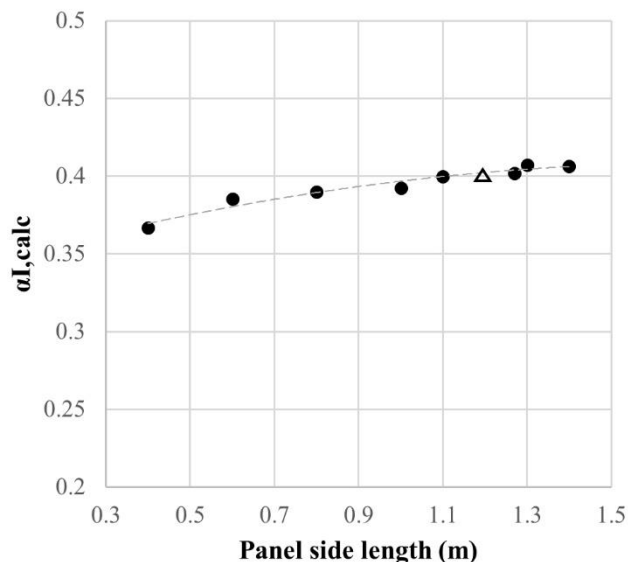


**Figure V.12** Effect of the panel side length on the coefficient  $\alpha_{I,calc}$ . Triangle dot indicates the value corresponding to the side length recommended in ASTM E519 [355] (1200 mm).

Figure V.13 illustrates the effect of the loading shoes depth on the coefficient  $\alpha_{I,calc}$ . With respect to the panel side length, the values investigated were 1/12<sup>th</sup> (0.083), 1/11<sup>th</sup> (0.091), 1/10<sup>th</sup> (0.1, as recommended by RILEM LUMB6), 1/9<sup>th</sup> (0.111, the reference panel), 1/8<sup>th</sup> (0.125, as recommended by ASTM E519), 1/7<sup>th</sup> (0.143), 1/6<sup>th</sup> (0.167), 1/4<sup>th</sup> (0.25), and 1/3<sup>rd</sup> (0.333). From 1/12<sup>th</sup> to 1/7<sup>th</sup>, there was no apparent influence, and the coefficient  $\alpha_{I,calc}$  remained almost constant and equal to 0.4. Conversely, larger shoes depths exerted such a confinement effect

## PAPER V

that the final results were affected. In the cases of 1/4<sup>th</sup> and 1/3<sup>rd</sup>, the failure mode of the wall changed and a compressive strut was formed between the two loaded corners, with parallel diagonal cracks connecting the edges of the shoes. The latter are extreme cases but may be found in practice.

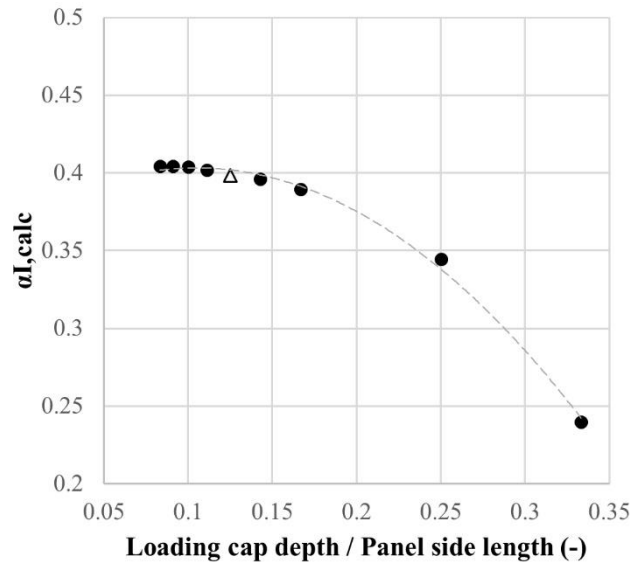


**Figure V.13** Effect of the loading cap depth on the coefficient  $\alpha_{I,calc}$ . The X-axis indicates the loading cap depth normalized with respect to the panel side length. The triangle dot indicates the value corresponding to the ratio recommended in ASTM E519 [355] (1/8<sup>th</sup>).

The coefficient  $\alpha_{I,calc}$  has shown little sensitivity to the size and confinement effects, provided that the panel length and the loading shoes depth lay within certain limits. This conclusion may depend on the specific dimensions of the blocks and joints conforming the walls, especially on the relative dimensions of the blocks with regard to the global geometry of the wall and setup.

### V.4.4 Validation

This section studies the applicability of the former findings to other masonry typologies and specimen sizes. Eight experimental campaigns carried out by other authors have been simulated [165,169,321,348,391,392]. The numerical analyses included the modelling of the

specific geometries of the walls, and the selection of proper input material properties, according to the procedures described below. The maximum loads predicted numerically were compared to the experimental ones.

Table V.6 presents the features of the eight selected campaigns. The different combinations of materials included clay bricks, concrete blocks, tuff blocks, and rubble masonry, combined with aerial lime, hydraulic lime, and cement mortars. The size of the analysed panels ranged from 0.9 to 1.63 m, and the thickness from 0.079 to 0.7 m. The input data were selected as follows. The compressive strengths  $f_c$  were directly obtained from the references. The compressive fracture energies were calculated by applying the same ratio  $G_{fc} / f_c$  used in this research. The Young's moduli  $E$  were derived from the experimental shear moduli  $G$ , which were calculated from the experimental data by using the coefficient  $\alpha_{xy}$  equal to 1.04 that is proposed in this research to calculate the shear stresses. The values of tensile strength  $f_t$  were obtained from the experimental maximum loads by means of the coefficient  $\alpha_{I,calc}$  equal to 0.4 that is proposed in this study. Finally, once the tensile strengths were defined, the tensile fracture energies  $G_{ft}$  were calculated by means of Equation 17.

Table V.6 includes in the last three columns the comparison between the experimental maximum loads and the numerically predicted loads. The average error was of 5.9%. This difference was very satisfactory, taking into account the great variety of geometries and materials being investigated. This good result validates the proposed coefficients  $\alpha_{I,calc}=0.4$  and  $\alpha_{xy}=1.04$  to determine the tensile strength and the shear modulus of masonry from the experimental outcomes of diagonal compression tests.

The validation with campaigns carried out by other authors leads to the following remarks. First, a value of 0.4 for the coefficient  $\alpha_I$  used to compute the tensile strength of masonry  $f_t$  has provided good estimations of the maximum experimental loads. This value takes into

## PAPER V

consideration non-linear effects, cracking, and stress redistributions. Even if it only constitutes an approximation to the complexity of the real behaviour of masonry, it provides estimations on the safe side with respect to the elastic solution ( $\alpha_I = 0.48$ ) and the ASTM E519 proposal ( $\alpha_I = 0.707$ ). Second, the use of a coefficient  $\alpha_{xy}$  equal to 1.04 to calculate the shear stresses has led to satisfactory estimations of the shear modulus of masonry  $G$ . Third, Equation V.17 proposed by Angelillo et al. [69] to estimate the tensile fracture energy  $G_{fi}$  from the tensile strength has provided good results for this type of problem characterized by a single localized crack.

**Table V.6** Validation analyses of additional experimental campaigns from literature. Comparison between experimental and numerically predicted maximum load.

Reference	Data-set		Input data					Comparison exp - num		
	Typology	Wall size (mm <sup>3</sup> )	$f_t$ (MPa)	$f_c$ (MPa)	$G_{ft}$ (N/m)	$G_{fc}$ (N/m)	E (MPa)	$P_{exp}$ (kN)	$P_{num}$ (kN)	$\Delta_{exp-num}$
Babaedarab ad et al. [391]	Clay brick + cement	1145 × 1220 × 92	0.263	24.0	15.70	36000	1769	70.0	66.6	+4.8%
Mahmood and Ingham [165]	Clay brick + cement lime	1170 × 1170 × 225	0.054	5.4	5.18	8100	3141	36.0	40.3	-12.0%
Milosevic et al. [321]	Rubble stone + air lime	1200 × 1200 × 700	0.014	7.41	1.98	11115	204	29.0	29.8	-2.6%
Milosevic et al. [321]	Rubble stone + hydraulic lime	1200 × 1200 × 700	0.162	8.01	11.2	12015	868	339.0	303.6	+10.4%
Parisi et al. [169]	Tuff block+ pozzolana	1230 × 1230 × 310	0.127	3.96	9.43	5940	1100	121.0	112.1	+7.4%
Rezaie et al. [348]	Rubble stone + hydraulic lime	900 × 900 × 400	0.060	0.76	5.58	1140	1191	53.0	52.5	+0.88%
Silva et al. [392]	Concrete block + cement	1626 × 1626 × 79	0.399	16.8	21.02	25200	8600	128.0	123.8	+3.4%
Silva et al. [392]	Clay brick + cement	1219 × 1219 × 92	0.289	13.2	16.78	19800	2700	81.0	76.5	+5.5%

## V.5 Conclusions

This paper has presented a combined experimental and numerical investigation on the use of the diagonal compression test to characterize the tensile strength and the shear modulus of masonry. A numerical macromodel has been calibrated with an experimental campaign that

involved tests in 5 brickwork walls built in Flemish bond. The following conclusions can be drawn from the numerical analyses carried out:

- In the linear range of the analyses, the numerical solution coincides qualitatively with the solution that Frocht derived theoretically for the elastic problem by photoelasticity. The numerical study has allowed showing that a wall compressed diagonally does not present a pure shear state of stresses. The approach of ASTM E519 has shown to overestimate the maximum principal stresses ( $\sigma_I = 0.707*P/A$  versus  $\sigma_I = 0.48*P/A$ ) and to underestimate the shear stresses ( $\tau_{xy} = 0.707*P/A$  versus  $\tau_{xy} = 1.04*P/A$ ) at the centre of the panel.
- Damage initiation is triggered when the maximum principal stresses at the centre of the panel reach the masonry tensile strength. Afterwards, a complex redistribution of stresses takes place until the maximum load is attained and the panel fails.
- A coefficient that correlates the maximum attained load and the input tensile strength has been back-calculated based on the numerical investigation. The tensile strength is calculated as the maximum applied load times a coefficient  $\alpha_I$  equal to 0.4, divided by the transverse area of the wall. The calculation of the coefficient  $\alpha_I$  accounts for cracking and stress redistributions, and allows the practical application of the experimental results to determine the tensile strength of masonry.
- The sensitivity of the coefficient  $\alpha_I$  to the variation of several parameters has been investigated numerically. The coefficient  $\alpha_I$  has resulted sensitive to the variation of the Young's modulus and tensile strength. Its value ranged from 0.38 to 0.45, and always remained below the corresponding elastic value of 0.48.

**PAPER V**

- The coefficient  $\alpha_I$  has shown little sensitivity to the variation of the size panel and the size of the loading shoes, provided that these dimensions were similar to the ones suggested by the standards. The coefficient has remained almost constant for walls between 0.6 m and 1.4 m wide, and for loading shoes depths spanning from  $1/6^{\text{th}}$  to  $1/12^{\text{th}}$  the length of the panel side.
- These findings have been validated by considering experimental results from eight campaigns carried out by other authors and available in literature. These campaigns covered a wide range of dimensions and components properties. The assumptions of a coefficient  $\alpha_I$  equal to 0.4 to compute the tensile strength of masonry from the experimental maximum load, and of a coefficient  $\alpha_{xy}$  equal to 1.04 to compute the shear stresses and determine the shear modulus, have allowed the numerical simulations to represent correctly the experimental loads.
- The experimental campaign presented herein involving brickwork walls has shown the particularities of the Flemish bond, as the development of the diagonal cracks through both mortar joints and bricks. With the coefficients proposed in this paper, the average tensile strength of the investigated masonry has been estimated equal to 0.15 MPa, while the average shear modulus has been estimated equal to 1890 MPa. The compressive strengths of the component materials were 18 MPa and 2.2 MPa for bricks and mortar respectively.
- The numerical model adopted in the research, based on an ad-hoc constitutive model for masonry and a crack-tracking technique for tensile crack localization, has proven to constitute a reliable tool for the assessment of masonry homogenized properties by means of comparisons with experimental results.

## 6.4. Discussion

The two previous sections have presented Papers IV and V on the characterisation of masonry in shear. This section exposes some remarks that can be drawn from the comparison of both papers, and include further comments in relation to Papers II and III. The individual conclusions of each paper are restated in Chapter 7.

A certain parallelism can be traced among papers of Chapter 5 and Chapter 6. This parallelism justifies the internal thematic coherence of the thesis. Paper II and Paper IV studied the standard procedures for the characterisation of masonry in laboratory, under compression and shear, respectively. Paper III and Paper V investigated techniques that could be used in situ to inspect existing buildings.

All four papers have investigated up to a certain extent the influence of the type of specimen. Paper IV found that couplets tested with a simple setup provided higher shear estimates than triplets. Paper V investigated the size effect of the specimens although only numerically. A minimal influence was found, except for very small specimens.

Paper V dealt with the determination of an elastic parameter, the shear elastic modulus. The experimental procedure included a loading protocol similar to the one applied in Paper II. The protocol consisted in the application of three loading cycles at low load levels, and the subsequent computation of the shear modulus as the chord modulus on the stress-strain curves, between two limits calculated according to the actual maximum attained load.

A further remark on the characterisation in shear is that experimental results presented a higher variability than those obtained in compression. This is especially true in the case of the variability observed in the determination of the tensile strength of masonry in Paper V, with a coefficient of variation above 20%, if compared with the variability observed in the

determination of the compressive strength in Paper II, with a coefficient of variation under 10% for specimens built with the same type of masonry and materials. This difference could be explained by the different brittleness associated to compression and shear failures, and by the type of failure. In compression tests, stresses are better distributed and the local variation of material properties is lumped through the whole section. In diagonal compression tests, the weakest-link postulate may apply and local properties may have a higher influence on the final performance of the specimen. As a result, the latter tests present this higher variability.

With regard to the use of Papers IV and V to characterise the traditional type of brickwork of Barcelona, the experimental values of cohesion, angle of friction, and tensile strength, seemed to compare well with the very few researches available in literature for similar materials. The values of cohesion and angle of friction laid between the limits proposed by the Italian Circolare for existing materials [62]. The value of the tensile strength was of the same magnitude that values found in situ on existing buildings made of brickwork. This is further evidence of the appropriateness of the selected component materials to replicate the behaviour of historical-like masonry.

In addition, Papers IV and V provided data about fracture energies, a sort of parameter which is often neglected in experimental characterisation. Paper IV provided new estimations for the cohesive fracture energy at zero normal stress, with a value of 15.2 N/m. Among the different empirical relationships available to determine the tensile fracture energy of masonry from the tensile strength, Paper V found numerically that the best fit was obtained by means of a modification from the Model Code 1990 expression [69]. The average result evaluated with this expression was 10.85 N/m. Last, Paper II had provided two estimations of the compressive fracture energy, which yielded an average value of 9750 N/m. Given the uncertainties around the experimental definition of these parameters, the values provided herein of cohesive fracture

energy at zero normal stress, tensile fracture energy, and compressive fracture energy, should be taken only as a qualitative reference for the type of material being investigated.

*This page is intentionally left blank.*

**7**

## **Conclusions**

*This page is intentionally left blank.*

## 7.1. Summary

This thesis has presented five experimental campaigns related to the characterisation of masonry. These campaigns constituted the base of five publications, which have been identified in this work as Papers I to V. Each campaign pursued specific scientific objectives, combined with the more general objective of replicating and characterising the historical type of brickwork traditionally used in Barcelona.

Chapter 2 has offered a literature review on the mechanical properties of masonry, the characterisation needs, and the current experimental procedures. Chapter 3 has presented the specific objectives of the thesis derived from the literature review.

Chapter 4 has described the materials used along the experimental campaigns. The need of having a historical-like mortar with a relatively fast hardening and low mechanical properties motivated the research included in Paper I (Section 4.4).

Chapter 5 has covered two investigations on the compressive characterisation of masonry. The first of them, constituting Paper II (Section 5.2), has dealt with the standard tests on prismatic specimens. The second one, presented as Paper III in Section 5.3, has delved into the use of extracted cylindrical specimens to characterise the mechanical behaviour of existing masonry structures.

Chapter 6 has included two additional papers on the shear characterisation of masonry. Paper IV (Section 6.2) has investigated the possibility of using couplets as an alternative to standard triplets for the determination of the cohesion and angle of friction of mortar bed joints. Finally, Paper V (Section 6.3) has studied the interpretation of the diagonal compression test, by means of numerical analyses calibrated with a specific experimental campaign.

## 7.2. Conclusions

The conclusions of this work can be summarized as follows.

### Literature review

- The mechanical properties that are required to perform a structural analysis depend on the level of detail considered in the modelling strategy. Based on the properties that are necessary for strategies that consider masonry as a homogeneous material, and on the properties required by the strength criteria provided in common building codes, the following six properties have been studied in detail: the compressive strength, the Young's modulus, the cohesion at zero normal stress, the coefficient of friction, the diagonal tensile strength, and the shear elastic modulus.
- Given the complex mechanical behaviour of masonry, its characterisation is complex and the procedures are not exempt of uncertainties. These uncertainties can be related to the geometry of the specimens, the boundary conditions, the loading protocol, the necessary instrumentation, and the interpretation of the results and post-processing of the tests.
- A review on the available characterisation techniques for masonry reveals the need of improvement or further definition for most of the studied testing procedures. This need of improvement may be related to contradictions between standards, inconsistent provisions, or lack of specific official standards for some tests. The uncertainties are related, in general, to the size of the specimen and the boundary conditions in the case of strength properties, and related to the loading protocol and instrumentation in the case of elastic properties. In most cases, uncertainties with regard to the interpretation and post-processing of results have been detected.

- The industrial and urbanistic development of Barcelona in the 19<sup>th</sup> century and first half of the 20<sup>th</sup> century motivated the proliferation of constructions based on masonry load bearing walls. The preferred type of masonry was brickwork made of lime mortar and handmade solid bricks. These bricks had average dimensions of  $300 \times 150 \times 50 \text{ mm}^2$ , which constitute a difference with respect to common smaller bricks of other places around the world. This type of masonry is in need of extensive characterisation, given that the current available information, although valuable, is scarce and incomplete.

#### **Modified hydraulic lime mortar**

- The incorporation of limestone filler additions to hydraulic lime based mortars shows several advantages depending on the amount of filler being added. The curing time and the mechanical property being analysed also have influence on the effect of these additions.
- Additions in volume between 12.5% and 25% can maximise the compressive and flexural strengths of NHL 3.5 based mortars. This improvement is due to the nucleation and filling effects offered by the small particles of filler.
- For a replacement in volume of 50%, the dilution effect prevails and the strengths of the mortar decrease with respect to the reference mix. This mortar proportioning has been used along the thesis to build masonry specimens with satisfactory results in terms of variability and final attained strengths.
- Limestone filler is an easily available industrial by-product and, thanks to its inert nature, it doesn't affect the composition of the resulting phases in the hardened mortar. It is therefore compatible with applications on traditional old mortars.

### Compression on standard masonry specimens

- Standard tests on prismatic masonry specimens built in laboratory present uncertainties related to: a) the geometry of the specimen for determining the compressive strength, and b) the loading protocol and post-processing for determining the Young's modulus. European and American standards differ in the type of specimen to be tested. In addition, no specific standard covers the determination of Young's modulus of masonry.
- For the particular case of masonry studied in this thesis, running bond walls and stack bond prisms have yielded similar results in terms of compressive strength and Young's modulus.
- Provisions of standards specifically devoted to the determination of Young's modulus in other materials have been applied. The application of initial loading-unloading cycles at low load levels has contributed to stabilise the measurements. The Young's modulus has been calculated as the chord modulus on the stress-strain curves, between two limits calculated according to the actual maximum attained load.
- Three masonry prisms were subjected to pseudo-cyclic loading until and beyond failure. Scientific literature on this topic for brickwork is scarce. The degradation of masonry stiffness for increasing strains was consistently captured. The stress-strain curves obtained through static loading can be used as a satisfactory estimation of the peak envelope of cyclic tests. In addition, the experimental results were compared to cyclic constitutive models available in literature. The model by Facconi et al. [92] provides a good simulation. The model by Sima et al. [297] has

required significant previous calibration to properly simulate the experimental results.

- In this case of the prismatic specimens, the empirical expressions provided by European and American codes for the prediction of the compressive strength of masonry from the properties of the components have yielded values in agreement with the experimental ones. Similarly, well-known analytical expressions derived by different authors have also provided good estimations of the compressive strength.
- A simple one-dimensional homogenisation spring model is able to satisfactorily evaluate the Young's modulus of masonry from the elastic properties of the components. The experimental characterisation of the latter is, however, challenging, given the instrumental difficulties related to the measurement of compressive strains in such small thicknesses as those of bricks and mortar joints. The ratios proposed by building codes to predict the Young's modulus of masonry from its compressive strength visibly overestimate the experimental results.

### **Compression on cylindrical specimens**

- The laboratory testing of cylindrical core samples extracted from masonry walls is a promising technique for the evaluation of the compressive parameters of existing masonry. This work has studied the possibility of using cylinders with diameter of 90 mm, in comparison with bigger cylinders of 150 mm that previous researches has shown to be able to provide good estimations of the actual masonry properties.
- Cylinders with diameter of 90 mm, constituted by two brick portions and one single mortar joint, are able to reproduce the expected mechanical behaviour of masonry.

Tests on these specimens have shown a failure sequence and a failure pattern consistent with those obtained on standard prismatic specimens.

- The reduction of the size of the core sample has a significant effect on the evaluation of the compressive parameters. In the case of compressive strength, a proportionality constant of 0.75 has been found to relate the results obtained from 90 mm and 150 mm specimens. That constant would be of application, in principle, only to masonry types similar to the ones investigated. In the case of Young's modulus, smaller cylinders also provide higher estimations of this mechanical property.
- In this case of cylindrical specimens, the empirical expressions provided by European and American codes for the prediction of the compressive strength of masonry from the properties of the components have underestimated the experimental values in the cases of low strength materials, while a better prediction has been obtained for the type of masonry built with stronger materials. The simpler expression by the American code, which depends only on the strength of the constituent bricks, seems to be more suitable for these low strength masonry types than the expression included in the European code. The latter depends also on the strength of mortar. Its predictions might be affected by the quality of the mortar strength determination, which is specially challenging for existing mortars.
- The dry procedure applied to drill the cylindrical cores has shown to be clean and efficient. It is therefore suitable for the extraction of specimens in existing buildings. The alternative of 90 mm cylinders is advantageous because it reduces the damage caused to the structure. In addition, it is easier to identify spots where to extract these smaller cylinder within the masonry walls.

**Shear on triplets and couplets**

- Standard shear tests on triplet specimens present uncertainties in the interpretation of the results, due to the non-simultaneous failure of the mortar joints. Complex testing setups on couplet specimens can be found in literature as alternatives to the triplet test. References dealing with the direct comparison between triplets and couplets are scarce.
- Couplet specimens tested with a very simple setup derived from the triplet testing setup are able to provide qualitatively similar results to those obtained with triplets, and to predict similar trends with regard to the dependency on the normal compression stress and with regard to dilatancy.
- From a quantitative point of view, tests on couplets provide consistently higher values of cohesion and angle of friction than triplets. The rate of increase for each one of the latter parameters seems to be related to the type of masonry and the dominant response of the materials. For the two types of masonry investigated in this particular campaign, the frictional response of rougher bricks motivates a higher increase of the angle of friction, while the cohesive response of smoother bricks motivates a higher increase of the cohesion value.
- The differences in the estimates obtained from standard triplets and couplets can be explained by several causes. These causes include differences in the stress distributions, size effects due to the larger area of brick-mortar interface in triplets, and bias in the interpretation of the results. The bias in the case of triplets is caused by the double peak phenomenon associated to the non-simultaneous failure of the two joints. In the case of couplets, the bias is related to the friction of the lateral faces of the specimen against the platens of the loading machine.

**Diagonal compression test**

- Diagonal compression tests are widely used to characterise the shear behaviour of masonry. They currently stand as a useful tool to perform comparison campaigns of strengthening and repair solutions, and as a valid tool for the inspection of existing buildings. The post-processing of the results presents uncertainties related to the definition of the actual state of stresses within the masonry panel.
- According to linear numerical analysis, a wall compressed diagonally does not present a pure shear state of stresses. The maximum principal stresses and the shear stresses at the centre of the panel do not have the same value but are equal  $\sigma_I = 0.48*P/A$  to  $\tau_{xy} = 1.04*P/A$  and respectively. These values are different that those assumed by the standard ASTM E519 ( $\sigma_I = 0.707*P/A$  and  $\tau_{xy} = 0.707*P/A$ ).
- When the maximum principal stresses at the centre of the panel reach the masonry tensile strength, damage initiation is triggered, and it is followed by a complex redistribution of stresses that eventually leads to the failure of the panel. Consequently, there is no a direct univocal correlation between the maximum attained load and the masonry tensile strength. A simplified correlation by means of a coefficient called  $\alpha_I$  has been investigated numerically. This coefficient accounts for cracking and stress redistributions.
- The calibration of the numerical analyses that simulate the experimental results used as benchmark has provided a value of 0.4 for coefficient  $\alpha_I$ . Its sensitivity to the variation of several parameters has been investigated numerically. The coefficient is sensitive to the input variations of Young's modulus and tensile strength, but always remains below the corresponding elastic value of 0.48. The coefficient is little sensitive to the variation of the size panel and the size of the

loading shoes, provided that these dimensions are similar to the ones suggested by the standards.

- The validity of these findings has been checked with the simulation of experimental campaigns carried out by other authors. The input data for the corresponding numerical analyses were obtained by applying the coefficients proposed herein for the determination of the tensile strength and the shear modulus. Simulations with these input data reproduced correctly the actual experimental loads.
- In addition, the numerical model adopted in this research has proven to constitute a reliable tool for the simulation of experimental results considering homogenised properties of masonry. This model is based on an ad-hoc constitutive model for masonry and a crack-tracking technique for tensile crack localisation.

### **Replication of historical-like masonry**

- The replication of historical-like masonry in laboratory is necessary given the intrinsic difficulties encountered in the experimental testing of existing masonry. Replicating masonry in laboratory could be used, among others, to study the structural response of this material under certain actions, to reproduce structural elements, to study strengthening solutions, or to provide reference values of mechanical properties. The replication presents however some challenges in relation to the choice of materials. In particular, the hardening time and final strength of the selected mortar are key parameters.
- Handmade solid fired clay bricks made by a local producer with traditional methods has been selected for the experimental campaigns carried out in this thesis, together with a modified hydraulic lime based commercial mortar. The combination of these two materials has shown to be able to satisfactorily reproduce the behaviour of

existing masonry and to quantitatively replicate the mechanical properties of existing masonry. The compressive parameters obtained with this replicated masonry compare well with those obtained from cylinders extracted from real buildings of Barcelona. With regard to the shear parameters obtained with this replicated masonry, they compare well with the few values that are available in literature and code provisions.

- In addition, the variability of the results observed for the replicated masonry and its components is also of similar magnitude to that of existing and historical materials.

### **Characterisation of traditional brick masonry of the city of Barcelona**

- Masonry made of handmade bricks and lime mortar was extensively used as a load bearing material in the city of Barcelona during the 19<sup>th</sup> c. and the first half of the 20<sup>th</sup> c. Up to date, this specific type of masonry has been only partially characterised. In the need of performing structural analyses due to renovation works or preventive studies, this material needs a better characterisation.
- This thesis presents experimental results from two sources: 1. From existing buildings through tests on extracted cylinders, 2. from replicated masonry in laboratory through standard tests. The size of the bricks and properties of the components make these results specific of the traditional brickwork of Barcelona. Nevertheless, brick masonry has been thoroughly used around the world along history. Qualitative and quantitative results presented herein may be of application to similar brickwork examples from other places.
- Tests on cylindrical specimens extracted from two existing buildings provide values of compressive strength that range from 5.28 to 7.83 MPa. Values of Young's modulus range from 1569 to 2304 MPa. Specimens from a third inspected

building provide higher estimations of both properties. The latter are not considered as representative of the real range given the exceptionality of this third construction, in terms of material and workmanship qualities.

- Standard tests on replicated masonry have provided the following average values: compressive strength 6.5 MPa, Young's modulus of 2318 MPa, cohesion at zero normal stress of 0.167 MPa, angle of friction of 33.71°, and tensile strength of 0.15 MPa.
- In addition, values of fracture energies have been estimated, e.g. cohesive fracture energy at zero normal stress, with a value of 15.2 N/m, tensile fracture energy of masonry of 10.85 N/m, and compressive fracture energy, with a value of 9750 N/m. Given the difficulties on the experimentation and interpretation of these properties, the range of the values should be assessed in the future with additional experiments.
- The former campaigns were intended to shed light on the mechanical properties of historical-like masonry. Given the variability of this type of material, it is always recommended to carry out specific and detailed inspections when dealing with existing structures.

### **7.3. Main contributions**

This work provides the following main contributions. The first three items of the list refer to more general observations. The last four items of the list refer to direct applications.

- The review of common procedures for the characterisation of basic mechanical properties of masonry and the identification of possible uncertainties related to each type of test. This identification provides a set of needs for research. Some of them

have been studied within this thesis, while some others may be of interest to other researchers for future work.

- The provision of new experimental evidence on two aspects of the characterisation in compression: the comparison between types of specimen –running bond walls and stack bond prisms-, and the effects of cyclic loading. The interest of this contribution is confirmed in the light of new works by other researchers that have investigated similar topics and have cited the corresponding publication [308,393–397].
- The preliminary investigation on the possibility of using couplet specimens composed of only one mortar joint to the standard triplet specimen composed of two mortar joints. The obtained results pointed out the need of improving the contact between the external faces of the specimen against the loading machine platens.
- The design of a mortar based on a natural hydraulic lime commercial premixed mortar that has been modified with the incorporation of limestone filler. This mortar combines the advantages of an industrially prepared product –easier to prepare and less variable- with convenient low values of compressive and flexural strengths. Being based on hydraulic lime, its hardening time adapts well to the schedule needs of a common laboratory. After 28 days, the compressive strength is sufficient and remains almost constant.
- The determination of a correlation factor that relates the compressive strength values determined with 90 mm cylinders to the values determined with 150 mm cylinders. Under the assumption that the latter provide a sufficiently good estimation of the actual compressive strength of masonry, which has been

calibrated in previous researches, the possibility of using smaller cylinders provides several advantages with respect to the bigger cylinders: the damage on the structure is reduced, and their extraction is easier, as well as the handling and testing in laboratory. In addition, given that the impact is reduced and it is easier to find convenient spots where to drill them, it is more feasible to extract a larger sample of cylinders from the structure. This fact results in more statistically significant determinations.

- The proposal of coefficients for the post-processing of the outcomes obtained with the diagonal compression test. These coefficients apply for the determination of the tensile strength and the shear elastic modulus of masonry. Better estimations of these parameters result in more accurate structural analyses and more respectful interventions.
- The mechanical characterisation of examples of the traditional type of brickwork used in Barcelona during the 19<sup>th</sup> c. and the first half of the 20<sup>th</sup> c. This characterisation includes results from existing masonry structures and from replicated masonry specimens built in laboratory.

#### **7.4. Suggestions for future work**

In general, when dealing with experimental procedures, the main suggestion should be to continue performing experimental campaigns in order to increase the significance of the conclusions. These additional campaigns could be either on the same materials, with the aim of increasing the statistical validity of the results, or on different material combinations, to expand the applicability of the results to other types of masonry. In addition, a general recommendation is to investigate and validate the experimental results with theoretical or numerical methods.

A last general remark with regard to the investigation on experimental procedures is about the coordination between researchers and institutions. An individual disconnected research is of interest for the characterisation of a specific type of masonry. The approach should be different if the goal is to reach significant sound conclusions and, eventually, reflect the experimental findings into a new standard or a modification of existing standards. In that case, coordinated campaigns should be performed, with consistent boundary conditions, loading protocols, and types of specimen.

Finally, this thesis closes with the following suggestions for future work.

- The further study of the size, shape, and slenderness effects on the determination of the compressive strength of masonry, preferably as a coordinated effort with the creation of a database of results. Individual attempts have been carried out in this sense, with the derivation of empirical expressions. These attempts would be much relevant if they were focused on the same objective. The study of the influence of the specimen type can be also done by means of numerical methods used as a virtual laboratory. Given the reduced size of the specimens, 3D micromodels would be affordable.
- The expansion of the database that correlates smaller and bigger cylinders for the characterisation of compressive parameters, together with the definitive validation of these two specimens as able to reproduce the actual properties of masonry. Combined with numerical investigations, this line of research could finalise with the implementation of a new standard for the inspection of existing buildings. If tests on cylinders in compression are combined with tests on cylinders for shear characterisation, a full inspection methodology could be proposed, only by considering tests on cylindrical specimens.

- The continuation of the study about the possibility of using couplets as an alternative to triplets for shear characterisation. New proposals should be done to reduce the friction between the lateral faces of the specimen against the precompression machine. However, the spirit of these proposals should be kept as simpler as possible. Increasing the complexity of the setup hinders its replicability by other researchers.
- The further validation of the coefficients obtained for the interpretation of the diagonal compression test. This validation could be done by means of other numerical tools, such as FEM micromodels or DEM, which account for the real texture of the masonry pattern. These tools would allow studying the influence of the masonry texture. In addition, a joint campaign that combines and compares experimental results obtained by means of diagonal compression tests and shear compression tests would be relevant.
- The further investigation of the expressions to predict masonry composite properties from the properties of the components. This approach remains a promising and powerful possibility for the mechanical characterisation of existing masonry. However, it still faces a double challenge: 1. The need of increasing the validity of the correlations, especially for cases of low strength masonry, 2. The difficulties to characterise the mechanical properties of the components. The latter constitutes a wide line of research that includes the study of, among others, the size of the samples to characterise bricks' compressive strength, the difficult determination of bricks' Young's modulus in the direction perpendicular to the larger faces, the determination of the actual compressive strength of existing

mortars, and the relation between the strength of mortars obtained from standard prismatic specimens to the actual strength of the mortar joint.

## **References**

*This page is intentionally left blank.*

- 
- [1] A.W. Hendry, *Structural Masonry*, Macmillan Press Ltd, 1998.
- [2] M. Como, *Statics of Historic Masonry Constructions*, Springer, 2013.
- [3] A.M. D’Altri, V. Sarhosis, G. Milani, J. Rots, S. Cattari, S. Lagomarsino, E. Sacco, A. Tralli, G. Castellazzi, S. de Miranda, *Modeling Strategies for the Computational Analysis of Unreinforced Masonry Structures: Review and Classification*, *Arch. Comput. Methods Eng.* (2019). doi:10.1007/s11831-019-09351-x.
- [4] P. Roca, P.B. Lourenço, A. Gaetani, *Historic construction and conservation. Materials, systems and damage*, Routledge, 2019.
- [5] L. Binda, C. Tiraboschi, S. Abbaneo, *Experimental research to characterise masonry materials*, *Mason. Int.* 10 (1997) 92–101.
- [6] A.W. Page, *The strength of brick masonry under biaxial tension-compression*, *Int. J. Mason. Constr.* 3 (1983) 26–31.
- [7] A.W. Page, *The biaxial compressive strength of brick masonry*, *Proc. Instn Civ. Engrs.* 71 (1981) 893–906.
- [8] M. Dhanasekar, A.W. Page, P.W. Kleeman, *Failure of brick masonry under biaxial stresses*, *Proc. Inst. Civ. Eng.* 79 (1985) 295–313. doi:10.1680/iicep.1985.992.
- [9] C. Calderini, S. Cattari, S. Lagomarsino, *In-plane strength of unreinforced masonry piers*, *Earthq. Eng. Struct. Dyn.* 38 (2009) 243–267. doi:10.1002/eqe.860.
- [10] European Committee for Standardization (CEN), *Eurocode 8 : Design of structures for earthquake resistance — Part 3: Assessment and retrofitting of buildings*, 3 (2004).
- [11] Ministero delle Infrastrutture e dei Trasporti, D.M 17 gennaio 2018 “Aggiornamento delle Norme tecniche per le Costruzioni,” (2018) 1–198.
- [12] P. Roca, M. Cervera, G. Gariup, L. Pelà, *Structural analysis of masonry historical constructions. Classical and advanced approaches*, *Arch. Comput. Methods Eng.* 17 (2010) 299–325. doi:10.1007/s11831-010-9046-1.
- [13] J. Heyman, *The stone skeleton*, *Int. J. Solids Struct.* 2 (1966) 249–279.

- [14] F.W. Smith, W.J. Harvey, A.E. Vardy, Three-hinge analysis of masonry arches, *Struct. Eng.* 68 (1990) 203–213.
- [15] S. Holzer, Numerical arch and vault analysis, *Wiadomości Konserw.* Nr 34 (2013) 7–17.
- [16] A. Chiozzi, G. Milani, A. Tralli, A Genetic Algorithm NURBS-based new approach for fast kinematic limit analysis of masonry vaults, *Comput. Struct.* 182 (2017) 187–204.  
doi:10.1016/j.compstruc.2016.11.003.
- [17] A. Andreu, L. Gil, P. Roca, Computational Analysis of Masonry Structures with a Funicular Model, *J. Eng. Mech.* 133 (2007) 473–480. doi:10.1061/(asce)0733-9399(2007)133:4(473).
- [18] P. Block, T. Ciblac, J. Ochsendorf, Real-time limit analysis of vaulted masonry buildings, *Comput. Struct.* 84 (2006) 1841–1852. doi:10.1016/j.compstruc.2006.08.002.
- [19] P. Block, L. Lachauer, Three-dimensional (3D) equilibrium analysis of gothic masonry vaults, *Int. J. Archit. Herit.* 8 (2014) 312–335. doi:10.1080/15583058.2013.826301.
- [20] A. Chiozzi, N. Grillanda, G. Milani, A. Tralli, UB-ALMANAC: An adaptive limit analysis NURBS-based program for the automatic assessment of partial failure mechanisms in masonry churches, *Eng. Fail. Anal.* 85 (2018) 201–220. doi:10.1016/j.engfailanal.2017.11.013.
- [21] M. Valente, G. Milani, Seismic assessment of historical masonry towers by means of simplified approaches and standard FEM, *Constr. Build. Mater.* 108 (2016) 74–104.  
doi:10.1016/j.conbuildmat.2016.01.025.
- [22] M. Betti, L. Galano, Seismic analysis of historic masonry buildings: The Vicarious Palace in Pescia (Italy), *Buildings.* 2 (2012) 63–82. doi:10.3390/buildings2020063.
- [23] A. Elyamani, P. Roca, O. Caselles, J. Clapes, Seismic safety assessment of historical structures using updated numerical models: The case of Mallorca cathedral in Spain, *Eng. Fail. Anal.* 74 (2017) 54–79.  
doi:10.1016/j.engfailanal.2016.12.017.
- [24] L. Pelà, A. Aprile, A. Benedetti, Seismic assessment of masonry arch bridges, *Eng. Struct.* 31 (2009) 1777–1788. doi:10.1016/j.engstruct.2009.02.012.
- [25] J. Lopez, S. Oller, E. Oñate, J. Lubliner, A homogeneous constitutive model for masonry, *Int. J. Numer. Methods Eng.* 46 (1999) 1651–1671. doi:10.1002/(SICI)1097-0207(19991210)46:10<1651::AID-

- NME718>3.0.CO;2-2.
- [26] L. Berto, A. Saetta, R. Scotta, R. Vitaliani, An orthotropic damage model for masonry structures, *Int. J. Numer. Methods Eng.* 55 (2002) 127–157. doi:10.1002/nme.495.
- [27] L. Pelà, M. Cervera, S. Oller, M. Chiumenti, A localized mapped damage model for orthotropic materials, *Eng. Fract. Mech.* 124–125 (2014) 196–216. doi:10.1016/j.engfracmech.2014.04.027.
- [28] DIANA FEA BV, DIANA FEA User's Manual - Release 10.3, 2019.
- [29] P.B. Lourenço, J.G. Rots, Multisurface interface model for analysis of masonry structures, *J. Eng. Mech.* (1997) 660–668. doi:10.1061/(ASCE)0733-9399(1997)123.
- [30] E. Çaktı, Ö. Saygılı, J. V. Lemos, C.S. Oliveira, Discrete element modeling of a scaled masonry structure and its validation, *Eng. Struct.* 126 (2016) 224–236. doi:10.1016/j.engstruct.2016.07.044.
- [31] M. Petracca, L. Pelà, R. Rossi, S. Zaghi, G. Camata, E. Spacone, Micro-scale continuous and discrete numerical models for nonlinear analysis of masonry shear walls, *Constr. Build. Mater.* 149 (2017) 296–314. doi:10.1016/j.conbuildmat.2017.05.130.
- [32] B. Pulatsu, E. Erdogmus, P.B. Lourenço, J. V. Lemos, K. Tuncay, Simulation of the in-plane structural behavior of unreinforced masonry walls and buildings using DEM, *Structures.* 27 (2020) 2274–2287. doi:10.1016/j.istruc.2020.08.026.
- [33] A. Penna, S. Lagomarsino, A. Galasco, A nonlinear macroelement model for the seismic analysis of masonry buildings, *Earthq. Eng. Struct. Dyn.* 43 (2014) 159–179. doi:10.1002/eqe.
- [34] S.Y. Chen, F.L. Moon, T. Yi, A macroelement for the nonlinear analysis of in-plane unreinforced masonry piers, *Eng. Struct.* 30 (2008) 2242–2252. doi:10.1016/j.engstruct.2007.12.001.
- [35] S. Lagomarsino, A. Penna, A. Galasco, S. Cattari, TREMURI program: An equivalent frame model for the nonlinear seismic analysis of masonry buildings, *Eng. Struct.* 56 (2013) 1787–1799. doi:10.1016/j.engstruct.2013.08.002.
- [36] I. Calì, M. Marletta, B. Pantò, A new discrete element model for the evaluation of the seismic behaviour of unreinforced masonry buildings, *Eng. Struct.* 40 (2012) 327–338. doi:10.1016/j.engstruct.2012.02.039.
- [37] R. Siano, P. Roca, G. Camata, L. Pelà, V. Sepe, E. Spacone, M. Petracca, Numerical investigation of

- non-linear equivalent-frame models for regular masonry walls, *Eng. Struct.* 173 (2018) 512–529.  
doi:10.1016/j.engstruct.2018.07.006.
- [38] G. Rinaldin, C. Amadio, L. Macorini, A macro-model with nonlinear springs for seismic analysis of URM buildings, *Earthq. Eng. Struct. Dyn.* 45 (2016) 2261–2281. doi:10.1002/eqe.
- [39] S. Saloustros, L. Pelà, M. Cervera, P. Roca, An Enhanced Finite Element Macro-Model for the Realistic Simulation of Localized Cracks in Masonry Structures: A Large-Scale Application, *Int. J. Archit. Herit.* 12 (2018) 432–447. doi:10.1080/15583058.2017.1323245.
- [40] L. Pelà, M. Cervera, P. Roca, An orthotropic damage model for the analysis of masonry structures, *Constr. Build. Mater.* 41 (2013) 957–967. doi:10.1016/j.conbuildmat.2012.07.014.
- [41] C. Chácará, F. Cannizzaro, B. Pantò, I. Calìò, P.B. Lourenço, Assessment of the dynamic response of unreinforced masonry structures using a macroelement modeling approach, *Earthq. Eng. Struct. Dyn.* 47 (2018) 2426–2446. doi:10.1002/eqe.3091.
- [42] B. Pantò, F. Cannizzaro, S. Caddemi, I. Calìò, 3D macro-element modelling approach for seismic assessment of historical masonry churches, *Adv. Eng. Softw.* 97 (2016) 40–59.  
doi:10.1016/j.advengsoft.2016.02.009.
- [43] E. Grande, M. Imbimbo, E. Sacco, A beam finite element for nonlinear analysis of masonry elements with or without fiber-reinforced plastic (FRP) reinforcements, *Int. J. Archit. Herit.* 5 (2011) 693–716.  
doi:10.1080/15583058.2010.490616.
- [44] D. Liberatore, D. Addessi, Strength domains and return algorithm for the lumped plasticity equivalent frame model of masonry structures, *Eng. Struct.* 91 (2015) 167–181.  
doi:10.1016/j.engstruct.2015.02.030.
- [45] E. Raka, E. Spacone, V. Sepe, G. Camata, Advanced frame element for seismic analysis of masonry structures : model formulation and validation, *Earthq. Eng. Struct. Dyn.* 44 (2015) 2489–2506.  
doi:10.1002/eqe.
- [46] P. Roca, C. Molins, A.R. Marí, Strength capacity of masonry wall structures by the equivalent frame method, *J. Struct. Eng.* 131 (2005) 1601–1610. doi:10.1061/(ASCE)0733-9445(2005)131.
- [47] S. Saloustros, L. Pelà, M. Cervera, A crack-tracking technique for localized cohesive-frictional damage,

- Eng. Fract. Mech. 150 (2015) 96–114. doi:10.1016/j.engfracmech.2015.10.039.
- [48] L. Leonetti, F. Greco, P. Trovalusci, R. Luciano, R. Masiani, A multiscale damage analysis of periodic composites using a couple-stress/Cauchy multidomain model: Application to masonry structures, *Compos. Part B Eng.* 141 (2018) 50–59. doi:10.1016/j.compositesb.2017.12.025.
- [49] G. Milani, P.B. Lourenço, A. Tralli, Homogenised limit analysis of masonry walls, Part I: Failure surfaces, *Comput. Struct.* 84 (2006) 166–180. doi:10.1016/j.compstruc.2005.09.005.
- [50] A. Zucchini, P.B. Lourenço, A micro-mechanical homogenisation model for masonry: Application to shear walls, *Int. J. Solids Struct.* 46 (2009) 871–886. doi:10.1016/j.ijsolstr.2008.09.034.
- [51] A. Orduña, P.B. Lourenço, Three-dimensional limit analysis of rigid blocks assemblages. Part II: Load-path following solution procedure and validation, *Int. J. Solids Struct.* 42 (2005) 5161–5180. doi:10.1016/j.ijsolstr.2005.02.011.
- [52] H. Smoljanović, Ž. Nikolić, N. Živaljić, A combined finite-discrete numerical model for analysis of masonry structures, *Eng. Fract. Mech.* 136 (2015) 1–14. doi:10.1016/j.engfracmech.2015.02.006.
- [53] L. Gambarotta, S. Lagomarsino, Damage models for the seismic response of brick masonry shear walls. Part I: The mortar joint model and its applications, *Earthq. Eng. Struct. Dyn.* 26 (1997) 423–439. doi:10.1002/(sici)1096-9845(199704)26:4<423::aid-eqe650>3.0.co;2-%23.
- [54] A.J. Aref, K.M. Dolatshahi, A three-dimensional cyclic meso-scale numerical procedure for simulation of unreinforced masonry structures, *Comput. Struct.* 120 (2013) 9–23. doi:10.1016/j.compstruc.2013.01.012.
- [55] R. Senthivel, P.B. Lourenço, Finite element modelling of deformation characteristics of historical stone masonry shear walls, *Eng. Struct.* 31 (2009) 1930–1943. doi:10.1016/j.engstruct.2009.02.046.
- [56] A.M. D’Altri, F. Messali, J. Rots, G. Castellazzi, S. de Miranda, A damaging block-based model for the analysis of the cyclic behaviour of full-scale masonry structures, *Eng. Fract. Mech.* 209 (2019) 423–448. doi:10.1016/j.engfracmech.2018.11.046.
- [57] R. Serpieri, M. Albarella, E. Sacco, A 3D microstructured cohesive–frictional interface model and its rational calibration for the analysis of masonry panels, *Int. J. Solids Struct.* 122–123 (2017) 110–127. doi:10.1016/j.ijsolstr.2017.06.006.

- [58] M. Betti, A. Vignoli, Numerical assessment of the static and seismic behaviour of the basilica of Santa Maria all’Impruneta (Italy), *Constr. Build. Mater.* 25 (2011) 4308–4324.  
doi:10.1016/j.conbuildmat.2010.12.028.
- [59] L. Macorini, B.A. Izzuddin, A non-linear interface element for 3D mesoscale analysis of brick-masonry structures, *Int. J. Numer. Methods Eng.* 85 (2011) 1584–1608. doi:10.1002/nme.3046.
- [60] European Committee for Standardization (CEN), Eurocode 6: Design of masonry structures - Part 1: General rules for reinforced and unreinforced masonry structures, (2005).
- [61] American Society of Civil Engineers, ASCE/SEI, 41-17, Seismic evaluation and retrofit of existing buildings, (2017). doi:10.1061/9780784414859.
- [62] Ministero delle Infrastrutture e dei Trasporti, Circolare 21 gennaio 2019 Istruzioni per l’applicazione dell’ “Aggiornamento delle ‘Norme tecniche per le costruzioni’” di cui al decreto ministeriale 17 gennaio 2018, (2019). <https://www.gazzettaufficiale.it/eli/gu/2019/02/11/35/so/5/sg/pdf>.
- [63] M. Kržan, S. Gostič, S. Cattari, V. Bosiljkov, Acquiring reference parameters of masonry for the structural performance analysis of historical buildings, *Bull. Earthq. Eng.* 13 (2015) 203–236.  
doi:10.1007/s10518-014-9686-x.
- [64] L. Binda, A. Saisi, C. Tiraboschi, Investigation procedures for the diagnosis of historic masonries, *Constr. Build. Mater.* 14 (2000) 199–233. doi:10.1016/S0950-0618(00)00018-0.
- [65] L. Gambarotta, Caratterizzazione sperimentale delle murature, in: *Stud. Della Risposta Sismica Di Edif. Muratura*, n.d.: pp. 1–59.
- [66] ACI, ASCE, TMS, ACI 530.1-11/ASCE 5-11/TMS 402-11 Building Code Requirements for Masonry Structures, (2005).
- [67] C. Chisari, L. Macorini, C. Amadio, B.A. Izzuddin, Identification of mesoscale model parameters for brick-masonry, *Int. J. Solids Struct.* 146 (2018) 224–240. doi:10.1016/j.ijsolstr.2018.04.003.
- [68] P.B. Lourenço, Current Experimental and Numerical Issues in Masonry Research, *SÍSMICA 2004 - 6° Congr. Nac. Sismol. e Eng. Sísmica* 6° Congr. Nac. Sismol. e Eng. Sísmica. (2004) 119–136.
- [69] M. Angelillo, P.B. Lourenço, G. Milani, Masonry behaviour and modelling, in: *Mech. Mason. Struct.*, Springer, 2014. doi:10.1007/978-3-7091-1774-3.

- [70] American Society for Testing and Materials, ASTM C1314-09 Standard Test Method for Compressive Strength of Masonry Prisms, ASTM Int. (2009) 1–10. doi:10.1520/C1314-14.2.
- [71] RILEM, TC76-LUMB1 Compressive strength of small walls and prisms, (1991).
- [72] European Committee for Standardization (CEN), EN 1052-1 Methods of test for masonry - Part 1: Determination of compressive strength, (1999).
- [73] I.E. Torroja, P.I.E.T.70, (1971).
- [74] R. Lumantarna, D.T. Biggs, J.M. Ingham, Uniaxial Compressive Strength and Stiffness of Field-Extracted and Laboratory-Constructed Masonry Prisms, *J. Mater. Civ. Eng.* 26 (2014) 567–575. doi:10.1061/(ASCE)MT.1943-5533.0000731.
- [75] A. Drougkas, P. Roca, C. Molins, Compressive strength and elasticity of pure lime mortar masonry, *Mater. Struct.* 49(3) (2016) 983–999. doi:DOI: 10.1617/s11527-015-0553-2 CITATIONS.
- [76] W.S. McNary, D.P. Abrams, *Mechanics of Masonry in Compression*, *J. Struct. Eng.* 111 (1985) 857–870.
- [77] H.B. Kaushik, D.C. Rai, S.K. Jain, Stress-Strain Characteristics of Clay Brick Masonry under Uniaxial Compression, *J. Mater. Civ. Eng.* 19 (2007) 728–739. doi:10.1061/(ASCE)0899-1561(2007)19:9(728).
- [78] B.D. Ewing, M.J. Kowalsky, Compressive Behavior of Unconfined and Confined Clay Brick Masonry, *J. Struct. Eng.* 130 (2004) 650–661. doi:10.1061/(ASCE)0733-9445(2004)130:4(650).
- [79] K.S. Gumaste, K.S. Nanjunda Rao, B. V Venkatarama Reddy, K.S. Jagadish, Strength and elasticity of brick masonry prisms and wallettes under compression, *Mater. Struct. Constr.* 40 (2007) 241–253. doi:10.1617/s11527-006-9141-9.
- [80] J.J. Hughes, A.K. Taylor, Compressive and flexural strength testing of brick masonry panels constructed with two contrasting traditionally produced lime mortars, *Int. RILEM Work. Repair Mortars Hist. Mason.* (2005) 162–177.
- [81] A. Costigan, S. Pavia, Compressive, flexural and bond strength of brick/lime mortar masonry, *Proc. PROHITEC 09.* (2009) 1609–1615.
- [82] L. Binda, A. Fontana, G. Frigerio, Mechanical Behaviour of Brick Masonries Derived From Unit and Mortar Characteristics, *Int. Brick Block Mason. Conf.* (1988).

- [83] L. Pelà, P. Roca, A. Benedetti, Mechanical Characterization of Historical Masonry by Core Drilling and Testing of Cylindrical Samples, *Int. J. Archit. Herit.* 3058 (2016) 150817093153002. doi:10.1080/15583058.2015.1077906.
- [84] N. Augenti, F. Parisi, Constitutive Models for Tuff Masonry under Uniaxial Compression, *J. Mater. Civ. Eng.* 22 (2010) 1102–1111. doi:10.1061/(ASCE)MT.1943-5533.0000119.
- [85] G. De Casa, G. Giglio, Contributo alla conoscenza del comportamento delle murature in blocchi di tufo vulcanico, 9th Int. Brick Block Mason. Conf. (1991) 141–148.
- [86] S. Ganduscio, L. La Mendola, G. Zingone, Comportamento ciclico di sezioni pressoinflesse in muratura, *La Mecc. Delle Murature Tra Teor. e Progett.* (1996).
- [87] D. V. Oliveira, P.B. Lourenço, P. Roca, Cyclic behaviour of stone and brick masonry under uniaxial compressive loading, *Mater. Struct.* 39 (2006) 247–257. doi:10.1617/s11527-005-9050-3.
- [88] M. Dhanasekar, N.G. Shrive, Strength and deformation of confined and unconfined grouted concrete masonry, *ACI Struct. J.* 99 (2002) 819–826.
- [89] K. Naraine, S.N. Sinha, Behavior of brick masonry under cyclic compressive loading, *J. Struct. Eng.* 115 (1989) 1432–1445.
- [90] M.M. AlShebani, S.N. Sinha, Stress-strain characteristics of brick masonry under uniaxial cyclic loading, *J. Struct. Eng.* 125 (1999) 600–604.
- [91] I. Galman, J. Kubica, Stress – Strain Characteristics of Brick Masonry Under Compressive Cyclic Loading, *Tech. Trans. Civ. Eng.* (2015). doi:10.4467/2353737XCT.15.162.4337.
- [92] L. Faconi, F. Minelli, F.J. Vecchio, Predicting Uniaxial Cyclic Compressive Behavior of Brick Masonry: New Analytical Model, *J. Struct. Eng.* 144 (2018) 4017213. doi:10.1061/(ASCE)ST.1943-541X.0001961.
- [93] R. Mattone, G. Pasero, M. Pavano, G. Pistone, R. Roccati, Prove sperimentali su campioni di varie dimensioni volte alla determinazione delle caratteristiche meccaniche delle vecchie murature, 6th Int. Brick Block Mason. Conf. (1982) 198–209.
- [94] G. de Felice, Experimental Investigation on Historic Brickwork Subjected to Eccentric Axial Loads, *Struct. Anal. Hist. Constr. New Delhi* 2006. (2006) 809–816.

- [95] American Society for Testing and Materials, ASTM C1197 In-situ measurement of masonry deformability properties using flat-jack method, (2014).
- [96] RILEM, LUMD3 In-situ strength/elasticity tests on masonry based on the flat-jack, (1991).
- [97] P. Gregorczyk, P.B. Lourenço, A Review on Flat-Jack Testing, *Eng. Civ. UM.* 9 (2000) 39–50.
- [98] L. Jurina, La caratterizzazione meccanica delle murature. Parte seconda: Martinetti piatti, in: *Semin. Internazionale C.I.A.S.*, 2007: pp. 133–150. [www.jurina.it](http://www.jurina.it).
- [99] American Society for Testing and Materials, ASTM C1196 In-situ compressive stress within solid unit masonry estimated using flat-jack measurements, (2014).
- [100] RILEM, LUMD2 In-situ stress tests on masonry based on the flat jack, (1991).
- [101] UIC, Leaflet 778-3R: Recommendations for the inspection, assessment and maintenance of masonry arch bridges. Final draft, (2008).
- [102] A. Brencich, E. Sterpi, Compressive Strength of Solid Clay Brick Masonry : Calibration of Experimental Tests and Theoretical Issues, in: P.B. Lourenço, C. Modena, P. Roca, S. Agrawal (Eds.), *SAHC 2006 - Struct. Anal. Hist. Constr.*, Macmillan India Ltd., 2006: pp. 757–766.
- [103] A. Brencich, D. Sabia, Experimental identification of a multi-span masonry bridge: The Tanaro Bridge, *Constr. Build. Mater.* 22 (2008) 2087–2099. doi:10.1016/j.conbuildmat.2007.07.031.
- [104] P. Matysek, Compressive strength of brick masonry in existing buildings — research on samples cut from the structures, in: C. Modena, F. da Porto, M.R. Valluzzi (Eds.), *Brick Block Mason. - Trends, Innov. Challenges*, Taylor & Francis Group, 2016: pp. 1741–1747.
- [105] L. Pelà, E. Canella, A. Aprile, P. Roca, Compression test of masonry core samples extracted from existing brickwork, *Constr. Build. Mater.* 119 (2016) 230–240. doi:10.1016/j.conbuildmat.2016.05.057.
- [106] L. Pelà, E. Canella, K. Kasioumi, P. Roca, D. Marastoni, Complete experimental characterization of lime mortar and clay brick masonry, in: C. Modena, F. da Porto, M.R. Valluzzi (Eds.), *Brick Block Mason. - Trends, Innov. Challenges*, Taylor & Francis Group, 2016: pp. 1799–1806.
- [107] E. Sassoni, C. Mazzotti, G. Pagliai, Comparison between experimental methods for evaluating the compressive strength of existing masonry buildings, *Constr. Build. Mater.* 68 (2014) 206–219. doi:10.1016/j.conbuildmat.2014.06.070.

- [108] P. Matysek, T. Stryzewska, S. Kanka, Experimental research of masonry compressive strength in the Auschwitz II - Birkenau former death camp buildings, *Eng. Fail. Anal.* 68 (2016) 263–274.  
doi:10.1016/j.engfailanal.2016.06.007.
- [109] S. Jafari, R. Esposito, J. Rots, Literature review on the assessment of masonry properties by tests on core samples, in: W.J. Quist, S.J.C. Granneman, R.P.J. van Hees (Eds.), 4th WTA Int. PhD Symp., Vlaanderen, 2017: pp. 172–180.
- [110] L. Pelà, S. Saloustros, P. Roca, Cylindrical samples of brick masonry with aerial lime mortar under compression : Experimental and numerical study, 227 (2019) 11–13.  
doi:10.1016/j.conbuildmat.2019.116782.
- [111] M. De Fomento, DB SE-F Seguridad estructural: Fábrica, (2019).
- [112] ACI, ASCE, TMS, Commentary on Specification for Masonry Structures (ACI 530.1-02/ASCE 6-02/TMS 602-02), Main. (2004) 85.
- [113] H.K. Hilsdorf, Investigation into the failure mechanism of brick masonry loaded in axial compression. Designing, Engineering and Constructing with Masonry Products., Houston, Texas, 1969.
- [114] C.L. Khoo, A.W. Hendry, Strength tests on brick and mortar under complex stresses for the development of a failure criterion for brickwork in compression, *Proc Br Ceram Soc.* 21 (1973) 57–66.
- [115] A. Ohler, Zur berechnung der druckfestigkeit von mauerwerk unter berücksichtigung der mehrachsigen spannungszustände in stein und mortel, *Bautechnik.* 63 (1986) 163–168.
- [116] L. Binda, G. Mirabella Roberti, C. Tiraboschi, S. Abbaneo, Measuring Masonry Material Properties, U.S.-Italy Work. Guidel. Seism. Eval. Rehabil. Unreinforced Mason. Build. (1994) 326–347.  
doi:10.1017/CBO9781107415324.004.
- [117] M. Drdácý, Non-Standard Testing of Mechanical Characteristics of Historic Mortars, *Int. J. Archit. Herit.* 5 (2011) 383–394. doi:10.1080/15583051003717788.
- [118] L. Pelà, P. Roca, A. Aprile, Combined In-Situ and Laboratory Minor Destructive Testing of Historical Mortars, *Int. J. Archit. Herit.* 12 (2018) 334–349. doi:10.1080/15583058.2017.1323247.
- [119] American Society for Testing and Materials, ASTM E111 Standard Test Method for Young's Modulus , Tangent Modulus , and Chord Modulus, (2010). doi:10.1520/E0111-04R10.

- [120] L. Binda, I. Papayianni, E. Toumbakari, R.P.J. van Hees, Mechanical tests on mortars and assemblages, *Characterisation Old Mortars with Respect to Their Repair—Final Rep. RILEM TC 167–COM*. (2004) 57–76. doi:10.1617/2912143675.005.
- [121] L. Binda, C. Tiraboschi, Flat-Jack Test: A slightly destructive technique for the diagnosis of brick and stone masonry structures, *Int. J. Restor. Build. Monum.* 5 (1999) 449–472.  
<http://www.stru.polimi.it/home/binda/lav246.PDF>.
- [122] I. Lombillo, L. Villegas, J. Elices, Minor destructive techniques applied to the mechanical characterization of historical rubble stone masonry structures, *Struct. Surv.* 28 (2010) 53–70.  
doi:10.1108/02630801011040860.
- [123] A. Simões, R. Bento, A. Gago, M. Lopes, Mechanical Characterization of Masonry Walls With Flat-Jack Tests, *Exp. Tech.* (2015) n/a-n/a. doi:10.1111/ext.12133.
- [124] E. Cescatti, M. Dalla Benetta, C. Modena, F. Casarin, Analysis and evaluations of flat jack test on a wide existing masonry buildings sample, *Brick Block Mason. Trends, Innov. Challenges - Proc. 16th Int. Brick Block Mason. Conf. IBMAC 2016*. (2016) 1485–1492. doi:10.1201/b21889-184.
- [125] I. Lombillo, Investigación teórico-experimental sobre ensayos ligeramente destructivos (MDT) utilizados para la caracterización mecánica in situ de estructuras de fábrica del patrimonio construido, PhD Thesis, Universidad de Cantabria, 2010.
- [126] UIC, Leaflet 778-3R: Recommendations for the inspection, assessment and maintenance of masonry arch bridges, 1995.
- [127] A.M. Wolde-Tinsae, J. Colville, R.H. Najib, Modulus of elasticity of clay brick masonry, *9th Int. Brick Block Mason. Conf.* (1991) 1136–1143.
- [128] A. Drougkas, C. Molins, P. Roca, Numerical prediction of the behavior, strength and elasticity of masonry in compression, *Eng. Struct.* 90 (2015) 15–28. doi:10.1016/j.engstruct.2015.02.011.
- [129] FEMA/ASCE, FEMA 356. Prestandard and Commentary for the Seismic Rehabilitation of Buildings, *Rehabil. Requir.* (2000).
- [130] MBIE-NZSEE, The seismic assessment of existing buildings: Technical guidelines for engineering assessments. Section C8 – Unreinforced masonry buildings, (2017) 195. [www.eq-assess.org.nz/new-](http://www.eq-assess.org.nz/new-)

home/part-c/c8/%0Ahttp://www.eq-assess.org.nz/dsa-epb/.

- [131] G.N. Pande, J.X. Liang, J. Middleton, Equivalent elastic moduli for brick masonry, *Comput. Geotech.* 8 (1989) 243–265. doi:10.1016/0266-352X(89)90045-1.
- [132] N. Makoond, L. Pelà, C. Molins, Dynamic elastic properties of brick masonry constituents, *Constr. Build. Mater.* 199 (2019) 756–770. doi:10.1016/j.conbuildmat.2018.12.071.
- [133] N. Makoond, A. Cabané, L. Pelà, C. Molins, Relationship between the static and dynamic elastic modulus of brick masonry constituents, *Constr. Build. Mater.* 259 (2020) 120386. doi:10.1016/j.conbuildmat.2020.120386.
- [134] P. Jukes, An investigation into the shear strength of masonry joints, PhD Thesis, University of Sussex, 1997.
- [135] European Committee for Standardization (CEN), EN 1052-3 Methods of test for masonry - Part 3: Determination of initial shear strength, (2007).
- [136] RILEM, MS-B.4 - Determination of shear strength index for masonry unit/mortar junction, *Mater. Struct.* 29 (1996) 459–463.
- [137] New Zealand Society for Earthquake Engineering, Assessment and improvement of the structural performance of buildings in earthquakes, 2006.
- [138] J.R. Riddington, K.H. Fong, P. Jukes, Numerical study of failure initiation in different joint shear tests, *Mason. Int.* 11 (1997) 44–50.
- [139] D.-H. Jiang, X.-S. Xiao, A New Masonry Shear Test Method Determining, in: 10th Int. Brick Block Mason. Conf., 1994: pp. 1013–1020.
- [140] G. Andreotti, F. Graziotti, G. Magenes, Expansion of mortar joints in direct shear tests of masonry samples: implications on shear strength and experimental characterization of dilatancy, *Mater. Struct. Constr.* 52 (2019) 1–16. doi:10.1617/s11527-019-1366-5.
- [141] S. Zhang, N. Richart, K. Beyer, Numerical evaluation of test setups for determining the shear strength of masonry, *Mater. Struct. Constr.* 51 (2018) 1–12. doi:10.1617/s11527-018-1236-6.
- [142] S. Stöckl, P. Hofmann, Tests on the shear bond behaviour in the bed-joints of masonry, in: J. De Courzy (Ed.), 8th Int. Brick Block Mason. Conf., Elsevier, 1986: pp. 292–303.

- [143] P. Roca, G. Araiza, Shear response of brick masonry small assemblages strengthened with bonded FRP laminates for in-plane reinforcement, *Constr. Build. Mater.* 24 (2010) 1372–1384.  
doi:10.1016/j.conbuildmat.2010.01.005.
- [144] R. Van Der Pluijm, Shear behaviour of bed joints, in: 6th North Am. Mason. Conf., 1993: pp. 125–136.
- [145] L. Pelà, K. Kasioumi, P. Roca, Experimental evaluation of the shear strength of aerial lime mortar brickwork by standard tests on triplets and non-standard tests on core samples, *Eng. Struct.* 136 (2017) 441–453. doi:10.1016/j.engstruct.2017.01.028.
- [146] C. Calderini, S. Cattari, S. Lagomarsino, The use of the diagonal compression test to identify the shear mechanical parameters of masonry, *Constr. Build. Mater.* 24 (2010) 677–685.  
doi:10.1016/j.conbuildmat.2009.11.001.
- [147] American Society for Testing and Materials, ASTM C1531 Standard test methods for in situ measurement of masonry mortar joint shear strength index, (2016).
- [148] RILEM, MS-D.6 - In situ measurement of masonry bed joint shear strength, *Mater. Struct.* 29 (1996) 470–475. doi:10.1007/bf02486276.
- [149] F. Graziotti, G. Guerrini, A. Rossi, G. Andreotti, G. Magenes, Proposal for an Improved Procedure and Interpretation of ASTM C1531 for the In Situ Determination of Brick-Masonry Shear Strength, *ASTM Int.* (2018) 13–33. doi:10.1520/stp161220170181.
- [150] F. Ferretti, S. Jafari, R. Esposito, J.G. Rots, C. Mazzotti, Investigation of the shear-sliding behavior of masonry through shove test: experimental and numerical studies, in: R. Aguilar (Ed.), *Struct. Anal. Hist. Constr.*, RILEM Bookseries, 2019: pp. 523–531. doi:10.1007/978-3-319-99441-3.
- [151] D. Marastoni, L. Pelà, A. Benedetti, P. Roca, Combining Brazilian Tests on masonry cores and Double Punch Tests for the mechanical characterization of historical mortars, *Constr. Build. Mater.* 112 (2016) 112–127. doi:10.1016/j.conbuildmat.2016.02.168.
- [152] A. Benedetti, L. Pelà, Experimental Characterization of Mortar By Testing on Small Specimens, 15th Int. Brick Block Mason. Conf. (2012).
- [153] C. Mazzotti, E. Sassoni, G. Pagliai, Determination of shear strength of historic masonries by moderately destructive testing of masonry cores, *Constr. Build. Mater.* 54 (2014) 421–431.

- doi:10.1016/j.conbuildmat.2013.12.039.
- [154] S. Jafari, J.G. Rots, R. Esposito, Core testing method to assess nonlinear shear-sliding behaviour of brick-mortar interfaces: A comparative experimental study, *Constr. Build. Mater.* 244 (2020) 118236. doi:10.1016/j.conbuildmat.2020.118236.
- [155] F. Ferretti, B. Ferracuti, C. Mazzotti, M. Savoia, Destructive and minor destructive tests on masonry buildings: Experimental results and comparison between shear failure criteria, *Constr. Build. Mater.* 199 (2019) 12–29. doi:10.1016/j.conbuildmat.2018.11.246.
- [156] ASTM, ASTM E519/E519M - 10. Standard Test Method for Diagonal Tension (Shear) in Masonry Assemblages, (2010).
- [157] RILEM, LUMB6 Diagonal tensile strength tests of small wall specimens, (1991).
- [158] COGUANOR, Método de ensayo. Determinación de la tracción diagonal (corte) en ensamblajes de mampostería, (2012).
- [159] I.N. de Normalización, NCh 2123 Albañilería confinada. Requisitos de diseño y cálculo, (2003).
- [160] M.M. Frocht, Recent advances in photoelasticity and an investigation of the stress distribution in square blocks subjected to diagonal compression, *Trans. Am. Soc. Mech. Eng.* 53 (1931) 135–153.
- [161] F.Y. Yokel, S.G. Fattal, A failure hypothesis for masonry shearwalls, 1975.
- [162] A. Brignola, S. Frumento, S. Lagomarsino, S. Podestà, Identification of Shear Parameters of Masonry Panels Through the In-Situ Diagonal Compression Test, *Int. J. Archit. Herit.* 3 (2008) 52–73. doi:10.1080/15583050802138634.
- [163] S. Chiostrini, L. Galano, A. Vignoli, On the Determination of Strength of Ancient Masonry Walls via Experimental Tests, 12th World Conf. Earthq. Eng. (2000) 1–8. <http://www.iitk.ac.in/nicee/wcee/article/2564.pdf>.
- [164] A. Borri, G. Castori, M. Corradi, E. Speranzini, Shear behavior of unreinforced and reinforced masonry panels subjected to in situ diagonal compression tests, *Constr. Build. Mater.* 25 (2011) 4403–4414. doi:10.1016/j.conbuildmat.2011.01.009.
- [165] H. Mahmood, J.M. Ingham, Diagonal Compression Testing of FRP-Retrofitted Unreinforced Clay Brick Masonry Wallettes, *J. Compos. Constr.* 15 (2011) 810–820. doi:10.1061/(ASCE)CC.1943-

- 5614.0000209.
- [166] N. Gattesco, I. Boem, A. Dudine, Diagonal compression tests on masonry walls strengthened with a GFRP mesh reinforced mortar coating, *Bull. Earthq. Eng.* 13 (2015) 1703–1726. doi:10.1007/s10518-014-9684-z.
- [167] X. Wang, C.C. Lam, V.P. Iu, Comparison of different types of TRM composites for strengthening masonry panels, *Constr. Build. Mater.* 219 (2019) 184–194. doi:10.1016/j.conbuildmat.2019.05.179.
- [168] L. Garcia-Ramonda, L. Pelà, P. Roca, G. Camata, In-plane shear behaviour by diagonal compression testing of brick masonry walls strengthened with basalt and steel textile reinforced mortars, *Constr. Build. Mater.* 240 (2020) 117905. doi:10.1016/j.conbuildmat.2019.117905.
- [169] F. Parisi, I. Iovinella, A. Balsamo, N. Augenti, A. Prota, In-plane behaviour of tuff masonry strengthened with inorganic matrix-grid composites, *Compos. Part B Eng.* 45 (2013) 1657–1666. doi:10.1016/j.compositesb.2012.09.068.
- [170] V. Turnšek, F. Čačovič, Some experimental results on the strength of brick masonry walls, *Proc. 2nd Int. Brick Mason. Conf.* (1971) 149–156. doi:10.1111/j.1365-2664.2009.01609.x.
- [171] L. Malyszko, In-plane shear and tensile strength test of small brickwork specimens, in: C. Modena, P.B. Lourenço, P. Roca (Eds.), *Struct. Anal. Hist. Constr.*, 2005: pp. 291–298.
- [172] V.Z. Bosiljkov, Y.Z. Totoev, J.M. Nichols, Shear modulus and stiffness of brickwork masonry: An experimental perspective, *Struct. Eng. Mech.* 20 (2005) 21–43. doi:10.12989/sem.2005.20.1.021.
- [173] P. Croce, M.L. Beconcini, P. Formichi, P. Cioni, F. Landi, C. Mochi, F. De Lellis, E. Mariotti, I. Serra, Shear modulus of masonry walls: A critical review, *Procedia Struct. Integr.* 11 (2018) 339–346. doi:10.1016/j.prostr.2018.11.044.
- [174] F. Autiero, G. De Martino, M. Di Ludovico, A. Prota, Mechanical performance of full-scale Pompeii-like masonry panels, *Constr. Build. Mater.* 251 (2020) 118964. doi:10.1016/j.conbuildmat.2020.118964.
- [175] R. Esposito, F. Messali, G.J.P. Ravenshorst, H.R. Schipper, J.G. Rots, Seismic assessment of a lab-tested two-storey unreinforced masonry Dutch terraced house, *Bull. Earthq. Eng.* 17 (2019) 4601–4623. doi:10.1007/s10518-019-00572-w.
- [176] D. García, J.T. San-José, L. Garmendia, R. San-Mateos, D. Garcia, J.T. San-Jose, L. Garmendia, R. San-

- Mateos, Experimental study of traditional stone masonry under compressive load and comparison of results with design codes, *Mater. Struct.* 45 (2012) 995–1006. doi:10.1617/s11527-011-9812-z.
- [177] R. Lumantarna, Material characterisation of New Zealand's clay brick unreinforced masonry buildings, PhD Thesis, The University of Auckland, 2012.
- [178] M.R. Valluzzi, F. Porto, C. Modena, Behaviour of multi-leaf stone masonry walls strengthened by different intervention techniques, *Hist. Constr.* (2001) 1023–1032.  
[http://www.civil.uminho.pt/masonry/Publications/Historical constructions/page 1023-1032 \\_89\\_.pdf](http://www.civil.uminho.pt/masonry/Publications/Historical%20constructions/page%201023-1032_%2089_.pdf).
- [179] N. Domède, G. Pons, A. Sellier, Y. Fritih, Mechanical behaviour of ancient masonry, *Mater. Struct.* 42 (2009) 123–133. doi:10.1617/s11527-008-9372-z.
- [180] Y. Boffill, H. Blanco, I. Lombillo, L. Villegas, Assessment of historic brickwork under compression and comparison with available equations, *Constr. Build. Mater.* 207 (2019) 258–272.  
doi:10.1016/j.conbuildmat.2019.02.083.
- [181] C. Knox, Assessment of Perforated Unreinforced Masonry Walls Responding In Plane, PhD Thesis, The University of Auckland, 2012.
- [182] P. Hauková, D. Frankeová, Z. Slízková, Characterisation of historic mortars for conservation diagnosis, in: J. Válek, J.J. Hughes, C.J.W.P. Groot (Eds.), *Hist. Mortars*, 2019: pp. 109–118.
- [183] J. Weber, T. Köberle, F. Pintér, Methods of microscopy to identify and characterise hydraulic binders in historic mortars - A methodological approach, in: J. Válek, J.J. Hughes, C.J.W.P. Groot (Eds.), *Hist. Mortars*, 2019: pp. 21–32.
- [184] C. Marinowitz, C. Nuewald-Burg, M. Pfeifer, Historic documents in understanding and evaluation of historic lime mortars, in: J. Válek, J.J. Hughes, C.J.W.P. Groot (Eds.), *Hist. Mortars*, 2012: pp. 15–24.
- [185] R.L. Bonett Díaz, Vulnerabilidad y riesgo sísmico de edificios. Aplicación a entornos urbanos en zonas de amenaza alta y moderada, PhD Thesis. Universitat Politècnica de Catalunya, 2003.
- [186] R. Moreno-González, Evaluación del riesgo sísmico en edificios mediante análisis estático no lineal: Aplicación a diversos escenarios sísmicos de Barcelona, PhD Thesis. Universitat Politècnica de Catalunya, 2006.
- [187] N. Lantada Zarzosa, Evaluación del riesgo sísmico mediante métodos avanzados y técnicas GIS.

- Aplicación a la ciudad de Barcelona., PhD Thesis, Universitat Politècnica de Catalunya, 2009.  
<http://www.tdx.cat/handle/10803/6259>.
- [188] R. Moreno-González, J.M. Bairán, Análisis del comportamiento sísmico de los edificios de obra de fábrica, típicos del distrito Eixample de Barcelona, *Inf. La Constr.* 63 (2011) 21–32.  
doi:10.3989/ic.10.045.
- [189] L.G. Pujades, A.H. Barbat, R. González-Drigo, J. Avila, S. Lagomarsino, Seismic performance of a block of buildings representative of the typical construction in the Eixample district in Barcelona (Spain), *Bull. Earthq. Eng.* 10 (2012) 331–349. doi:10.1007/s10518-010-9207-5.
- [190] R. Gonzalez-Drigo, A. Avila-Haro, A.H. Barbat, L.G. Pujades, Y.F. Vargas, S. Lagomarsino, S. Cattari, Modernist unreinforced masonry (URM) buildings of barcelona: Seismic vulnerability and risk assessment, *Int. J. Archit. Herit.* 9 (2015) 214–230. doi:10.1080/15583058.2013.766779.
- [191] R. Gonzalez-Drigo, J. Avila-Haro, L.G. Pujades, A.H. Barbat, Non-linear static procedures applied to high-rise residential URM buildings, *Bull. Earthq. Eng.* 15 (2017) 149–174. doi:10.1007/s10518-016-9951-2.
- [192] J.C. Jiménez Pacheco, Evaluación sísmica de edificios de mampostería no reforzada típicos de Barcelona: modelización y revisión de la aplicación del Método del Espectro de Capacidad, PhD Thesis, Universitat Politècnica de Catalunya, 2016.
- [193] J. Jiménez-Pacheco, R. González-Drigo, L.G. Pujades Beneit, A.H. Barbat, J. Calderón-Brito, Traditional High-rise Unreinforced Masonry Buildings: Modeling and Influence of Floor System Stiffening on Their Overall Seismic Response, *Int. J. Archit. Herit.* 00 (2020) 1–38.  
doi:10.1080/15583058.2019.1709582.
- [194] S. Cara, A. Aprile, L. Pelà, P. Roca, Seismic Risk Assessment and Mitigation at Emergency Limit Condition of Historical Buildings along Strategic Urban Roadways. Application to the “Antiga Esquerra de L’Eixample” Neighborhood of Barcelona, *Int. J. Archit. Herit.* 12 (2018) 1055–1075.  
doi:10.1080/15583058.2018.1503376.
- [195] J. Rosell i Colomina, La Construcció en l’arquitectura de Barcelona a finals del segle XVIII, PhD Thesis. Universitat Politècnica de Catalunya, 1996. <http://www.tesisenred.net/handle/10803/6101>.

- [196] C. Cornadó, Comportament mecànic-estructural dels edificis històrics de murs d'obra de fàbrica de maó de l'Eixample de Barcelona, PhD dissertation, Universitat Politècnica de Catalunya, 2015.
- [197] A. Paricio Casademunt, *Secrets d'un sistema constructiu. L'Eixample*, Edicions UPC, 2001.
- [198] C. Rieger, M. Benavente (Transl.), *Elementos de toda la arquitectura civil*, 1763.  
[http://www.sedhc.es/bibliotecaD/1763\\_Ch\\_Rieger\\_Elementos\\_de\\_toda\\_la\\_arquitectura\\_civil.pdf](http://www.sedhc.es/bibliotecaD/1763_Ch_Rieger_Elementos_de_toda_la_arquitectura_civil.pdf).
- [199] M. Fornés Gurrea, *Observaciones sobre la práctica del arte de edificar*, 1841.
- [200] P.C. Espinosa, *Manual de construcciones de albañilería*, 1859.
- [201] R. Marcos Bausá, *Manual del albañil*, 1879.  
[http://www.cehopu.cedex.es/img/bibliotecaD/1879\\_Ricardo\\_Marcos\\_y\\_Bausa\\_Manual\\_del\\_albanil](http://www.cehopu.cedex.es/img/bibliotecaD/1879_Ricardo_Marcos_y_Bausa_Manual_del_albanil).
- [202] F. Ger Lobe, *Tratado de construcción civil*, 1898.
- [203] E. Barberot, L. Álvarez Valdés (Transl.), *Tratado práctico de Edificación*, 1927.
- [204] J.M. Adell Argilés, *La arquitectura de ladrillos del siglo XIX: Racionalidad y modernidad*, *Inf. La Construcción*. 44 (1992) 5–15. <http://informesdelaconstruccion.revistas.csic.es>.
- [205] J.M. Montaner, *Antiga arquitectura industrial per a la ciutat contemporània*, *Barcelona Soc.* (2010) 49–54.
- [206] R. Lacuesta, *Arquitectura industrial catalana en el darrer quart del segle XIX i primer quart del segle XX*, *Catalan Hist. Rev.* 187 (2017) 175–187. doi:10.2436/20.1000.01.139.
- [207] P. Hereu, J. Oliveras, A. Paricio, C. Rodríguez, M. Rosselló, J. Serra, *El Teixit residencial en la formació de la metròpolis moderna: el cas de Barcelona (1840-1936)*. Vol. 2, *Les operacions de creació d'habitatge dins l'Eixample (1860-1936)*, *Iniciativa Digital Politècnica*, 2015.
- [208] V. Rodríguez Fornós, *Del forn a la bòbila. La fabricació de material d'obra al terme de Gavà (Baix Llobregat)*, *Centre d'Estudis de Gavà*, 2018.
- [209] G. Magenes, A. Penna, A. Galasco, M. Rota, *Experimental characterisation of stone masonry mechanical properties*, in: *8th Int. Mason. Conf.*, 2010: pp. 247–256.
- [210] G. Guerrini, I. Senaldi, S. Scherini, S. Morganti, G. Magenes, K. Beyer, A. Penna, *Material Characterization for the Shaking-Table Test of the Scaled Prototype of a Stone Masonry Building*

- Aggregate, in: Proc. XVII Convegno ANIDIS "L'Ingegneria Sismica Ital.", 2017.
- [211] J. Lanas, J.L. Pérez Bernal, M.A. Bello, J.I. Álvarez Galindo, Mechanical properties of natural hydraulic lime-based mortars, *Cem. Concr. Res.* 34 (2004) 2191–2201. doi:10.1016/j.cemconres.2004.02.005.
- [212] R.G. Blezard, The History of Calcareous Cements, in: P. Hewlett (Ed.), *Lea's Chem. Cem. Concr.*, Fourth Edi, Elsevier Ltd., 2003: pp. 1–23. doi:10.1016/B978-0-7506-6256-7.50013-8.
- [213] D. Krivánková, C.L. Nunes, Z. Slízková, D. Frankeová, K. Niedoba, High-Performance Repair Mortars for Application in Severe Weathering Environments : Frost Resistance Assessment, in: J.J. Hughes, J. Válek, C.J.W.P. Groot (Eds.), *Hist. Mortars*, Springer International, 2019: pp. 155–168.
- [214] C.J.W.P. Groot, J.T.M. Gunneweg, Choosing Mortar Compositions for Repointing of Historic Masonry Under Severe Environmental Conditions, in: J.J. Hughes, J. Válek, C.J.W.P. Groot (Eds.), *Hist. Mortars*, Springer International, 2019: pp. 143–154.
- [215] R. Veiga, Air lime mortars : What else do we need to know to apply them in conservation and rehabilitation interventions ? A review, *Constr. Build. Mater.* 157 (2017) 132–140. doi:10.1016/j.conbuildmat.2017.09.080.
- [216] D. Gulotta, S. Goidanich, C. Tedeschi, T.G. Nijland, L. Toniolo, Commercial NHL-containing mortars for the preservation of historical architecture . Part 1 : Compositional and mechanical characterisation, *Constr. Build. Mater.* 38 (2013) 31–42. doi:10.1016/j.conbuildmat.2012.08.029.
- [217] M.R. Veiga, A. Fragata, A.L. Velosa, A.C. Magalhaes, G. Margalha, Lime-Based Mortars : Viability for Use as Substitution Renders in Historical Buildings, *Int. J. Archit. Herit.* 4 (2010) 177–195. doi:10.1080/15583050902914678.
- [218] A. Kalagri, I. Karatasios, V. Kilikoglou, The effect of aggregate size and type of binder on microstructure and mechanical properties of NHL mortars, *Constr. Build. Mater.* 53 (2014) 467–474. doi:10.1016/j.conbuildmat.2013.11.111.
- [219] S. Pavia, O. Brennan, Portland Cement-Lime Mortars for Conservation, in: J.J. Hughes, J. Válek, C.J.W.P. Groot (Eds.), *Hist. Mortars*, Springer International, 2019: pp. 129–142.
- [220] P. Maravelaki-Kalaitzaki, A. Bakolas, I. Karatasios, V. Kilikoglou, Hydraulic lime mortars for the restoration of historic masonry in Crete, *Cem. Concr. Res.* 35 (2005) 1577–1586.

- doi:10.1016/j.cemconres.2004.09.001.
- [221] P. Faria, V. Silva, Natural Hydraulic Lime Mortars : Influence of the Aggregates, in: J.J. Hughes, J. Válek, C.J.W.P. Groot (Eds.), *Hist. Mortars*, Springer International, 2019: pp. 185–199.
- [222] R. Hanley, S. Pavia, A study of the workability of natural hydraulic lime mortars and its influence on strength, *Mater. Struct.* 41(2) (2008) 373–381. doi:10.1617/s11527-007-9250-0.
- [223] B.A. Silva, A.P. Ferreira Pinto, A. Gomes, Natural hydraulic lime versus cement for blended lime mortars for restoration works, *Constr. Build. Mater.* 94 (2015) 346–360.  
doi:10.1016/j.conbuildmat.2015.06.058.
- [224] C. Torney, A.M. Forster, P.F.G. Banfill, E.M. Szadurski, The effects of site practice on the physical properties of proprietary stone restoration mortar, *Constr. Build. Mater.* 75 (2015) 359–367.  
doi:10.1016/j.conbuildmat.2014.11.040.
- [225] D. Gulotta, S. Goidanich, C. Tedeschi, L. Toniolo, Commercial NHL-containing mortars for the preservation of historical architecture. Part 2: Durability to salt decay, *Constr. Build. Mater.* 96 (2015) 198–208. doi:10.1016/j.conbuildmat.2015.08.006.
- [226] P. Lopez-Arce, M. Tagnit-Hammou, B. Menendez, J.D. Mertz, M. Guiavarc’h, A. Kaci, S. Aggoun, A. Cousture, Physico-chemical stone-mortar compatibility of commercial stone-repair mortars of historic buildings from Paris, *Constr. Build. Mater.* 124 (2016) 424–441.  
doi:10.1016/j.conbuildmat.2016.07.076.
- [227] L. Gil, E. Bernat-Masó, F. Cañavate, Changes in Properties of Cement and Lime Mortars When Incorporating Fibers from End-of-Life Tires, *Fibers.* 4 (2016) 7. doi:10.3390/fib4010007.
- [228] F. Iucolano, B. Liguori, D. Caputo, F. Colangelo, R. Cioffi, Recycled plastic aggregate in mortars composition: Effect on physical and mechanical properties, *Mater. Des.* 52 (2013) 916–922.  
doi:10.1016/j.matdes.2013.06.025.
- [229] J. Grilo, A.S. Silva, P. Faria, A. Gameiro, R. Veiga, A. Velosa, Mechanical and mineralogical properties of natural hydraulic lime-metakaolin mortars in different curing conditions, *Constr. Build. Mater.* 51 (2014) 287–294. doi:10.1016/j.conbuildmat.2013.10.045.
- [230] B. Liguori, D. Caputo, F. Iucolano, Fiber-reinforced lime-based mortars : Effect of zeolite addition,

- Constr. Build. Mater. 77 (2015) 455–460. doi:10.1016/j.conbuildmat.2014.12.067.
- [231] S. Xu, J. Wang, Q. Jiang, S. Zhang, Study of natural hydraulic lime-based mortars prepared with masonry waste powder as aggregate and diatomite / fly ash as mineral admixtures, *J. Clean. Prod.* 119 (2016) 118–127. doi:10.1016/j.jclepro.2016.01.069.
- [232] M.M. Barbero-Barrera, N. Flores Medina, C. Guardia-Martín, Influence of the addition of waste graphite powder on the physical and microstructural performance of hydraulic lime pastes, *Constr. Build. Mater.* 149 (2017) 599–611. doi:10.1016/j.conbuildmat.2017.05.156.
- [233] S. Thirumalini, R. Ravi, M. Rajesh, Experimental investigation on physical and mechanical properties of lime mortar : Effect of organic addition, *J. Cult. Herit.* 31 (2018) 97–104. doi:10.1016/j.culher.2017.10.009.
- [234] R. Ravi, T. Selvaraj, S.K. Sekar, Characterization of Hydraulic Lime Mortar Containing *Opuntia ficus-indica* as a Bio-Admixture for Restoration Applications, *Int. J. Archit. Herit.* 10 (2016) 714–725. doi:10.1080/15583058.2015.1109735.
- [235] Y. Benachour, C.A. Davy, F. Skoczylas, H. Houari, Effect of a high calcite filler addition upon microstructural, mechanical, shrinkage and transport properties of a mortar, *Cem. Concr. Res.* 38 (2008) 727–736. doi:10.1016/j.cemconres.2008.02.007.
- [236] M. Galetakis, G. Alevizos, K. Leventakis, Evaluation of fine limestone quarry by-products, for the production of building elements - An experimental approach, *Constr. Build. Mater.* 26 (2012) 122–130. doi:10.1016/j.conbuildmat.2011.05.011.
- [237] D. Manning, Exploitation and Use of Quarry Fines. Report No. 087/MIST2/DACM/01, Mineral Solutions, 2004.
- [238] E. Petavratzi, S. Wilson, Sustainable utilisation of quarry by-products, *Sustainable Aggregates*, 2008.
- [239] A.K.H. Kwan, S.K. Ling, Filler technology for improving robustness and reducing cementitious paste volume of SCC, *Constr. Build. Mater.* 153 (2017) 875–885. doi:10.1016/j.conbuildmat.2017.07.160.
- [240] M. Gesoglu, E. Güneysi, M.E. Kocabag, V. Bayram, K. Mermerdas, Fresh and hardened characteristics of self compacting concretes made with combined use of marble powder, limestone filler, and fly ash, *Constr. Build. Mater.* 37 (2012) 160–170. doi:10.1016/j.conbuildmat.2012.07.092.

- [241] E. Bacarji, R.D.T. Filho, E.A.B. Koenders, E.P. Figueiredo, J.L.M.P. Lopes, Sustainability perspective of marble and granite residues as concrete fillers, *Constr. Build. Mater.* 45 (2013) 1–10. doi:10.1016/j.conbuildmat.2013.03.032.
- [242] V. Bonavetti, H. Donza, G. Menéndez, O. Cabrera, E.F. Irassar, Limestone filler cement in low w / c concrete : A rational use of energy, *Cem. Concr. Res.* 33 (2003) 865–871. doi:10.1016/S0008-8846(02)01087-6.
- [243] M. Bederina, Z. Makhloufi, T. Bouziani, Effect of limestone fillers the physic-mechanical properties of limestone concrete, *Phys. Procedia.* 21 (2011) 28–34. doi:10.1016/j.phpro.2011.10.005.
- [244] B. Menadi, S. Kenai, J. Khatib, A. Aït-Mokhtar, Strength and durability of concrete incorporating crushed limestone sand, *Constr. Build. Mater.* 23 (2009) 625–633. doi:10.1016/j.conbuildmat.2008.02.005.
- [245] F.M. Lea, *The chemistry of cement and concrete* 3rd ed., Chemical Publishing Co. Inc., 1971.
- [246] I. Soroka, N. Stern, Calcareous fillers and the compressive strength of portland cement, *Cem. Concr. Res.* 6 (1976) 367–376. doi:10.1016/0008-8846(76)90099-5.
- [247] R.F. Feldman, V.S. Ramachandran, P.J. Sereda, Influence of CaCO<sub>3</sub> on the hydration of 3CaO·Al<sub>2</sub>O<sub>3</sub>, *J. Am. Ceram. Soc.* 48 (1965) 25–30.
- [248] D. Wang, C. Shi, N. Farzadnia, Z. Shi, H. Jia, Z. Ou, A review on use of limestone powder in cement-based materials : Mechanism, hydration and microstructures, *Constr. Build. Mater.* 181 (2018) 659–672. doi:10.1016/j.conbuildmat.2018.06.075.
- [249] B. Benabed, H. Soualhi, B. Ase, L. Azzouz, E. Kadri, S. Kenai, Effect of limestone powder as a partial replacement of crushed quarry sand on properties of self-compacting repair mortars, *J. Build. Mater. Struct.* 3 (2016) 15–30.
- [250] M. Aqel, D.K. Panesar, Hydration kinetics and compressive strength of steam-cured cement pastes and mortars containing limestone filler, *Constr. Build. Mater.* 113 (2016) 359–368. doi:10.1016/j.conbuildmat.2016.03.031.
- [251] A. Fragata, R. Veiga, *Air Lime Mortars : The Influence of Calcareous Aggregate and Filler Addition*, *Mater. Sci. Forum.* 636–637 (2010) 1280–1285. doi:10.4028/www.scientific.net/MSF.636-637.1280.

- [252] T. Skoulidis, D. Charalambous, K. Tsakona, Amelioration of the properties of hydrated lime for the consolidation of the surface or/and the mass of building materials of monuments or new buildings or statures and ornaments, in: 8th Int. Congr. Deterior. Conserv. Stone, 1996: pp. 1599–1605.
- [253] A.M. Forster, N. Razali, P. Banfill, E. Szadurski, C. Torney, The influence of calcitic filler in hydraulic lime mortars for use in high temperature and high humidity climatic conditions : A preliminary investigation, in: J.J. Hughes, J. Válek, C. Groot (Eds.), *Hist. Mortars*, Springer International, 2019: pp. 201–211. doi:<https://doi.org/10.1007/978-3-319-91606-4>.
- [254] European Committee for Standardization (CEN), EN 459-1 Building lime - Part 1: Definitions, specifications and conformity criteria, (2010).
- [255] European Committee for Standardization (CEN), EN 933-1 Test for geometrical properties of aggregates - Part 1: Determination of particle size distribution. Sieving method, (1997).
- [256] European Committee for Standardization (CEN), EN 1015-3 Methods of test for mortar for masonry - Part 3: Determination of consistence of fresh mortar (by flow table), (1999).
- [257] European Committee for Standardization (CEN), EN 1015-11 Methods of test for mortar for masonry - Part 11: Determination of flexural and compressive strength of hardened mortar, (1999).
- [258] European Committee for Standardization (CEN), EN 196-1 Methods of testing cement - Part 1: Determination of strength, (2005).
- [259] A. Moropoulou, A. Bakolas, P. Moundoulas, E. Aggelakopoulou, S. Anagnostopoulou, Strength development and lime reaction in mortars for repairing historic masonries, *Cem. Concr. Compos.* 27 (2005) 289–294. doi:[10.1016/j.cemconcomp.2004.02.017](https://doi.org/10.1016/j.cemconcomp.2004.02.017).
- [260] A. Costigan, An experimental study of the physical properties of lime mortar and their effect on lime-mortar masonry, PhD dissertation, University of Dublin, 2013.
- [261] G. Allen, *Hydraulic lime mortar for stone, brick and block masonry*, Routledge, 2003. doi:<https://doi.org/10.4324/9781315781273>.
- [262] B.A. Silva, A.P. Ferreira Pinto, A. Gomes, Influence of natural hydraulic lime content on the properties of aerial lime-based mortars, *Constr. Build. Mater.* 72 (2014) 208–218. doi:[10.1016/j.conbuildmat.2014.09.010](https://doi.org/10.1016/j.conbuildmat.2014.09.010).

- [263] N. Copsey, Hiding in plain sight: hot mixed lime mortars, *Loggia*. 28 (2015) 118–131.
- [264] M. Apostolopoulou, E.T. Delegou, E. Alexakis, M. Kalofonou, K.C. Lampropoulos, E. Aggelakopoulou, A. Bakolas, A. Moropoulou, Study of the historical mortars of the Holy Aedicule as a basis for the design , application and assessment of repair mortars : A multispectral approach applied on the Holy Aedicule, *Constr. Build. Mater.* 181 (2018) 618–637. doi:10.1016/j.conbuildmat.2018.06.016.
- [265] F. Parisi, N. Augenti, A. Prota, Implications of the spandrel type on the lateral behavior of unreinforced masonry walls, *Earthq. Eng. Struct. Dyn.* 43 (2014) 1867–1887. doi:10.1002/eqe.2441.
- [266] G. Rinaldin, C. Amadio, N. Gattesco, Review of experimental cyclic tests on unreinforced and strengthened masonry spandrels and numerical modelling of their cyclic behaviour, *Eng. Struct.* 132 (2017) 609–623. doi:10.1016/j.engstruct.2016.11.063.
- [267] C.L. Knox, D. Dizhur, J.M. Ingham, Two-Story Perforated URM Wall Subjected to Cyclic In-Plane Loading, *J. Struct. Eng.* 144 (2018) 04018037. doi:10.1061/(asce)st.1943-541x.0002021.
- [268] J. Segura, L. Pelà, P. Roca, Monotonic and cyclic testing of clay brick and lime mortar masonry in compression, *Constr. Build. Mater.* 193 (2018) 453–466. doi:10.1016/j.conbuildmat.2018.10.198.
- [269] N. Shetty, G. Livitsanos, N. Van Roy, D.G. Aggelis, D. Van Hemelrijck, M. Wevers, E. Verstryngge, Quantification of progressive structural integrity loss in masonry with Acoustic Emission-based damage classification, *Constr. Build. Mater.* 194 (2019) 192–204. doi:10.1016/j.conbuildmat.2018.10.215.
- [270] J. Segura, L. Pelà, P. Roca, A. Cabané, Experimental analysis of the size effect on the compressive behaviour of cylindrical samples core-drilled from existing brick masonry, *Constr. Build. Mater.* 228 (2019) 116759. doi:10.1016/j.conbuildmat.2019.116759.
- [271] A.W. Hendry, B.P. Sinha, S.R. Davies, *Design of masonry structures*, 3rd ed., Taylor & Francis, 2004.
- [272] P.B. Lourenco, Masonry structures, overview, in: *Encycl. Earthq. Eng.*, Springer-Verlag Berlin Heidelberg, 2014: pp. 1–9. doi:10.1007/978-3-642-36197-5\_111-1.
- [273] P.B. Lourenço, F. Fernandes, F. Castro, Handmade clay bricks: chemical, physical and mechanical properties., *Int. J. Archit. Herit.* 4 (2009) 38–58.
- [274] G. López-Patiño, J.M. Adam, P. Verdejo Gimeno, G. Milani, Causes of damage to industrial brick masonry chimneys, *Eng. Fail. Anal.* 74 (2017) 188–201. doi:10.1016/j.engfailanal.2017.01.014.

- [275] A.P. Russell, J.M. Ingham, Prevalence of New Zealand ' S Unreinforced Masonry Buildings, *Bull. New Zeal. Soc. Earthq. Eng.* 43 (2010) 182–202.
- [276] L.S. Hogan, I. Giongo, K.Q. Walsh, J.M. Ingham, D. Dizhur, Full-scale Experimental Pushover Testing of an Existing URM Building, *Structures*. 15 (2018) 66–81. doi:10.1016/j.istruc.2018.04.007.
- [277] M. Ispir, A. Ilki, Behavior of Historical Unreinforced Brick Masonry Walls under Monotonic and Cyclic Compression, *Arab. J. Sci. Eng.* 38 (2013) 1993–2007. doi:10.1007/s13369-013-0567-4.
- [278] A. Amirzadeh, R.K. Strand, R.E. Hammann, M.S. Bhandari, Determination and Assessment of Optimum Internal Thermal Insulation for Masonry Walls in Historic Multifamily Buildings, *J. Archit. Eng.* 24 (2018) 1–12. doi:10.1061/(ASCE)AE.1943-5568.0000320.
- [279] D. Liberatore, A. Marotta, L. Sorrentino, Estimation of solid clay brick unreinforced masonry compressive strength based on mortar and unit mechanical parameters, in: 9th Int. Mason. Conf., Guimaraes, 2014: pp. 1715–1722.  
[http://www.researchgate.net/publication/277139966\\_Estimation\\_of\\_solid\\_clay\\_brick\\_unreinforced\\_masonry\\_compressive\\_strength\\_based\\_on\\_mortar\\_and\\_unit\\_mechanical\\_parameters](http://www.researchgate.net/publication/277139966_Estimation_of_solid_clay_brick_unreinforced_masonry_compressive_strength_based_on_mortar_and_unit_mechanical_parameters).
- [280] D. Ferretti, E. Coisson, D. Ugolotti, E. Lenticchia, Use of EC6-like equations to estimate the compressive strength of masonry made of solid clay bricks and lime mortar, in: C. Modena, F. da Porto, M.R. Valluzzi (Eds.), *Brick Block Mason. - Trends, Innov. Challenges*, Taylor & Francis Group, London, 2016: pp. 1561–1570.
- [281] S.G. Fattal, L.E. Cattaneo, *Structural performance of masonry walls under compression and flexure*, The National Bureau of Standards, 1976.  
[http://books.google.it/books/about/Structural\\_performance\\_of\\_masonry\\_walls.html?id=SqTSeEOTnnsC&pgis=1](http://books.google.it/books/about/Structural_performance_of_masonry_walls.html?id=SqTSeEOTnnsC&pgis=1).
- [282] A.T. Vermeltfoort, Compression properties of masonry and its components, 10th Int. Brick/Block Mason. Conf. (1994) 1433–1442.
- [283] L. Binda, C. Tiraboschi, G. Mirabella Roberti, Problemi di misura dei parametri meccanici della muratura e dei suoi componenti, in: *La Mecc. Delle Murature Tra Teor. e Progett.*, 1996.
- [284] W. Mann, M. Betzler, Investigations on the effect of different forms of tests samples to test the

- compressive strength of masonry, 10th Int. Brick/Block Mason. Conf. (1994) 1305–1314.
- [285] European Committee for Standardization (CEN), EN 772-1:2011 Methods of Test for Masonry Units - Part 1: Determination of Compressive Strength, (2011).
- [286] European Committee for Standardization (CEN), UNE-EN 772-6 Métodos de ensayo de piezas para fábrica de albañilería - Parte 6: Determinación de la resistencia a flexotracción de las piezas de hormigón de árido para fábrica de albañilería, (2002).
- [287] European Committee for Standardization (CEN), EN 12390-13 Testing hardened concrete - Part 13: Determination of secant modulus of elasticity in compression, (2013).
- [288] American Society for Testing and Materials, ASTM C 469-02 Standard Test Method for Static Modulus of Elasticity and Poisson's Ratio of Concrete in Compression, (2002) 2–6. doi:10.1520/C0469.
- [289] European Committee for Standardization (CEN), EN 14580 Natural stone test methods. Determination of static elastic modulus, (2006).
- [290] K. Naraine, S.N. Sinha, Loading and unloading stress-strain curves for brick masonry, *J. Struct. Eng.* 115 (1989) 2631–2644.
- [291] P.B. Lourenço, J. Pina-Henriques, Validation of analytical and continuum numerical methods for estimating the compressive strength of masonry, *Comput. Struct.* 84 (2006) 1977–1989. doi:10.1016/j.compstruc.2006.08.009.
- [292] European Committee for Standardization (CEN), Eurocode 2: Design of concrete structures. General rules and rules for buildings, (2004).
- [293] J. Eibl, E. Keintzel, V. Vratsanou, Determination of earthquake duration dependent behaviour factors for unreinforced brick masonry panels by nonlinear time history calculations, *Elev. World Conf. Earthq. Eng.* (1996).
- [294] K. Subramaniam, S.N. Sinha, Analytical Model for Cyclic Compressive Behavior of Brick Masonry, *ACI Struct. J.* 92 (1995) 288–294.
- [295] M.M. AlShebani, Cyclic residual strains of brick masonry, in: *Proc., Int. Conf. Struct. Eng. Mech. Comput.*, 2001.
- [296] M.E. Nazar, S.N. Sinha, Loading-unloading curves of interlocking grouted stabilised sand-flyash brick

- masonry, *Mater. Struct. Constr.* 40 (2007) 667–678. doi:10.1617/s11527-006-9177-x.
- [297] J.F. Sima, P. Roca, C. Molins, Nonlinear response of masonry wall structures subjected to cyclic and dynamic loading, *Eng. Struct.* 33 (2011) 1955–1965. doi:10.1016/j.engstruct.2011.02.033.
- [298] F.J. Crisafulli, *Seismic Behaviour of Reinforced Concrete Structures with Masonry Infills*, University of Canterbury, 1997.
- [299] K. Naraine, S. Sinha, Cyclic behavior of brick masonry under biaxial compression, *J. Struct. Eng.* 117 (1991) 1336–1355.
- [300] I. Galman, *Ściany z ceramicznej cegły pełnej cyklicznie ściskane w swej płaszczyźnie lub zginane prostopadle do płaszczyzny*, Silesian University of Technology, Poland, 2012.
- [301] P.B. Lourenço, Recent Advances in Masonry Modelling: Micromodelling and Homogenisation, *Multiscale Model. Solid Mech.* (2009) 251–294. doi:10.1142/9781848163089\_0006.
- [302] A. Carpinteri, B. Chiaia, P. Bocca, Size dependence of strength and fracture properties of brick masonry walls, *J. Eng. Mech.* 123 (1997) 816–822.
- [303] P.B. Lourenço, Two aspects related to the analysis of masonry structures: size effect and parameter sensitivity. Report n 03.21.1.31.25, 1997.
- [304] Deutsches Institut für Normung (DIN), DIN 18555-9: Testing of mortar containing mineral binders - Part 9: Determining the compressive strength of hardened mortar, (1999).
- [305] M. Tomazevic, *Earthquake-resistant design of masonry buildings*, Imperial College Press, 1999. doi:<https://doi.org/10.1142/p055>.
- [306] A. Mohammed, T.G. Hughes, A. Mustapha, The effect of scale on the structural behaviour of masonry under compression, *Constr. Build. Mater.* 25 (2011) 303–307. doi:10.1016/j.conbuildmat.2010.06.025.
- [307] C.L. Knox, D. Dizhur, J.M. Ingham, Experimental study on scale effects in clay brick masonry prisms and wall panels investigating compression and shear related properties, *Constr. Build. Mater.* 163 (2018) 706–713. doi:10.1016/j.conbuildmat.2017.12.149.
- [308] J.A. Thamboo, M. Dhanasekar, Correlation between the performance of solid masonry prisms and wallettes under compression, *J. Build. Eng.* 22 (2019) 429–438. doi:10.1016/j.job.2019.01.007.

- [309] R.H. Atkinson, B.P. Amadei, S. Saeb, S. Sture, Response of masonry bed joints in direct shear, *J. Struct. Eng.* 115 (1989) 2276–2296. doi:10.5940/jcrsj.32.Supplement\_78.
- [310] M. Tomaževič, Shear resistance of masonry walls and Eurocode 6: Shear versus tensile strength of masonry, *Mater. Struct. Constr.* 42 (2009) 889–907. doi:10.1617/s11527-008-9430-6.
- [311] J.R. Riddington, P. Jukes, A comparison between panel, joint and code shear strength, in: N.G. Shrive, A. Huizer (Eds.), *10th Int. Brick Block Mason. Conf.*, Masonry Council of Canada, 1994: pp. 1481–1490. doi:10.1017/CBO9781107415324.004.
- [312] S. Zhang, K. Beyer, Numerical investigation of the role of masonry typology on shear strength, *Eng. Struct.* 192 (2019) 86–102. doi:10.1016/j.engstruct.2019.04.026.
- [313] D. Malomo, M.J. DeJong, A. Penna, Influence of bond pattern on the in-plane behaviour of URM piers, *Int. J. Archit. Herit.* 00 (2019) 1–20. doi:10.1080/15583058.2019.1702738.
- [314] P. Jukes, J. Riddington, A review of masonry joint shear strength test methods, *Mason. Int.* 11 (1997) 37–43.
- [315] M. Montazerolghaem, W. Jaeger, A Comparative Numerical Evaluation of Masonry Initial Shear Test Methods and Modifications Proposed for EN 1052-3, in: *9th Int. Mason. Conf.*, 2014: pp. 1–10.
- [316] R. Popal, A New Shear Test Method for Mortar Bed Joints, Dissertation, University of Calgary, 2013.
- [317] R. Popal, S.L. Lissel, Numerical evaluation of existing mortar joint shear tests and a new test method, in: *8th Int. Mason. Conf.*, 2010: pp. 795–802.
- [318] P.B. Lourenço, L.F. Ramos, Characterization of cyclic behavior of dry masonry joints, *J. Struct. Eng.* 130 (2004) 779–786. doi:10.1061/(ASCE)0733-9445(2004)130.
- [319] A.T. Vermeltoort, Shear Strength Variation Due To Mortar Strength Variation and the Use of a Triplet Shear Test Set-Up, in: *15th Int. Brick Block Mason. Conf.*, 2012.
- [320] O.P. Cavalheiro, G.M. Pedroso, Experimental data on hollow block prisms using direct shear test, in: *12th Int. Brick/Block Mason. Conf.*, 2000: pp. 433–440.
- [321] J. Milosevic, A.S. Gago, M. Lopes, R. Bento, Experimental assessment of shear strength parameters on rubble stone masonry specimens, *Constr. Build. Mater.* 47 (2013) 1372–1380. doi:10.1016/j.conbuildmat.2013.06.036.

- [322] F. Ferretti, C. Mazzotti, R. Esposito, J.G. Rots, Shear-sliding behavior of masonry: Numerical micro-modeling of triplet tests, in: G. Meschke, B. Pichler, J.G. Rots (Eds.), *Comput. Model. Concr. Struct. - Proc. Conf. Comput. Model. Concr. Struct. EURO-C 2018*, CRC Press, 2018: pp. 941–954. doi:10.1201/9781315182964-109.
- [323] D. Marastoni, *Advanced Minor Destructive Testing for the Assessment of Existing Masonry*, PhD Thesis, Università di Bologna, 2016.
- [324] P.B. Lourenco, J.O. Barros, J.T. Oliveira, Shear testing of stack bonded masonry, *Constr. Build. Mater.* 18 (2004) 125–132. doi:10.1016/j.conbuildmat.2003.08.018.
- [325] G. Vasconcelos, P.B. Lourenço, Experimental characterization of stone masonry in shear and compression, *Constr. Build. Mater.* 23 (2009) 3337–3345. doi:10.1016/j.conbuildmat.2009.06.045.
- [326] J.R. Riddington, P. Jukes, A masonry joint shear strength test method, *Proc. Inst. Civ. Eng. Struct. Build.* 104 (1994) 267–274. doi:10.1680/istbu.1994.26777.
- [327] B.P. Sinha, A.W. Hendry, Further investigations of bond tension, bond shear and the effect of precompression on shear strength of model brick masonry couplets, *Br. Ceram. Res. Assoc. March* (1966).
- [328] J.C.G. Chin Wah, *Shear resistance of masonry walls*, PhD Thesis, University of London, 1972.
- [329] S.J. Lawrence, *Couplet and triplet tests for the measurement of bond strength of brickwork*, Experimental Building Station, 1977.
- [330] A. Rahman, T. Ueda, Experimental investigation and numerical modeling of peak shear stress of Brick Masonry mortar joint under compression, *J. Mater. Civ. Eng.* 26 (2014) 1–13. doi:10.1061/(ASCE)MT.1943-5533.0000958.
- [331] N. Augenti, F. Parisi, Constitutive modelling of tuff masonry in direct shear, *Constr. Build. Mater.* 25 (2011) 1612–1620. doi:10.1016/j.conbuildmat.2010.10.002.
- [332] P. Schubert, A. Caballero Gonzalez, *Vergleichende Untersuchungen nach DIN 18555-5 und DIN EN 1052-3. Part 1 and Part 2*. Research reports F449 and F449/2, 1996.
- [333] F. Fouchal, F. Lebon, I. Titeux, Contribution to the modelling of interfaces in masonry construction, *Constr. Build. Mater.* 23 (2009) 2428–2441. doi:10.1016/j.conbuildmat.2008.10.011.

- [334] J. Segura, D. Aponte, L. Pelà, P. Roca, Influence of recycled limestone filler additions on the mechanical behaviour of commercial premixed hydraulic lime based mortars, *Constr. Build. Mater.* 238 (2020) 117722. doi:10.1016/j.conbuildmat.2019.117722.
- [335] E. Bernat-Maso, Analysis of unreinforced and TRM-strengthened brick masonry walls subjected to eccentric axial load, PhD Thesis, Universitat Politècnica de Catalunya, 2014.
- [336] P.B. Lourenço, Computational strategies for masonry structures, PhD Thesis, Delft University of Technology, 1996.
- [337] M. Bisoffi-Sauve, S. Morel, F. Dubois, Modelling mixed mode fracture of mortar joints in masonry buildings, *Eng. Struct.* 182 (2019) 316–330. doi:10.1016/j.engstruct.2018.11.064.
- [338] G.P.A.G. van Zijl, Modeling masonry shear-compression: Role of dilatancy highlighted, *J. Eng. Mech.* 130 (2004) 1289–1296. doi:10.1061/(ASCE)0733-9399(2004)130:11(1289).
- [339] N. Mojsilović, M. Petrović, X.R. Anglada, Masonry elements with multi-layer bed joints: Behaviour under monotonic and static-cyclic shear, *Constr. Build. Mater.* 100 (2015) 149–162. doi:10.1016/j.conbuildmat.2015.09.065.
- [340] S. Ali, A.W. Page, A failure criterion for mortar joints in brickwork subjected to combined shear and tension, *Mason. Int.* 9 (1986) 43–54.
- [341] W.S. Lei, A generalized weakest-link model for size effect on strength of quasi-brittle materials, *J. Mater. Sci.* 53 (2018) 1227–1245. doi:10.1007/s10853-017-1574-8.
- [342] M. Shadlou, E. Ahmadi, M.M. Kashani, Micromechanical modelling of mortar joints and brick-mortar interfaces in masonry Structures: A review of recent developments, *Structures.* 23 (2020) 831–844. doi:10.1016/j.istruc.2019.12.017.
- [343] A. Rahgozar, A. Hosseini, Experimental and numerical assessment of in-plane monotonic response of ancient mortar brick masonry, *Constr. Build. Mater.* 155 (2017) 892–909. doi:10.1016/j.conbuildmat.2017.08.079.
- [344] V. Alecci, M. Fagone, T. Rotunno, M. De Stefano, Shear strength of brick masonry walls assembled with different types of mortar, *Constr. Build. Mater.* 40 (2013) 1038–1045. doi:10.1016/j.conbuildmat.2012.11.107.

- [345] L. Binda, A. Fontana, G. Mirabella, Mechanical behavior and stress distribution in multiple-leaf stone walls, in: 10th Int. Brick Block Mason. Conf., 1994: pp. 51–59.
- [346] M. Uranjek, V. Bokan-Bosiljkov, Influence of freeze-thaw cycles on mechanical properties of historical brick masonry, *Constr. Build. Mater.* 84 (2015) 416–428. doi:10.1016/j.conbuildmat.2015.03.077.
- [347] V. Alecci, F. Focacci, L. Rovero, G. Stipo, M. De Stefano, Intrados strengthening of brick masonry arches with different FRCM composites: Experimental and analytical investigations, *Compos. Struct.* 176 (2017) 898–909. doi:10.1016/j.compstruct.2017.06.023.
- [348] A. Rezaie, M. Godio, K. Beyer, Experimental investigation of strength, stiffness and drift capacity of rubble stone masonry walls, *Constr. Build. Mater.* 251 (2020) 118972. doi:10.1016/j.conbuildmat.2020.118972.
- [349] N. Augenti, F. Parisi, Learning from Construction Failures due to the 2009 L’Aquila, Italy, Earthquake, *J. Perform. Constr. Facil.* 24 (2010) 536–555. doi:10.1061/(ASCE)CF.1943-5509.0000122.
- [350] G. Magenes, G.M. Calvi, In-plane seismic response of brick masonry walls, *Earthq. Eng. Struct. Dyn.* 26 (1997) 1091–1112.
- [351] V. Turnšek, P. Sheppard, The shear and flexural resistance of masonry walls, in: *Int. Res. Conf. Earthq. Eng.*, 1980: pp. 517–573. doi:10.1017/CBO9781107415324.004.
- [352] A. Incerti, V. Rinaldini, C. Mazzotti, The evaluation of masonry shear strength by means of different experimental techniques: A comparison between full-scale and laboratory tests, *Brick Block Mason. Trends, Innov. Challenges - Proc. 16th Int. Brick Block Mason. Conf. IBMAC 2016.* (2016) 1645–1652. doi:10.1201/b21889-204.
- [353] M. Basili, G. Marcari, F. Vestroni, Nonlinear analysis of masonry panels strengthened with textile reinforced mortar, *Eng. Struct.* 113 (2016) 245–258. doi:10.1016/j.engstruct.2015.12.021.
- [354] R. Sousa, H. Sousa, J. Guedes, Diagonal compressive strength of masonry samples - Experimental and numerical approach, *Mater. Struct. Constr.* 46 (2013) 765–786. doi:10.1617/s11527-012-9933-z.
- [355] American Society for Testing and Materials, ASTM E 519 Standard Test Method for Diagonal Tension ( Shear ) in Masonry Assemblages, (2010).
- [356] M. Del Zoppo, M. Di Ludovico, A. Balsamo, A. Prota, In-plane shear capacity of tuff masonry walls

- with traditional and innovative Composite Reinforced Mortars (CRM), *Constr. Build. Mater.* 210 (2019) 289–300. doi:10.1016/j.conbuildmat.2019.03.133.
- [357] S. Casacci, C. Gentilini, A. Di Tommaso, D. V. Oliveira, Shear strengthening of masonry wallettes resorting to structural repointing and FRCM composites, *Constr. Build. Mater.* 206 (2019) 19–34. doi:10.1016/j.conbuildmat.2019.02.044.
- [358] M. Corradi, A. Borri, A database of the structural behavior of masonry in shear, *Bull. Earthq. Eng.* 16 (2018) 3905–3930. doi:10.1007/s10518-018-0328-6.
- [359] A. Benedetti, In Plane Behaviour of Masonry Walls Reinforced with Mortar Coatings and Fibre Meshes, *Int. J. Archit. Herit.* 13 (2019) 1029–1041. doi:10.1080/15583058.2019.1618972.
- [360] G.P. Lignola, A. Bilotta, F. Ceroni, Assessment of the effect of FRCM materials on the behaviour of masonry walls by means of FE models, *Eng. Struct.* 184 (2019) 145–157. doi:10.1016/j.engstruct.2019.01.035.
- [361] M. Del Zoppo, M. Di Ludovico, A. Prota, Analysis of FRCM and CRM parameters for the in-plane shear strengthening of different URM types, *Compos. Part B Eng.* 171 (2019) 20–33. doi:10.1016/j.compositesb.2019.04.020.
- [362] S. Türkmen, B.T. De Vries, S.N.M. Wijte, A.T. Vermeltfoort, In-plane behaviour of clay brick masonry wallettes retrofitted with single-sided fabric-reinforced cementitious matrix and deep mounted carbon fibre strips, *Bull. Earthq. Eng.* 18 (2020) 725–765. doi:10.1007/s10518-019-00596-2.
- [363] M. Shabdin, M. Zargarán, N.K.A. Attari, Experimental diagonal tension (shear) test of Un-Reinforced Masonry (URM) walls strengthened with textile reinforced mortar (TRM), *Constr. Build. Mater.* 164 (2018) 704–715. doi:10.1016/j.conbuildmat.2017.12.234.
- [364] A. Incerti, A.R. Tilocca, F. Ferretti, C. Mazzotti, Influence of masonry texture on the shear strength of FRCM reinforced panels, in: R. Aguilar (Ed.), *Struct. Anal. Hist. Constr., RILEM Bookseries*, 2019: pp. 1623–1631. doi:10.1007/978-3-319-99441-3.
- [365] J. Segura, E. Bernat-Masó, V.D. Mendizábal, L. Pelà, P. Roca, L. Gil, Experimental comparison of two testing setups for characterizing the shear mechanical properties of masonry (under review), *Constr. Build. Mater.* (2020).

- [366] C. Loth, Flemish bond: A hallmark of traditional architecture, *Inst. Class. Archit. Art.* (2011).
- [367] T. Li, N. Galati, J.G. Tumialan, A. Nanni, Analysis of unreinforced masonry concrete walls strengthened with glass fiber-reinforced polymer bars, *ACI Struct. J.* 102 (2005) 569–577. doi:10.14359/14561.
- [368] N. Ismail, R.B. Petersen, M.J. Masia, J.M. Ingham, Diagonal shear behaviour of unreinforced masonry wallettes strengthened using twisted steel bars, *Constr. Build. Mater.* 25 (2011) 4386–4393. doi:10.1016/j.conbuildmat.2011.04.063.
- [369] A. Borri, M. Corradi, G. Castori, A. De Maria, A method for the analysis and classification of historic masonry, *Bull. Earthq. Eng.* 13 (2015) 2647–2665. doi:10.1007/s10518-015-9731-4.
- [370] V. Alecci, S. Barducci, A. D’Ambrisi, M. De Stefano, F. Focacci, R. Luciano, R. Penna, Shear capacity of masonry panels repaired with composite materials: Experimental and analytical investigations, *Compos. Part B Eng.* 171 (2019) 61–69. doi:10.1016/j.compositesb.2019.04.013.
- [371] J. Milosevic, M. Lopes, A.S. Gago, R. Bento, Testing and modeling the diagonal tension strength of rubble stone masonry panels, *Eng. Struct.* 52 (2013) 581–591. doi:10.1016/j.engstruct.2013.03.019.
- [372] A. Borri, G. Castori, M. Corradi, Determination of Shear Strength of Masonry Panels Through Different Tests, *Int. J. Archit. Herit.* 9 (2015) 913–927. doi:10.1080/15583058.2013.804607.
- [373] F. Parisi, C. Balestrieri, D. Asprone, Nonlinear micromechanical model for tuff stone masonry: Experimental validation and performance limit states, *Constr. Build. Mater.* 105 (2016) 165–175. doi:10.1016/j.conbuildmat.2015.12.078.
- [374] A. Gabor, E. Ferrier, E. Jacquelin, P. Hamelin, Analysis and modelling of the in-plane shear behaviour of hollow brick masonry panels, *Constr. Build. Mater.* 20 (2006) 308–321. doi:10.1016/j.conbuildmat.2005.01.032.
- [375] S. Zhang, S.M. Taheri Mousavi, N. Richart, J.F. Molinari, K. Beyer, Micro-mechanical finite element modeling of diagonal compression test for historical stone masonry structure, *Int. J. Solids Struct.* 112 (2017) 122–132. doi:10.1016/j.ijsolstr.2017.02.014.
- [376] R. Faria, J. Oliver, A rate dependent plastic-damage constitutive model for large scale computations in concrete structures, CIMNE, 1993.
- [377] M. Petracca, L. Pelà, R. Rossi, S. Oller, G. Camata, E. Spacone, Multiscale computational first order

- homogenization of thick shells for the analysis of out-of-plane loaded masonry walls, *Comput. Methods Appl. Mech. Eng.* 315 (2017) 273–301. doi:10.1016/j.cma.2016.10.046.
- [378] M. Petracca, L. Pelà, R. Rossi, S. Oller, G. Camata, E. Spacone, Regularization of first order computational homogenization for multiscale analysis of masonry structures, *Comput. Mech.* 57 (2016) 257–276. doi:10.1007/s00466-015-1230-6.
- [379] J. Lubliner, J. Oliver, S. Oller, E. Oñate, A plastic-damage model for concrete, *Int. J. Solids Struct.* 26 (1989) 252. doi:10.1016/0148-9062(89)91126-1.
- [380] R. Clemente, Análisis estructural de edificios históricos mediante modelos localizados de fisuración, PhD Thesis, Universitat Politècnica de Catalunya, 2006.
- [381] L. Pelà, M. Cervera, P. Roca, Continuum damage model for orthotropic materials: Application to masonry, *Comput. Methods Appl. Mech. Eng.* 200 (2011) 917–930. doi:10.1016/j.cma.2010.11.010.
- [382] L. Pelà, Continuum damage model for nonlinear analysis of masonry structures, PhD Thesis, Universitat Politècnica de Catalunya, 2009.
- [383] S. Saloustros, L. Pelà, M. Cervera, P. Roca, Finite element modelling of internal and multiple localized cracks, *Comput. Mech.* 59 (2017) 299–316. doi:10.1007/s00466-016-1351-6.
- [384] S. Saloustros, M. Cervera, L. Pelà, Tracking multi-directional intersecting cracks in numerical modelling of masonry shear walls under cyclic loading, *Meccanica.* 53 (2018) 1757–1776. doi:10.1007/s11012-017-0712-3.
- [385] S. Saloustros, M. Cervera, L. Pelà, Challenges, Tools and Applications of Tracking Algorithms in the Numerical Modelling of Cracks in Concrete and Masonry Structures, *Arch. Comput. Methods Eng.* 26 (2019) 961–1005. doi:10.1007/s11831-018-9274-3.
- [386] COMET, Coupled Mechanical and Thermal analysis, (2016). <https://www.cimne.com/comet>.
- [387] GiD v.14, The personal pre- and post-processor, (2018). <https://www.gidhome.com/>.
- [388] CEB-FIP, Model Code 1990, (1993).
- [389] CEB-FIP, Model Code 2010, (2012).
- [390] S.G. Fattal, The capacity of unreinforced masonry shear walls under membrane loads, in: *Earthq. Resist.*

- Mason. Constr. Natl. Work., 1977: pp. 177–197.
- [391] S. Babaeidarabad, F. De Caso, A. Nanni, URM walls strengthened with fabric-reinforced cementitious matrix composite subjected to diagonal compression, *J. Compos. Constr.* 18 (2014). doi:10.1061/(ASCE)CC.1943-5614.0000441.
- [392] P.F. Silva, P. Yu, A. Nanni, Monte Carlo simulation of shear capacity of URM walls retrofitted by polyurea reinforced GFRP grids, *J. Compos. Constr.* 12 (2008) 405–415. doi:10.1061/(ASCE)1090-0268(2008)12:4(405).
- [393] I.S. Koltsida, A.K. Tomor, C.A. Booth, Strain evolution of brick masonry under cyclic compressive loading, *Mater. Struct. Constr.* 52 (2019). doi:10.1617/s11527-019-1379-0.
- [394] N. Mojsilović, Masonry subjected to semi-cyclic compression: Inelastic response modelling, *Constr. Build. Mater.* 263 (2020). doi:10.1016/j.conbuildmat.2020.120147.
- [395] J. Veríssimo-Anacleto, M. Ludovico-Marques, P. Neto, An empirical model for compressive strength of the limestone masonry based on number of courses – An experimental study, *Constr. Build. Mater.* 258 (2020). doi:10.1016/j.conbuildmat.2020.119508.
- [396] J. Thamboo, J. Bandara, S. Perera, S. Navaratnam, K. Poologanathan, M. Corradi, Experimental and analytical study of masonry subjected to uniaxial cyclic compression, *Materials (Basel)*. 13 (2020) 1–17. doi:10.3390/ma13204505.
- [397] J. Thamboo, M. Dhanasekar, Assessment of the characteristics of lime mortar bonded brickwork wallettes under monotonic and cyclic compression, *Constr. Build. Mater.* 261 (2020). doi:10.1016/j.conbuildmat.2020.120003.